# APPENDIX A

# RELAP5/MOD2 MODELS NOT EMPLOYED IN EVALUATIONS

Several special component and constitutive models are included within RELAP5/MOD2-B&W which will not be used for evaluation model calculations. These models include: reflood heat transfer, noncondensible gas heat transfer degradation, the original INEL simple gap conductance model, jet mixing, and the turbine component. These sections will not be described within this report; however, a reference back to the original INEL release of RELAP5/MOD2 code manual[1] will be given for completeness.

The reflood heat transfer option will not be used in the RELAP5 evaluation model calculations. It is described in sections 3.1.3.6, 3.2.8, and 3.2.9 of Reference 1. The reflood portion of the LBLOCA transient will be performed by the BEACH code[123], a derivative of RELAP5/MOD2.

Two noncondensible gas heat transfer degradation models are available within RELAP5/MOD2-B&W. An original INEL model and a new mechanistic model option added by B&W are formulated within the code. A complete description of the INEL model can be found in Reference 1.

A new detailed gap conductance model which included clad swell and rupture calculations as well as metal water reaction calculations was added for evaluation model calculations. The original simple gap conductance model described in section 3.2.10 of Reference 1 will therefore not be used.

The turbine and jet mixer special component models will not be used for licensing calculations. A complete description of these models is found in Reference 1 sections 3.1.5.5 and 3.1.5.3.

# APPENDIX B

## LIST OF SYMBOLS

(Variables which are not dimensioned have SI units)

| | |
|---|---|
| $A$ | Cross-sectional area ($m^2$), coefficient matrix in hydrodynamics, coefficient in pressure and velocity equations |
| $A_1$ | Coefficient in heat conduction equation at boundaries |
| $A_L$ | Surge line cross sectional area ($m^2$) |
| $A_t$ | Throat area ($m^2$) |
| $a$ | Speed of sound (m/s), interfacial area per unit volume ($m^{-1}$), coefficient in gap conductance, coefficient in heat conduction equation, absorption coefficient |
| $B$ | Coefficient matrix, drag coefficient, coefficient in pressure and velocity equations |
| $B_1$ | Coefficient in heat conduction equation at boundaries |
| $b$ | Coefficient in heat conduction equation, source vector in hydrodynamics |
| $B_x$ | Body force in x-coordinate direction ($m/s^2$) |
| $B_y$ | Body force in y-coordinate direction ($m/s^2$) |
| $C$ | Coefficient of virtual mass, general vector function, coefficient in pressure, and velocity equations, delay neutron precursors in reactor kinetics, concentration |

| | |
|---|---|
| $C_o$ | Coefficient in noncondensible energy equation (J/kg-K) |
| $C_d$ | Drag coefficient |
| $C_g$ | Dimensional constant in correlation for $\Gamma_g$ |
| $C_p$ | Specific heat at constant pressure (J/kg-K) |
| $C_v$ | Specific heat at constant volume (J/kg-K) |
| c | Coefficient in heat conduction equation, coefficient in new time volume-average velocity equation |
| D | Coefficient of relative Mach number, diffusivity, diameter (m), heat conduction boundary condition matrix, coefficient in pressure and velocity equations |
| $D_o$ | Coefficient in noncondensible energy equation ($J/kg-K^2$) |
| $D_1$ | Coefficient of heat conduction equation at boundaries |
| d | Coefficient in heat conduction equation, droplet diameter (m) |
| DISS | Energy dissipation function ($w/m^3$) |
| E | Total energy ($U + v^2/2$) (J/kg), emissivity, Young's modulus, term in iterative heat conduction algorithm, coefficient in pressure equation |

| | |
|---|---|
| e | Interfacial roughness |
| Eu | Euler number |
| F | Term in iterative heat conduction algorithm, gray-body factor with subscript, frictional loss coefficient, vertical stratification factor |
| FIF, FIG | Interphase drag coefficients (liquid, vapor) ($s^{-1}$) |
| FI | Interphase drag coefficient ($m^3$/kg-s) |
| FWF, FWG | Wall drag coefficients (liquid, vapor) ($s^{-1}$) |
| f | Interphase friction factor, vector for liquid velocities in hydrodynamics, delayed neutron fraction |
| $G_{head}$ | Pressure drop across valve due to gravity (Pa) |
| G | Mass velocity (kg/s), shear stress, gradient, coefficient in heat conduction, vector quantity, fraction of delayed neutrons in reactor kinetics |
| $G_c$ | Dynamic pressure for valve (Pa) |
| Gr | Grashof number |
| g | Gravitational constant ($m/s^2$), temperature jump distance (m), vector for vapor velocities in hydrodynamics |
| $g_{Z,g}$ | Acceleration due to gravity ($m/s^2$) |

| | |
|---|---|
| H | Elevation (m), volumetric heat transfer coefficient ($w/K-m^3$), head (m), clad non-dimensional heating ramp rate |
| HLOSSF | Form or frictional losses (liquid) (m/s) |
| HLOSSG | Form or frictional losses (vapor) (m/s) |
| h | Specific enthalpy (J/kg), heat transfer coefficient ($w/m^2-K$), energy transfer coefficient for $\Gamma_g$, head ratio |
| $h_L$ | Dynamic head loss (m) |
| I | Identity matrix, moment of inertia ($N-m-s^2$) |
| J | Junction velocity (m/s) |
| K | Energy form loss coefficient, metal-water rate constant ($g^2/cm^4-s$) |
| k | Thermal conductivity (w/m-K) |
| $k_B$ | Boltzmann constant |
| $k_s$ | Spring constant |
| L | Length, limit function |
| $L_L$ | Surge line length (m) |
| $\ell\ell$ | Liquid level (m) |
| M | Mach number, molecular weight, pump two-phase multiplier, mass transfer rate, mass (kg) |

| | |
|---|---|
| $N$ | Number of system nodes, number density (#/$m^3$), pump speed (rad/s) |
| $Nu$ | Nusselt number |
| $n$ | Unit vector, order of equation system, moles of gap gas (kg mole) |
| $P_{Br}$ | Valve closing back pressure (Pa) |
| $P$ | Pressure (Pa), reactor power (w), channel perimeter (m), turbine power (J/s) |
| $P_D$ | Nitrogen pressure in dome (Pa) |
| $P_f$ | Relates reactor power to heat generation rate in heat structures, immediate fission power (MeV/s) |
| $P_o$ | Atmospheric pressure (Pa) |
| $p$ | Wetted perimeter (m), particle probability function |
| PCV | Specified pressure required to close a valve (Pa) |
| Pr | Prandtl number |
| $Q$ | Volumetric heat addition rate ($w/m^3$), space dependent function, volumetric flow rate ($m^3/s$) |
| $Q_D$ | Total heat transfer to vapor dome (w) |
| $Q_f$ | Immediate fission energy per fission (MeV) |
| $q$ | Heat transfer rate (w), heat flux ($w/m^2$) |

| | |
|---|---|
| $q_t$ | Specified time dependent, space dependent factor in the source term of heat conduction |
| R | Reynolds number, radius (m), surface roughness in gap conductance, radiation resistance term, gas constant (cal/gmole-K) |
| $R_e$ | Reynolds number |
| $Re_p$ | The particle Reynolds number |
| $R_n$, $R_s$ | Universal gas constants (noncondensible, steam) (N-m/kg-K) |
| r | Reaction fraction for turbine |
| S | Chen's boiling suppression factor, stress gradient, specific entropy (J/kg-K), shape factor, real constant, source term in heat conduction or reactor kinetics (w) |
| s | Surface, Laplace transform variable |
| T | Temperature (K), trip |
| $T_c$ | Critical temperature (K) |
| $T_R$ | Reduced temperature (K) |
| $T_t$ | Specified time dependent function in heat conduction |
| t | Time (s) |

| | |
|---|---|
| U | Specific internal energy (J/kg), vector of dependent variables |
| u | Radial displacement in gap conductance (m) |
| V | Volume ($m^3$), specific volume ($m^3/kg$), control quantity |
| $V_V$ | Volume of noncondensible in accumulator dome ($m^3$) |
| VFDP, VGDP | Coefficient for pressure change in momentum equations (liquid, vapor) (m/s-Pa) |
| VIS | Numerical viscosity terms in momentum equations ($m^2/s^2$) |
| $VIS_F$, $VIS_G$ | Numerical viscosity terms in momentum equations (liquid, vapor) ($m^2/s^2$) |
| VUNDER, VOVER | Separator model parameters (liquid, vapor) |
| v | Mixture velocity (m/s), phasic velocity (m/s), flow ratio, liquid surge line velocity (m/s) |
| $v_c$ | Choking velocity (m/s) |
| W | Weight of valve disk, weighting function in reactor kinetics, relaxation parameter in heat conduction, shaft work per unit mass flow rate |
| $W_{crit}$ | Critical Weber number |
| We | Weber number |

| | |
|---|---|
| w | Humidity ratio |
| X | Static quality, mass fraction, conversion from MeV/s to watts |
| x | Spatial coordinate (m), vector of hydrodynamic variables |
| Y | Control variable |
| Z | Two-phase friction correlation factor, function in reactor kinetics |
| z | Elevation change coordinate (m) |

Symbols

| | |
|---|---|
| $\alpha$ | Void fraction, subscripted volume fraction, angular acceleration ($rad/s^2$), coefficient for least squares fit, speed ratio |
| $\beta$ | Coefficient of isobaric thermal expansion ($K^{-1}$), effective delayed neutron fraction in reactor kinetics |
| $\Gamma$ | Volumetric mass exchange rate ($kg/m^3$-s) |
| $\Delta P_f$ | Dynamic pressure loss (Pa) |
| $\Delta P_s$ | Increment in steam pressure (Pa) |
| $\Delta V_s$ | Increment in specific volume of steam ($m^3/kg$) |
| $\Delta t$ | Increment in time variable (s) |

| | |
|---|---|
| $\Delta t_c$ | Courant time step (s) |
| $\Delta x$ | Increment in spatial variable (m) |
| $\beta$ | Area ratio, truncation error measure, film thickness (m), impulse function, Deryagin number |
| $\epsilon$ | Coefficient, strain function, emissivity, tabular function of area ratio, surface roughness, wall vapor generation/condensation flag |
| $\zeta$ | Diffusion coefficient, multiplier or horizontal stratification terms the right side of heat conduction equation in finite difference form |
| $\eta$ | Efficiency, bulk/saturation enthalpy flag |
| $\theta$ | Relaxation time in correlation for Q, angular position (rad) |
| $\kappa$ | Coefficient of isothermal compressibility ($Pa^{-1}$) |
| $\Lambda$ | Prompt neutron generation time, Baroczy dimensionless property index |
| $\lambda$ | Eigenvalue, interface velocity parameter, friction factor, decay constant in reactor kinetics |
| $\mu$ | Viscosity (kg/m-s) |
| $\nu$ | Kinematic viscosity ($m^2/s$), Poisson's ratio |
| $\xi$ | Exponential function, RMS precision |
| $\pi$ | 3.141592654 |

| | |
|---|---|
| $\rho$ | Density ($kg/m^3$), reactivity in reactor kinetics (dollars) |
| $\Sigma_f$ | Fission cross section |
| $\Sigma'$ | Depressurization rate (Pa/s) |
| $\sigma$ | Surface tension ($J/m^2$), stress, flag used in heat conduction equations to indicate transient or steady state |
| $\tau$ | Shear stresses (N), torque (N-m), fuel-clad gap (m) |
| $\phi$ | Donored property, Lockhart-Martinelli two-phase parameter, neutron flux in reactor kinetics, angle of inclination of valve assembly |
| $\chi$ | Lockhart-Martinelli parameter |
| $\psi$ | Coefficient, fission rate (#/s) |
| $\omega$ | Angular velocity (rad/s), function variable in reactor kinetics |

Subscripts

| | |
|---|---|
| a | Average value |
| B | Boron, dissolved solid |
| b | Bubble |
| CHF | Value at critical heat flux |

| | |
|---|---|
| c | Vena contracta, continuous phase, cladding, critical property, cross section |
| cm | Cladding midpoint |
| con | Condensation |
| cr | Critical property or condition |
| D | Drive line, vapor dome |
| d | Droplet, delay in control component |
| e | Thermodynamic equilibrium, equivalent quality in hydraulic volumes, value ring exit, elastic deformation |
| exp | Used to indicate explicit velocities in choking |
| F | Wall friction, fuel |
| FB, FBB | Film boiling, Bromley film boiling |
| f | Liquid phase |
| fg | Phasic difference (i.e., vapor term-liquid term) |
| fp | Onset of vapor pull-through |
| fr | Frictional |
| g | Vapor phase, gap |
| ge | Incipient liquid entrainment |

| | |
|---|---|
| H | Head |
| HE | Homogeneous equilibrium |
| HF | Homogeneous frozen |
| hy | Hydraulic |
| I | Interface, delayed neutron group index |
| IB | Incipience of boiling |
| i | Inlet, interface |
| j, j+1, j-1 | Spatial noding indices, junctions |
| K | Spatial noding indices, volumes |
| L | Spatial noding index, volumes, laminar |
| $\ell$ | Left boundary in heat conduction |
| M | Rightmost boundary in heat conduction |
| m | Mixture property, motor, mesh point |
| NB | Nucleate boiling |
| n | Noncondensible component of vapor phase |
| o | Reference value |
| R | Rated values |

| | |
|---|---|
| r | Relative Mach number, right boundary in heat conduction |
| S | Suction region |
| s | Steam component of vapor phase |
| sat | Saturated quantity |
| T | Point of minimum area, turbulent |
| TB | Transition film boiling |
| t | Turbulent, tangential |
| tt | Fully turbulent |
| up | Upstream quantity |
| v | Mass mean Mach number, vapor quantity, valve |
| w | Wall, water |
| wall | Wall of tank |
| wg, wf | Wall to vapor, wall to liquid |
| 1 | Upstream station, multiple junction index, vector index |
| 1$\phi$ | Single-phase value |
| 2 | Downstream station, multiple junction index, vector index |

| | |
|---|---|
| $2\phi$ | Two-phase value |
| $\tau$ | Torque |
| $\vec{\ }$ | Vector |
| $\approx$ | Matrix |

Superscripts

| | |
|---|---|
| b | Boundary gradient weight factor in heat conduction, vector quantities |
| exp | Old time terms in velocity equation |
| I | Imaginary part of complex number |
| m-1, m, m+1 | Mesh points in heat conduction finite difference equation or mean value |
| n, n+1 | Time level index |
| n + 1/2 | An average of quantities with superscripts n and n + 1 |
| o | Initial value |
| R | Real part of complex number |
| r | Right boundary in heat conduction |
| s | Saturation property, space gradient weight factor in heat conduction |
| v | Volume gradient weight factor in heat conduction |

| | |
|---|---|
| w | Wall |
| 1 | Vector index, coefficient in velocity equation |
| 2 | Vector index |
| * | Total derivative of a saturation property with respect to pressure, local variable, bulk/saturation property |
| ' | Derivative |
| - | Vector, average quantity |
| . | Donored quantity |
| - | Unit momentum for mass exchange, intermediate time variable |
| ^ | Linearized quantity, quality based on total mixture mass |

# APPENDIX C

# EM CRITICAL FLOW TABLES

The new evaluation model choked flow tables are listed in tabular form in this Appendix. They are listed in the following sections:

C.1 Moody Critical Flow Table.

C.2 Extended Henry-Fauske Critical Flow Table.

C.3 Homogeneous Equilibrium Critical Flow Table.

C.4 Murdock-Bauman Critical Flow Table.

## C.1 MOODY CRITICAL FLOW TABLE

GXX(1) = STAGNATION PRESSURE (PSIA)
GXX(EVEN) = MAXIMUM FLOW RATE (LBM/FT**2-SEC)
GXX(ODD) = STAGNATION ENTHALPY (BTU/LB)

NG = NUMBER OF PAIRS OF FLOW AND ENTHALPY VALUES PER PRESSURE
NPI = NUMBER OF PRESSURE VALUES

```
      DATA  NG, NPI / 17, 21 /

      DATA G01 /      1.0E0,  214.71E0,  69.733E0,   20.11E0, 173.340E0,
     1   10.95E0, 276.948E0,    7.54E0, 380.555E0,    5.76E0, 484.163E0,
     2    4.65E0, 587.771E0,    3.91E0, 691.378E0,    3.37E0, 794.986E0,
     3    2.96E0, 898.593E0,    2.64E0,1002.201E0,    2.38E0,1105.809E0,
     4    2.50E0,1112.678E0,    2.00E0,1238.828E0,    1.80E0,1369.999E0,
     5    1.60E0,1507.606E0,    1.40E0,1652.162E0,    1.30E0,1803.545E0/

      DATA G02 /      5.0E0,  527.49E0,  130.196E0,   90.72E0, 230.286E0,
     1   50.86E0, 330.376E0,   35.44E0, 430.465E0,   27.21E0, 530.555E0,
     2   22.09E0, 630.645E0,   18.60E0, 730.734E0,   16.06E0, 830.824E0,
     3   14.13E0, 930.913E0,   12.62E0,1031.003E0,   11.39E0,1131.093E0,
     4   11.70E0,1142.565E0,    9.80E0,1264.479E0,    8.60E0,1390.263E0,
     5    7.70E0,1521.800E0,    7.10E0,1659.584E0,    6.60E0,1803.492E0/

      DATA G03 /     10.0E0,  767.75E0,  161.261E0,  171.18E0, 259.470E0,
     1   97.76E0, 357.678E0,   68.64E0, 455.887E0,   52.93E0, 554.096E0,
     2   43.09E0, 652.305E0,   36.34E0,750.513E0,   31.42E0, 848.722E0,
     3   27.67E0, 946.931E0,   24.73E0,1045.140E0,   22.35E0,1143.348E0,
     4   22.90E0,1157.466E0,   19.30E0,1277.542E0,   17.10E0,1400.619E0,
     5   15.40E0,1529.045E0,   14.20E0,1663.351E0,   13.10E0,1803.425E0/

      DATA G04 /     14.7E0,  943.01E0,  180.179E0,  242.34E0, 277.210E0,
     1  140.17E0, 374.240E0,   98.93E0, 471.270E0,   76.51E0, 568.300E0,
     2   62.40E0, 665.331E0,   52.69E0, 762.361E0,   45.60E0, 859.391E0,
     3   40.19E0, 956.421E0,   35.93E0,1053.452E0,   32.49E0,1150.482E0,
     4   33.10E0,1166.3770E0,  28.20E0,1258.449E0,   24.90E0,1406.903E0,
     5   22.60E0,1533.437E0,   20.80E0,1665.624E0,   19.30E0,1803.363E0/

      DATA G05 /     50.0E0, 1787.76E0,  250.212E0,  706.24E0, 342.600E0,
     1  432.14E0, 434.988E0,  312.25E0, 527.376E0,  244.68E0, 619.764E0,
     2  201.24E0, 712.153E0,  170.93E0, 804.541E0,  148.58E0, 896.929E0,
     3  131.40E0, 989.317E0,  117.79E0,1081.705E0,  106.74E0,1174.093E0,
     4  107.50E0,1196.581E0,   92.90E0,1312.998E0,   83.20E0,1428.913E0,
     5   76.00E0,1548.789E0,   70.40E0,1673.458E0,   65.80E0,1802.893E0/

      DATA G06 /    100.0E0, 2546.50E0,  298.538E0, 1252.95E0, 387.401E0,
     1  802.83E0, 476.264E0,  591.90E0, 565.127E0,  469.15E0, 653.989E0,
     2  388.73E0, 742.852E0,  331.92E0, 831.715E0,  289.63E0, 920.578E0,
     3  256.92E0,1009.440E0,  230.86E0,1098.303E0,  209.60E0,1187.166E0,
     4  209.20E0,1214.890E0,  182.30E0,1330.371E0,  164.50E0,1442.897E0,
     5  151.10E0,1558.489E0,  140.30E0,1678.248E0,  131.60E0,1802.229E0/
```

```
 DATA G07 /    200.0E0, 3608.16E0, 355.506E0, 2153.39E0, 439.789E0,
1 1463.65E0, 524.071E0, 1108.91E0, 608.354E0,  893.05E0, 692.637E0,
2  747.78E0, 776.920E0,  643.27E0, 861.202E0,  564.45E0, 945.485E0,
3  502.88E0,1029.768E0,  453.44E0,1114.051E0,  412.87E0,1198.334E0,
4  407.00E0,1234.101E0,  357.60E0,1349.174E0,  325.00E0,1458.103E0,
5  300.00E0,1568.929E0,  279.90E0,1683.135E0,  263.30E0,1800.900E0/

 DATA G08 /    400.0E0, 5084.55E0, 424.167E0, 3560.62E0, 502.210E0,
1 2601.91E0, 580.252E0, 2044.87E0, 658.294E0, 1683.97E0, 736.337E0,
2 1413.45E0, 814.379E0, 1244.89E0, 892.421E0, 1101.42E0, 970.464E0,
3  987.66E0,1048.506E0,  895.23E0,1126.548E0,  818.64E0,1204.591E0,
4  792.40E0,1253.154E0,  701.20E0,1368.603E0,  641.80E0,1473.887E0,
5  595.90E0,1579.509E0,  558.50E0,1687.509E0,  527.30E0,1798.245E0/

 DATA G09 /    600.0E0, 6192.24E0, 471.697E0, 4682.13E0, 544.893E0,
1 3588.84E0, 618.089E0, 2897.01E0, 691.285E0, 2426.85E0, 764.481E0,
2 2087.61E0, 837.677E0, 1831.53E0, 910.873E0, 1631.43E0, 984.069E0,
3 1470.77E0,1057.265E0, 1338.95E0,1130.461E0, 1228.83E0,1203.657E0,
4 1172.40E0,1262.896E0, 1040.80E0,1379.241E0,  956.20E0,1482.588E0,
5  890.60E0,1585.098E0,  837.00E0,1689.262E0,  792.00E0,1795.591E0/

 DATA G10 /    800.0E0, 7103.30E0, 509.811E0, 5630.54E0, 578.769E0,
1 4472.42E0, 647.726E0, 3689.49E0, 716.684E0, 3135.77E0, 785.641E0,
2 2725.47E0, 854.599E0, 2409.78E0, 923.557E0, 2159.53E0, 992.514E0,
3 1956.33E0,1061.472E0, 1788.08E0,1130.429E0, 1646.48E0,1199.387E0,
4 1550.10E0,1268.822E0, 1378.50E0,1386.128E0, 1269.40E0,1488.245E0,
5 1184.90E0,1588.533E0, 1115.70E0,1689.882E0, 1057.40E0,1792.940E0/

 DATA G11 /   1000.0E0, 7883.70E0, 542.551E0, 6458.25E0, 607.589E0,
1 5277.33E0, 672.628E0, 4434.96E0, 737.666E0, 3818.11E0, 802.705E0,
2 3349.91E0, 867.743E0, 2983.26E0, 932.782E0, 2688.66E0, 997.820E0,
3 2446.89E0,1062.859E0, 2244.95E0,1127.898E0, 2073.79E0,1192.936E0,
4 1928.00E0,1272.169E0, 1715.80E0,1390.601E0, 1582.30E0,1491.960E0,
5 1479.30E0,1590.602E0, 1394.80E0,1689.784E0, 1323.60E0,1790.290E0/

 DATA G12 /   1200.0E0, 8566.61E0, 571.853E0, 7194.59E0, 633.149E0,
1 6018.53E0, 694.445E0, 5141.21E0, 755.741E0, 4478.45E0, 817.037E0,
2 3964.05E0, 878.333E0, 3554.43E0, 939.629E0, 3221.01E0,1000.925E0,
3 2944.51E0,1062.221E0, 2711.61E0,1123.517E0, 2512.78E0,1184.813E0,
4 2306.00E0,1274.362E0, 2052.90E0,1393.811E0, 1895.20E0,1494.624E0,
5 1773.90E0,1591.920E0, 1674.40E0,1689.289E0, 1590.60E0,1787.642E0/

 DATA G13 /   1400.0E0, 9171.02E0, 598.830E0, 7857.52E0, 656.477E0,
1 6705.77E0, 714.125E0, 5813.30E0, 771.773E0, 5119.72E0, 829.420E0,
2 4569.95E0, 887.068E0, 4125.04E0, 944.716E0, 3758.28E0,1002.364E0,
3 3450.98E0,1060.011E0, 3189.90E0,1117.659E0, 2965.42E0,1175.307E0,
4 2684.80E0,1275.682E0, 2390.20E0,1396.083E0, 2208.30E0,1496.504E0,
5 2068.80E0,1592.681E0, 1954.50E0,1688.499E0, 1858.30E0,1784.994E0/

 DATA G14 /   1600.0E0, 9708.52E0, 624.202E0, 8458.62E0, 678.235E0,
1 7345.72E0, 732.268E0, 6454.71E0, 786.300E0, 5743.98E0, 840.333E0,
2 5169.19E0, 894.366E0, 4696.66E0, 948.399E0, 4302.13E0,1002.431E0,
```

```
3 3968.12E0,1056.464E0, 3681.89E0,1110.497E0, 3433.97E0,1164.530E0,
4 3067.10E0,1275.712E0, 2729.00E0,1397.285E0, 2522.30E0,1497.542E0,
5 2364.50E0,1592.855E0, 2235.40E0,1687.403E0, 2126.80E0,1782.347E0/

 DATA G15 /   1800.0E0,10186.24E0, 648.490E0, 9005.71E0, 698.875E0,
1 7943.45E0, 749.258E0, 7068.47E0, 799.642E0, 6353.40E0, 850.027E0,
2 5763.77E0, 900.411E0, 5271.40E0, 950.795E0, 4855.02E0,1001.179E0,
3 4498.77E0,1051.564E0, 4190.73E0,1101.948E0, 3921.87E0,1152.332E0,
4 3448.60E0,1275.998E0, 3067.70E0,1398.372E0, 2836.40E0,1498.413E0,
5 2660.50E0,1592.891E0, 2516.90E0,1686.228E0, 2396.00E0,1779.701E0/

 DATA G16 /   2000.0E0,10608.22E0, 672.111E0, 9504.17E0, 718.734E0,
1 8503.14E0, 765.356E0, 7657.68E0, 811.979E0, 6950.77E0, 858.601E0,
2 6356.68E0, 905.224E0, 5852.74E0, 951.846E0, 5420.97E0, 998.468E0,
3 5047.45E0,1045.091E0, 4721.42E0,1091.713E0, 4434.55E0,1138.336E0,
4 3833.80E0,1257.411E0, 3408.30E0,1398.751E0, 3151.70E0,1498.725E0,
5 2957.50E0,1592.538E0, 2799.20E0,1684.851E0, 2666.10E0,1777.056E0/

 DATA G17 /   2200.0E0,10975.67E0, 695.462E0, 9956.80E0, 738.132E0,
1 9027.41E0, 780.802E0, 8224.65E0, 823.471E0, 7538.67E0, 866.141E0,
2 6951.18E0, 908.811E0, 6444.80E0, 951.481E0, 6004.98E0, 994.150E0,
3 5620.04E0,1036.820E0, 5280.64E0,1079.490E0, 4979.37E0,1122.159E0,
4 4220.10E0,1274.756E0, 3749.80E0,1398.911E0, 3467.80E0,1498.821E0,
5 3255.10E0,1592.023E0, 3082.30E0,1683.386E0, 2937.10E0,1774.411E0/

 DATA G18 /   2400.0E0,11209.60E0, 718.953E0,10316.18E0, 757.431E0,
1 9486.43E0, 795.909E0, 8750.33E0, 834.387E0, 8105.54E0, 872.866E0,
2 7541.38E0, 911.344E0, 7046.15E0, 949.822E0, 6609.24E0, 988.300E0,
3 6221.66E0,1026.779E0, 5875.90E0,1065.257E0, 5565.81E0,1103.735E0,
4 4619.20E0,1271.798E0, 4096.70E0,1397.651E0, 3787.00E0,1497.913E0,
5 3554.70E0,1590.843E0, 3366.60E0,1681.584E0, 3208.80E0,1771.765E0/

 DATA G19 /   2600.0E0,11428.29E0, 744.475E0,10644.57E0, 778.232E0,
1 9914.50E0, 811.988E0, 9254.60E0, 845.745E0, 8664.25E0, 879.502E0,
2 8137.27E0, 913.259E0, 7666.18E0, 947.016E0, 7243.77E0, 980.772E0,
3 6863.58E0,1014.529E0, 6520.03E0,1048.286E0, 6208.34E0,1082.043E0,
4 5012.40E0,1270.621E0, 4441.80E0,1397.239E0, 4105.40E0,1497.515E0,
5 3854.20E0,1589.972E0, 3651.40E0,1679.930E0, 3481.50E0,1769.120E0/

 DATA G20 /   2800.0E0,11589.07E0, 770.686E0,10931.29E0, 799.200E0,
110314.45E0, 827.715E0, 9746.45E0, 856.230E0, 9227.42E0, 884.745E0,
2 8754.35E0, 913.260E0, 8323.15E0, 941.774E0, 7929.53E0, 970.289E0,
3 7569.46E0, 998.804E0, 7239.24E0,1027.319E0, 6935.60E0,1055.834E0,
4 5411.00E0,1269.067E0, 4789.20E0,1396.501E0, 4425.40E0,1496.853E0,
5 4154.90E0,1588.914E0, 3937.10E0,1678.177E0, 3755.00E0,1766.475E0/

 DATA G21 /   3000.0E0,11604.42E0, 801.845E0,11109.66E0, 823.687E0,
110640.97E0, 845.529E0,10200.60E0, 867.371E0, 9788.61E0, 889.213E0,
2 9403.93E0, 911.055E0, 9044.98E0, 932.898E0, 8709.95E0, 954.740E0,
3 8397.01E0, 976.582E0, 8104.38E0, 998.424E0, 7830.38E0,1020.266E0;
4 5816.40E0,1267.043E0, 5139.50E0,1395.404E0, 4747.10E0,1495.908E0,
5 4456.80E0,1587.660E0, 4223.80E0,1676.323E0, 4029.40E0,1763.830E0/
```

## C.2 EXTENDED HENRY-FAUSKE CRITICAL FLOW TABLE

PE( 1,I) = STAGNATION PRESSURE (PSIA)
PE(EVEN,I) = MAXIMUM FLOW RATE (LB/FT**2-SEC)
PE( ODD,I) = STAGNATION ENTHALPY (BTU/LB)

NPHE = NUMBER OF PRESSURE VALUES
NHHE = NUMBER OF PAIRS OF ENTHALPY AND FLOW VALUES PER PRESSURE

```
DATA NHHE,NPHE / 11,16 /

 DATA PE01 /  10.0,  2293.0,  64.630,  2255.0,  74.271,
1  2204.0,  83.914,  2140.0,  93.560,  2059.0, 103.210,
2  1955.0, 112.866,  1820.0, 122.527,  1647.0, 132.195,
3  1415.0, 141.871,  1108.0, 151.556,   768.0, 161.261/

 DATA PE02 /  14.7,  2788.0,  74.023,  2744.0,  84.605,
1  2684.0,  95.190,  2609.0, 105.780,  2512.0, 116.377,
2  2388.0, 126.981,  2227.0, 137.594,  2014.0, 148.217,
3  1735.0, 158.852,  1369.0, 169.501,   943.0, 180.179/

 DATA PE03 /  50.0,  5174.0, 108.576,  5094.0, 122.624,
1 4989.0,  136.686,  4853.0, 150.766,  4679.0, 164.868,
2 4449.0,  178.996,  4156.0, 193.154,  3771.0, 207.349,
3 3273.0,  221.585,  2646.0, 235.869,  1787.8, 250.212/

 DATA PE04 / 100.0,  7314.0, 131.690,  7203.0, 148.066,
1 7059.0,  164.470,  6870.0, 180.909,  6624.0, 197.390,
2 6304.0,  213.922,  5895.0, 230.515,  5361.0, 247.176,
3 4691.0,  263.917,  3853.0, 280.749,  2546.5, 298.538/

 DATA PE05 / 200.0, 10316.0, 159.379, 10157.0, 178.555,
1 9940.0,  197.788,  9668.0, 217.089,  9303.0, 236.474,
2 8846.0,  255.958,  8256.0, 275.557,  7513.0, 295.289,
3 6567.0,  315.174,  5460.0, 335.236,  3608.2, 355.506/

 DATA PE06 /  400.0, 14530.0, 191.387, 14278.0, 213.823,
1 13967.0,  236.367, 13556.0, 259.042, 13043.0, 281.874,
2 12377.0,  304.892, 11537.0, 328.128, 10496.0, 351.621,
3 9199.0,   375.416,  7708.0, 399.574,  5084.6, 424.167/

 DATA PE07 /  600.0, 17719.0, 212.798, 17412.0, 237.429,
1 17020.0,  262.216, 16499.0, 287.192, 15845.0, 312.394,
2 15027.0,  337.865, 13996.0, 363.658, 12730.0, 389.838,
3 11153.0,  416.489,  9378.0, 443.724,  6192.2, 471.697/

 DATA PE08 /  800.0, 20397.0, 229.413, 20026.0, 255.753,
1 19544.0,  282.295, 18943.0, 309.081, 18176.0, 336.159,
2 17231.0,  363.591, 16028.0, 391.452, 14557.0, 419.842,
3 12758.0,  448.894, 10734.0, 478.793,  7103.3, 509.811/
```

```
 DATA PE09 / 1000.0, 22751.0, 243.188, 22316.0, 270.943,
1 21779.0,  298.941, 21080.0, 327.236, 20219.0, 355.890,
2 19140.0,  384.982, 17782.0, 414.616, 16138.0, 444.930,
3 14147.0,  476.119, 11891.0, 508.470,  7883.7, 542.551/

 DATA PE10 / 1200.0, 24864.0, 255.011, 24372.0, 283.995,
1 23760.0,  313.263, 23001.0, 342.879, 22039.0, 372.919,
2 20839.0,  403.484, 19364.0, 434.707, 17546.0, 466.775,
3 15369.0,  499.957, 12891.0, 534.672,  8566.6, 571.853/

 DATA PE11 / 1400.0, 26793.0, 265.587, 26256.0, 295.666,
1 25596.0,  326.069, 24745.0, 356.869, 23706.0, 388.160,
2 22400.0,  420.065, 20806.0, 452.751, 18847.0, 486.459,
3 16460.0,  521.548, 13753.0, 558.615,  9171.0, 598.830/

 DATA PE12 / 1600.0, 28582.0, 275.051, 28009.0, 306.109,
1 27278.0,  337.529, 26357.0, 369.396, 25230.0, 401.819,
2 23832.0,  434.945, 22100.0, 468.978, 20014.0, 504.219,
3 17468.0,  541.136, 14547.0, 580.548,  9708.5, 624.202/

 DATA PE13 / 1800.0, 30263.0, 283.684, 29633.0, 315.637,
1 28856.0,  347.990, 27868.0, 380.836, 26676.0, 414.304,
2 25180.0,  448.564, 23329.0, 483.862, 21090.0, 520.563,
3 18388.0,  559.264, 15234.0, 601.066, 10186.3, 648.990/

 DATA PE14 / 2000.0, 31856.0, 291.617, 31201.0, 324.390,
1 30358.0,  357.598, 29294.0, 391.347, 28034.0, 425.781,
2 26436.0,  461.098, 24486.0, 497.583, 22124.0, 535.676,
3 19264.0,  576.119, 15855.0, 620.360, 10608.2, 672.111/

 DATA PE15 / 2200.0, 33369.0, 298.970, 32664.0, 332.498,
1 31782.0,  366.495, 30655.0, 401.079, 29295.0, 436.411,
2 27643.0,  472.715, 25603.0, 510.319, 23115.0, 549.741,
3 20073.0,  591.888, 16430.0, 638.625, 10975.7, 695.462/

 DATA PE16/ 2400.0,  34803.0, 305.833, 34045.0, 340.062,
1 33104.0, 374.792,  31947.0, 410.154, 30531.0, 446.326,
2 28787.0, 483.557,  26642.0, 522.220, 24030.0, 562.918,
3 20862.0, 606.736,  16975.0, 656.028, 11209.6, 718.953/
```

## C.3 HOMOGENEOUS EQUILIBRIUM MODEL CRITICAL FLOW TABLES

TXX(1) = STAGNATION PRESSURE (PSIA)
TXX(EVEN) = CRITICAL FLOW RATE (LBM/SEC-FT2)
TXX(ODD) = STAGNATION ENTHALPY (BTU/LBM)

NGHT = NUMBER OF PAIRS OF FLOW RATE AND ENTHALPY VALUES PER PRESSURE
NPT = NUMBER OF PRESSURE VALUES

```
      DATA NGHT, NPT / 27,21 /

      DATA T01 /                                                      1.0E0,
     1  716.13E0,   8.030E0,  711.91E0,  18.057E0,  658.45E0,  28.062E0,
     2  681.49E0,  38.054E0,  535.31E0,  48.038E0,  447.12E0,  58.019E0,
     3  442.29E0,  67.999E0,   20.41E0,  69.733E0,   6.75E0, 173.340E0,
     4    5.02E0, 276.948E0,    4.17E0, 380.555E0,   3.65E0, 484.163E0,
     5    3.29E0, 587.771E0,    3.01E0, 691.378E0,   2.80E0, 794.986E0,
     6    2.62E0, 898.594E0,    2.48E0,1002.201E0,   2.35E0,1105.809E0,
     7    2.35E0,1114.029E0,    2.18E0,1186.541E0,   1.97E0,1260.427E0,
     8    1.81E0,1336.135E0,    1.67E0,1423.810E0,   1.55E0,1514.346E0,
     9    1.46E0,1607.840E0,    1.38E0,1704.280E0,   1.31E0,1803.545E0/

      DATA T02 /                                                      5.0E0,
     1 1681.25E0,   8.042E0, 1665.45E0,  38.065E0, 1579.07E0,  68.010E0,
     2 1378.69E0,  87.975E0, 1162.01E0, 107.955E0,  852.83E0, 117.953E0,
     3  385.75E0, 127.958E0,   83.89E0, 130.196E0,   31.49E0, 230.286E0,
     4   23.69E0, 330.376E0,   19.80E0, 430.465E0,   17.36E0, 530.555E0,
     5   15.65E0, 630.645E0,   14.36E0, 730.734E0,   13.35E0, 830.824E0,
     6   12.52E0, 930.914E0,   11.83E0,1031.003E0,   11.25E0,1131.093E0,
     7   11.22E0,1139.325E0,   10.47E0,1213.338E0,    9.53E0,1288.228E0,
     8    8.80E0,1364.831E0,    8.20E0,1443.519E0,    7.71E0,1524.467E0,
     9    7.30E0,1607.747E0,    6.90E0,1704.209E0,    6.56E0,1803.492E0/

      DATA T03 /                                                     10.0E0,
     1 2391.40E0,   8.057E0, 2236.70E0,  78.004E0, 2047.90E0, 107.967E0,
     2 1724.77E0, 127.970E0, 1505.41E0, 137.983E0, 1192.82E0, 148.006E0,
     3  659.12E0, 158.038E0,  151.52E0, 161.261E0,   60.84E0, 259.470E0,
     4   46.07E0, 357.678E0,   38.62E0, 455.887E0,   33.92E0, 554.096E0,
     5   30.60E0, 652.305E0,   28.10E0, 750.513E0,   26.13E0, 848.722E0,
     6   24.53E0, 946.931E0,   23.18E0,1045.140E0,   22.04E0,1143.348E0,
     7   22.01E0,1146.574E0,   20.69E0,1221.805E0,   18.86E0,1297.280E0,
     8   17.44E0,1374.284E0,   16.28E0,1453.321E0,   15.32E0,1534.604E0,
     9   14.50E0,1618.208E0,   13.80E0,1704.121E0,   13.12E0,1803.425E0/

      DATA T04 /                                                     14.7E0,
     1 2904.72E0,   8.071E0, 2774.33E0,  78.016E0, 2495.47E0, 117.977E0,
     2 2216.69E0, 137.995E0, 1750.08E0, 158.049E0, 1384.01E0, 168.094E0,
     3  789.99E0, 178.152E0,  209.49E0, 180.179E0,   87.60E0, 277.210E0,
     4   66.61E0, 374.240E0,   55.94E0, 471.270E0,   49.19E0, 568.300E0,
     5   44.41E0, 665.331E0,   40.80E0, 762.361E0,   37.95E0, 859.391E0,
```

```
6   35.63E0, 956.421E0,   33.68E0,1053.452E0,   32.03E0,1150.482E0,
7   31.98E0,1154.345E0,   30.06E0,1230.480E0,   27.45E0,1306.438E0,
8   25.40E0,1383.809E0,   23.74E0,1463.184E0,   22.36E0,1544.795E0,
9   21.18E0,1628.719E0,   20.17E0,1714.939E0,   19.28E0,1803.363E0/

 DATA T05 /                                                    50.0E0,
1 5371.63E0,   8.175E0, 5190.51E0, 108.067E0, 4775.18E0, 158.130E0,
2 4009.67E0, 198.393E0, 3318.03E0, 218.632E0, 2105.91E0, 238.966E0,
3  703.71E0, 249.174E0,  571.57E0, 250.212E0,  389.44E0, 277.928E0,
4  267.62E0, 351.839E0,  192.22E0, 490.421E0,  159.83E0, 619.764E0,
5  144.72E0, 712.153E0,  133.23E0, 804.541E0,  124.11E0, 896.929E0,
6  116.64E0, 989.317E0,  110.38E0,1081.705E0,  105.03E0,1174.093E0,
7  104.66E0,1184.119E0,   99.07E0,1254.716E0,   91.70E0,1323.151E0,
8   85.78E0,1391.904E0,   80.85E0,1461.887E0,   76.11E0,1543.804E0,
9   72.09E0,1627.948E0,   68.62E0,1714.337E0,   65.60E0,1802.894E0/

 DATA T06 /                                                   100.0E0,
1 7600.63E0,   8.324E0, 7337.38E0, 128.187E0, 6764.11E0, 188.413E0,
2 5606.26E0, 239.065E0, 4208.59E0, 269.774E0, 3474.36E0, 280.078E0,
3 2333.70E0, 290.420E0,  989.42E0, 298.538E0,  721.04E0, 325.197E0,
4  564.01E0, 369.629E0,  412.34E0, 476.264E0,  329.23E0, 609.558E0,
5  282.31E0, 742.852E0,  260.32E0, 831.715E0,  242.80E0, 920.578E0,
6  228.41E0,1009.440E0,  216.31E0,1098.303E0,  205.95E0,1187.166E0,
7  205.33E0,1194.192E0,  194.62E0,1269.141E0,  180.35E0,1339.551E0,
8  168.93E0,1409.519E0,  159.42E0,1480.449E0,  151.30E0,1552.838E0,
9  144.28E0,1626.855E0,  137.31E0,1713.484E0,  131.25E0,1802.229E0/

 DATA T07 /                                                   200.0E0,
110751.06E0,   8.620E0,10327.76E0, 158.476E0, 9241.84E0, 239.264E0,
2 8058.31E0, 280.257E0, 5812.39E0, 321.858E0, 3688.74E0, 342.949E0,
3 1759.85E0, 353.581E0, 1685.31E0, 355.506E0, 1515.39E0, 363.934E0,
4 1139.95E0, 406.075E0,  940.63E0, 456.645E0,  778.11E0, 532.500E0,
5  631.88E0, 658.924E0,  528.84E0, 819.061E0,  475.74E0, 945.485E0,
6  448.14E0,1029.768E0,  424.86E0,1114.051E0,  404.87E0,1198.334E0,
7  402.87E0,1210.131E0,  384.10E0,1280.034E0,  355.73E0,1353.710E0,
8  333.37E0,1425.503E0,  314.79E0,1497.762E0,  298.97E0,1571.261E0,
9  285.28E0,1646.255E0,  273.29E0,1722.810E0,  262.69E0,1800.900E0/

 DATA T08 /                                                   400.0E0,
115203.90E0,   9.212E0,14540.28E0, 189.071E0,13309.29E0, 270.329E0,
211259.93E0, 332.672E0, 8740.94E0, 375.266E0, 5255.00E0, 407.962E0,
3 3105.55E0, 419.039E0, 2818.39E0, 424.168E0, 2475.99E0, 439.776E0,
4 2091.97E0, 470.993E0, 1858.15E0, 502.210E0, 1539.99E0, 572.448E0,
5 1347.66E0, 642.686E0, 1155.65E0, 751.945E0, 1013.44E0, 876.813E0,
6  935.86E0, 970.464E0,  860.17E0,1087.527E0,  800.37E0,1204.591E0,
7  795.86E0,1216.493E0,  775.13E0,1271.230E0,  720.21E0,1341.438E0,
8  672.03E0,1417.029E0,  633.05E0,1491.300E0,  600.27E0,1566.139E0,
9  572.15E0,1642.145E0,  547.66E0,1719.505E0,  526.11E0,1798.245E0/

 DATA T09 /                                                   600.0E0,
118618.66E0,   9.803E0,18103.35E0, 169.421E0,16833.40E0, 270.700E0,
214751.27E0, 343.512E0,11204.24E0, 408.123E0, 7987.71E0, 441.582E0,
```

```
     3 4173.67E0, 464.480E0, 3768.85E0, 471.697E0, 3048.55E0, 508.295E0,
     4 2660.54E0, 544.893E0, 2206.12E0, 618.089E0, 1847.98E0, 720.564E0,
     5 1598.54E0, 837.677E0, 1486.45E0, 910.873E0, 1395.25E0, 984.069E0,
     6 1319.13E0,1057.265E0, 1254.32E0,1130.461E0, 1198.26E0,1203.657E0,
     7 1190.77E0,1215.928E0, 1173.16E0,1262.896E0, 1082.18E0,1340.030E0,
     8 1016.37E0,1408.262E0,  954.91E0,1484.762E0,  903.95E0,1560.997E0,
     9  860.60E0,1638.031E0,  823.13E0,1716.199E0,  790.29E0,1795.591E0/

      DATA T10 /                                                    800.0E0,
    121495.90E0,  10.393E0,20695.34E0, 200.012E0,19081.41E0, 301.983E0,
    216623.91E0, 375.727E0,13495.09E0, 430.431E0, 9141.10E0, 476.098E0,
     3 5199.07E0, 499.841E0, 4606.04E0, 509.811E0, 4101.00E0, 530.499E0,
     4 3572.38E0, 564.977E0, 3163.63E0, 606.352E0, 2724.61E0, 675.310E0,
     5 2320.01E0, 778.746E0, 1974.80E0, 923.557E0, 1857.32E0, 992.514E0,
     6 1758.77E0,1061.472E0, 1674.52E0,1130.429E0, 1601.39E0,1199.387E0,
     7 1599.58E0,1201.250E0, 1575.19E0,1255.513E0, 1444.57E0,1339.288E0,
     8 1353.25E0,1410.638E0, 1280.53E0,1478.126E0, 1210.09E0,1555.829E0,
     9 1150.71E0,1633.910E0, 1099.71E0,1712.893E0, 1055.23E0,1792.940E0/

      DATA T11 /                                                   1000.0E0,
    124029.48E0,  10.981E0,23096.00E0, 210.517E0,20845.04E0, 333.571E0,
    217336.14E0, 419.454E0,13305.23E0, 476.061E0, 9253.32E0, 511.794E0,
     3 5593.07E0, 536.693E0, 5360.70E0, 542.551E0, 4399.43E0, 588.078E0,
     4 3734.83E0, 646.612E0, 3169.41E0, 731.162E0, 2854.64E0, 802.705E0,
     5 2638.81E0, 867.743E0, 2466.26E0, 932.782E0, 2324.07E0, 997.821E0,
     6 2204.17E0,1062.859E0, 2101.26E0,1127.898E0, 2011.64E0,1192.936E0,
     7 1992.55E0,1210.394E0, 1947.82E0,1266.456E0, 1784.28E0,1352.309E0,
     8 1671.66E0,1425.265E0, 1582.13E0,1494.115E0, 1507.04E0,1561.913E0,
     9 1442.48E0,1629.779E0, 1377.37E0,1709.586E0, 1320.92E0,1790.290E0/

      DATA T12 /                                                   1200.0E0,
    126318.85E0,  11.569E0,25241.12E0, 221.027E0,23173.53E0, 333.875E0,
    220471.70E0, 408.632E0,16445.88E0, 476.035E0,11934.79E0, 523.846E0,
     3 6472.79E0, 562.204E0, 6049.68E0, 571.853E0, 5568.88E0, 590.242E0,
     4 5097.52E0, 614.760E0, 4519.85E0, 657.667E0, 4112.88E0, 700.575E0,
     5 3622.62E0, 774.130E0, 3230.02E0, 859.944E0, 2926.91E0, 951.888E0,
     6 2724.25E0,1031.573E0, 2536.18E0,1123.517E0, 2430.66E0,1184.813E0,
     7 2407.37E0,1201.318E0, 2347.06E0,1263.089E0, 2139.70E0,1353.651E0,
     8 2001.03E0,1428.978E0, 1892.11E0,1499.365E0, 1801.41E0,1568.314E0,
     9 1723.77E0,1637.122E0, 1656.18E0,1706.277E0, 1587.34E0,1787.642E0/

      DATA T13 /                                                   1400.0E0,
    128423.09E0,  12.156E0,27421.06E0, 211.368E0,25287.74E0, 334.181E0,
    222242.52E0, 419.757E0,17361.80E0, 499.447E0,12557.47E0, 548.676E0,
     3 7095.83E0, 588.776E0, 6683.12E0, 598.830E0, 5658.27E0, 644.948E0,
     4 4962.20E0, 696.831E0, 4439.64E0, 754.478E0, 3963.13E0, 829.421E0,
     5 3688.03E0, 887.068E0, 3464.35E0, 944.716E0, 3277.60E0,1002.364E0,
     6 3118.52E0,1060.011E0, 2980.82E0,1117.659E0, 2860.05E0,1175.307E0,
     7 2827.79E0,1194.086E0, 2787.21E0,1241.299E0, 2526.46E0,1341.691E0,
     8 2352.10E0,1420.820E0, 2218.97E0,1493.200E0, 2109.54E0,1563.395E0,
     9 2016.60E0,1633.103E0, 1936.14E0,1702.966E0, 1854.56E0,1784.994E0/
```

```
 DATA T14 /                                                      1600.0E0,
130380.68E0,  12.741E0,29111.17E0, 231.954E0,26342.19E0, 366.053E0,
222067.79E0, 464.563E0,15699.63E0, 548.276E0, 8599.02E0, 602.066E0,
3 7531.45E0, 616.772E0, 7267.39E0, 624.202E0, 6283.48E0, 667.428E0,
4 5642.15E0, 710.654E0, 4937.82E0, 780.897E0, 4517.75E0, 840.333E0,
5 4218.70E0, 894.366E0, 3973.36E0, 948.399E0, 3767.13E0,1002.431E0,
6 3590.46E0,1056.464E0, 3436.84E0,1110.497E0, 3301.60E0,1164.530E0,
7 3252.42E0,1189.014E0, 3203.28E0,1239.587E0, 2882.68E0,1344.071E0,
8 2679.74E0,1425.221E0, 2526.18E0,1498.984E0, 2400.68E0,1570.241E0,
9 2294.50E0,1640.826E0, 2202.85E0,1711.435E0, 2122.55E0,1782.348E0/

 DATA T15 /                                                      1800.0E0,
132218.38E0,  13.326E0,30781.42E0, 242.471E0,27490.19E0, 387.615E0,
222773.30E0, 487.560E0,15821.59E0, 573.754E0, 8589.41E0, 630.734E0,
3 7857.19E0, 646.795E0, 7806.53E0, 648.490E0, 6876.29E0, 688.797E0,
4 6044.93E0, 744.220E0, 5470.07E0, 799.642E0, 5073.59E0, 850.027E0,
5 4754.88E0, 900.411E0, 4490.93E0, 950.795E0, 4267.42E0,1001.179E0,
6 4074.81E0,1051.564E0, 3906.50E0,1101.948E0, 3757.71E0,1152.332E0,
7 3680.50E0,1186.215E0, 3618.59E0,1239.460E0, 3394.22E0,1298.836E0,
8 3109.78E0,1390.193E0, 2912.11E0,1468.170E0, 2756.26E0,1541.440E0,
9 2626.84E0,1613.133E0, 2499.56E0,1696.332E0, 2391.32E0,1779.701E0/

 DATA T16 /                                                      2000.0E0,
133955.66E0,  13.909E0,32613.64E0, 232.777E0,29236.62E0, 387.847E0,
224722.20E0, 487.530E0,18371.14E0, 573.194E0, 9715.11E0, 645.003E0,
3 8655.25E0, 661.733E0, 8302.92E0, 672.111E0, 7264.52E0, 718.734E0,
4 6562.68E0, 765.356E0, 6041.26E0, 811.979E0, 5631.87E0, 858.601E0,
5 5298.39E0, 905.224E0, 5019.40E0, 951.846E0, 4781.25E0, 998.469E0,
6 4574.70E0,1045.091E0, 4393.22E0,1091.713E0, 4232.05E0,1138.336E0,
7 4201.10E0,1148.283E0, 4112.19E0,1185.706E0, 4021.18E0,1240.893E0,
8 3584.17E0,1351.059E0, 3324.89E0,1435.455E0, 3102.61E0,1523.952E0,
9 2927.42E0,1608.933E0, 2783.04E0,1693.009E0, 2660.89E0,1777.056E0/

 DATA T17 /                                                      2200.0E0,
135607.23E0,  14.492E0,34096.21E0, 243.279E0,30883.91E0, 388.082E0,
226527.79E0, 487.510E0,19443.82E0, 585.859E0,10853.33E0, 659.615E0,
3 9433.73E0, 677.129E0, 8756.94E0, 695.462E0, 7803.37E0, 738.132E0,
4 7126.33E0, 780.802E0, 6608.61E0, 823.471E0, 6194.12E0, 866.141E0,
5 5851.60E0, 908.811E0, 5561.87E0, 951.481E0, 5312.35E0, 994.150E0,
6 5094.36E0,1036.820E0, 4901.66E0,1079.490E0, 4729.64E0,1122.159E0,
7 4637.43E0,1149.415E0, 4548.59E0,1187.522E0, 4510.73E0,1218.025E0,
8 3988.37E0,1339.694E0, 3683.13E0,1427.787E0, 3428.14E0,1518.459E0,
9 3229.88E0,1604.716E0, 3067.72E0,1689.682E0, 2931.24E0,1774.411E0/

 DATA T18 /                                                      2400.0E0,
137184.51E0,  15.073E0,35898.96E0, 223.542E0,32783.10E0, 377.694E0,
226889.76E0, 510.759E0,19090.97E0, 612.528E0,10166.01E0, 693.052E0,
3 9303.38E0, 714.054E0, 9076.25E0, 718.953E0, 8262.73E0, 757.431E0,
4 7645.11E0, 795.909E0, 7153.80E0, 834.387E0, 6749.86E0, 872.866E0,
5 6409.55E0, 911.344E0, 6117.39E0, 949.822E0, 5862.79E0, 988.300E0,
6 5638.20E0,1026.779E0, 5438.06E0,1065.257E0, 5258.18E0,1103.735E0,
7 5075.29E0,1153.449E0, 4935.95E0,1222.206E0, 4672.68E0,1270.727E0,
```

```
     8 4333.15E0,1344.672E0, 3999.72E0,1433.843E0, 3756.82E0,1512.909E0,
     9 3534.24E0,1600.480E0, 3353.62E0,1686.350E0, 3202.40E0,1771.765E0/

      DATA T19 /                                                    2600.0E0,
    138696.59E0,  15.653E0,36813.83E0, 264.310E0,33210.24E0, 409.968E0,
    227825.36E0, 522.481E0,19896.25E0, 625.813E0,10829.86E0, 709.590E0,
    3 9699.24E0, 733.410E0, 9407.96E0, 744.475E0, 8710.29E0, 778.232E0,
    4 8155.16E0, 811.988E0, 7698.71E0, 845.745E0, 7314.08E0, 879.502E0,
    5 6983.79E0, 913.259E0, 6695.85E0, 947.016E0, 6441.74E0, 980.772E0,
    6 6215.19E0,1014.529E0, 6011.47E0,1048.286E0, 5826.93E0,1082.043E0,
    7 5703.57E0,1107.711E0, 5518.77E0,1160.241E0, 5446.62E0,1197.675E0,
    8 5320.20E0,1227.844E0, 4834.08E0,1315.521E0, 4474.94E0,1397.239E0,
    9 4129.57E0,1494.237E0, 3750.08E0,1633.563E0, 3474.36E0,1769.120E0/

      DATA T20 /                                                    2800.0E0,
    140150.85E0,  16.232E0,38230.31E0, 264.699E0,34648.04E0, 410.174E0,
    228674.42E0, 534.279E0,20589.80E0, 639.301E0,11213.02E0, 727.621E0,
    310138.64E0, 753.572E0, 9699.30E0, 770.686E0, 9126.99E0, 799.200E0,
    4 8649.96E0, 827.715E0, 8243.83E0, 856.230E0, 7892.20E0, 884.745E0,
    5 7583.59E0, 913.260E0, 7309.70E0, 941.774E0, 7064.33E0, 970.289E0,
    6 6842.75E0, 998.804E0, 6641.28E0,1027.319E0, 6457.00E0,1055.834E0,
    7 6124.36E0,1121.221E0, 5885.61E0,1205.299E0, 5392.81E0,1282.213E0,
    8 4929.99E0,1372.797E0, 4567.09E0,1461.125E0, 4297.59E0,1540.859E0,
    9 4081.41E0,1617.173E0, 3901.13E0,1692.106E0, 3747.13E0,1766.475E0/

      DATA T21 /                                                    3000.0E0,
    41553.34E0,  16.811E0,39752.96E0, 254.984E0,36393.30E0, 399.685E0,
    230895.16E0, 522.232E0,22518.30E0, 638.147E0,11703.88E0, 745.797E0,
    310519.37E0, 775.147E0, 9873.87E0, 801.845E0, 9458.94E0, 823.687E0,
    4 9094.64E0, 845.529E0, 8771.22E0, 867.371E0, 8481.36E0, 889.213E0,
    5 8219.52E0, 911.055E0, 7981.34E0, 932.898E0, 7763.38E0, 954.740E0,
    6 7562.87E0, 976.582E0, 7377.56E0, 998.424E0, 7205.58E0,1020.266E0,
    7 6928.15E0,1060.464E0, 6563.23E0,1135.614E0, 6448.04E0,1179.815E0,
    8 5515.02E0,1328.310E0, 5042.64E0,1425.647E0, 4714.22E0,1509.351E0,
    9 4459.17E0,1587.660E0, 4218.81E0,1676.323E0, 4020.72E0,1763.830E0/
```

## C.4 MURDOCK-BAUMAN CRITICAL FLOW TABLE FOR SUPERHEATED VAPOR

```
GXX(1)     = STAGNATION PRESSURE (PSIA)
GXX(EVEN)  = CRITICAL FLOW RATE (LB/FT**2-SEC)
GXX(ODD)   = STAGNATION ENTHALPY (BTU/LB)

NHB = NUMBER OF PAIRS OF ENTHALPY AND FLOW VALUES PER PRESSURE
NPB = NUMBER OF PRESSURE VALUES

DATA  NHB,NPB  /7,21/


 DATA G01 /      1.0E0,    2.38E0,1105.809E0,    2.35E0,1141.101E0,
1    1.97E0,1262.297E0,    1.72E0,1388.407E0,    1.55E0,1520.487E0,
2    1.42E0,1658.914E0,    1.31E0,1803.546E0/
 DATA G02 /      5.0E0,   11.39E0,1131.093E0,   11.24E0,1166.678E0,
1    9.79E0,1265.265E0,    8.59E0,1390.877E0,    7.73E0,1522.229E0,
2    7.08E0,1659.809E0,    6.55E0,1803.492E0/
 DATA G03 /     10.0E0,   22.35E0,1143.348E0,   22.03E0,1179.286E0,
1   19.50E0,1269.014E0,   17.14E0,1393.975E0,   15.44E0,1524.411E0,
2   14.15E0,1660.929E0,   13.11E0,1803.426E0/
 DATA G04 /     14.7E0,   32.49E0,1150.482E0,   31.99E0,1186.845E0,
1   28.54E0,1272.574E0,   25.13E0,1396.898E0,   22.67E0,1526.466E0,
2   20.78E0,1661.983E0,   19.27E0,1803.363E0/
 DATA G05 /     50.0E0,  106.74E0,1174.093E0,  104.68E0,1213.137E0,
1   94.06E0,1300.260E0,   83.80E0,1419.135E0,   76.25E0,1542.013E0,
2   70.36E0,1669.933E0,   65.55E0,1802.894E0/
 DATA G06 /    100.0E0,  209.60E0,1187.166E0,  204.53E0,1230.033E0,
1  180.06E0,1341.546E0,  163.13E0,1451.412E0,  150.18E0,1564.360E0,
2  139.82E0,1681.289E0,  131.15E0,1802.229E0/
 DATA G07 /    200.0E0,  412.87E0,1198.334E0,  401.31E0,1244.107E0,
1  357.56E0,1349.071E0,  324.65E0,1458.026E0,  299.54E0,1568.876E0,
2  279.41E0,1683.108E0,  262.51E0,1800.901E0/
 DATA G08 /    400.0E0,  818.64E0,1204.591E0,  790.41E0,1256.322E0,
1  703.94E0,1366.109E0,  642.58E0,1472.057E0,  595.71E0,1578.268E0,
2  557.86E0,1686.873E0,  525.85E0,1798.245E0/
 DATA G09 /    600.0E0, 1228.83E0,1203.657E0, 1178.21E0,1261.308E0,
1 1045.74E0,1376.982E0,  957.72E0,1480.958E0,  890.56E0,1584.001E0,
2  836.07E0,1688.703E0,  789.92E0,1795.592E0/
 DATA G10 /    800.0E0, 1646.48E0,1199.387E0, 1567.52E0,1262.925E0,
1 1390.36E0,1380.495E0, 1274.14E0,1484.244E0, 1186.07E0,1585.860E0,
2 1114.88E0,1688.525E0, 1054.63E0,1792.941E0/
 DATA G11 /   1000.0E0, 2073.79E0,1192.936E0, 1960.40E0,1262.293E0,
1 1731.88E0,1384.776E0, 1588.70E0,1487.875E0, 1480.61E0,1587.889E0,
2 1393.68E0,1688.413E0, 1320.03E0,1790.291E0/
 DATA G12 /   1200.0E0, 2512.78E0,1184.813E0, 2357.14E0,1260.858E0,
1 2082.05E0,1383.259E0, 1907.73E0,1487.326E0, 1778.05E0,1587.107E0,
2 1674.23E0,1686.865E0, 1586.33E0,1787.642E0/
 DATA G13 /   1400.0E0, 2965.42E0,1175.307E0, 2760.30E0,1257.989E0,
1 2432.47E0,1382.074E0, 2226.80E0,1489.933E0, 2075.80E0,1586.409E0,
2 1955.33E0,1685.352E0, 1853.38E0,1784.995E0/
```

```
 DATA G14 /   1600.0E0, 3433.97E0,1164.530E0, 3170.87E0,1253.837E0,
1 2782.86E0,1381.242E0, 2545.77E0,1486.701E0, 2375.82E0,1585.793E0,
2 2236.96E0,1683.872E0, 2121.17E0,1782.348E0/
 DATA G15 /   1800.0E0, 3921.87E0,1152.332E0, 3591.34E0,1248.253E0,
1 3132.78E0,1380.778E0, 2864.44E0,1486.632E0, 2672.07E0,1585.260E0,
2 2519.08E0,1682.426E0, 2389.71E0,1779.702E0/
 DATA G16 /   2000.0E0, 4434.55E0,1138.336E0, 4025.84E0,1240.864E0,
1 3481.81E0,1380.692E0, 3182.73E0,1486.729E0, 2970.49E0,1584.810E0,
2 2801.69E0,1681.012E0, 2658.99E0,1777.056E0/
 DATA G17 /   2200.0E0, 4979.37E0,1122.159E0, 4471.88E0,1233.895E0,
1 3840.73E0,1378.038E0, 3505.97E0,1485.080E0, 3271.12E0,1583.219E0,
2 3085.68E0,1679.026E0, 2930.18E0,1774.411E0/
 DATA G18 /   2400.0E0, 5565.81E0,1103.735E0, 4921.76E0,1227.612E0,
1 4200.33E0,1375.616E0, 3829.65E0,1483.534E0, 3572.20E0,1581.681E0,
2 3370.29E0,1677.062E0, 3202.31E0,1771.766E0/
 DATA G19 /   2600.0E0, 6208.34E0,1082.043E0, 5373.43E0,1222.124E0,
1 4560.22E0,1373.439E0, 4153.64E0,1482.096E0, 3873.69E0,1580.196E0,
2 3655.51E0,1675.119E0, 3475.38E0,1769.121E0/
 DATA G20 /   2800.0E0, 6935.60E0,1055.834E0, 5824.61E0,1217.519E0,
1 4919.99E0,1371.516E0, 4477.81E0,1480.770E0, 4175.53E0,1578.765E0,
2 3941.31E0,1673.198E0, 3749.39E0,1766.476E0/
 DATA G21 /   3000.0E0, 7830.38E0,1020.266E0, 6273.03E0,1213.858E0,
1 5279.13E0,1369.856E0, 4802.02E0,1479.560E0, 4477.62E0,1577.390E0,
2 4227.69E0,1671.299E0, 4024.33E0,1763.831E0/
```

```
 DATA PM(25,17),PM(26,17),PM(27,17),PM(28,17),PM(29,17),PM(30,17),
1     PM(31,17),PM(32,17),PM(33,17),PM(34,17),PM(35,17),PM(36,17),
2     PM(37,17),PM(38,17),PM(39,17),PM(40,17),PM(41,17),PM(42,17),
3     PM(43,17),PM(44,17),PM(45,17),PM(46,17),PM(47,17),PM(48,17)/
4 0.68143584E 03, 0.11157809E 05, 0.68609809E 03, 0.10765562E 05,
5 0.69076033E 03, 0.10467344E 05, 0.69542258E 03, 0.10284563E 05,
6 0.70008482E 03, 0.10275959E 05, 0.70474707E 03, 0.10180133E 05,
7 0.70940931E 03, 0.10112706E 05, 0.71407156E 03, 0.10047270E 05,
8 0.71873380E 03, 0.89878104E 04, 0.76535625E 03, 0.78172752E 04,
9 0.81197870E 03, 0.69030697E 04, 0.85860115E 03, 0.62502254E 04/

 DATA PM(49,17),PM(50,17),PM(51,17),PM(52,17),PM(53,17),PM(54,17),
1     PM(55,17),PM(56,17),PM(57,17),PM(58,17),PM(59,17)/
2 0.90522360E 03, 0.57611957E 04, 0.95184605E 03, 0.53897722E 04,
3 0.99846850E 03, 0.50810573E 04, 0.10450909E 04, 0.48154370E 04,
4 0.10917134E 04, 0.45892802E 04, 0.11378696E 04/

 DATA PM( 1,18),PM( 2,18),PM( 3,18),PM( 4,18),PM( 5,18),PM( 6,18),
1     PM( 7,18),PM( 8,18),PM( 9,18),PM(10,18),PM(11,18),PM(12,18),
2     PM(13,18),PM(14,18),PM(15,18),PM(16,18),PM(17,18),PM(18,18),
3     PM(19,18),PM(20,18),PM(21,18),PM(22,18),PM(23,18),PM(24,18)/
4 0.22000000E 04, 0.12813458E 05, 0.69546232E 03, 0.12797706E 05,
5 0.69588902E 03, 0.12737513E 05, 0.69631572E 03, 0.12703856E 05,
6 0.69674241E 03, 0.12670456E 05, 0.69716911E 03, 0.12612354E 05,
7 0.69759581E 03, 0.12579734E 05, 0.69802250E 03, 0.12547358E 05,
8 0.69844920E 03, 0.12515223E 05, 0.69887590E 03, 0.12459599E 05,
9 0.69930260E 03, 0.12428195E 05, 0.69972929E 03, 0.12063798E 05/

 DATA PM(25,18),PM(26,18),PM(27,18),PM(28,18),PM(29,18),PM(30,18),
1     PM(31,18),PM(32,18),PM(33,18),PM(34,18),PM(35,18),PM(36,18),
2     PM(37,18),PM(38,18),PM(39,18),PM(40,18),PM(41,18),PM(42,18),
3     PM(43,18),PM(44,18),PM(45,18),PM(46,18),PM(47,18),PM(48,18)/
4 0.70399626E 03, 0.11751453E 05, 0.70826323E 03, 0.11464110E 05,
5 0.71253020E 03, 0.11375772E 05, 0.71679717E 03, 0.11364155E 05,
6 0.72106414E 03, 0.11429088E 05, 0.72533111E 03, 0.11397517E 05,
7 0.72959808E 03, 0.11351836E 05, 0.73386505E 03, 0.11291398E 05,
8 0.73813202E 03, 0.10144490E 05, 0.78080172E 03, 0.84951054E 04,
9 0.82347142E 03, 0.74811964E 04, 0.86614112E 03, 0.68680311E 04/

 DATA PM(49,18),PM(50,18),PM(51,18),PM(52,18),PM(53,18),PM(54,18),
1     PM(55,18),PM(56,18),PM(57,18),PM(58,18),PM(59,18)/
2 0.90881083E 03, 0.64129876E 04, 0.95148053E 03, 0.60360975E 04,
3 0.99415023E 03, 0.57181600E 04, 0.10368199E 04, 0.54250196E 04,
4 0.10794896E 04, 0.51763832E 04, 0.11217326E 04/
```

## C.3 HOMOGENEOUS EQUILIBRIUM MODEL CRITICAL FLOW TABLES

```
TXX(1)      = STAGNATION PRESSURE  (PSIA)
TXX(EVEN).  = CRITICAL FLOW RATE   (LBM/SEC-FT2)
TXX(ODD)    = STAGNATION ENTHALPY  (BTU/LBM)

NGHT = NUMBER OF PAIRS OF FLOW RATE AND ENTHALPY VALUES PER
       PRESSURE
NPT  = NUMBER OF PRESSURE VALUES

DATA NGHT, NPT / 27,21 /

 DATA T01 /                                                      1.0E0,
1  716.13E0,   8.030E0,  711.91E0,  18.057E0,  658.45E0,  28.062E0,
2  681.49E0,  38.054E0,  535.31E0,  48.038E0,  447.12E0,  58.019E0,
3  442.29E0,  67.999E0,   20.41E0,  69.733E0,    6.75E0, 173.340E0,
4    5.02E0, 276.948E0,    4.17E0, 380.555E0,    3.65E0, 484.163E0,
5    3.29E0, 587.771E0,    3.01E0, 691.378E0,    2.80E0, 794.986E0,
6    2.62E0, 898.594E0,    2.48E0,1002.201E0,    2.35E0,1105.809E0,
7    2.35E0,1114.029E0,    2.18E0,1186.541E0,    1.97E0,1260.427E0,
8    1.81E0,1336.135E0,    1.67E0,1423.810E0,    1.55E0,1514.346E0,
9    1.46E0,1607.840E0,    1.38E0,1704.280E0,    1.31E0,1803.545E0/

 DATA T02 /                                                      5.0E0,
1 1681.25E0,   8.042E0, 1665.45E0,  38.065E0, 1579.07E0,  68.010E0,
2 1378.69E0,  87.975E0, 1162.01E0, 107.955E0,  852.83E0, 117.953E0,
3  385.75E0, 127.958E0,   83.89E0, 130.196E0,   31.49E0, 230.286E0,
4   23.69E0, 330.376E0,   19.80E0, 430.465E0,   17.36E0, 530.555E0,
5   15.65E0, 630.645E0,   14.36E0, 730.734E0,   13.35E0, 830.824E0,
6   12.52E0, 930.914E0,   11.83E0,1031.003E0,   11.25E0,1131.093E0,
7   11.22E0,1139.325E0,   10.47E0,1213.338E0,    9.53E0,1288.228E0,
8    8.80E0,1364.831E0,    8.20E0,1443.519E0,    7.71E0,1524.467E0,
9    7.30E0,1607.747E0,    6.90E0,1704.209E0,    6.56E0,1803.492E0/

 DATA T03 /                                                     10.0E0,
1 2391.40E0,   8.057E0, 2236.70E0,  78.004E0, 2047.90E0, 107.967E0,
2 1724.77E0, 127.970E0, 1505.41E0, 137.983E0, 1192.82E0, 148.006E0,
3  659.12E0, 158.038E0,  151.52E0, 161.261E0,   60.84E0, 259.470E0,
4   46.07E0, 357.678E0,   38.62E0, 455.887E0,   33.92E0, 554.096E0,
5   30.60E0, 652.305E0,   28.10E0, 750.513E0,   26.13E0, 848.722E0,
6   24.53E0, 946.931E0,   23.18E0,1045.140E0,   22.04E0,1143.348E0,
7   22.01E0,1146.574E0,   20.69E0,1221.805E0,   18.86E0,1297.280E0,
8   17.44E0,1374.284E0,   16.28E0,1453.321E0,   15.32E0,1534.604E0,
9   14.50E0,1618.208E0,   13.80E0,1704.121E0,   13.12E0,1803.425E0/

 DATA T04 /                                                     14.7E0,
1 2904.72E0,   8.071E0, 2774.33E0,  78.016E0, 2495.47E0, 117.977E0,
2 2216.69E0, 137.995E0, 1750.08E0, 158.049E0, 1384.01E0, 168.094E0,
3  789.99E0, 178.152E0,  209.49E0, 180.179E0,   87.60E0, 277.210E0,
4   66.61E0, 374.240E0,   55.94E0, 471.270E0,   49.19E0, 568.300E0,
5   44.41E0, 665.331E0,   40.80E0, 762.361E0,   37.95E0, 859.391E0,
```

```
6   35.63E0, 956.421E0,   33.68E0,1053.452E0,   32.03E0,1150.482E0,
7   31.98E0,1154.345E0,   30.06E0,1230.480E0,   27.45E0,1306.438E0,
8   25.40E0,1383.809E0,   23.74E0,1463.184E0,   22.36E0,1544.795E0,
9   21.18E0,1628.719E0,   20.17E0,1714.939E0,   19.28E0,1803.363E0/

 DATA T05 /                                                    50.0E0,
1 5371.63E0,   8.175E0, 5190.51E0, 108.067E0, 4775.18E0, 158.130E0,
2 4009.67E0, 198.393E0, 3318.03E0, 218.632E0, 2105.91E0, 238.966E0,
3  703.71E0, 249.174E0,  571.57E0, 250.212E0,  389.44E0, 277.928E0,
4  267.62E0, 351.839E0,  192.22E0, 490.421E0,  159.83E0, 619.764E0,
5  144.72E0, 712.153E0,  133.23E0, 804.541E0,  124.11E0, 896.929E0,
6  116.64E0, 989.317E0,  110.38E0,1081.705E0,  105.03E0,1174.093E0,
7  104.66E0,1184.119E0,   99.07E0,1254.716E0,   91.70E0,1323.151E0,
8   85.78E0,1391.904E0,   80.85E0,1461.887E0,   76.11E0,1543.804E0,
9   72.09E0,1627.948E0,   68.62E0,1714.337E0,   65.60E0,1802.894E0/

 DATA T06 /                                                   100.0E0,
1 7600.63E0,   8.324E0, 7337.38E0, 128.187E0, 6764.11E0, 188.413E0,
2 5606.26E0, 239.065E0, 4208.59E0, 269.774E0, 3474.36E0, 280.078E0,
3 2333.70E0, 290.420E0,  989.42E0, 298.538E0,  721.04E0, 325.197E0,
4  564.01E0, 369.629E0,  412.34E0, 476.264E0,  329.23E0, 609.558E0,
5  282.31E0, 742.852E0,  260.32E0, 831.715E0,  242.80E0, 920.578E0,
6  228.41E0,1009.440E0,  216.31E0,1098.303E0,  205.95E0,1187.166E0,
7  205.33E0,1194.192E0,  194.62E0,1269.141E0,  180.35E0,1339.551E0,
8  168.93E0,1409.519E0,  159.42E0,1480.449E0,  151.30E0,1552.838E0,
9  144.28E0,1626.855E0,  137.31E0,1713.484E0,  131.25E0,1802.229E0/

 DATA T07 /                                                   200.0E0,
110751.06E0,   8.620E0,10327.76E0, 158.476E0, 9241.84E0, 239.264E0,
2 8058.31E0, 280.257E0, 5812.39E0, 321.858E0, 3688.74E0, 342.949E0,
3 1759.85E0, 353.581E0, 1685.31E0, 355.506E0, 1515.39E0, 363.934E0,
4 1139.95E0, 406.075E0,  940.63E0, 456.645E0,  778.11E0, 532.500E0,
5  631.88E0, 658.924E0,  528.84E0, 819.061E0,  475.74E0, 945.485E0,
6  448.14E0,1029.768E0,  424.86E0,1114.051E0,  404.87E0,1198.334E0,
7  402.87E0,1210.131E0,  384.10E0,1280.034E0,  355.73E0,1353.710E0,
8  333.37E0,1425.503E0,  314.79E0,1497.762E0,  298.97E0,1571.261E0,
9  285.28E0,1646.255E0,  273.29E0,1722.810E0,  262.69E0,1800.900E0/

 DATA T08 /                                                   400.0E0,
115203.90E0,   9.212E0,14540.28E0, 189.071E0,13309.29E0, 270.329E0,
211259.93E0, 332.672E0, 8740.94E0, 375.266E0, 5255.00E0, 407.962E0,
3 3105.55E0, 419.039E0, 2818.39E0, 424.168E0, 2475.99E0, 439.776E0,
4 2091.97E0, 470.993E0, 1858.15E0, 502.210E0, 1539.99E0, 572.448E0,
5 1347.66E0, 642.686E0, 1155.65E0, 751.945E0, 1013.44E0, 876.813E0,
6  935.86E0, 970.464E0,  860.17E0,1087.527E0,  800.37E0,1204.591E0,
7  795.86E0,1216.493E0,  775.13E0,1271.230E0,  720.21E0,1341.438E0,
8  672.03E0,1417.029E0,  633.05E0,1491.300E0,  600.27E0,1566.139E0,
9  572.15E0,1642.145E0,  547.66E0,1719.505E0,  526.11E0,1798.245E0/

 DATA T09 /                                                   600.0E0,
118618.66E0,   9.803E0,18103.35E0, 169.421E0,16833.40E0, 270.700E0,
214751.27E0, 343.512E0,11204.24E0, 408.123E0, 7987.71E0, 441.582E0,
```

```
3 4173.67E0, 464.480E0, 3768.85E0, 471.697E0, 3048.55E0, 508.295E0,
4 2660.54E0, 544.893E0, 2206.12E0, 618.089E0, 1847.98E0, 720.564E0,
5 1598.54E0, 837.677E0, 1486.45E0, 910.873E0, 1395.25E0, 984.069E0,
6 1319.13E0,1057.265E0, 1254.32E0,1130.461E0, 1198.26E0,1203.657E0,
7 1190.77E0,1215.928E0, 1173.16E0,1262.896E0, 1082.18E0,1340.030E0,
8 1016.37E0,1408.262E0,  954.91E0,1484.762E0,  903.95E0,1560.997E0,
9  860.60E0,1638.031E0,  823.13E0,1716.199E0,  790.29E0,1795.591E0/

 DATA T10 /                                                    800.0E0,
121495.90E0,  10.393E0,20695.34E0, 200.012E0,19081.41E0, 301.983E0,
216623.91E0, 375.727E0,13495.09E0, 430.431E0, 9141.10E0, 476.098E0,
3 5199.07E0, 499.841E0, 4606.04E0, 509.811E0, 4101.00E0, 530.499E0,
4 3572.38E0, 564.977E0, 3163.63E0, 606.352E0, 2724.61E0, 675.310E0,
5 2320.01E0, 778.746E0, 1974.80E0, 923.557E0, 1857.32E0, 992.514E0,
6 1758.77E0,1061.472E0, 1674.52E0,1130.429E0, 1601.39E0,1199.387E0,
7 1599.58E0,1201.250E0, 1575.19E0,1255.513E0, 1444.57E0,1339.288E0,
8 1353.25E0,1410.638E0, 1280.53E0,1478.126E0, 1210.09E0,1555.829E0,
9 1150.71E0,1633.910E0, 1099.71E0,1712.893E0, 1055.23E0,1792.940E0/

 DATA T11 /                                                   1000.0E0,
124029.48E0,  10.981E0,23096.00E0, 210.517E0,20845.04E0, 333.571E0,
217336.14E0, 419.454E0,13305.23E0, 476.061E0, 9253.32E0, 511.794E0,
3 5593.07E0, 536.693E0, 5360.70E0, 542.551E0, 4399.43E0, 588.078E0,
4 3734.83E0, 646.612E0, 3169.41E0, 731.162E0, 2854.64E0, 802.705E0,
5 2638.81E0, 867.743E0, 2466.26E0, 932.782E0, 2324.07E0, 997.821E0,
6 2204.17E0,1062.859E0, 2101.26E0,1127.898E0, 2011.64E0,1192.936E0,
7 1992.55E0,1210.394E0, 1947.82E0,1266.456E0, 1784.28E0,1352.309E0,
8 1671.66E0,1425.265E0, 1582.13E0,1494.115E0, 1507.04E0,1561.913E0,
9 1442.48E0,1629.779E0, 1377.37E0,1709.586E0, 1320.92E0,1790.290E0/

 DATA T12 /                                                   1200.0E0,
126318.85E0,  11.569E0,25241.12E0, 221.027E0,23173.53E0, 333.875E0,
220471.70E0, 408.632E0,16445.88E0, 476.035E0,11934.79E0, 523.846E0,
3 6472.79E0, 562.204E0, 6049.68E0, 571.853E0, 5568.88E0, 590.242E0,
4 5097.52E0, 614.760E0, 4519.85E0, 657.667E0, 4112.88E0, 700.575E0,
5 3622.62E0, 774.130E0, 3230.02E0, 859.944E0, 2926.91E0, 951.888E0,
6 2724.25E0,1031.573E0, 2536.18E0,1123.517E0, 2430.66E0,1184.813E0,
7 2407.37E0,1201.318E0, 2347.06E0,1263.089E0, 2139.70E0,1353.651E0,
8 2001.03E0,1428.978E0, 1892.11E0,1499.365E0, 1801.41E0,1568.314E0,
9 1723.77E0,1637.122E0, 1656.18E0,1706.277E0, 1587.34E0,1787.642E0/

 DATA T13 /                                                   1400.0E0,
128423.09E0,  12.156E0,27421.06E0, 211.368E0,25287.74E0, 334.181E0,
222242.52E0, 419.757E0,17361.80E0, 499.447E0,12557.47E0, 548.676E0,
3 7095.83E0, 588.776E0, 6683.12E0, 598.830E0, 5658.27E0, 644.948E0,
4 4962.20E0, 696.831E0, 4439.64E0, 754.478E0, 3963.13E0, 829.421E0,
5 3688.03E0, 887.068E0, 3464.35E0, 944.716E0, 3277.60E0,1002.364E0,
6 3118.52E0,1060.011E0, 2980.82E0,1117.659E0, 2860.05E0,1175.307E0,
7 2827.79E0,1194.086E0, 2787.21E0,1241.299E0, 2526.46E0,1341.691E0,
8 2352.10E0,1420.820E0, 2218.97E0,1493.200E0, 2109.54E0,1563.395E0,
9 2016.60E0,1633.103E0, 1936.14E0,1702.966E0, 1854.56E0,1784.994E0/
```

```
 DATA T14 /                                                      1600.0E0,
130380.68E0,  12.741E0,29111.17E0, 231.954E0,26342.19E0, 366.053E0,
222067.79E0, 464.563E0,15699.63E0, 548.276E0, 8599.02E0, 602.066E0,
3 7531.45E0, 616.772E0, 7267.39E0, 624.202E0, 6283.48E0, 667.428E0,
4 5642.15E0, 710.654E0, 4937.82E0, 780.897E0, 4517.75E0, 840.333E0,
5 4218.70E0, 894.366E0, 3973.36E0, 948.399E0, 3767.13E0,1002.431E0,
6 3590.46E0,1056.464E0, 3436.84E0,1110.497E0, 3301.60E0,1164.530E0,
7 3252.42E0,1189.014E0, 3203.28E0,1239.587E0, 2882.68E0,1344.071E0,
8 2679.74E0,1425.221E0, 2526.18E0,1498.984E0, 2400.68E0,1570.241E0,
9 2294.50E0,1640.826E0, 2202.85E0,1711.435E0, 2122.55E0,1782.348E0/

 DATA T15 /                                                      1800.0E0,
132218.38E0,  13.326E0,30781.42E0, 242.471E0,27490.19E0, 387.615E0,
222773.30E0, 487.560E0,15821.59E0, 573.754E0, 8589.41E0, 630.734E0,
3 7857.19E0, 646.795E0, 7806.53E0, 648.490E0, 6876.29E0, 688.797E0,
4 6044.93E0, 744.220E0, 5470.07E0, 799.642E0, 5073.59E0, 850.027E0,
5 4754.88E0, 900.411E0, 4490.93E0, 950.795E0, 4267.42E0,1001.179E0,
6 4074.81E0,1051.564E0, 3906.50E0,1101.948E0, 3757.71E0,1152.332E0,
7 3680.50E0,1186.215E0, 3618.59E0,1239.460E0, 3394.22E0,1298.836E0,
8 3109.78E0,1390.193E0, 2912.11E0,1468.170E0, 2756.26E0,1541.440E0,
9 2626.84E0,1613.133E0, 2499.56E0,1696.332E0, 2391.32E0,1779.701E0/.

 DATA T16 /                                                      2000.0E0,
133955.66E0,  13.909E0,32613.64E0, 232.777E0,29236.62E0, 387.847E0,
224722.20E0, 487.530E0,18371.14E0, 573.194E0, 9715.11E0, 645.003E0,
3 8655.25E0, 661.733E0, 8302.92E0, 672.111E0, 7264.52E0, 718.734E0,
4 6562.68E0, 765.356E0, 6041.26E0, 811.979E0, 5631.87E0, 858.601E0,
5 5298.39E0, 905.224E0, 5019.40E0, 951.846E0, 4781.25E0, 998.469E0,
6 4574.70E0,1045.091E0, 4393.22E0,1091.713E0, 4232.05E0,1138.336E0,
7 4201.10E0,1148.283E0, 4112.19E0,1185.706E0, 4021.18E0,1240.893E0,
8 3584.17E0,1351.059E0, 3324.89E0,1435.455E0, 3102.61E0,1523.952E0,
9 2927.42E0,1608.933E0, 2783.04E0,1693.009E0, 2660.89E0,1777.056E0/

 DATA T17 /                                                      2200.0E0,
135607.23E0,  14.492E0,34096.21E0, 243.279E0,30883.91E0, 388.082E0,
226527.79E0, 487.510E0,19443.82E0, 585.859E0,10853.33E0, 659.615E0,
3 9433.73E0, 677.129E0, 8756.94E0, 695.462E0, 7803.37E0, 738.132E0,
4 7126.33E0, 780.802E0, 6608.61E0, 823.471E0, 6194.12E0, 866.141E0,
5 5851.60E0, 908.811E0, 5561.87E0, 951.481E0, 5312.35E0, 994.150E0,
6 5094.36E0,1036.820E0, 4901.66E0,1079.490E0, 4729.64E0,1122.159E0,
7 4637.43E0,1149.415E0, 4548.59E0,1187.522E0, 4510.73E0,1218.025E0,
8 3988.37E0,1339.694E0, 3683.13E0,1427.787E0, 3428.14E0,1518.459E0,
9 3229.88E0,1604.716E0, 3067.72E0,1689.682E0, 2931.24E0,1774.411E0/

 DATA T18 /                                                      2400.0E0,
137184.51E0,  15.073E0,35898.96E0, 223.542E0,32783.10E0, 377.694E0,
226889.76E0, 510.759E0,19090.97E0, 612.528E0,10166.01E0, 693.052E0,
3 9303.38E0, 714.054E0, 9076.25E0, 718.953E0, 8262.73E0, 757.431E0,
4 7645.11E0, 795.909E0, 7153.80E0, 834.387E0, 6749.86E0, 872.866E0,
5 6409.55E0, 911.344E0, 6117.39E0, 949.822E0, 5862.79E0, 988.300E0,
6 5638.20E0,1026.779E0, 5438.06E0,1065.257E0, 5258.18E0,1103.735E0,
7 5075.29E0,1153.449E0, 4935.95E0,1222.206E0, 4672.68E0,1270.727E0,
```

```
8 4333.15E0,1344.672E0, 3999.72E0,1433.843E0, 3756.82E0,1512.909E0,
9 3534.24E0,1600.480E0, 3353.62E0,1686.350E0, 3202.40E0,1771.765E0/

 DATA T19 /                                                    2600.0E0,
138696.59E0,  15.653E0,36813.83E0, 264.310E0,33210.24E0, 409.968E0,
227825.36E0, 522.481E0,19896.25E0, 625.813E0,10829.86E0, 709.590E0,
3 9699.24E0, 733.410E0, 9407.96E0, 744.475E0, 8710.29E0, 778.232E0,
4 8155.16E0, 811.988E0, 7698.71E0, 845.745E0, 7314.08E0, 879.502E0,
5 6983.79E0, 913.259E0, 6695.85E0, 947.016E0, 6441.74E0, 980.772E0,
6 6215.19E0,1014.529E0, 6011.47E0,1048.286E0, 5826.93E0,1082.043E0,
7 5703.57E0,1107.711E0, 5518.77E0,1160.241E0, 5446.62E0,1197.675E0,
8 5320.20E0,1227.844E0, 4834.08E0,1315.521E0, 4474.94E0,1397.239E0,
9 4129.57E0,1494.237E0, 3750.08E0,1633.563E0, 3474.36E0,1769.120E0/

 DATA T20 /                                                    2800.0E0,
140150.85E0,  16.232E0,38230.31E0, 264.699E0,34648.04E0, 410.174E0,
228674.42E0, 534.279E0,20589.80E0, 639.301E0,11213.02E0, 727.621E0,
310138.64E0, 753.572E0, 9699.30E0, 770.686E0, 9126.99E0, 799.200E0,
4 8649.96E0, 827.715E0, 8243.83E0, 856.230E0, 7892.20E0, 884.745E0,
5 7583.59E0, 913.260E0, 7309.70E0, 941.774E0, 7064.33E0, 970.289E0,
6 6842.75E0, 998.804E0, 6641.28E0,1027.319E0, 6457.00E0,1055.834E0,
7 6124.36E0,1121.221E0, 5885.61E0,1205.299E0, 5392.81E0,1282.213E0,
8 4929.99E0,1372.797E0, 4567.09E0,1461.125E0, 4297.59E0,1540.859E0,
9 4081.41E0,1617.173E0, 3901.13E0,1692.106E0, 3747.13E0,1766.475E0/

 DATA T21 /                                                    3000.0E0,
-141553.34E0,  16.811E0,39752.96E0, 254.984E0,36393.30E0, 399.685E0,
230895.16E0, 522.232E0,22518.30E0, 638.147E0,11703.88E0, 745.797E0,
310519.37E0, 775.147E0, 9873.87E0, 801.845E0, 9458.94E0, 823.687E0,
4 9094.64E0, 845.529E0, 8771.22E0, 867.371E0, 8481.36E0, 889.213E0,
5 8219.52E0, 911.055E0, 7981.34E0, 932.898E0, 7763.38E0, 954.740E0,
6 7562.87E0, 976.582E0, 7377.56E0, 998.424E0, 7205.58E0,1020.266E0,
7 6928.15E0,1060.464E0, 6563.23E0,1135.614E0, 6448.04E0,1179.815E0,
8 5515.02E0,1328.310E0, 5042.64E0,1425.647E0, 4714.22E0,1509.351E0,
9 4459.17E0,1587.660E0, 4218.81E0,1676.323E0, 4020.72E0,1763.830E0/
```

## C.4 MURDOCK-BAUMAN CRITICAL FLOW TABLE FOR SUPERHEATED VAPOR

```
GXX(1)    = STAGNATION PRESSURE (PSIA)
GXX(EVEN) = CRITICAL FLOW RATE (LB/FT**2-SEC)
GXX(ODD)  = STAGNATION ENTHALPY (BTU/LB)

NHB = NUMBER OF PAIRS OF ENTHALPY AND FLOW VALUES PER PRESSURE
NPB = NUMBER OF PRESSURE VALUES

DATA  NHB,NPB  /7,21/


 DATA G01 /      1.0E0,    2.38E0,1105.809E0,    2.35E0,1141.101E0,
1    1.97E0,1262.297E0,    1.72E0,1388.407E0,    1.55E0,1520.487E0,
2    1.42E0,1658.914E0,    1.31E0,1803.546E0/
 DATA G02 /      5.0E0,   11.39E0,1131.093E0,   11.24E0,1166.678E0,
1    9.79E0,1265.265E0,    8.59E0,1390.877E0,    7.73E0,1522.229E0,
2    7.08E0,1659.809E0,    6.55E0,1803.492E0/
 DATA G03 /     10.0E0,   22.35E0,1143.348E0,   22.03E0,1179.286E0,
1   19.50E0,1269.014E0,   17.14E0,1393.975E0,   15.44E0,1524.411E0,
2   14.15E0,1660.929E0,   13.11E0,1803.426E0/
 DATA G04 /     14.7E0,   32.49E0,1150.482E0,   31.99E0,1186.845E0,
1   28.54E0,1272.574E0,   25.13E0,1396.898E0,   22.67E0,1526.466E0,
2   20.78E0,1661.983E0,   19.27E0,1803.363E0/
 DATA G05 /     50.0E0,  106.74E0,1174.093E0,  104.68E0,1213.137E0,
1   94.06E0,1300.260E0,   83.80E0,1419.135E0,   76.25E0,1542.013E0,
2   70.36E0,1669.933E0,   65.55E0,1802.894E0/
 DATA G06 /    100.0E0,  209.60E0,1187.166E0,  204.53E0,1230.033E0,
1  180.06E0,1341.546E0,  163.13E0,1451.412E0,  150.18E0,1564.360E0,
2  139.82E0,1681.289E0,  131.15E0,1802.229E0/
 DATA G07 /    200.0E0,  412.87E0,1198.334E0,  401.31E0,1244.107E0,
1  357.56E0,1349.071E0,  324.65E0,1458.026E0,  299.54E0,1568.876E0,
2  279.41E0,1683.108E0,  262.51E0,1800.901E0/
 DATA G08 /    400.0E0,  818.64E0,1204.591E0,  790.41E0,1256.322E0,
1  703.94E0,1366.109E0,  642.58E0,1472.057E0,  595.71E0,1578.268E0,
2  557.86E0,1686.873E0,  525.85E0,1798.245E0/
 DATA G09 /    600.0E0, 1228.83E0,1203.657E0, 1178.21E0,1261.308E0,
1 1045.74E0,1376.982E0,  957.72E0,1480.958E0,  890.56E0,1584.001E0,
2  836.07E0,1688.703E0,  789.92E0,1795.592E0/
 DATA G10 /    800.0E0, 1646.48E0,1199.387E0, 1567.52E0,1262.925E0,
1 1390.36E0,1380.495E0, 1274.14E0,1484.244E0, 1186.07E0,1585.860E0,
2 1114.88E0,1688.525E0, 1054.63E0,1792.941E0/
 DATA G11 /   1000.0E0, 2073.79E0,1192.936E0, 1960.40E0,1262.293E0,
1 1731.88E0,1384.776E0, 1588.70E0,1487.875E0, 1480.61E0,1587.889E0,
2 1393.68E0,1688.413E0, 1320.03E0,1790.291E0/
 DATA G12 /   1200.0E0, 2512.78E0,1184.813E0, 2357.14E0,1260.858E0,
1 2082.05E0,1383.259E0, 1907.73E0,1487.326E0, 1778.05E0,1587.107E0,
2 1674.23E0,1686.865E0, 1586.33E0,1787.642E0/
 DATA G13 /   1400.0E0, 2965.42E0,1175.307E0, 2760.30E0,1257.989E0,
1 2432.47E0,1382.074E0, 2226.80E0,1489.933E0, 2075.80E0,1586.409E0,
2 1955.33E0,1685.352E0, 1853.38E0,1784.995E0/
```

```
 DATA G14 /   1600.0E0, 3433.97E0,1164.530E0, 3170.87E0,1253.837E0,
1 2782.86E0,1381.242E0, 2545.77E0,1486.701E0, 2375.82E0,1585.793E0,
2 2236.96E0,1683.872E0, 2121.17E0,1782.348E0/
 DATA G15 /   1800.0E0, 3921.87E0,1152.332E0, 3591.34E0,1248.253E0,
1 3132.78E0,1380.778E0, 2864.44E0,1486.632E0, 2672.07E0,1585.260E0,
2 2519.08E0,1682.426E0, 2389.71E0,1779.702E0/
 DATA G16 /   2000.0E0, 4434.55E0,1138.336E0, 4025.84E0,1240.864E0,
1 3481.81E0,1380.692E0, 3182.73E0,1486.729E0, 2970.49E0,1584.810E0,
2 2801.69E0,1681.012E0, 2658.99E0,1777.056E0/
 DATA G17 /   2200.0E0, 4979.37E0,1122.159E0, 4471.88E0,1233.895E0,
1 3840.73E0,1378.038E0, 3505.97E0,1485.080E0, 3271.12E0,1583.219E0,
2 3085.68E0,1679.026E0, 2930.18E0,1774.411E0/
 DATA G18 /   2400.0E0, 5565.81E0,1103.735E0, 4921.76E0,1227.612E0,
1 4200.33E0,1375.616E0, 3829.65E0,1483.534E0, 3572.20E0,1581.681E0,
2 3370.29E0,1677.062E0, 3202.31E0,1771.766E0/
 DATA G19 /   2600.0E0, 6208.34E0,1082.043E0, 5373.43E0,1222.124E0,
1 4560.22E0,1373.439E0, 4153.64E0,1482.096E0, 3873.69E0,1580.196E0,
2 3655.51E0,1675.119E0, 3475.38E0,1769.121E0/
 DATA G20 /   2800.0E0, 6935.60E0,1055.834E0, 5824.61E0,1217.519E0,
1 4919.99E0,1371.516E0, 4477.81E0,1480.770E0, 4175.53E0,1578.765E0,
2 3941.31E0,1673.198E0, 3749.39E0,1766.476E0/
 DATA G21 /   3000.0E0, 7830.38E0,1020.266E0, 6273.03E0,1213.858E0,
1 5279.13E0,1369.856E0, 4802.02E0,1479.560E0, 4477.62E0,1577.390E0,
2 4227.69E0,1671.299E0, 4024.33E0,1763.831E0/
```

# APPENDIX D

# THERMODYNAMIC PROPERTIES

The thermodynamic state variables used by RELAP5/MOD2 are contained in tabular form within a controlled library. This library was generated by the STH2X water property subroutines transmitted with the base RELAP code release. RELAP5 attaches this library during each execution. Through interpolation the values of pressure, temperature, specific volume, internal energy, entropy, enthalpy, thermal expansion, compressibility, and heat capacity are acquired using a subset of this list and the phase as the independent variables. Single-phase values are stored for 57 temperatures and 36 pressure points. Saturation values for 47 temperatures and 27 pressures are also included in this file.

# APPENDIX E

# RELAP5/MOD2 INTERNALLY STORED MATERIAL DEFAULT PROPERTIES

RELAP5/MOD2 has the thermal conductivity and volumetric heat capacity stored internally for gap gas, carbon steel, stainless steel, uranium dioxide, and zirconium. These values may be selected by the user for use in the heat structure heat conduction calculations. If chosen the following values or tables are used.

| | Material | Temperature (F) | Thermal Conductivity (Btu/hr-ft-F) |
|---|---|---|---|
| 1. | Gap Gas (constant value) | - | 0.41562 |
| 2. | Carbon Steel (constant value) | - | 26.607 |
| 3. | Stainless Steel | 32. | 7.5 |
| | | 1700. | 14.506 |
| 4. | Uranium Dioxide | 500. | 3.341 |
| | | 650. | 2.671 |
| | | 800. | 2.677 |
| | | 950. | 2.439 |
| | | 1100. | 2.242 |
| | | 1250. | 2.078 |
| | | 1400. | 1.940 |
| | | 1500. | 1.823 |
| | | 1700. | 1.724 |
| | | 1850. | 1.639 |
| | | 2000. | 1.568 |
| | | 2150. | 1.507 |
| | | 2300. | 1.457 |
| | | 2450. | 1.415 |
| | | 2600. | 1.382 |
| | | 3100. | 1.323 |
| | | 3600. | 1.333 |
| | | 4100. | 1.406 |
| | | 4600. | 1.538 |
| | | 5100. | 1.730 |
| 5. | Zirconium | 392. | 6.936 |
| | | 752. | 8.092 |
| | | 1112. | 9.827 |
| | | 1472. | 10.983 |
| | | 1832. | 12.717 |
| | | 2192. | 14.451 |
| | | 2552. | 17.341 |
| | | 2912. | 20.809 |
| | | 3272. | 25.433 |
| | | 3632. | 31.792 |
| | | 3992. | 39.306 |

| | Material | Temperature (F) | Volumetric Heat Btu/ft$^3$-F |
|---|---|---|---|
| 1. | Gap Gas (constant value) | - | $7.5 \cdot 10^{-5}$ |
| 2. | Carbon Steel (constant value) | - | 57.816 |
| 3. | Stainless Steel | 200. | 57.114 |
| | | 300. | 59.118 |
| | | 400. | 61.122 |
| | | 500. | 63.126 |
| | | 600. | 64.629 |
| | | 700. | 66.130 |
| | | 800. | 67.134 |
| | | 1000. | 69.138 |
| | | 2000. | 80.160 |
| 4. | Uranium Dioxide | 32. | 34.45 |
| | | 122. | 38.35 |
| | | 212. | 40.95 |
| | | 392. | 43.55 |
| | | 752. | 46.80 |
| | | 2012. | 51.35 |
| | | 2732. | 52.65 |
| | | 3092. | 56.55 |
| | | 3452. | 63.05 |
| | | 3812. | 72.80 |
| | | 4352. | 89.70 |
| | | 4532. | 94.25 |
| | | 4712. | 98.15 |
| | | 4892. | 100.1 |
| | | 5144. | 101.4 |
| | | 8000. | 101.4 |
| 5. | Zirconium | 0. | 28.392 |
| | | 1480. | 34.476 |
| | | 1675. | 85.176 |
| | | 1787.5 | 34.470 |
| | | 3500. | 34.476 |

# APPENDIX F

## HEAT TRANSFER REGIMES AND CORRELATIONS IDENTIFICATION

The heat transfer mode, heat transfer correlations, and CHF correlations are identified by a set of flags, and these flags are printed out in the heat slab section of the major edit as MODE. The values of these flags and the corresponding mode/correlations are described below.

Heat Transfer Mode

| Mode | Description |
|---|---|
| 1 | Single-phase liquid convection at critical and super critical pressure |
| 2 | Single-phase liquid convection at subcritical pressure |
| 3 | Subcooled nucleate boiling ($T_f < T_{sat} - 0.05$) |
| 4 | Saturated nucleate boiling ($T_f \geq T_{sat} - 0.05$) |
| 5 | Subcooled transition film boiling |
| 6 | Saturated transition film boiling |
| 7 | Subcooled film boiling |
| 8 | Saturated film boiling |
| 9 | Single-phase vapor convection |
| 10 | Condensation when void equals one |
| 11 | Condensation when void is less than one |
| 12 | Air-water mixture heat transfer |
| 13 | High AFW spray heat transfer |
| 14 | Interpolation between AFW and normal heat slab transfer mode |
| 30-31 | NCG condensation degradation |

Heat Transfer Correlation Flag

A three digit code, IJK is used to identify the heat transfer correlation. If IJK = 0, EM heat transfer is not used. The first digit, I, represents CHFLCK and FMLOCK; I=0 if CHF has not been exceeded, I=1 if CHF has been exceeded (CHFLCK=T) and I=2 if CHF has been exceeded and $\Delta T_{sat} \geq 166.667$ K (300 F)(FMLOCK=T). JK represents the heat transfer correlations. In major edits IJK is identified under the heading of EM-MODE-HT. The values of JK and the corresponding correlations are given below.

| JK | EM-MODE-HT | Correlation |
|---|---|---|
| - | Single-phase liquid | |
| | 1 | Dittus-Boelter |
| | 2 | Rohsenow-Choi |
| - | Nucleate Boiling | |
| | 3 | Dittus-Boelter |
| | 4 | Thom |
| | 5 | Thom/Schrock & Grossman interpolation |
| | 6 | Schrock & Grossman |
| | 7 | Schrock & Grossman/McEligot (steam) interpolation |
| | 8 | Schrock & Grossman/Rohsenow-Choi (steam) interpolation |
| | 9 | Chen |
| | 10 | Chen/McEligot (steam) interpolation |
| | 11 | Chen/Rohsenow-Choi (steam) interpolation |
| | 12 | Thom/Chen interpolation |
| | 13 | Thom/Schrock & Grossman to Chen interpolation |

14 Schrock & Grossman to Chen interpolation

15 Chen/Schrock & Grossman combination to McEligot (steam) interpolation

16 Chen/Schrock & Grossman combination to Rohsenow-Choi (steam) interpolation

- Single-Phase Steam

17 McEligot & Radiation

18 Rohsenow-Choi & Radiation

- Transition Boiling

19 McDonough, Milich and King

- Film Boiling

20 Temporary film boiling - CSO/Condie-Bengston IV

23 Film boiling - CSO/Condie-Bengston IV

- Condensation

31 Dittus-Boelter

CHF Correlation Flag

A three digit code, LMN, is used to identify the CHF correlation. In major edits, it is identified under EM-MODE-CHF. The values of LMN and corresponding correlations are given below.

| EM-MODE-CHF | Correlation |
|---|---|
| High Flow - High Pressure | |
| 100 | B&W-2 |
| 200 | BWC |
| 300 | BWCMV |
| 400 | BWUMV |

High Flow - Low Pressure

| | |
|---|---|
| 10 | Interpolation between high pressure and Barnett |
| 20 | Barnett |
| 30 | Barnett-Modified Barnett Interpolation |
| 40 | Modified Barnett |

Low Flow

| | |
|---|---|
| 1 | High flow - low flow interpolation |
| 2 | Low flow (MacBeth)<br>(MacBeth > Griffith) |
| 3 | Low flow ( Griffith ) |
| 4 | Minimum value for $q_{crit}$ (90,000 Btu/hr-ft$^2$) is used |

Note: For all flow conditions the CHF value is taken from the transition boiling correlation for $\alpha_g > 0.8$. This condition is identified by adding 50 to the appropriate value of EM-MODE-CHF in the above table. If the transition value of CHF is less than the minimum value of 90,000 Btu/hr-ft$^2$, the minimum value is used and 55 is added to EM-MODE-CHF.

# APPENDIX G

# BENCHMARKS

Two benchmarks are included with this report to verify the RELAP5/MOD2-B&W formulation and implementation. A LBLOCA benchmark, Semiscale MOD1 test S-04-6, and a SBLOCA benchmark, LOFT test L3-5, were performed and are documented in this appendix.

## G.1. LBLOCA Benchmark of Semiscale MOD1 Experiment S-04-6

### G.1.1. Introduction

Test S-04-6 was one of the 200 percent offset shear double-ended cold leg break tests conducted in the Semiscale MOD1 test facility. RELAP5/MOD2-B&W was used to predict the test, first using the INEL Cycle 36.04 options (base case) and second using the B&W installed evaluation model (EM) options. Both cases predicted higher break mass flow rates than shown by the data, and, as a result, the predicted depressurization rates were higher than the data. The predicted cladding temperature at the peak power location of the high powered rod using the EM option was higher than the Cycle 36.04 prediction. Both cases predicted higher cladding temperatures than measured. From this study it is concluded that the EM option would properly predict the system behavior during the blowdown phase of a PWR large break loss of coolant accident (LBLOCA).

### G.1.2. Description of Experiment

An isometric view of the Semiscale MOD1 test facility used for the cold leg break tests is shown in Figure G.1-1. It is a small scale model of a typical four-loop recirculating steam generator PWR. It consists of the following major PWR components: a pressure vessel with the core simulator, lower and upper plenums, and downcomer; an intact loop with a steam generator, a pump and a pressurizer; a broken loop with a simulated steam generator and a simulated pump; emergency coolant systems (ECC) in both loops that included an accumulator, and high and low pressure injection pumps; and a pressure suppression system with a suppression tank.

The configuration of the electrically-heated 40-rod bundle, shown in Figure G.1-2, is typical of a 15 by 15 fuel assembly (0.422 inch rod outside diameter and 0.563 inch pitch) except that the heated length of the test rods is 5.5 feet compared with 12 feet for commercial rods. The bundle has an inlet peaked axial power profile (peak at 26 inches from the bottom of the heated section). Three of the four center rods have a peak power density of 12 kw/ft and the fourth rod is unpowered. Of the remaining 36 rods, 33 rods have a peak power density of 11.46 kw/ft and three rods are unpowered.

The transient was initiated after the system reached steady-state by breaking two rupture assemblies that allowed the flow of the primary fluid into the suppression tank through two blowdown nozzles, each having a break area of 0.00262 $ft^2$. The suppression system was maintained at a constant pressure of 34.8 psia. At blowdown initiation, the power to the primary coolant pump was reduced and the pump was allowed to coast down to a speed of 1500 rpm, which was then maintained for the duration of the test. During the transient, the power to the core was automatically controlled to simulate the thermal response of nuclear rods. The measurements made during the transient included pressure, flow, density, and fluid temperatures at different locations in the primary and secondary systems, and surface temperatures at different elevations of the selected heated rods. The sequence of events relative to the transient initiation is given in Table G.1-1.

## G.1.3. RELAP5 Input Model

The nodalization of the RELAP5 input model for the Semiscale MOD1 test facility is shown in Figure G.1-32. The nodalization of the primary system is very similar to the RELAP4 model given in Reference 7. The geometry and other needed input information for the primary system was obtained from this RELAP4 model.[7] The geometry and other input information for the secondary side of

the steam generator were obtained from the RELAP5/MOD0 input model given in Reference 8. The input information obtained from the RELAP4 and the RELAP5/MOD0 input models were verified using the geometry values given in Reference 6.

The RELAP5 base input model consisted of 89 volumes, 98 junctions, and 50 heat structures. Some of the important features of the model are given below.

1. The core was modeled with two channels to account for the radially peaked power profile. The fluid volumes associated with the three high powered rods were modeled as a hot channel. The remaining core fluid volumes were modeled as an average channel. Each channel was axially divided into six volumes in order to make the model consistent with the EM plant model. The axial division coincided with selected axial steps in the power shape curve. Crossflow junctions were used to connect the hot and average channel volumes.

2. The active heater rods in each channel were modeled using ten heat slabs, that is, one heat slab per power step.

3. The pressurizer was modeled using an eight-equal-volume pipe component.

4. The accumulator was modeled using the accumulator component.

5. The high and low pressure pumps were simulated using time-dependent volumes and junctions.

6. The suppression system was modeled as a time-dependent volume.

7. Break nozzles were modeled as trip valves.

8. The homologous curves for the intact loop pump were obtained from the RELAP4 input model.[7] The measured pump speed versus time data were input to simulate the pump coast down during the transient.

9. The measured power versus time data were input to simulate the electrical power supplied to the heater rods during the transient.

10. The moisture separator on the secondary side of the steam generator was simulated using the separator component.

11. Nonequilibrium and nonhomogeneous options were selected for each volume and junction.

12. The break junctions and the pressurizer surge line junction were treated as choked flow junctions using a discharge coefficient of one.

G.1.3.1. EM Input Options

The following modifications to the base model were made to select the EM options. These options are the same as those used in the EM plant model.

1. The equilibrium option was selected for the core inlet, outlet, and core volumes.

2. The homogeneous option was selected for the core inlet, outlet, and the normal (vertical) core junctions.

3. The EM heat transfer option with the B&W high pressure CHF correlation (B&W-2) was selected for all the core heat slabs. The post-CHF lock-in option was selected that would force permanent film boiling if CHF is exceeded and conditions would permit a return to nucleate boiling.

4. The 90/10 weighting factor was used in the underrelaxation of the interphase heat transfer.

5. Choked Flow Models

   Subcooled: Extended Henry-Fauske.
   Two-phase and superheated region: Moody/Murdock-Bauman.
   Static properties.
   Homogeneous option (slip ratio = 1.0).
   Quality switching for the subcooled to two-phase transition.

6. The break junctions in the base model were selected as EM choked flow junctions. An additional junction and a time-dependent volume were added at each break plane. These junctions were used to switch the flow from choked flow to a flow calculated by the RELAP5 momentum equations when the system pressure was close to the suppression tank pressure and choked flow was no longer appropriate. The non-choking option was selected for these junctions. When the velocity calculated using the orifice equation is less than the choked junction velocity, the choked junction is closed and the second junction is opened, and will remain open during the remainder of the transient.

G.1.4. Transient Simulation

The base case and the EM case were run with constant boundary conditions to obtain steady-state test conditions. The steam generator secondary side pressure was adjusted to obtain the desired primary system conditions. Once the system reached steady-state, a steady-state post processor was used to replace the assumed initial conditions with the correct steady-state conditions in the input files. The measured and the predicted steady-state conditions are given in Table G.1-2. Trips were used to initiate the sequence of events, given in Table G.1-1, during the transient.

## G.1.5. Results and Discussion

The measured and the predicted pressure variations near the vessel side break are shown in Figure G.1-3. Both Cycle 36.04 and the EM predicted lower pressures than the data during the entire transient. The EM calculated a faster depressurization rate than Cycle 36.04. As a result, the pressure near the break location reached the suppression tank pressure at about 18 seconds in the EM case, and at 25.7 seconds in the base case as compared to 37 seconds in the test. The depressurization rate in both cases could be adjusted to match the data by varying the discharge coefficients. However, in the present study no attempt was made to adjust the discharge coefficients.

The pressure response near the pump side break is shown in Figure G.1-4. The predicted pressure response near this break location, using the EM option, was similar to the prediction near the vessel side break. Between 1.0 and 8.0 seconds, the base case predicted a higher pressure than the data. The difference between the measured and the input values of the HPI flow rates near this break location is the cause of this difference. The break plane pressure reached the suppression tank pressure at 15.8 seconds in the EM test case, and 25.6 seconds in the base case as compared to 27.0 seconds in the test.

The pressure responses at other locations in the primary system are shown in Figures G.1-5 through G.1-9. From these figures it can be concluded that the pressure response in the primary system is similar to the pressure response near the vessel side break shown in Figure G.1-3. The Cycle 36.04 pressure response near the broken loop simulated pump suction side, as shown in Figure G.1-6, supports the conclusion made from Figure G.1-4 that the HPI flow rate difference is the cause for the prediction of higher pressure than the data in the 1.0 to 8.0 second time period.

The pressure responses in the intact and the broken loop accumulators, shown in Figures G.1-10 and G.1-11 respectively, are consistent with the primary system pressure response. The sudden drop in measured pressure in the broken loop accumulator at about 2.5 seconds was caused by the opening of a valve in the surge line before the onset of injection.[7] In the present model, the initial pressure in this accumulator was set to 520 psia as was done in the RELAP4 model given in Reference 7.

The mass flow rates at different locations in the primary system are shown in Figures G.1-12 through G.1-18. In the test, the mass flow rate was estimated from the measured density and the volume flow rate. The mass flow rates given in the data report[5] were digitized to generate the comparison plots. During the digitalization the oscillations in the original data plots were smoothened out.

Figure G.1-12 shows that, near the vessel side break, both Cycle 36.04 and the EM predicted higher flow rates than the data. Both cases correctly predicted the transition from single-phase conditions to two-phase conditions which occurred at about 2.8 seconds. When the system pressure was close to the suppression tank pressure large spikes were observed in the data as well as in the prediction. These spikes were caused by the movement of liquid slugs from the accumulator injection location to the break. In the EM case, downflow of liquid into the downcomer occurred at about 19.2 seconds. This liquid flashes, thereby, resulting in a large vapor upflow that pushes fluid from the downcomer to the cold legs. The positive spike in the break flow rate (Figure G.1-12) and the negative spike in the flow from the intact loop cold leg to the downcomer, as shown in Figure G.1-17, at about 19.2 seconds were caused by this flashing of liquid in the downcomer.

The data as well as the prediction show that the core inlet flow remains negative during the entire blowdown period as shown in Figure G.1-18. For the first second after the initiation of the transient, both cases predicted higher values than the measured negative flow rate. From 7 to 12 seconds the EM predicted higher negative flow rates than the data and the Cycle 36.04 prediction.

The flow rates from the intact and the broken loop accumulators are shown in Figures G.1-19 and G.1-20, respectively. The starting points for the accumulator injection as well as the flow rates are consistent with the pressure response near the injection location. The spike in the broken loop accumulator flow data was caused by the opening of a valve[7] and therefore the actual flow did not start until about 3 seconds after transient initiation. The oscillations in the Cycle 36.04 prediction of this accumulator flow were due to the time steps taken by the code. They were larger than those allowed by the Courant limit. Similar oscillations were observed in an EM case when the code used the same time step as in the Cycle 36.04 case. The EM case discussed here was run using time steps which were smaller than that allowed by the Courant limit and it calculated a smooth flow rate as shown in Figure G.1-20.

The density variations near the vessel side and the pump side breaks and near the core inlet are shown in Figures G.1-21, G.1-22, and G.1-23, respectively. The underprediction of density near the vessel side break was due to the prediction of a faster depressurization rate. The spikes in the data as well as in the predictions, during the later part of the transient, were caused by movement of liquid slugs from the ECC injection location to the break. Near the pump side break, the EM underpredicted the density during the entire transient. Cycle 36.04 overpredicted the density from 1.5 to 6.0 seconds and underpredicted it during the remainder of the transient which is consistent with the

pressure prediction shown in Figure G.1-4. Both Cycle 36.04 and the EM overpredicted the density near the core inlet as shown in Figure G.1-23. Higher predicted flows from the core during the early part of the transient and lower predicted core heat transfer are the causes of the high density fluid near the core inlet (Figure G.1-23).

Fluid temperature variations at different locations in the primary system are shown in Figures G.1-24 through G.1-29. The calculated liquid and vapor temperatures are shown in these figures. These figures show that, once the system fluid condition has switched from subcooled liquid to two-phase mixture, the liquid and vapor temperatures generally remain near saturation during the major portion of the blowdown period. During the accumulator injection period, the data as well as the prediction show subcooled liquid and saturated steam at the injection location (Figure G.1-27). As the liquid slugs move toward the break, the fluid conditions along the path change from a saturation condition to saturated steam and subcooled liquid (Figures G.1-25 and G.1-26). The effect of lower core heat transfer during the later part of the transient can be observed in the fluid conditions near the core inlet (Figure G.1-28) and exit (Figure G.1-29).

The cladding temperature variations at the peak power location in the average and the high powered rods are shown in Figures G.1-30 and G.1-31, respectively. From an examination of the data given in Reference 5, it was observed that the cladding temperatures of the rods near the vessel wall were much higher than those of other rods (data D8-27 in Figure G.1-30). The unpowered rods in the bundle could reduce the temperatures of the nearby heated rods. However, test S-04-5, which is the counterpart of test S-04-6 (with all rods powered) showed a similar trend in the results. For most of the inner rods, both tests gave about the same temperatures at the peak power locations. Therefore, only

the cladding temperatures for the inner rods should be used for comparing the data with predictions.

The predicted cladding surface temperatures are shown in Figures G.1-30 and G.1-31. In the test, the thermocouples were located in the creases of the inner sheath. In the model, the cladding was modeled using two radial nodes. Therefore, the inner node temperature would and should be closer to the data. However, in RELAP5 only surface temperatures are stored in the plot file. At steady-state, the calculated temperature of the inner node, in both cases, was found to be close to the data. During the transient the difference between the surface temperature and the inner node temperature was about 10 F. Hence, the surface temperature is sufficient for comparison purposes.

The EM CHF correlations were found to be conservative in predicting DNB. Cycle 36.04 predicted DNB early by about 1 second for the average powered rods and correctly predicted DNB for the high powered rods. The EM predicted DNB early by about 2 seconds for the average powered rods and for the high powered rods the EM predicted DNB within 0.1 seconds after the initiation of the transient whereas DNB in the test occurred at about 3 seconds after the initiation of the transient.

Cycle 36.04 and the EM predicted higher cladding temperatures than the data during the entire transient period. For the high powered rods the EM calculated cladding temperature was much higher than the data as well as that calculated by Cycle 36.04. For the average powered rods the EM calculated cladding temperature was lower than that calculated by Cycle 36.04 after about 11 seconds. The higher core heat transfer predicted by the EM was due to the higher core flow rate prediction.

## G.1.6. Summary and Conclusion

Semiscale MOD1 large break LOCA test S-04-6 was simulated using RELAP5/MOD2-B&W with one case using the Cycle 36.04 options and the other using the EM options. In both cases a discharge coefficient of 1.0 was used for both the subcooled and two-phase break flow regimes. The EM options selected in this study are the same as those selected for actual plant modeling. As expected, both cases predicted higher break flow rates, faster system depressurization rates, and higher cladding temperatures than the data; the EM generally predicted higher values for these parameters than Cycle 36.04.

The consistency between the transient behavior predicted by the RELAP5/MOD2-B&W evaluation model version and the test data, given allowances for the effects of the EM discharge and core heat transfer models, supports application of B&W's EM version for conservative calculations of blowdown during large LOCA transients. When applied according to Appendix K requirements using a spectrum of effective break area-discharge coefficient combinations, RELAP5/MOD2-B&W should prove effective in defining limiting end-of-blowdown conditions.

Table G.1-1. Sequence of Events During Test S-04-6.

| Event | Time (sec) |
|---|---|
| Blowdown Initiated | 0.0 |
| ECC Accumulators Initiated | 0.0 |
| HPI Pumps Started | 0.0 |
| Steam Generator Feedwater and Discharge Valves Closed | 1.0 |
| LPI Started | 30.0 |

Table G.1-2. Conditions at Blowdown Initiation.

| Parameter | Data | Cycle 36.04 | EM |
|---|---|---|---|
| Core Power, kw (Btu/s) | 1.44 (1364.86) | 1.44 | 1.44 |
| Cold Leg Fluid Temperature, F | 543.0 | 543.5 | 543.0 |
| Hot Leg Fluid Temperature, F | 610.0 | 610.3 | 609.5 |
| Pressurizer Pressure, psia | 2252.0 | 2253.3 | 2252.6 |
| Pump Speed, RPM | 2400.0 | 2400.0 | 2400.0 |
| ICL Flow Rate, lbm/s | 15.5 | 15.4 | 15.4 |
| Steam Generator Pressure, psia | 850.0 | 809.5 | 803.5 |
| Pressure Suppression Tank Pressure, psia | 34.8 | 34.8 | 34.8 |

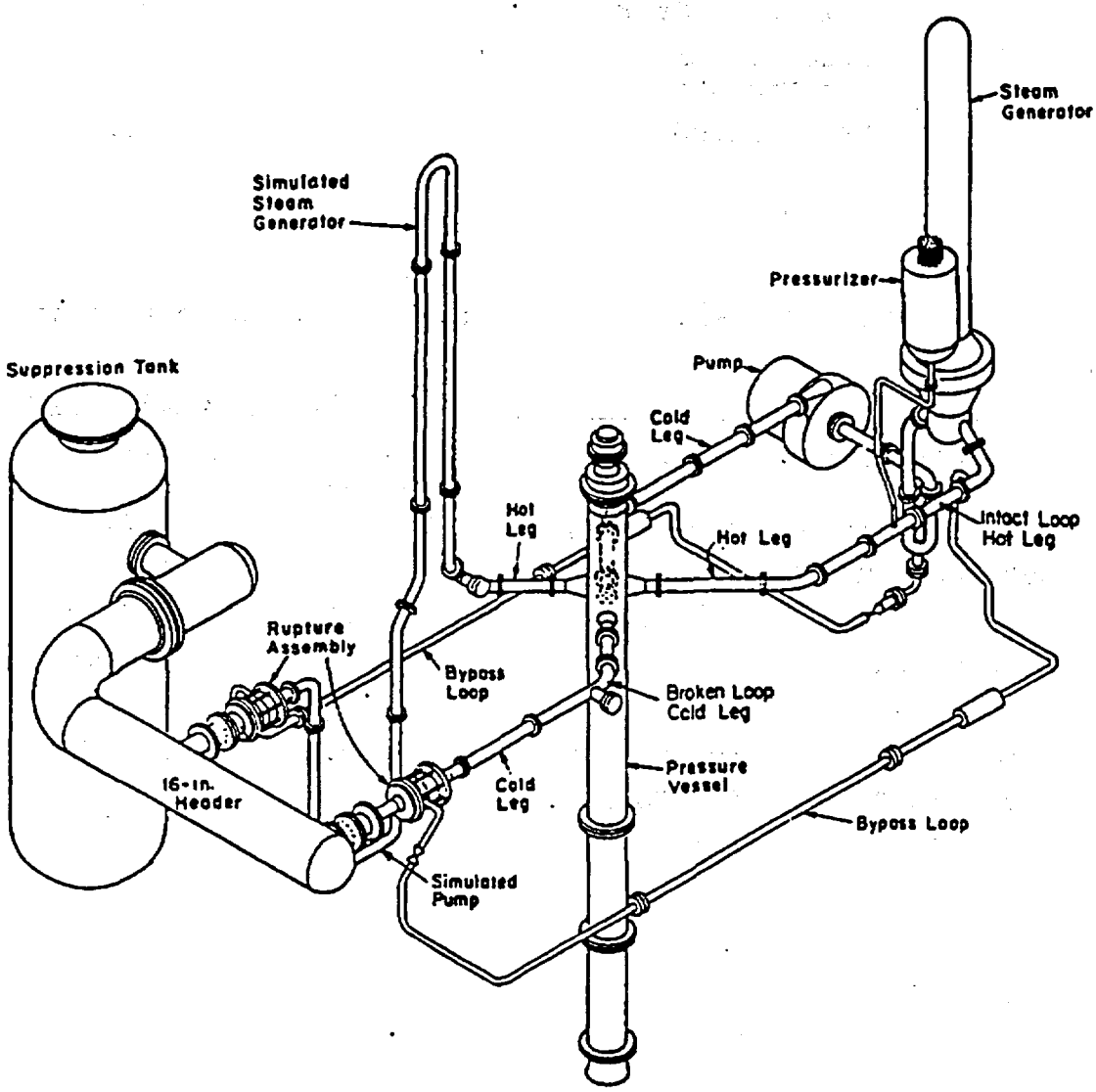


Figure G.1- 1. Semiscale MOD1 Test Facility - Cold Leg Break Configuration.

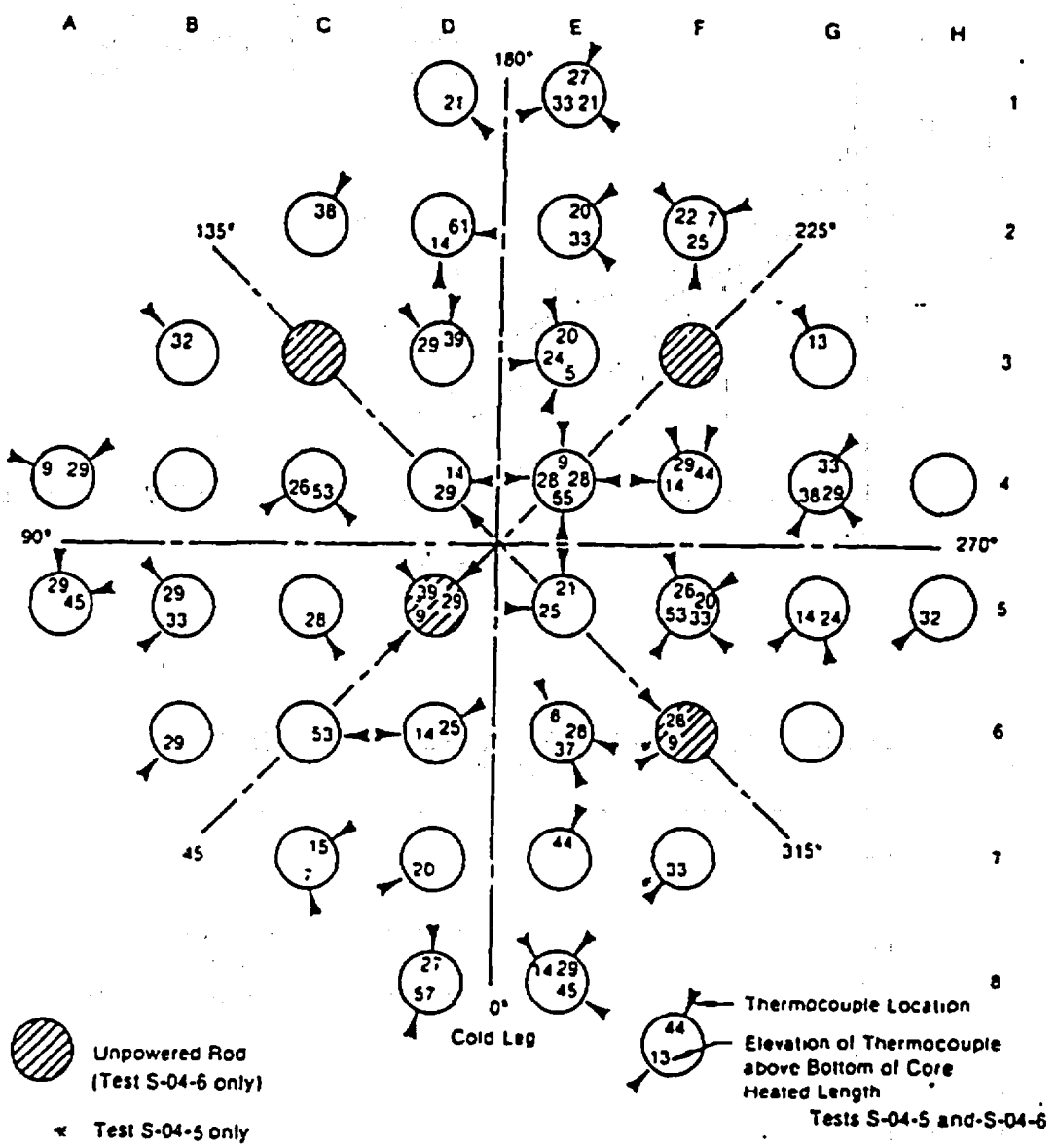


Figure G.1- 2. Semiscale MOD1 Rod Locations for Test S-04-6.

FIGURE G.1-3. SEMISCALE MOD1 TEST S-04-6; PRESSURE NEAR THE VESSEL SIDE BREAK.

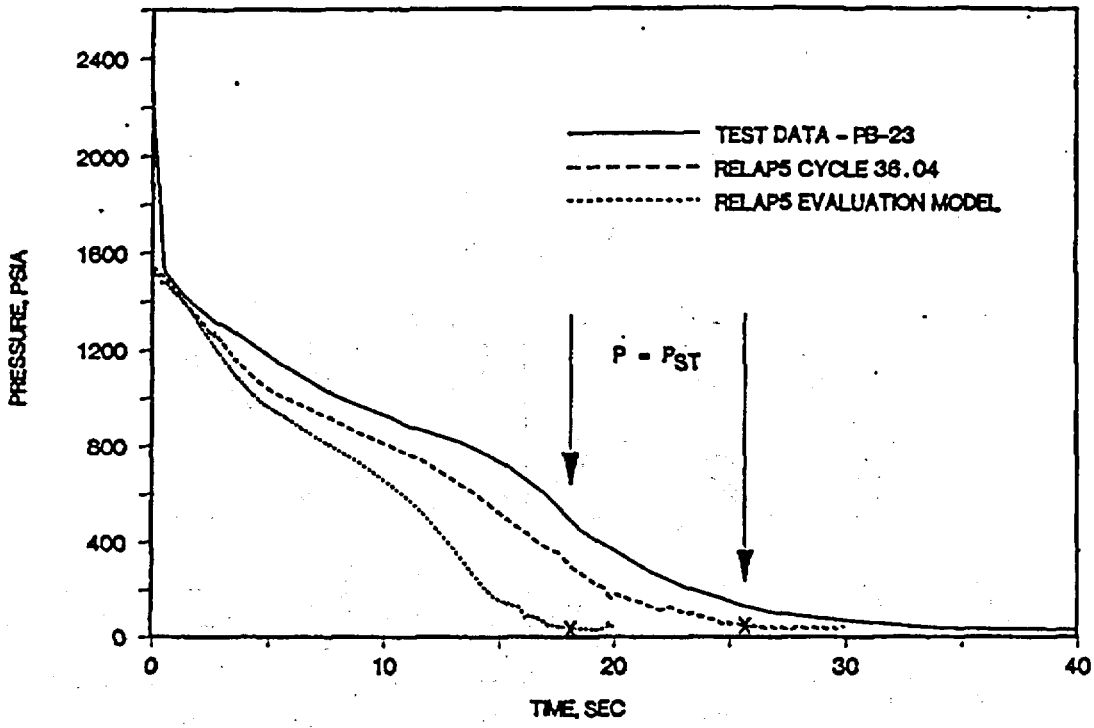


FIGURE G.1-4. SEMISCALE MOD1 TEST S-04-6; PRESSURE NEAR THE PUMP SIDE BREAK.

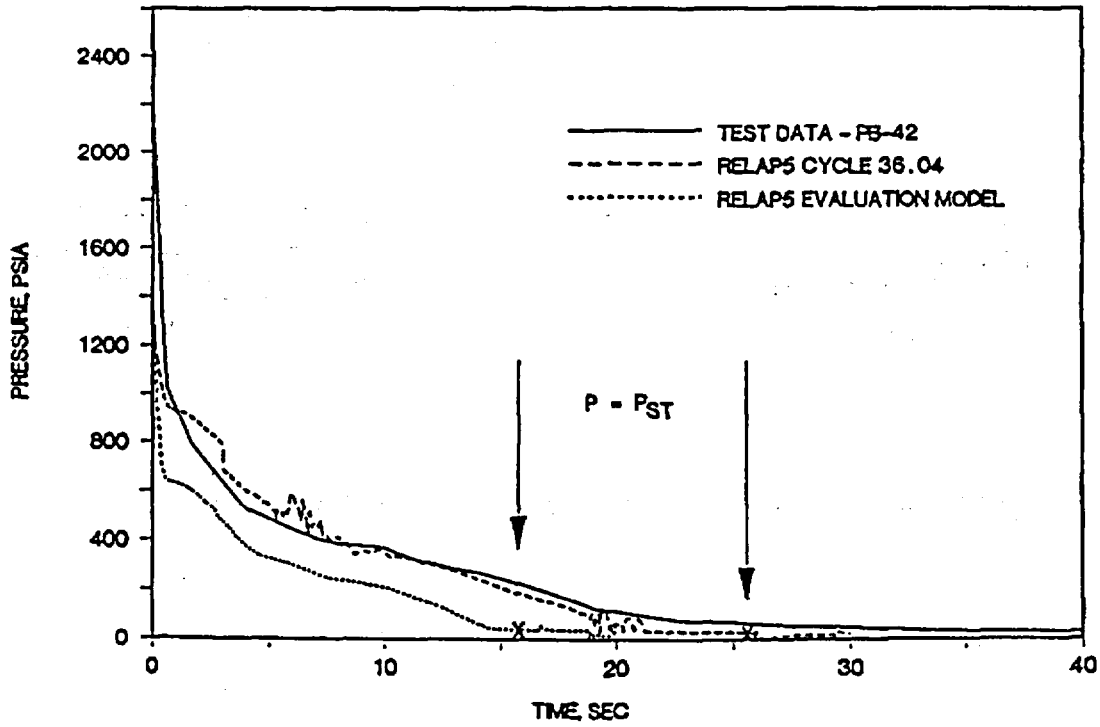

FIGURE G.1-5. SEMISCALE MOD1 TEST S-04-6; PRESSURE NEAR THE INTACT LOOP PUMP EXIT.

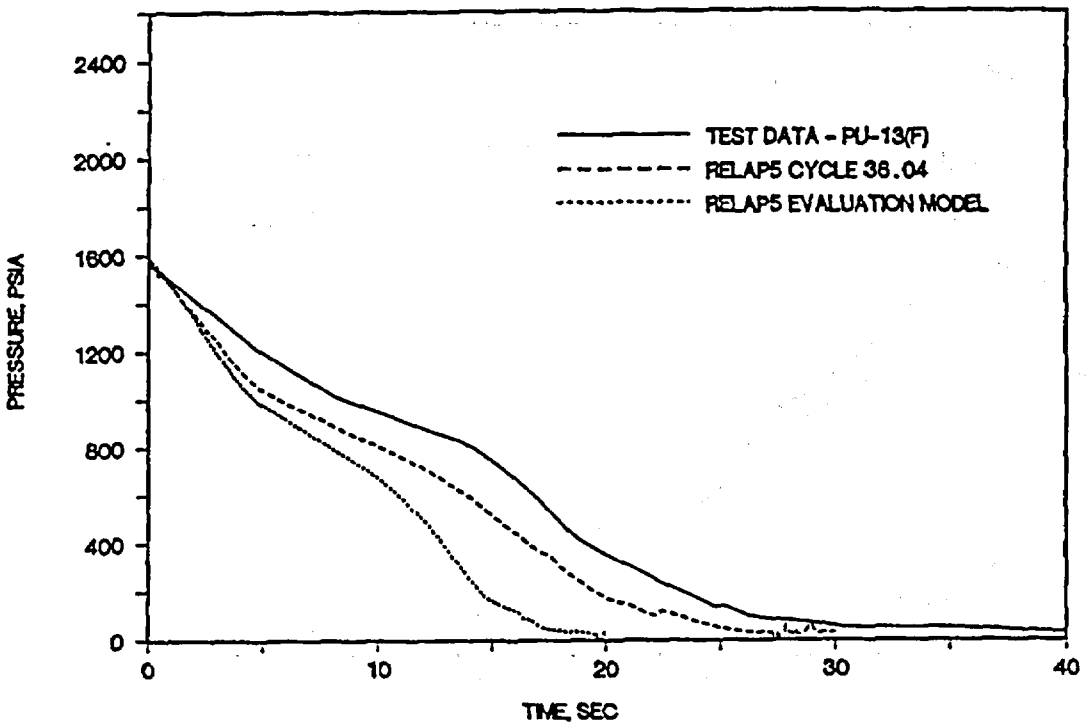


FIGURE G.1-6. SEMISCALE MOD1 TEST S-04-6; PRESSURE IN THE BROKEN LOOP NEAR THE PUMP SIMULATOR INLET.

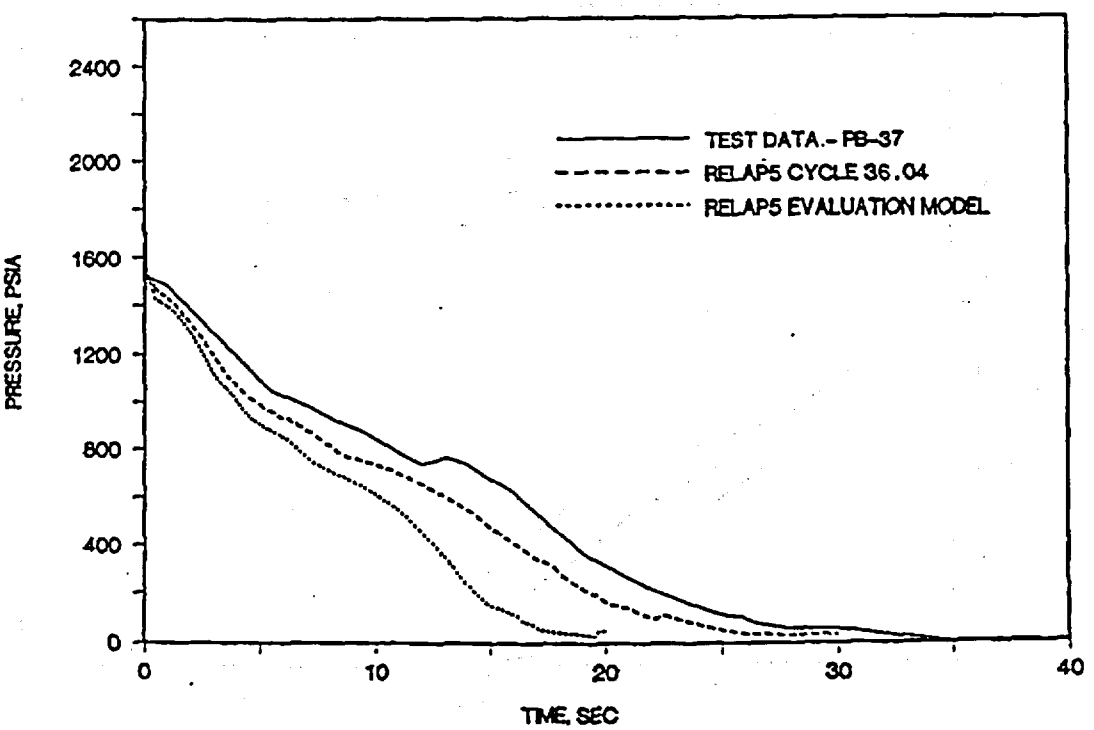

FIGURE G.1-7. SEMISCALE MOD1 TEST S-04-6; PRESSURE IN THE LOWER PLENUM.

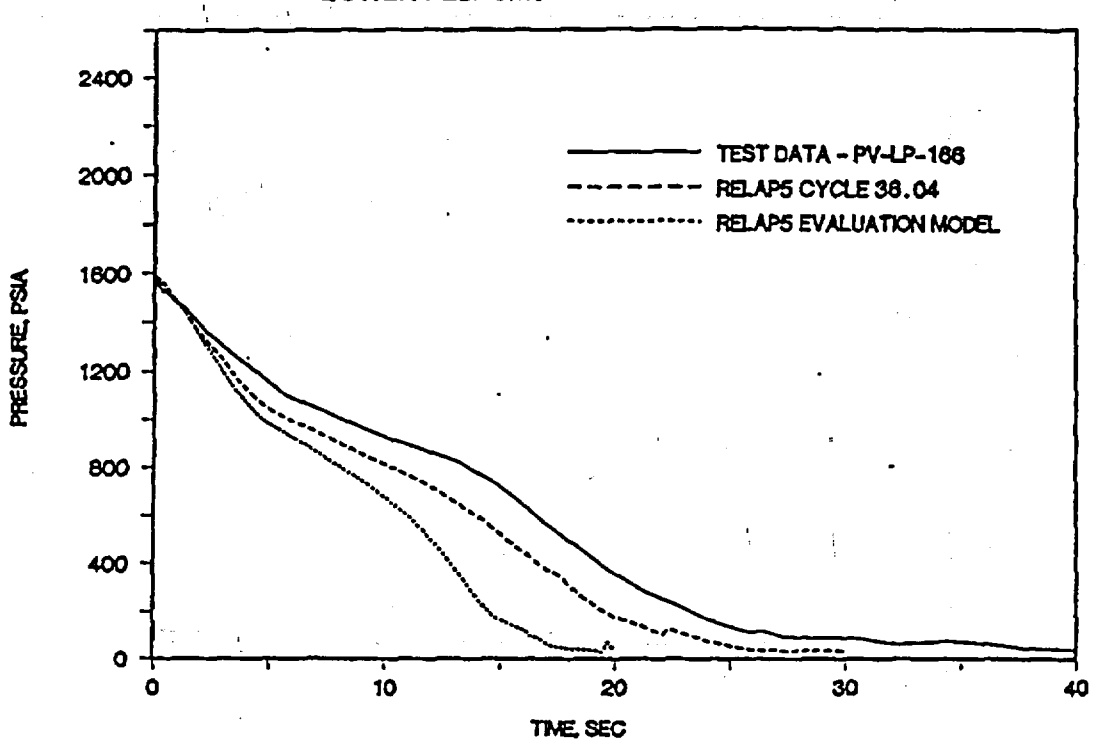


FIGURE G.1-8. SEMISCALE MOD1 TEST S-04-6; PRESSURE IN THE UPPER PLENUM.

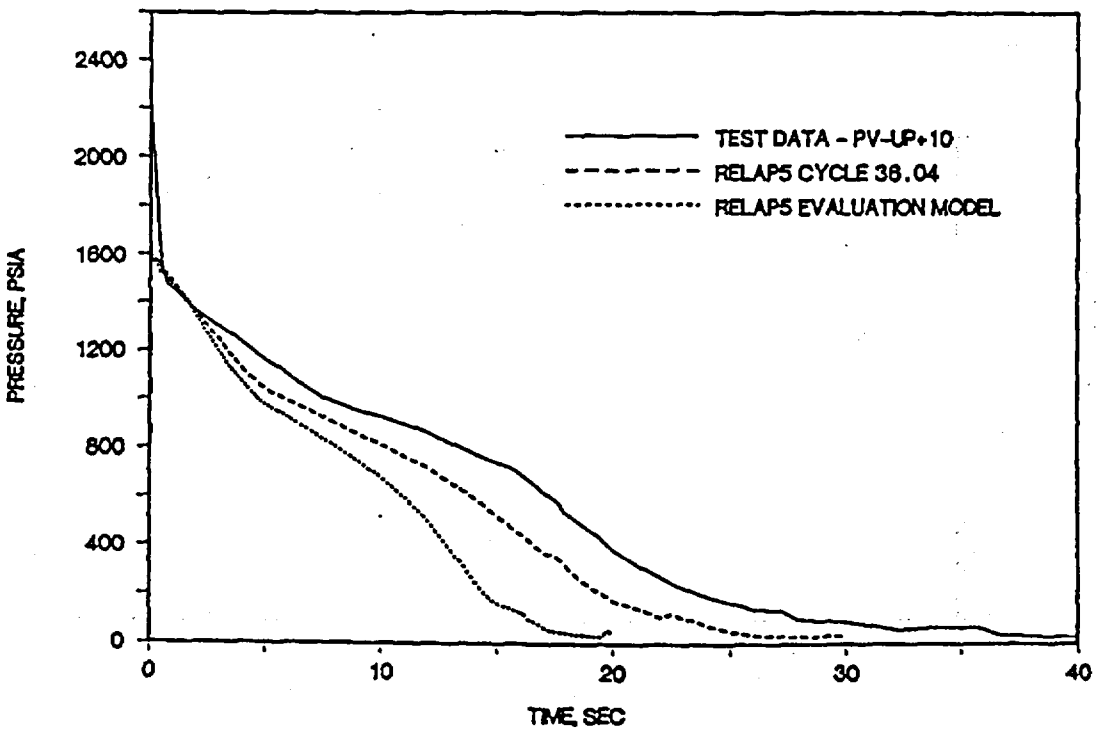

FIGURE G.1-9. SEMISCALE MOD1 TEST S-04-6; PRESSURE NEAR THE TOP OF THE PRESSURIZER.

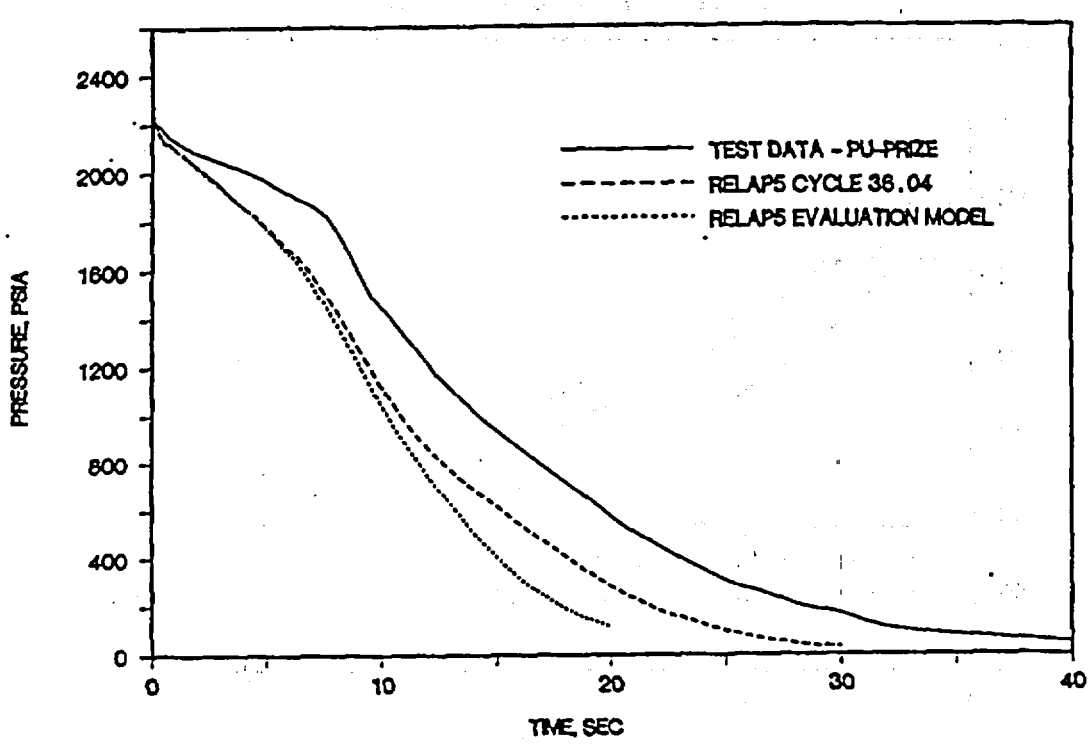


FIGURE G.1-10. SEMISCALE MOD1 TEST S-04-6; PRESSURE IN THE INTACT LOOP ACCUMULATOR.

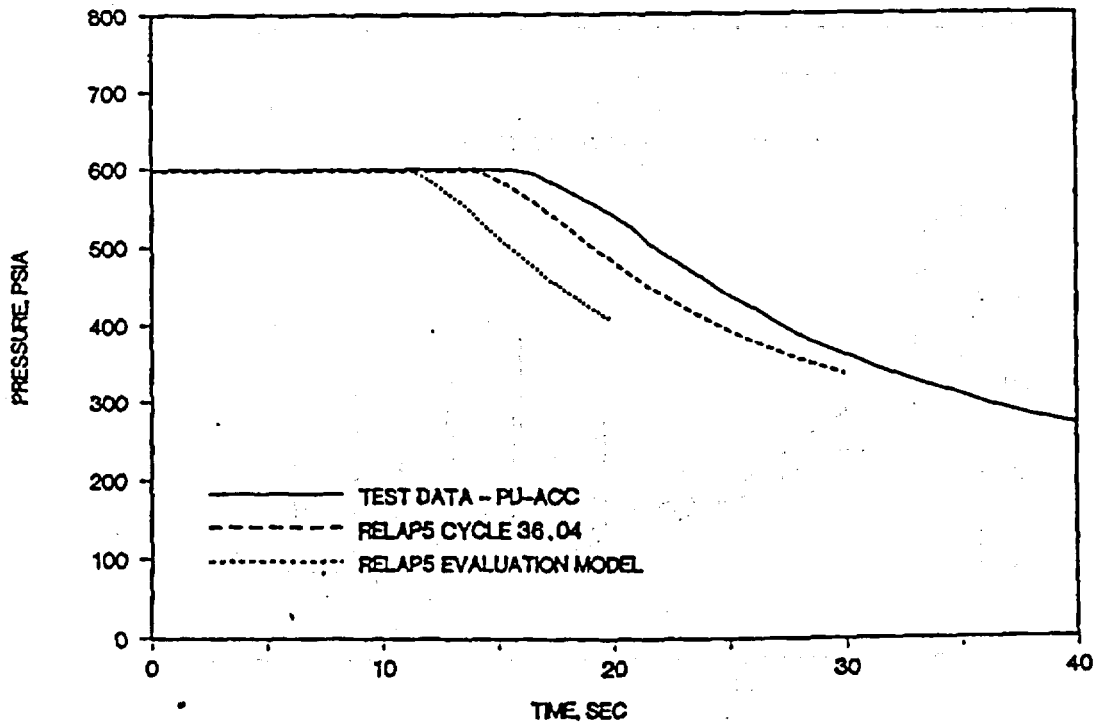

FIGURE G.1-11. SEMISCALE MOD1 TEST S-04-6; PRESSURE IN THE BROKEN LOOP ACCUMULATOR.

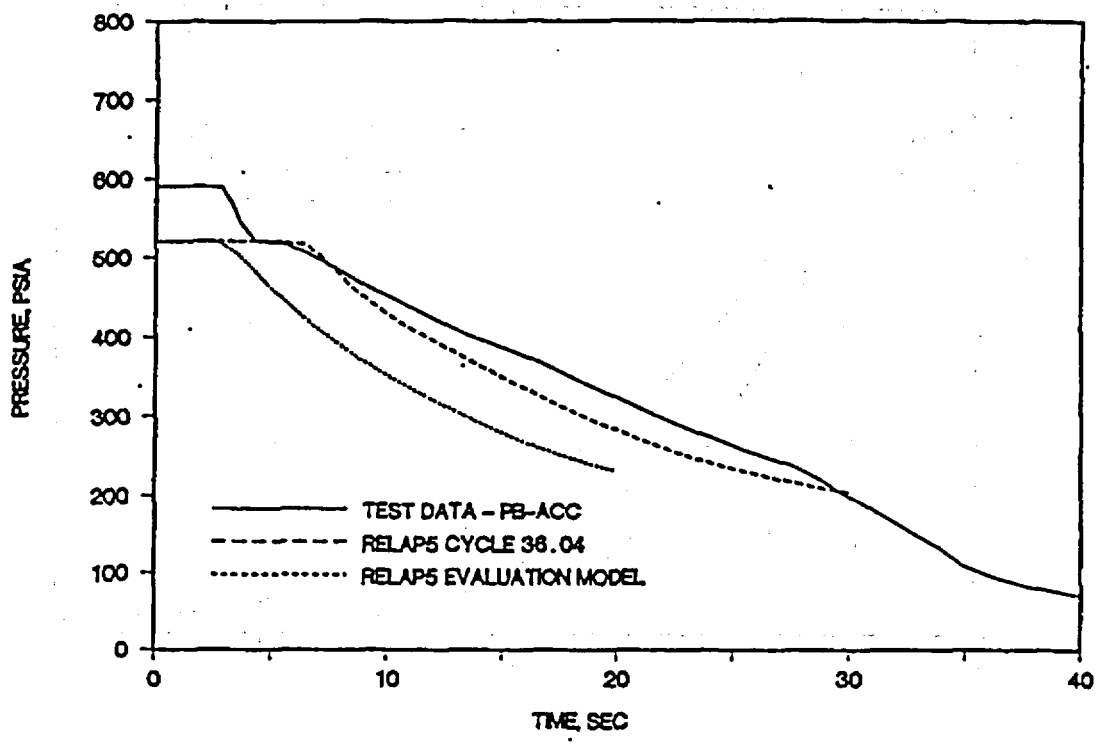


FIGURE G.1-12. SEMISCALE MOD1 TEST S-04-6; MASS FLOW RATE NEAR THE VESSEL SIDE BREAK.

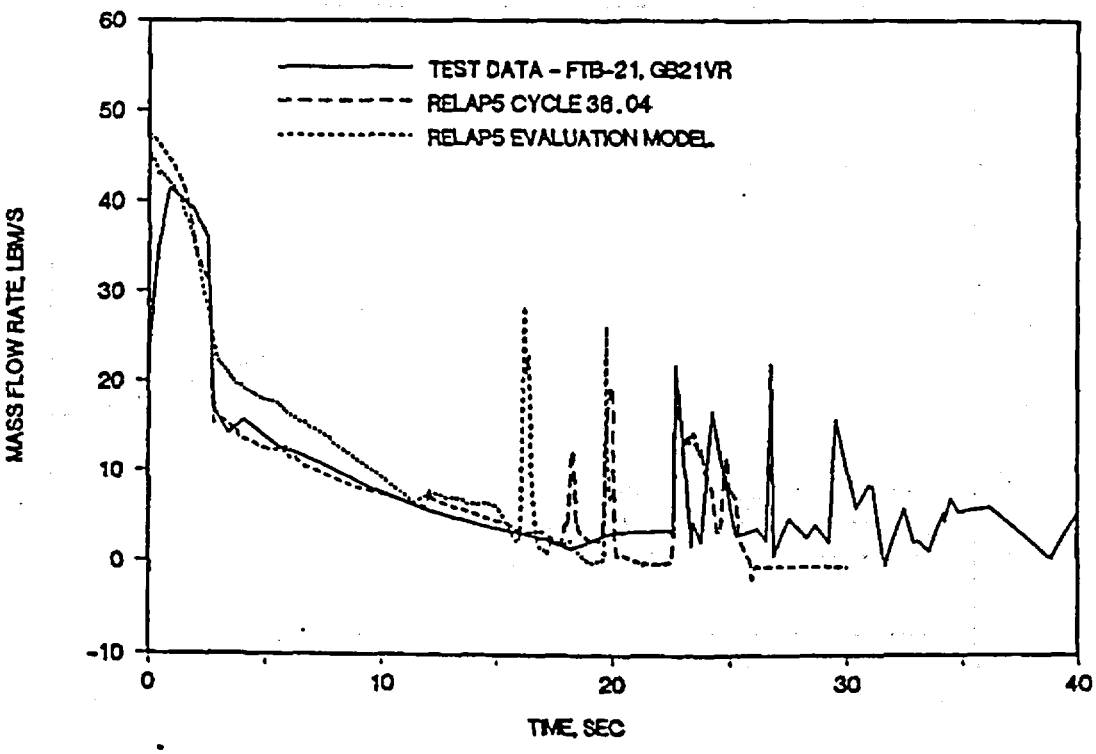

FIGURE G.1-13. SEMISCALE MOD1 TEST S-04-6; MASS FLOW RATE NEAR PUMP SIDE BREAK (BEFORE ECC INJECTION POINT).

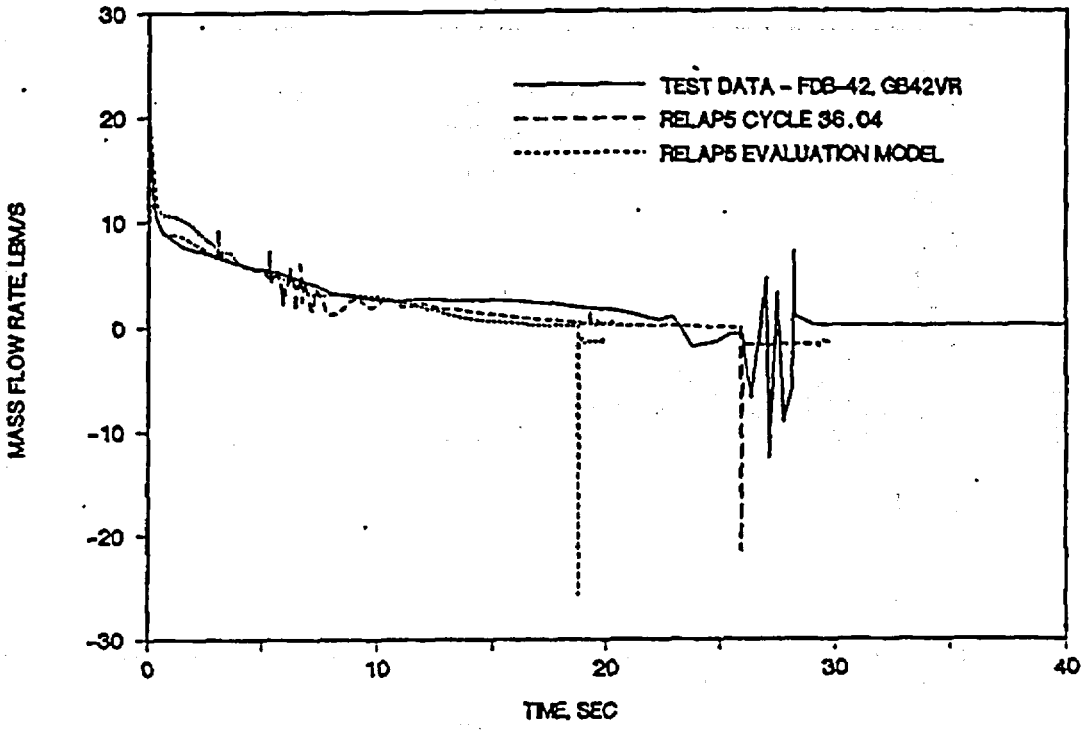


FIGURE G.1-14. SEMISCALE MOD1 TEST S-04-6; MASS FLOW RATE IN THE INTACT LOOP HOT LEG.

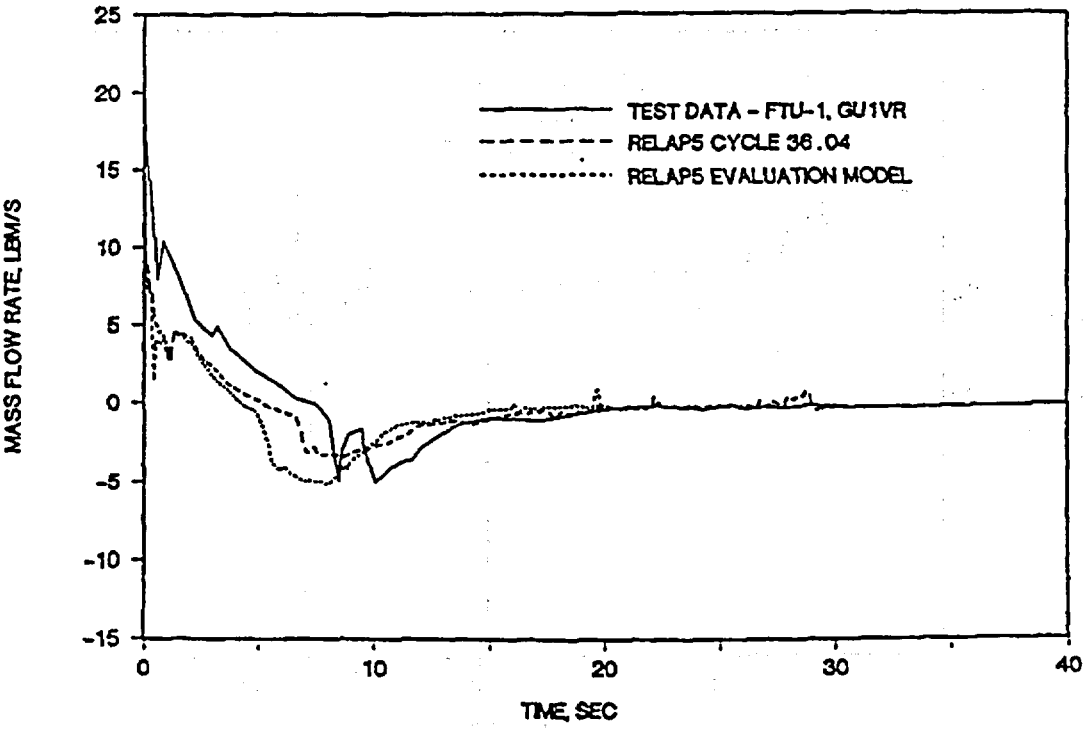

FIGURE G.1-15. SEMISCALE MOD1 TEST S-04-6; MASS FLOW RATE NEAR THE PUMP SIMULATOR INLET.

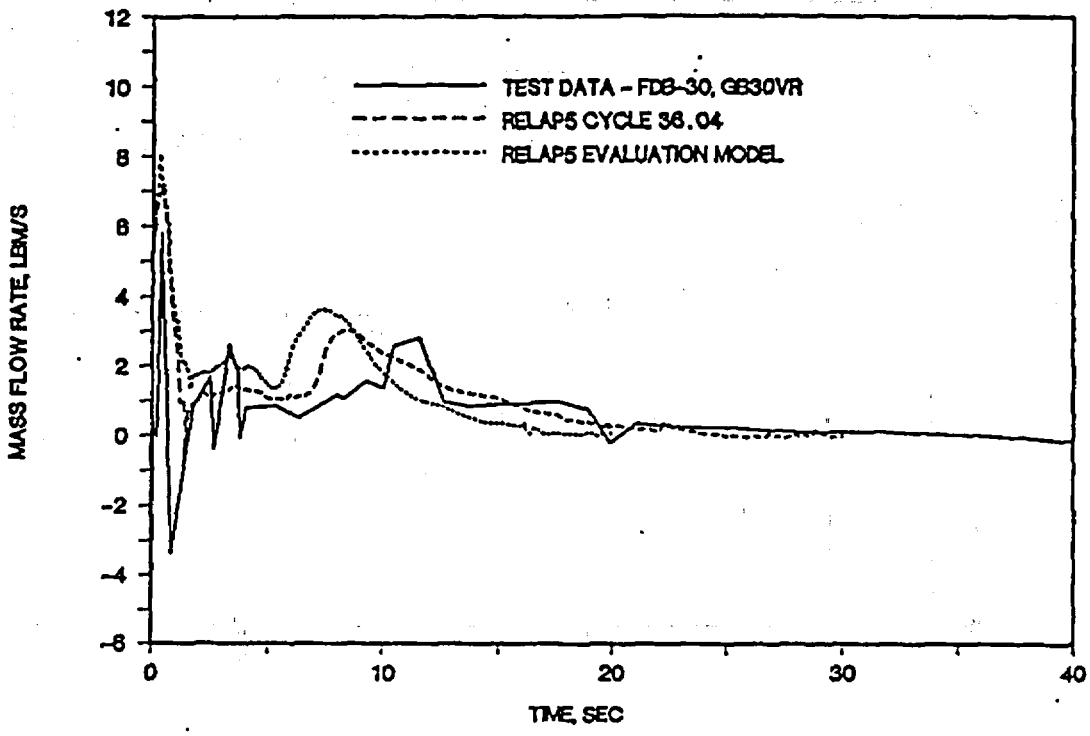


FIGURE G.1-16. SEMISCALE MOD1 TEST S-04-6; MASS FLOW RATE IN INTACT LOOP COLD LEG (BEFORE ACCUMULATOR INJECTION POINT).

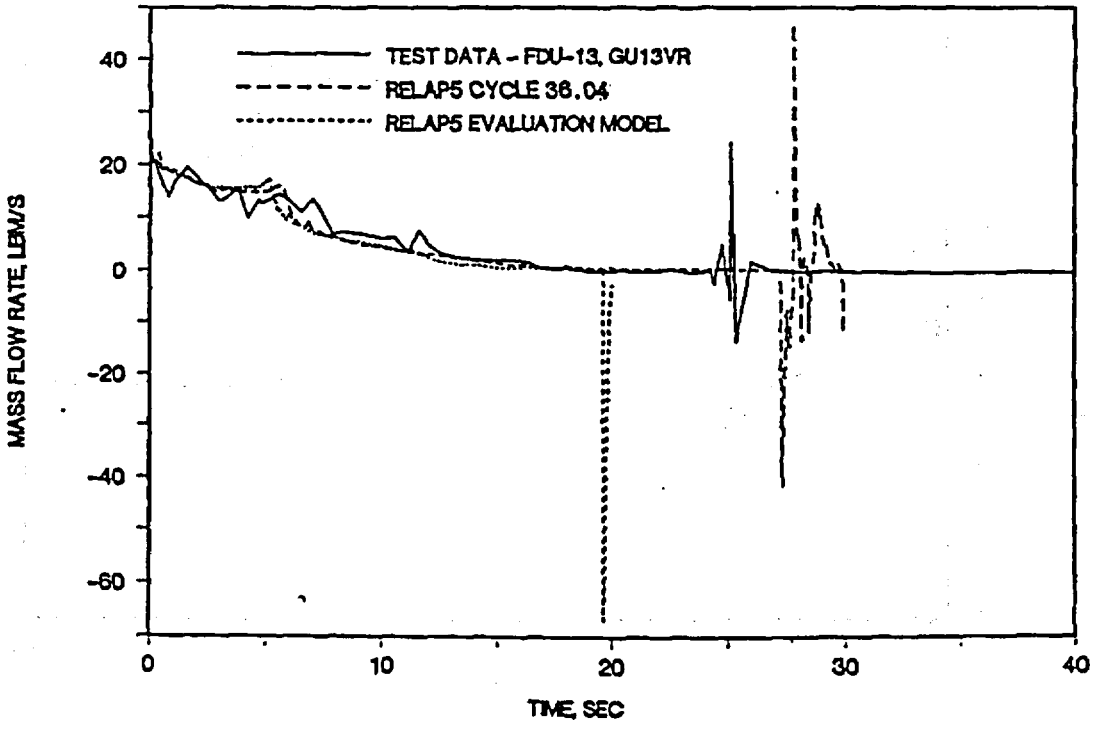

FIGURE G.1-17. SEMISCALE MOD1 TEST S-04-6; DOWNCOMER INLET FLOW RATE FROM THE INTACT LOOP.

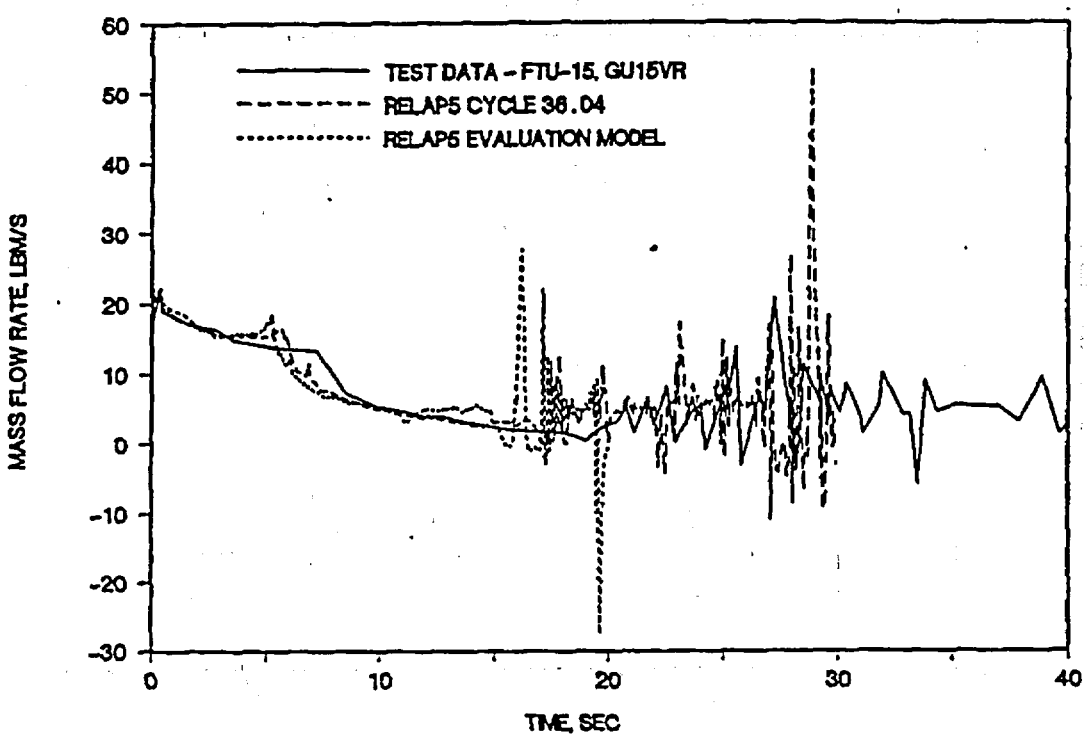


FIGURE G.1-18. SEMISCALE MOD1 TEST S-04-6: MASS FLOW RATE AT THE CORE INLET.

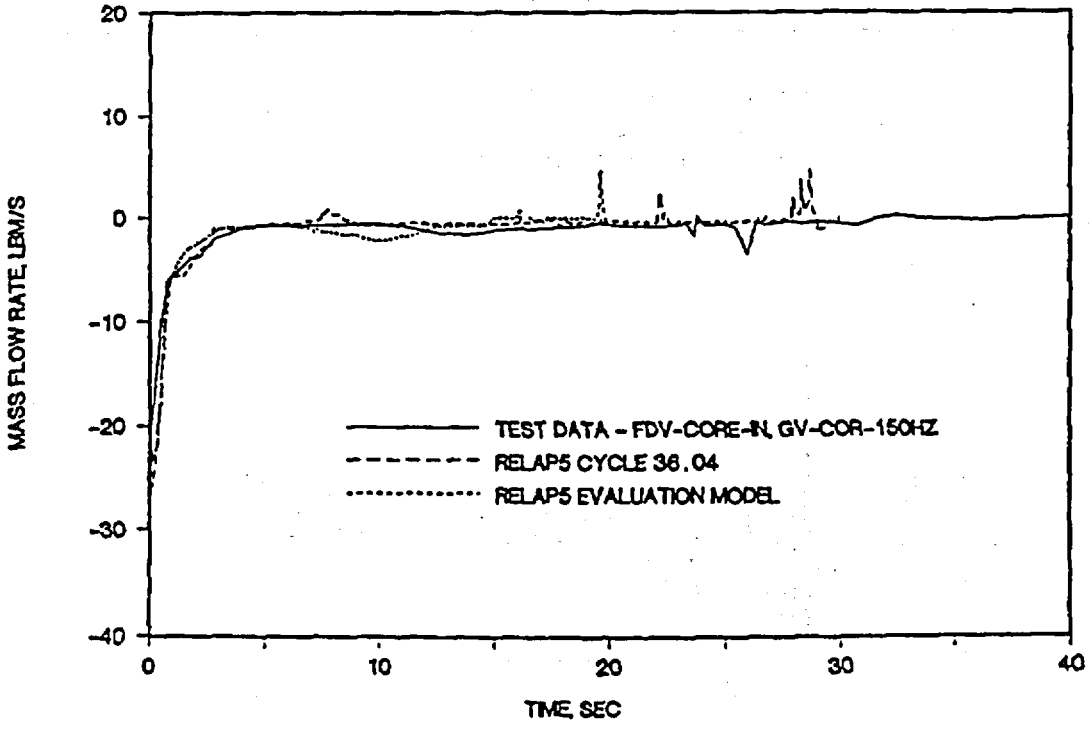

FIGURE G.1-19. SEMISCALE MOD1 TEST S-04-6; MASS FLOW RATE FROM THE INTACT LOOP ACCUMULATOR.

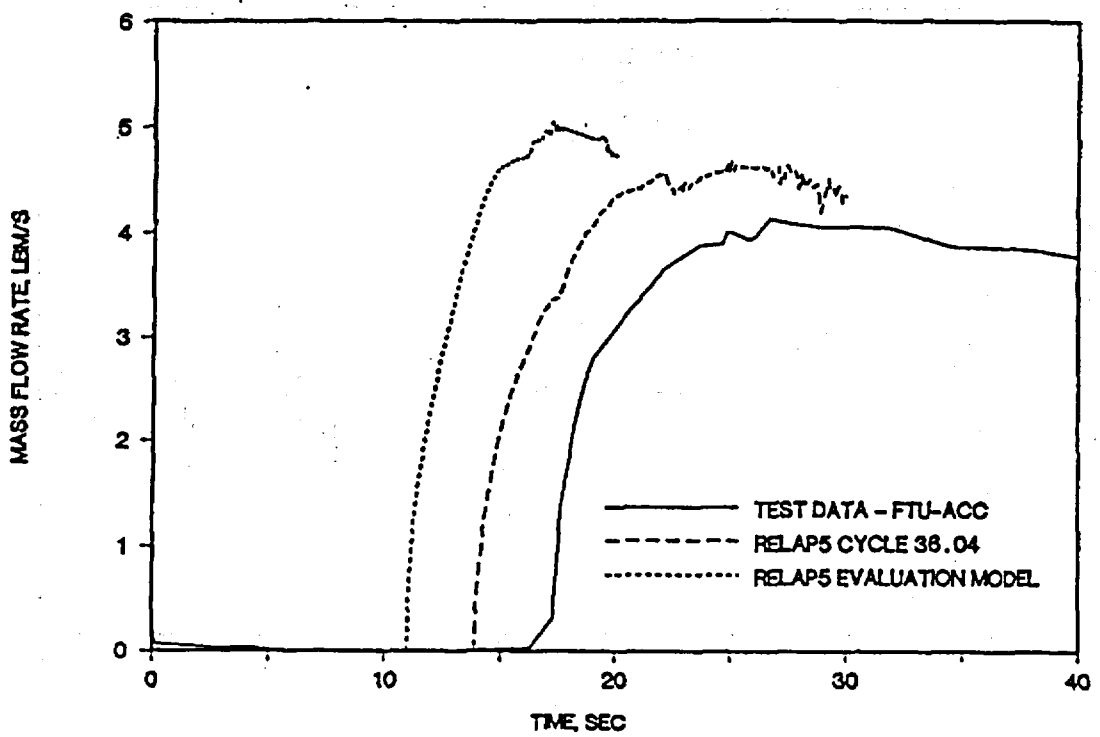


FIGURE G.1-20. SEMISCALE MOD1 TEST S-04-6; MASS FLOW RATE FROM THE BROKEN LOOP ACCUMULATOR.

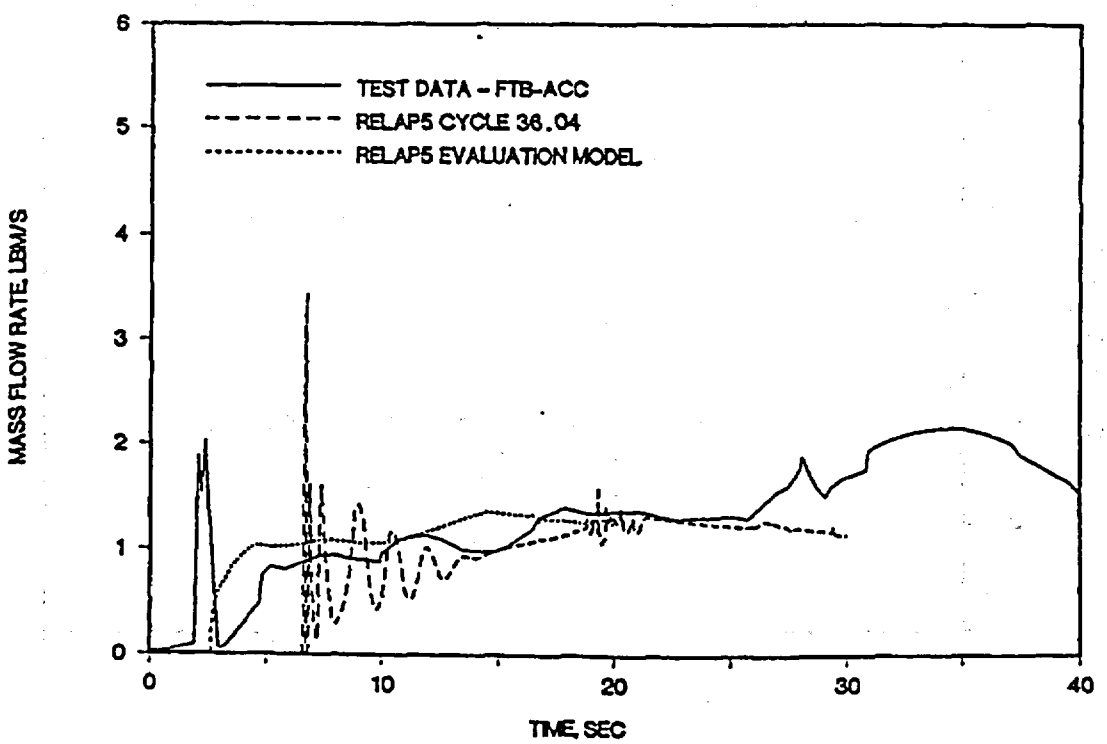

FIGURE G.1-21. SEMISCALE MOD1 TEST S-04-6; DENSITY NEAR THE VESSEL SIDE BREAK.

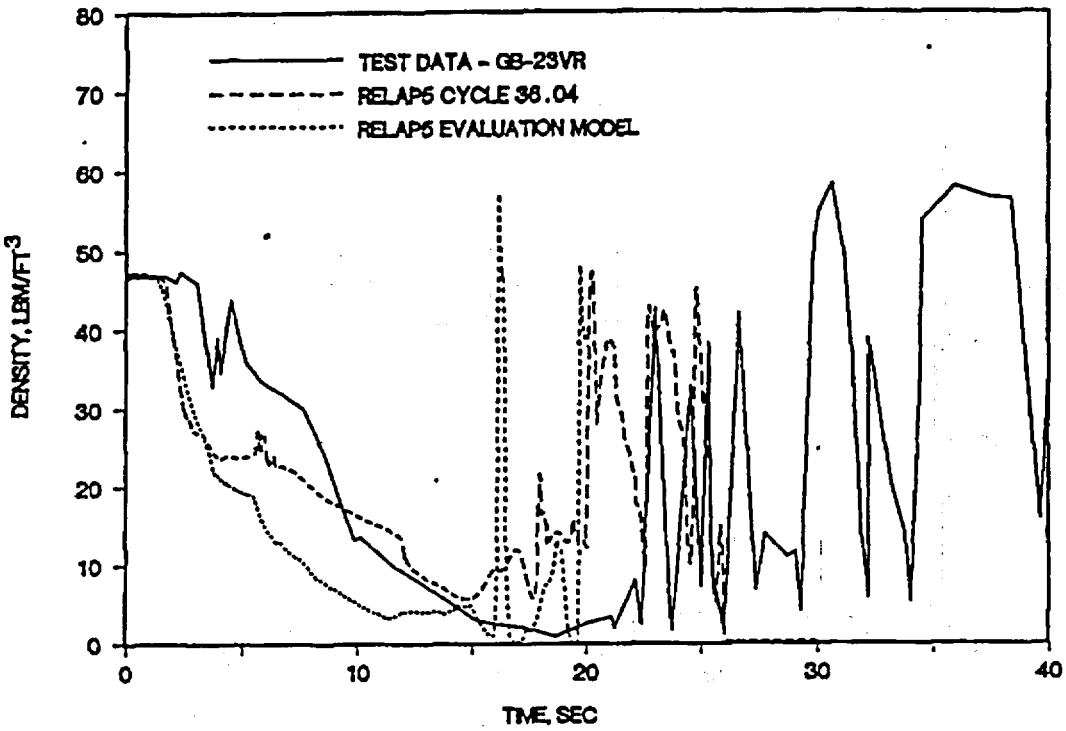


FIGURE G.1-22. SEMISCALE MOD1 TEST S-04-6; DENSITY NEAR THE PUMP SIDE BREAK (BEFORE THE ECC INJECTION LOCATION).

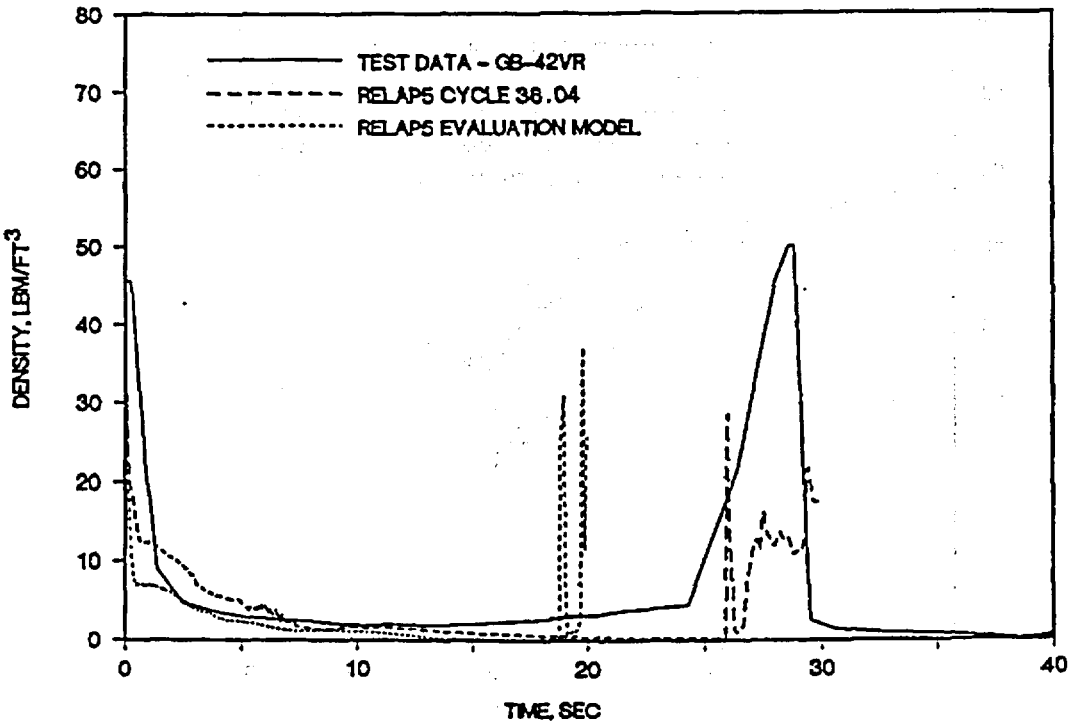

FIGURE G.1-23. SEMISCALE MOD1 TEST S-04-6; DENSITY NEAR THE CORE INLET.

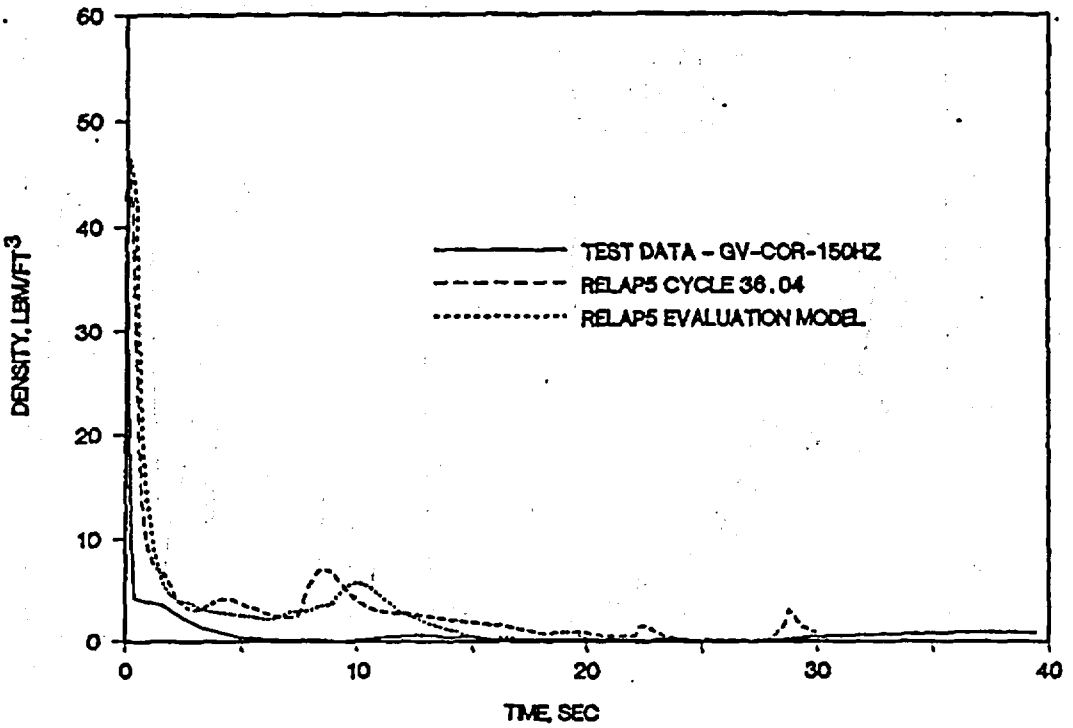


FIGURE G.1-24. SEMISCALE MOD1 TEST S-04-6; FLUID TEMPERATURE NEAR THE VESSEL SIDE BREAK.

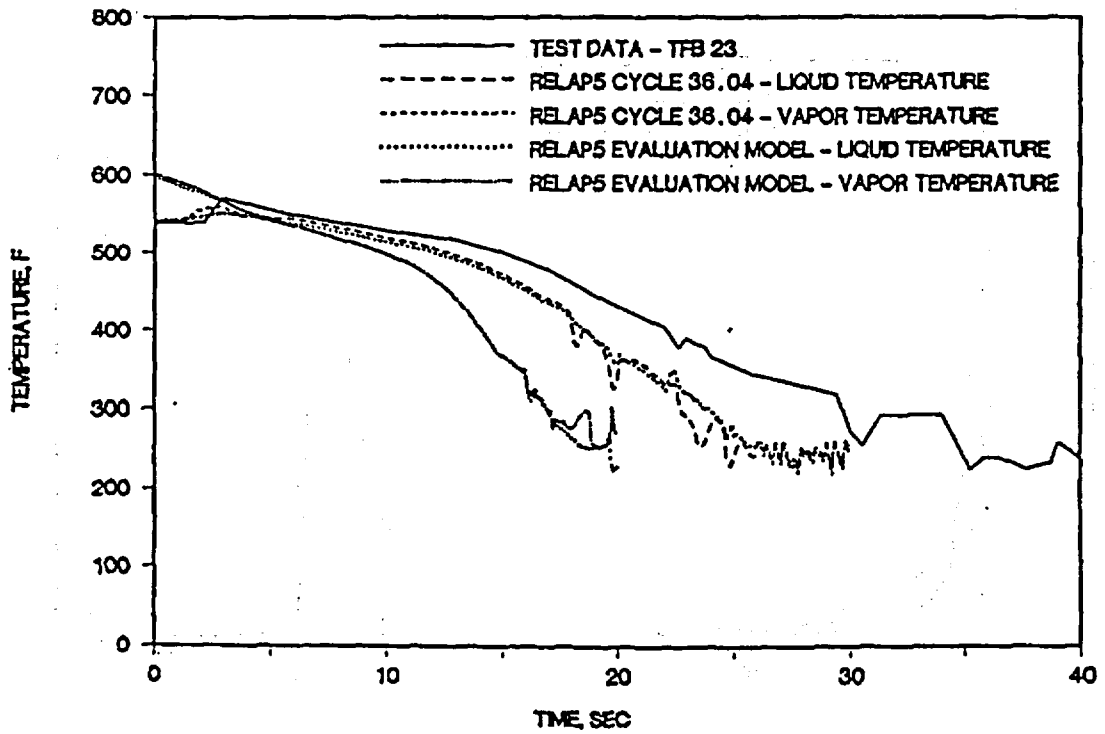

FIGURE G.1-25. SEMISCALE MOD1 TEST S-04-6; FLUID TEMPERATURE NEAR PUMP SIDE BREAK (BEFORE ECC INJECTION LOCATION).

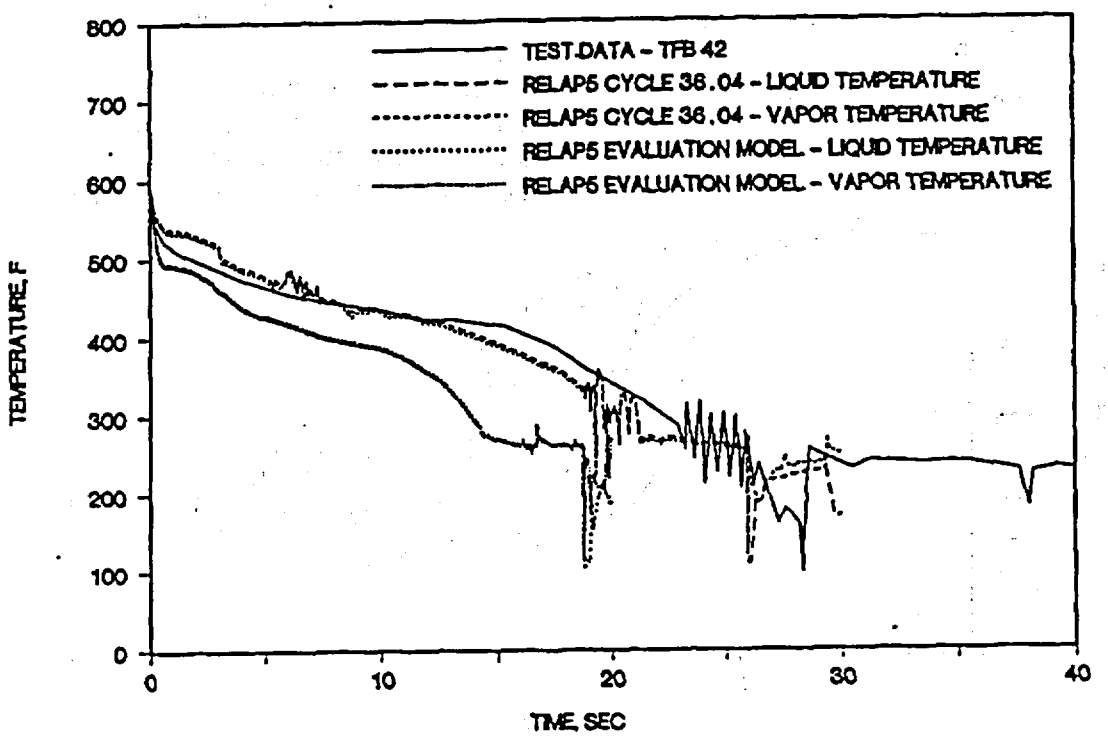


FIGURE G.1-26. SEMISCALE MOD1 TEST S-04-6; FLUID TEMPERATURE IN THE INTACT LOOP HOT LEG.

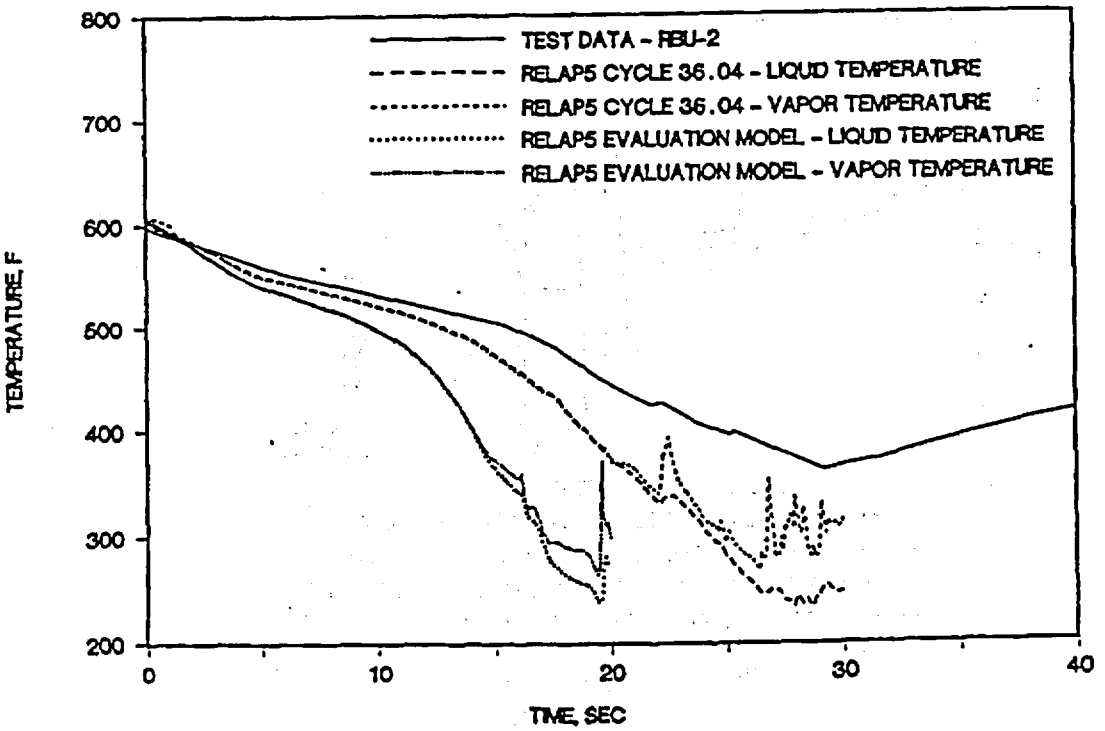

FIGURE G.1-27. SEMISCALE MOD1 TEST S-04-6; FLUID TEMPERATURE IN INTACT LOOP COLD LEG (NEAR ECC INJECTION POINT).

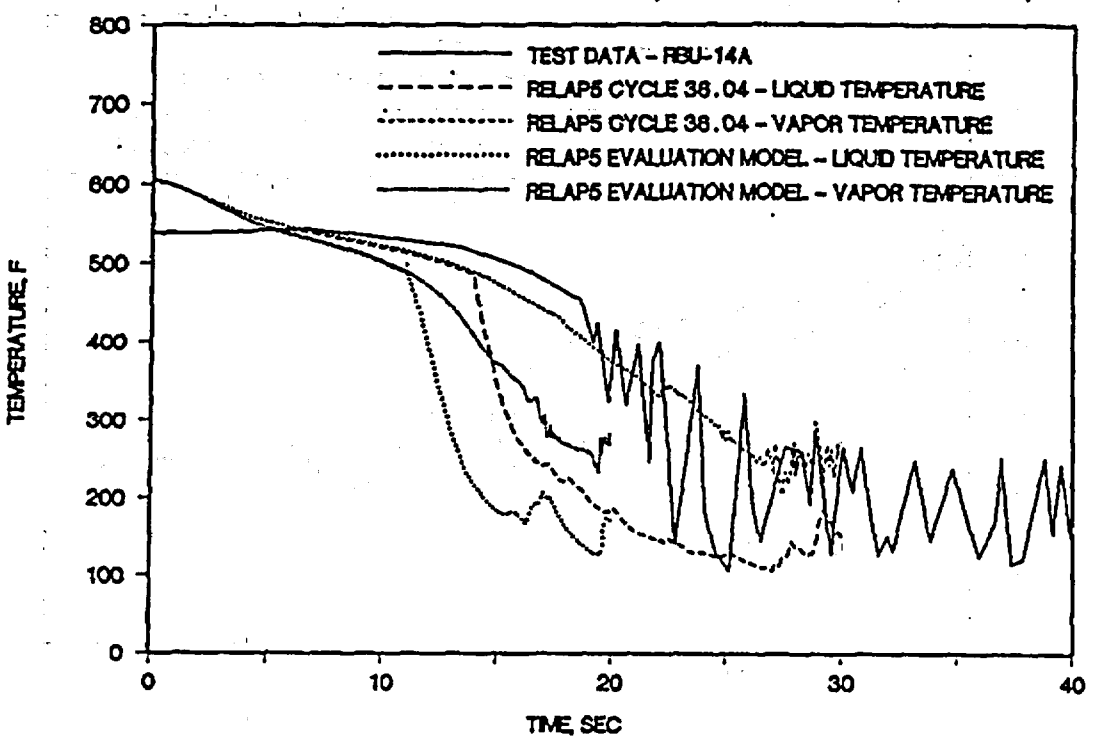


FIGURE G.1-28. SEMISCALE MOD1 TEST S-04-6; FLUID TEMPERATURE NEAR THE CORE INLET.

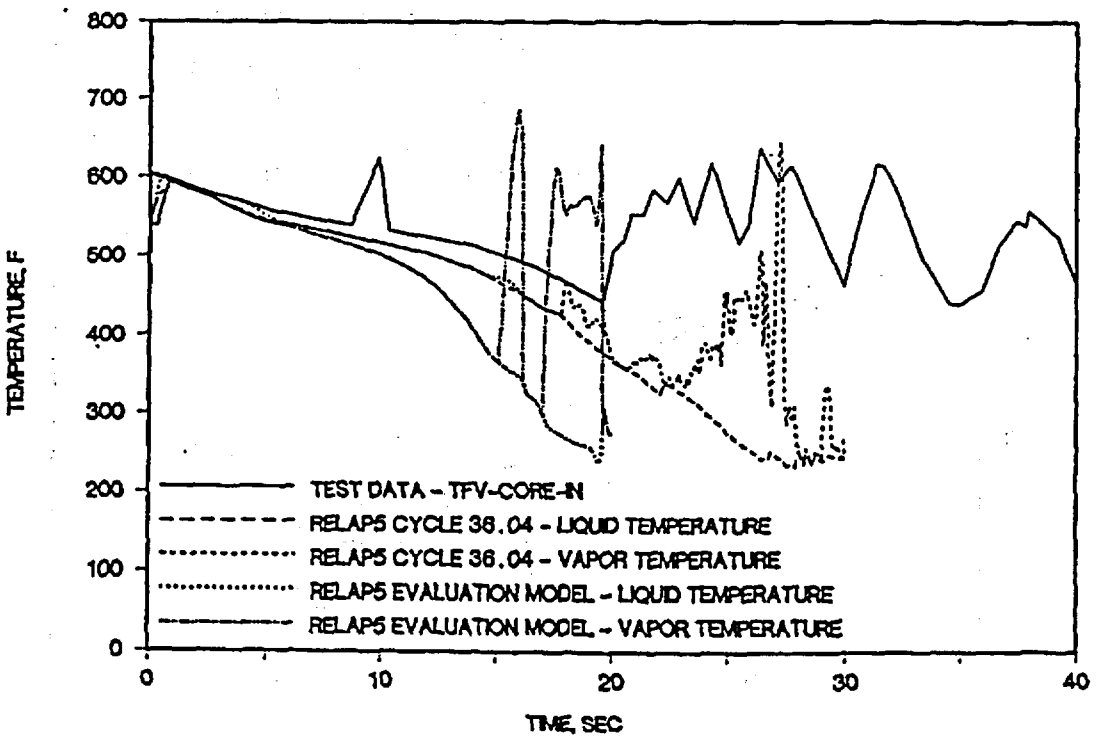

FIGURE G.1-29. SEMISCALE MOD1 TEST S-04-6; FLUID TEMPERATURE IN UPPER PLENUM.

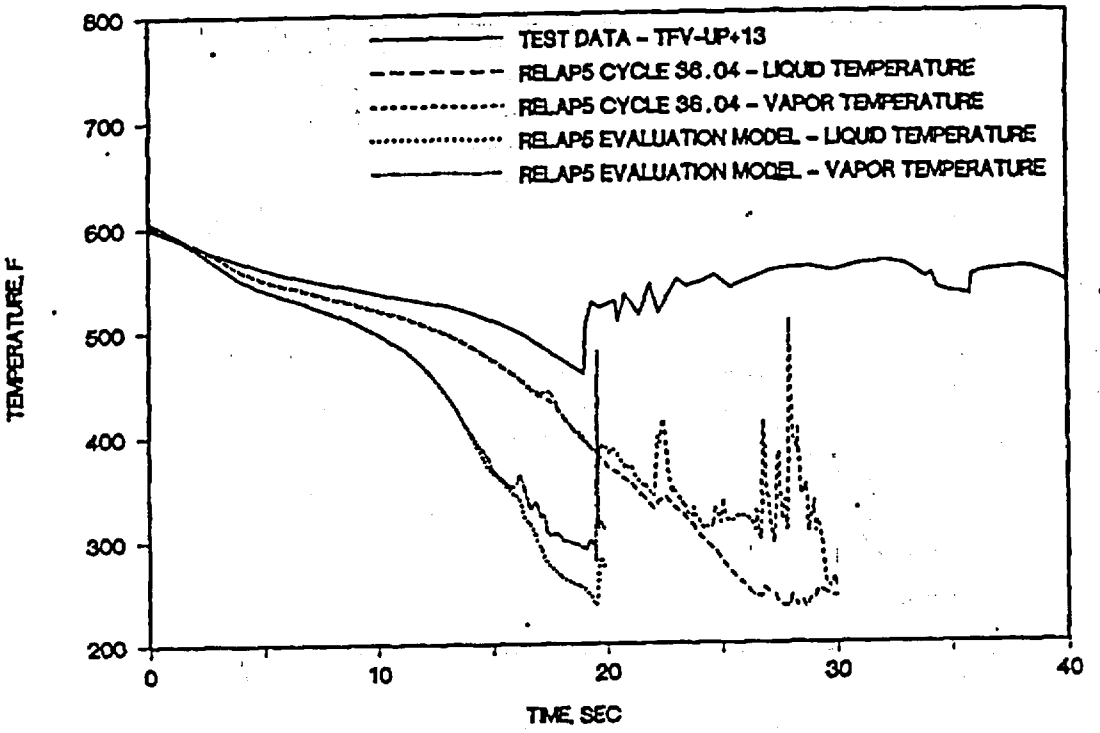


FIGURE G.1-30. SEMISCALE MOD1 TEST S-04-6; AVERAGE POWER ROD CLADDING TEMPERATURE AT PEAK POWER LOCATION.

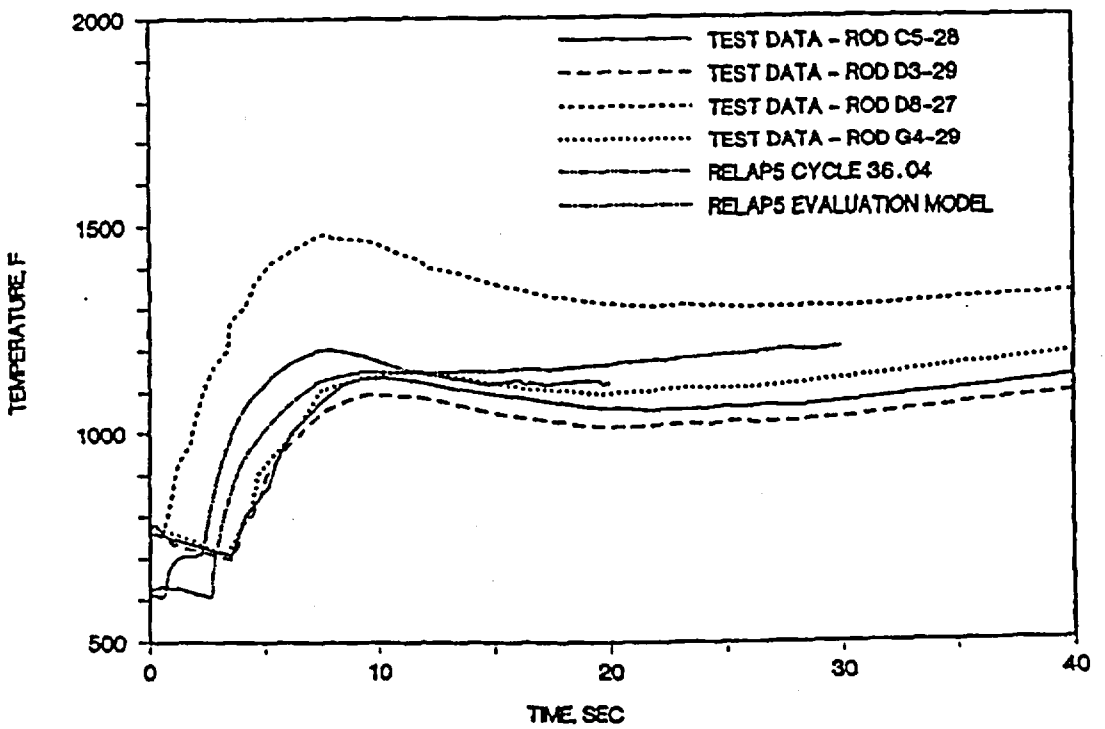

FIGURE G.1-31. SEMISCALE MOD1 TEST S-04-6; HIGH POWER ROD CLADDING TEMPERATURE NEAR PEAK POWER LOCATION.

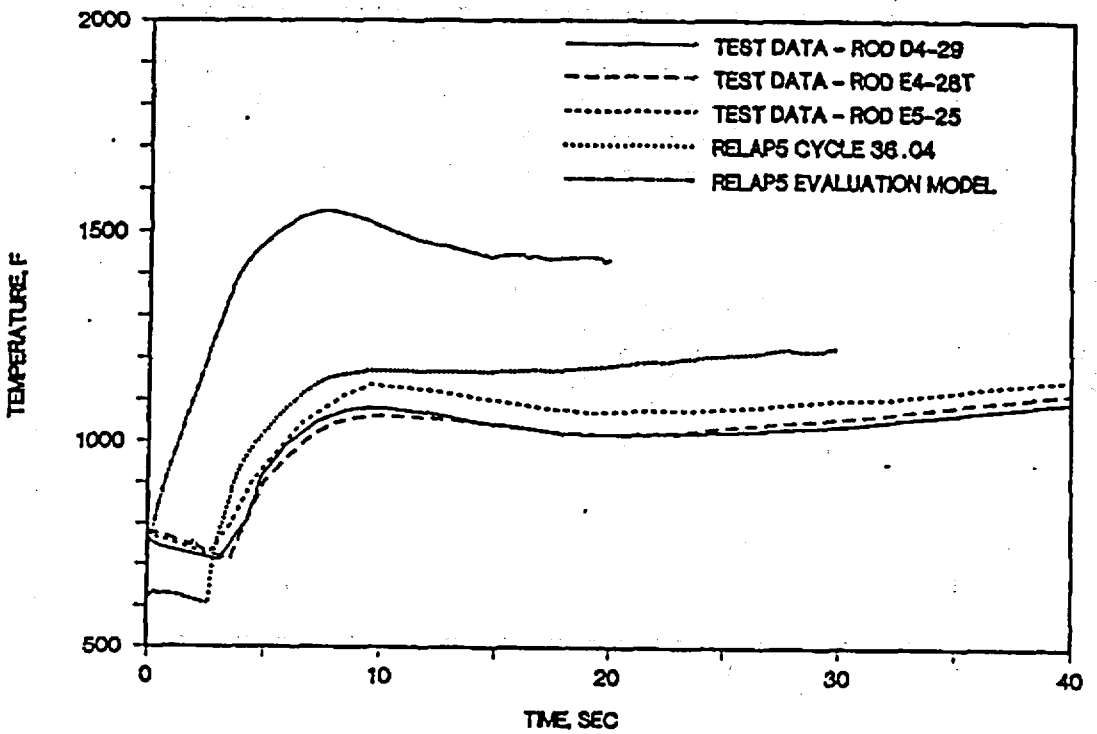

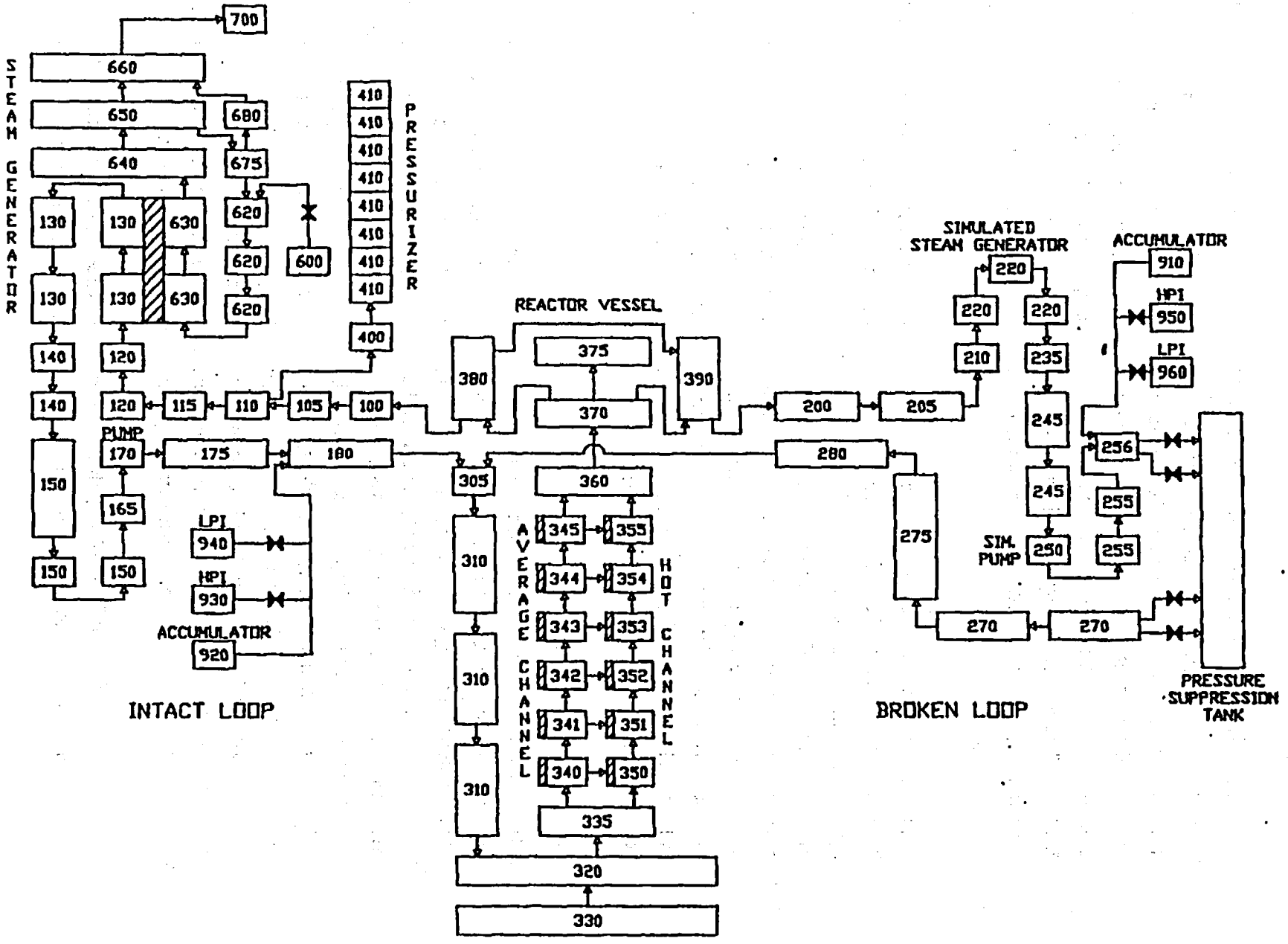


Figure G.1-32. RELAP5 Node and Junction Diagram.

## G.2. SBLOCA Benchmark of LOFT Experiment L3-5

Small break LOCA (SBLOCA) events are challenging to predict due to the variety of scenarios which may evolve during a transient. Particularly key to SBLOCA mitigation is continuous core energy removal via the break, steam generator, and absorption through ECCS fluid heating, while maintaining adequate vessel liquid inventory such that clad temperature excursions remain below 2200 F.

Vessel inventory is determined by system boundary flows (HPIS and break) and the liquid distribution within the reactor coolant system. In terms of code models, the system heat transfer, two-phase flow, and choked flow models predominately determine this behavior. Demonstration that these code models are adequate is provided through benchmark calculations. In particular, prediction of integral system transient tests from prototypical PWR scaled facilities provide a good measure of a code's ability to calculate SBLOCA phenomena.

### G.2.1. Introduction

LOFT experiment L3-5[4] was designed to investigate the response of the primary system to a SBLOCA. This experiment addresses the 4-inch diameter equivalent (2.5%) small break transient. The break was located in the intact loop cold leg pipe between the RC pumps and the reactor vessel inlet nozzle. The RC pumps were tripped immediately following leak initiation. This experiment was selected to benchmark the RELAP5/MOD2-B&W computer code because a 4-inch diameter break is characterized by a leak flow exceeding HPIS flow and by a relatively slow system depressurization since the steam generator becomes ineffective in removing decay heat, thereby resulting in a severe system inventory depletion.

The B&W version of RELAP5/MOD2 was benchmarked against the L3-5 experiment to demonstrate the analytical capability of the code

in predicting the various modes of a SBLOCA transient. The RELAP5 model for the L3-5 experiment was obtained from Appendix B of the report EGG-LOFT-5480.[2] The model was verified against the system design data provided in NUREG/CR-0247[3] (LOFT System and Test Description).

Section G.2.2 presents a description of the LOFT L3-5 experiment. The RELAP5 model is provided in section G.2.3 along with minor input changes that are required to achieve stable initial conditions. Section G.2.4 discusses the results of the analysis and compares the test data with the RELAP5 prediction. Conclusions are presented in section G.2.5.

## G.2.2. Description of Experiment

The LOFT integral test facility was designed to simulate the major components of a four-loop PWR, thereby producing data on the thermal, hydraulic, nuclear and structural processes expected to occur during a LOCA. As shown in Figure G.2-1, the experimental facility consists of the reactor vessel, intact loop (scaled to represent three operational loops), ECC system, broken loop, and blowdown suppression system. The reactor vessel contains 1300 66-inch long nuclear fuel rods with a total power output of 50 MWt. The intact loop includes a hot leg, a steam generator, the pressurizer, two parallel RC pumps and a cold leg. The broken loop is primarily used for large LOCA experiments and contains a hot leg, a steam generator, pump simulators, a cold leg, and isolation values. The ECCS is comprised of the accumulator system, the LPIS and the HPIS.

The L3-5 experiment simulates a small break depressurization with a 0.6374-inch diameter break orifice in the intact loop cold leg between the RC pump and the reactor vessel. The RC pump is tripped at leak initiation. The HPIS is injected into the reactor vessel downcomer, while the accumulator is isolated from the intact loop. The reactor was scrammed approximately 5

seconds before blowdown initiation. When the control rods were fully inserted, the intact cold leg blowdown was initiated. The RC pumps were manually tripped at 0.8 seconds after blowdown initiation. The sequence of events for the experiment is presented in Table G.2-2. HPIS flow was initiated automatically when the primary system pressure dropped to 1900 psia. The leak was isolated at 2309 seconds. The secondary system auxiliary feed pump was started at approximately 2 minutes after scram and was operated for about 30 minutes. The initial plant operating conditions are provided in Table G.2-1.

G.2.3. RELAP5 Model of LOFT L3-5

The RELAP5/MOD2-B&W computer code was used to perform the benchmark analysis of experiment L3-5. This code is based on a one-dimensional, two fluid, nonequilibrium hydrodynamic formulation and uses a finite difference scheme for both fluid paths and heated paths. Inputs for the basic RELAP5 model shown in Figure G.2-2 are contained in Appendix B of the LOFT report. As indicated in the report, this model was used in the post-test analysis of LOFT experiments L3-1, L3-5 and L3-6 by EG&G. The results of the post-test analysis demonstrated that this model can accurately simulate the overall system response to a SBLOCA, including the primary system pressure and inventory.

The nodalization used for the benchmark analysis is shown in Figure G.2-3. It is basically the same as that shown in Figure G.2-2 except minor changes made to the steam generator separator component and the HPIS. In the original nodalization, the separator arrangement shown in Figure G.2-2 is incorrect and results in an elevation discrepancy between the downcomer and the boiler sections. The revised separator model shown in Figure G.2-3 consists of a separator volume (500) and a bypass volume (503). Volume 503 will permit a direct path from the steam dome to the downcomer. The HPIS was injected via the ECCS piping (600) to the RV downcomer in the original model. Volume 60

caused flow instability due to steam backflow from the downcomer. This volume and junction 630 were removed from the original model including the LPIS, which was not used in the experiment. The revised model as shown in Figure G.2-3 permits HPIS injection directly into the downcomer.

The revised model for the L3-5 benchmark analysis consists of 116 volumes, 124 junctions and 120 heat structures. Inputs for the major components have been verified against the design data presented in the LOFT System and Test Description Report (NUREG/CR-0247) to assure that the model closely represents the LOFT system. A steady-state calculation was made to achieve the desired initial conditions. A comparison of the measured initial conditions with the calculated values is presented in Table G.2-1. Considering the discrete nature of steam generator heat transfer in RELAP5, the initialized primary system pressures and temperatures are acceptable for the benchmark analysis.

The transient analysis was performed using the basic Best Estimate (BE) option, INEL's RELAP5/MOD2 version 36.04. The Ransom-Trapp choked flow model with a discharge coefficient of 1.0, nonhomogeneous and nonequilibrium hydrodynamic modeling, and the original system CHF, heat transfer, and fuel pin models were used. The core heat generation was simulated with a tabular input of power versus time. An additional change was made during a restart at 200 seconds. The break nozzle volume, 181 in Figure G.2-2, caused severe leak flow oscillations. This volume is approximately 3.6% of the cold leg volume (180) and was removed at the restart to prevent flow instability. Volume 180 was used as the leak node for the remainder of the analysis.

## G.2.4. Transient Calculation

The blowdown was initiated 4.8 seconds after the reactor scram as shown in Table G.2-2, and the RC pumps were tripped 0.8 seconds after the blowdown initiation. The main feedwater flow was

terminated immediately following the reactor trip, and the auxiliary feedwater flow was started 67.8 seconds later. HPIS flow was initiated automatically when the primary system pressure dropped to 1900 psia. The calculated and measured core pressures are shown in Figure G.2-4. The calculated depressurization rate is slower than actually occurred during the initial subcooled phase of the blowdown, but exceeded the experiment thereafter as the primary system approached saturation. The post-test analysis in EGG-LOFT-5480 seems to confirm that RELAP5's Ransom-Trapp model underpredicts leak flow. In addition, the model tends to overpredict low quality two-phase flow, but underpredict high quality mixture flow as it occurred after 150 seconds. This flow characteristic has been verified by hand calculation using the HEM choked flow model with the same inlet conditions. Figure G.2-10 shows the calculated and measured leak node pressures. This figure demonstrates that the leak flowrate has a significant impact on the primary system depressurization rate for the 4-inch diameter equivalent break (2.5%). The short-term and long-term secondary side pressure responses are presented in Figures G.2-5 and G.2-11 respectively. It can be seen that RELAP5 predicted the secondary side pressure response quite well. The pressurizer liquid level is shown in Figure G.2-6. Again, this plot reflects the slower depressurization predicted by RELAP5. The pump coastdown and the loop flow degradation are shown in Figures G.2-7 and G.2-8 respectively. The measured loop flow does not seem to agree with the pump coastdown. This is probably caused by errors in flow measurement that were not quantified during the test.

In the RELAP5 calculation, the pumps coasted down in approximately 29 seconds. Natural circulation was calculated to occur thereafter, and reflux mode circulation was calculated at about 440 seconds. In this mode of cooling, vapor from the reactor core flows upward into the steam generator tubes where it is condensed. The condensate returns via the hot leg pipe to the reactor vessel. The reflux mode continued for the remainder of

the transient because the primary system pressure never dropped below the secondary side pressure due to the benchmarks slower primary system depressurization shown in Figure G.2-10. Injecting the HPIS directly into the primary system instead of the ECC piping resulted in good agreement between the calculated and measured flow rates as shown in Figure G.2-9.

G.2.5. Conclusion

The L3-5 experiment confirmed the dominance of the breakflow as the prime decay heat removal mechanism. Although there is a discrepancy between calculated and measured primary system depressurization as noted previously, the RELAP5 prediction of the L3-5 experiment is quite good. The code predicted the overall system response, including primary and secondary system pressure, pump coastdown, natural circulation, and long term core cooling. Correct characterization of the primary coolant pumps is not imperative to the proper simulation of the test because the pumps coasted down rapidly following the trip. But event times and depressurization rates are dependent upon proper characterization of the leak flow. The experimental data (Figure 35-7 in NUREG/CR-1695) shows a distinct liquid level in the cold leg piping 130 seconds after blowdown initiation. Thus, calculation of this stratification is important for accurate break mass flow calculation.

There are two core bypass flow paths as shown in Figure G.2-2. One is from the inlet annulus to the upper plenum and the other is the reflood assist bypass valve in the broken loop. These paths mitigate the differential pressure that can be developed across the reactor vessel as a result of steam generation in the core, and allow steam venting through the inlet annulus to the break without clearing the loop seal. Continuous primary system depressurization was observed in both the calculation and the test as shown in Figure G.2-10.

The comparison plots provided in the later part of this appendix demonstrate that the RELAP5 code is acceptable for SBLOCA simulation. The overall prediction was quite good confirming the code's predictive ability, which various other RELAP5 users have also observed through integral system SBLOCA calculations of tests from the OTIS, MIST, LOFT, and Semiscale test facilities. Numerous full size PWR plant transient calculations have also confirmed the predictive capabilities of the code. Based on these observations, the code has been demonstrated to be acceptable and reliable in predicting SBLOCA transient behavior for PWR geometries.

Table G.2-1. Initial Conditions for LOFT L3-5.

| Parameter | Measured Value * | RELAP5 Model |
|---|---|---|
| Primary System Mass Flow Rate (Kg/s) | 476.4 | 484.9 |
| Hot Leg Temperature (K) | 576. | 579.4 |
| Cold Leg Temperature (K) | 558. | 560.9 |
| Core Power Level (MW) | 49. | 48.9 |
| Pressurizer Water Volume ($m^3$) | 0.68 | 0.66 |
| Pressurizer Pressure (Pa) | 14.88E6 | 14.959E6 |
| Hot Leg Pressure (Pa) | 14.86E6 | 14.945E6 (V105) |
| SG Secondary Side Flow Rate (Kg/s) | 26.4 | 26.4 |
| SG Secondary Side Pressure (Pa) | 5.58E6 | 5.56E6 (V530) |
| SG Secondary Side Water Level (m) | 3.14 | 2.758 |

*Based on Nominal values in Table 2-2 of NUREG/CR-1695.

Table G.2-2. Sequence of Events for LOFT L3-5.

| Event | Time (sec) | |
|---|---|---|
| | Experiment* | RELAP5 |
| Reactor Scrammed | 0.0 | 0.0 |
| LOCA Initiated | 4.8 | 4.8 |
| RC Pump Tripped | 5.6 | 5.6 |
| HPIS Initiated | 8.8 | 10.6 |
| Pressurizer Emptied | 27.0 | 40.8 |
| RC Pump Coastdown | 35.0** | 20.0 |
| SG Auxiliary Feedwater Initiated | 67.8 | 67.8 |
| Secondary Side Pressure Exceeded Primary Side | 749.8 | -- |
| SG Auxiliary Feedwater Terminated | 1804.8 | -- |
| Leak Isolation | 2313.9 | 1500.0 |

*Based on data in Table 2-1 of NUREG/CR-1695.
**From Figure 35-45 in NUREG/CR-1695.

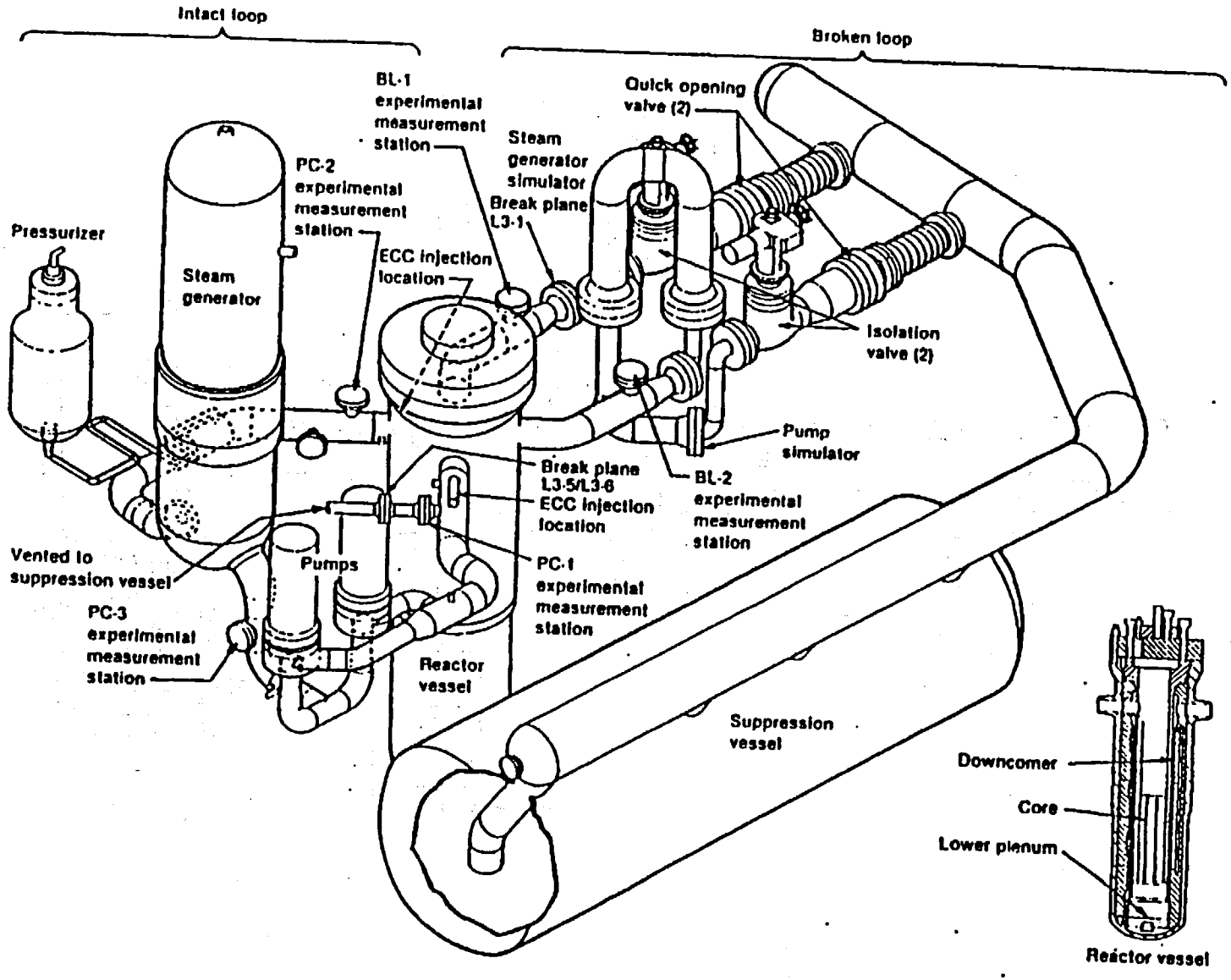


Figure G.2- 1. LOFT System Configuration.

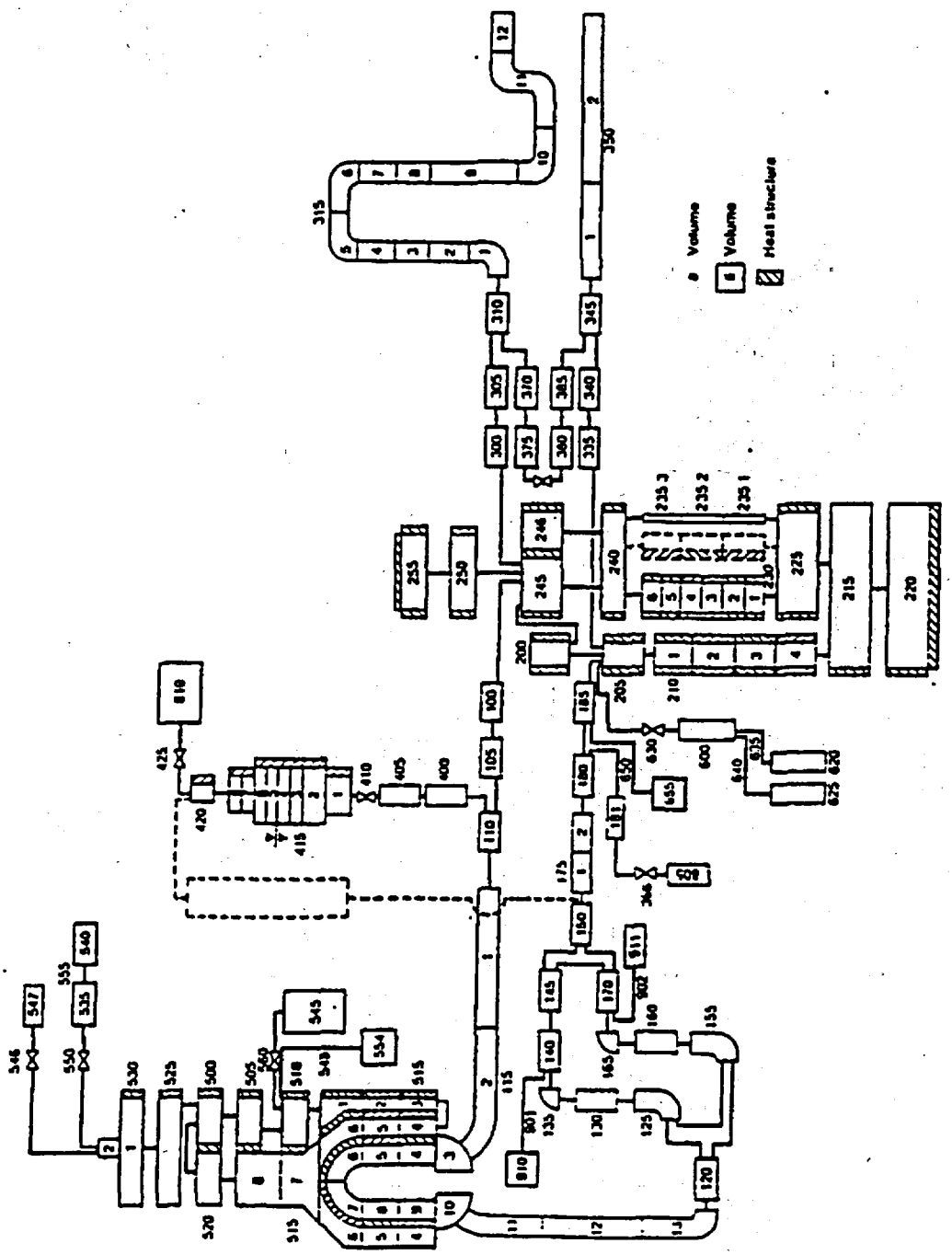


Figure G.2- 2. RELAP5 LOFT Nodalization for Test L-3-5.

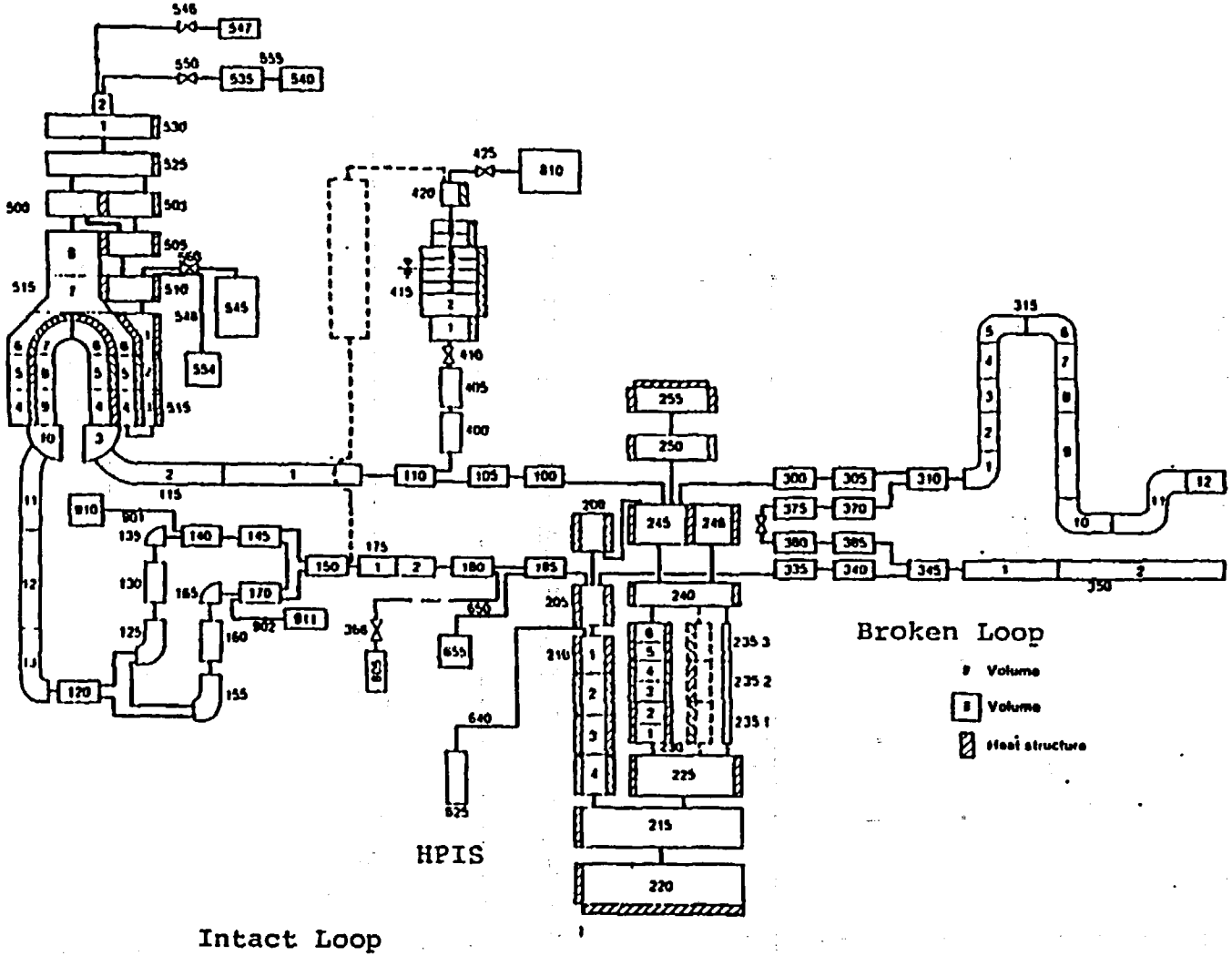


Figure G.2- 3. RELAP5 Nodalization for LOFT Test L-3-5 Benchmark Analysis.

FIGURE G.2-4. LOFT TEST L-3-5; CORE PRESSURE.

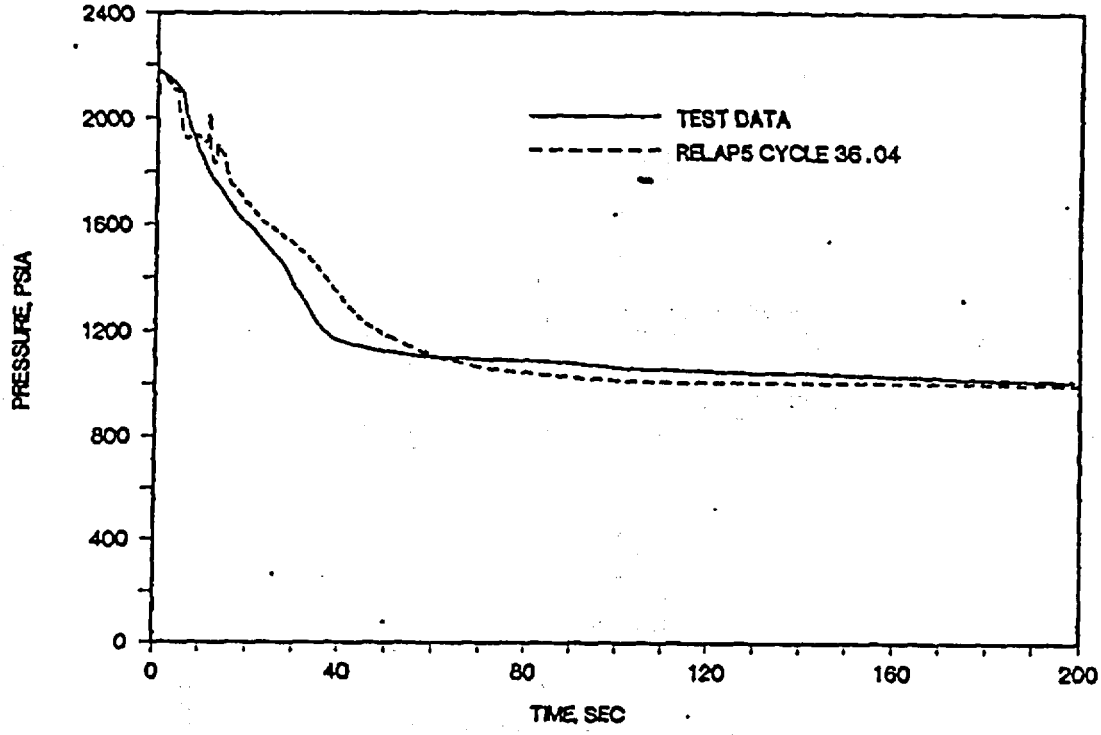


FIGURE G.2-5. LOFT TEST L-3-5; STEAM GENERATOR PRSSURE.

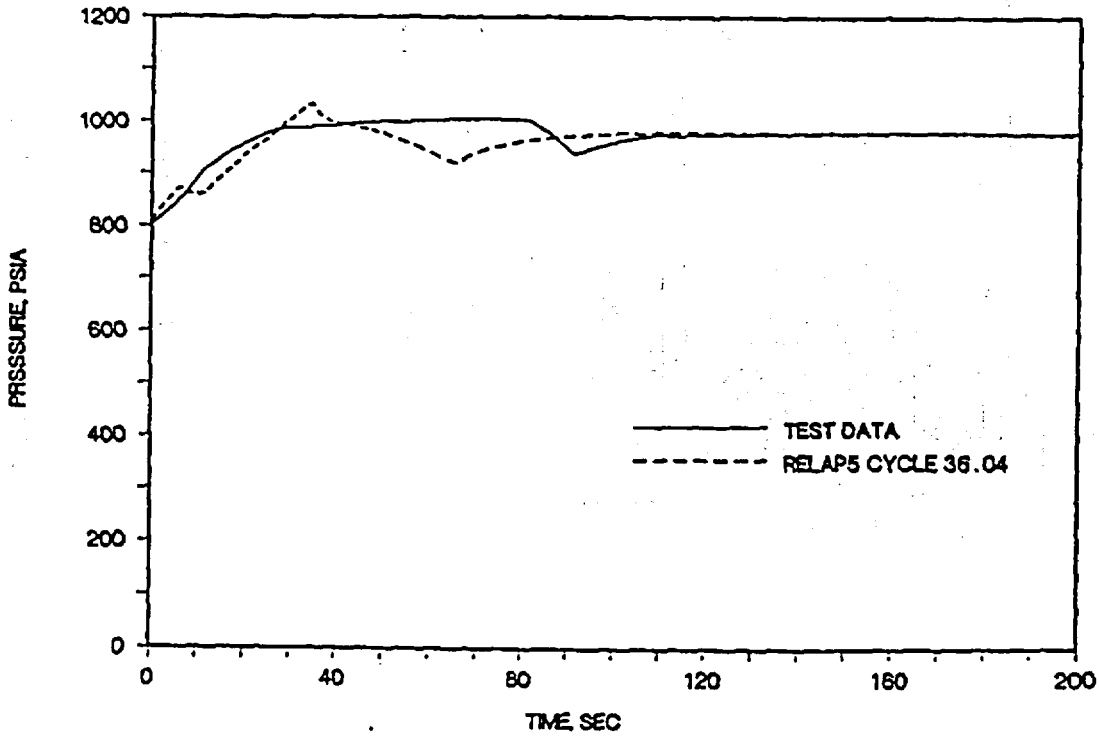

FIGURE G.2-6. LOFT TEST L-3-5; PRESSURIZER WATER LEVEL.

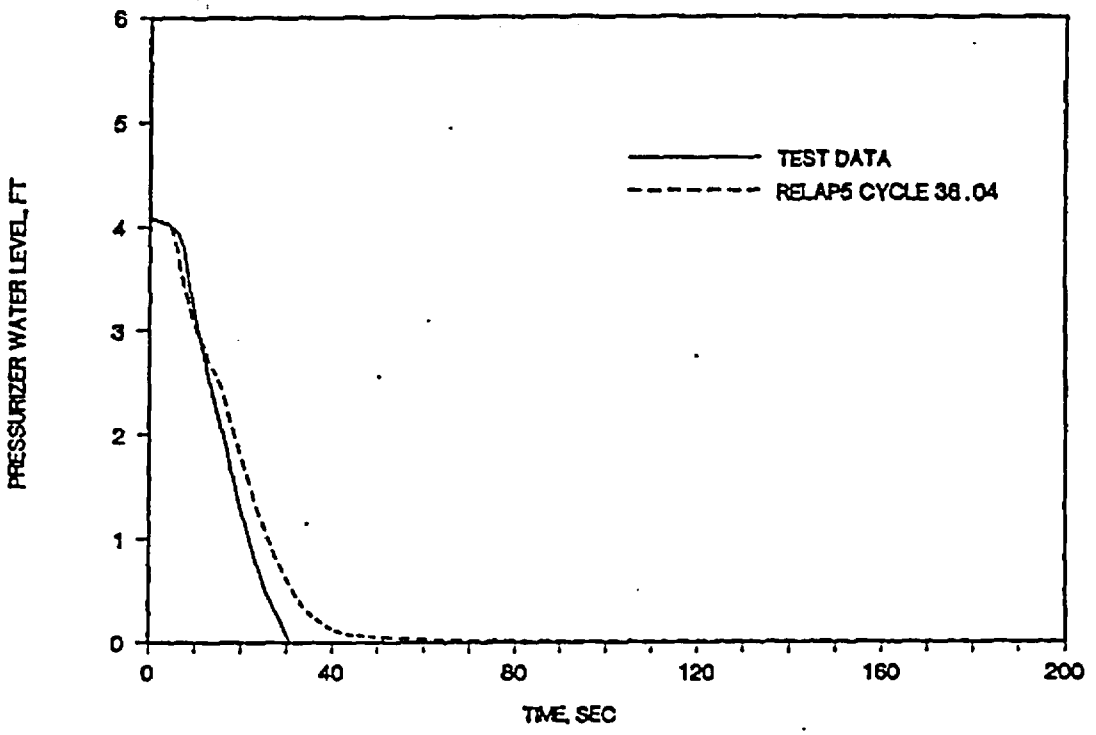


FIGURE G.2-7. LOFT TEST L-3-5; PUMP VELOCITY.

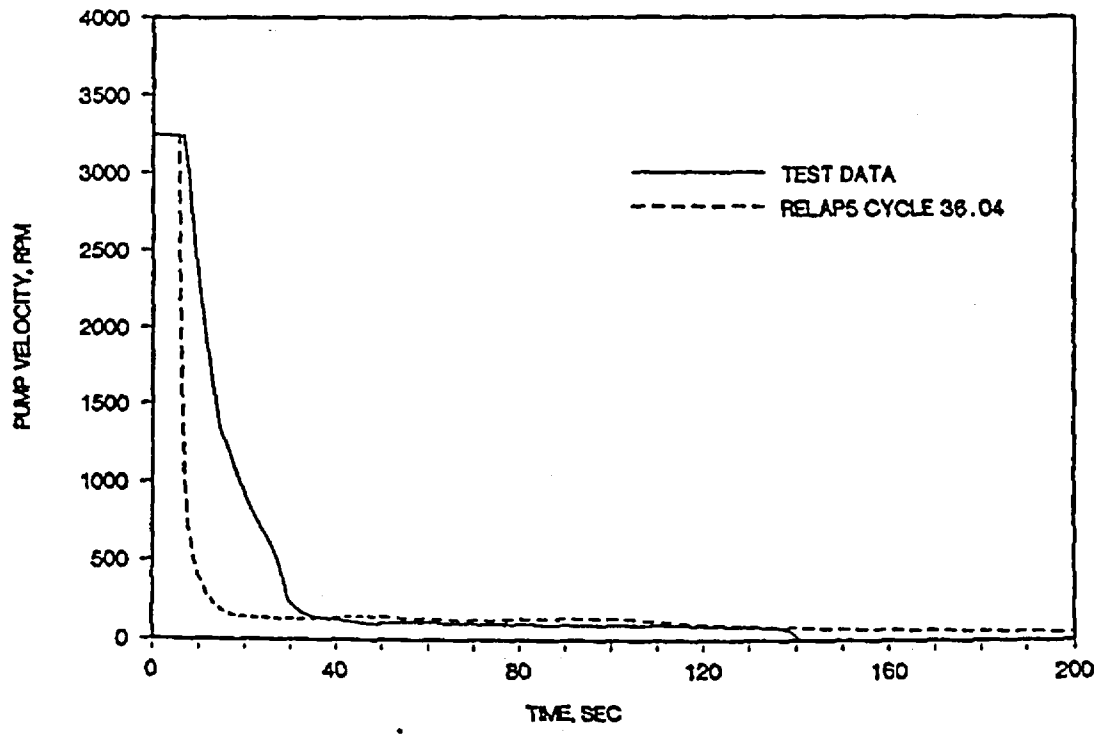

FIGURE G.2-8. LOFT TEST L-3-5; HOT LEG MASS FLOW RATE.

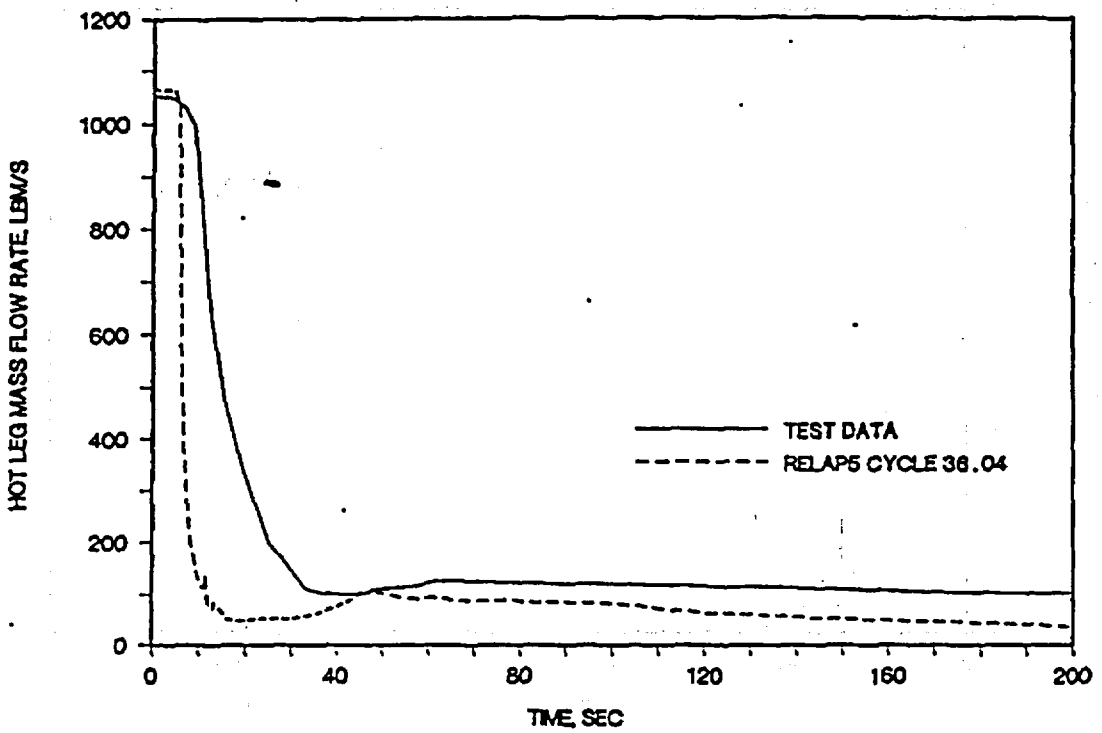


FIGURE G.2-9. LOFT TEST L-3-5; HPIS MASS FLOW RATE.

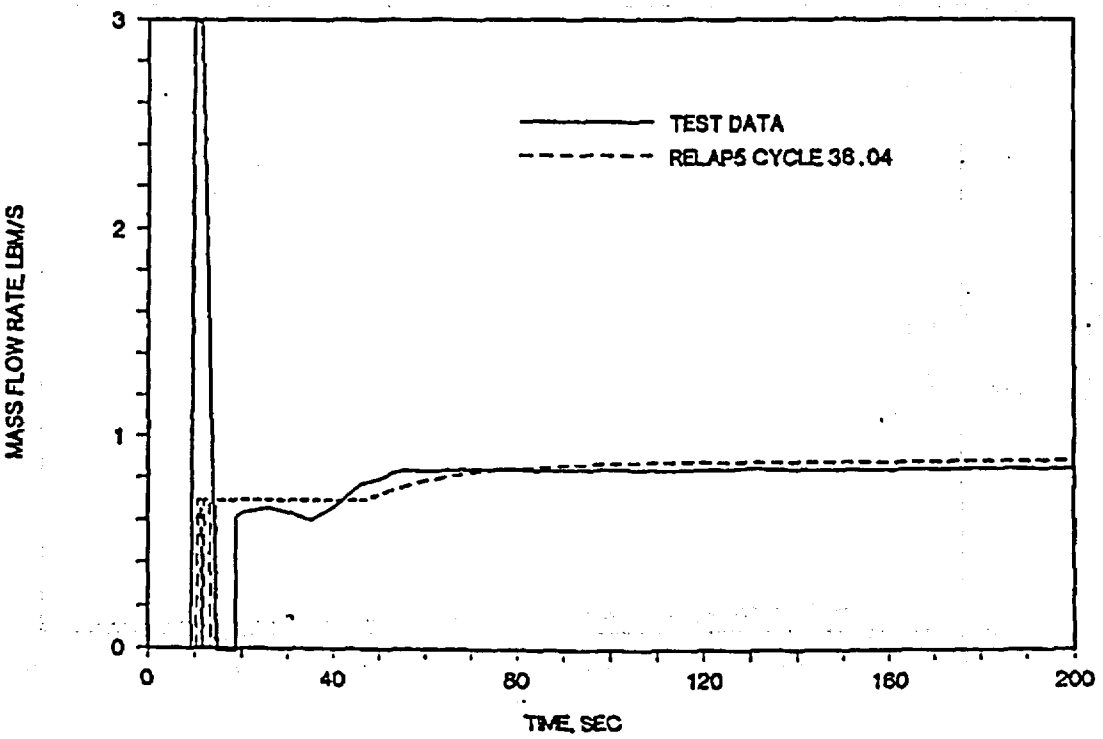

FIGURE G.2-10. LOFT TEST L-3-5; LEAK NODE PRESSURE.

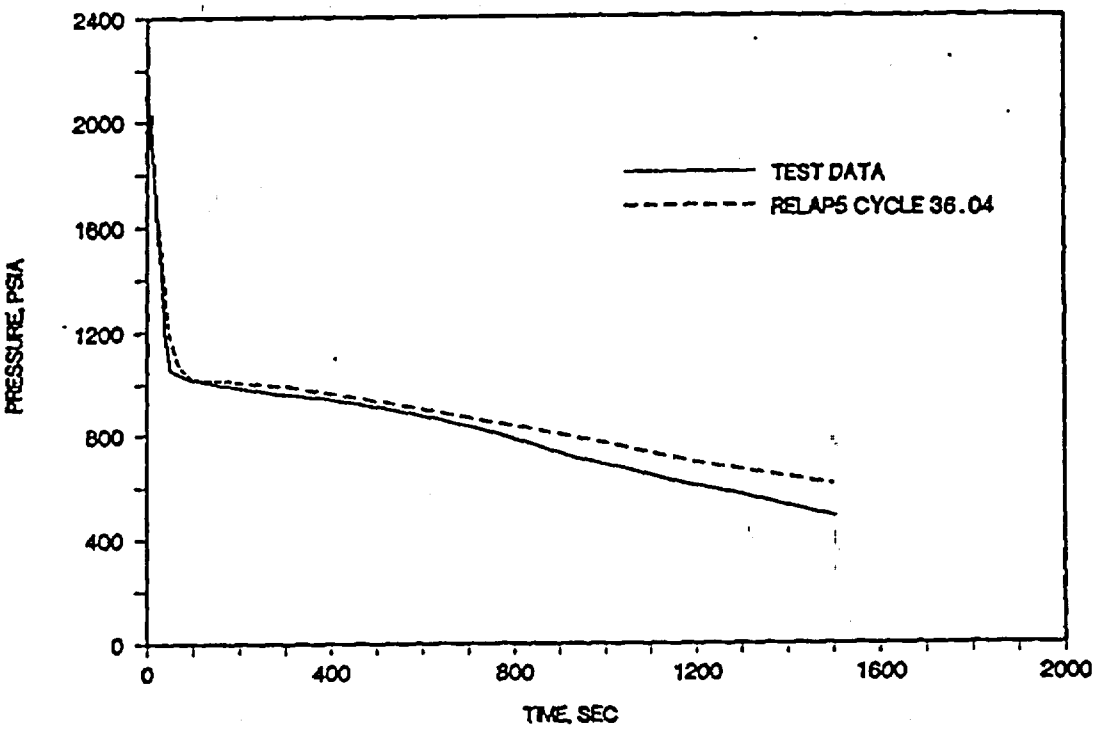


FIGURE G.2-11. LOFT TEST L-3-5; STEAM GENERATOR PRESSURE.

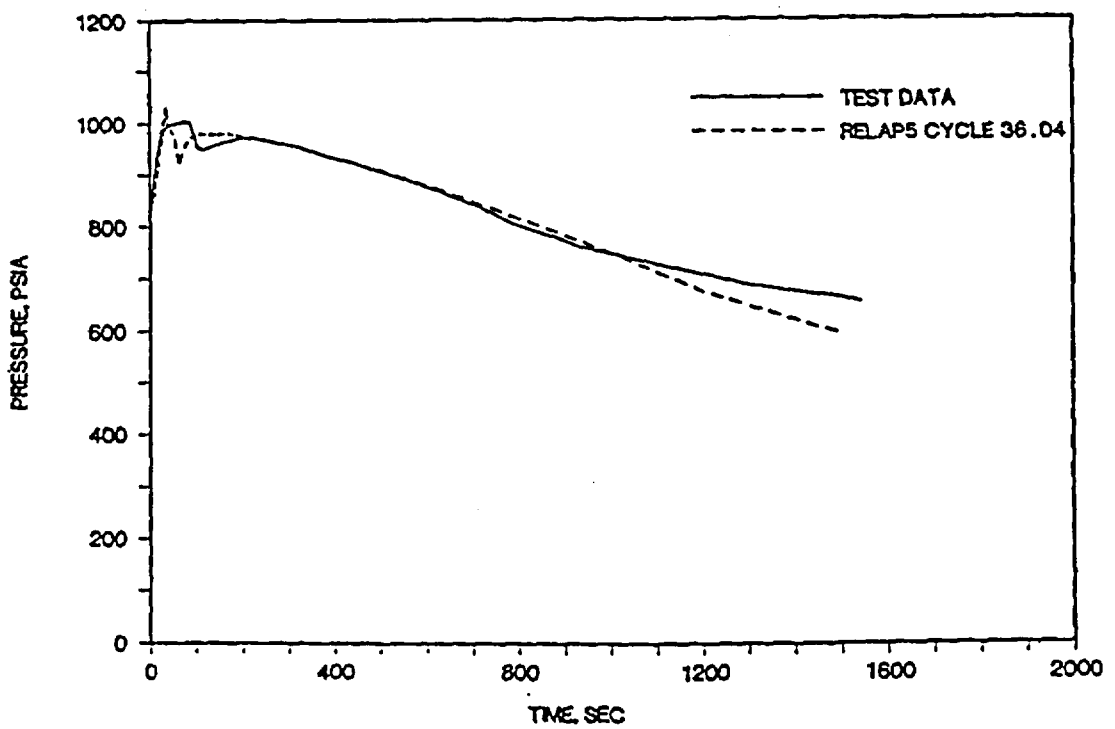

## G.3. Conclusion - Large and Small LOCA Benchmark

The B&W benchmark analyses of the large and small LOCA experiments (S-04-6 and L-3-5) show that the B&W RELAP5 code correctly calculates the major system variables during the blowdown, such as the primary and secondary system pressures, leak flows, and ECC injection. These parameters determine the system blowdown rate and mass inventory that significantly affect the fuel cladding temperature behavior during and after the blowdown. With accurately predicted blowdown hydraulic data an overall agreement in the cladding temperature between the calculation and the experiment can be assured. The results of the benchmark presented in the preceding pages have demonstrated that the RELAP5 code is adequate and reliable in predicting overall system thermal hydraulic responses to a LOCA. Furthermore, the results of the S-04-6 benchmark with the EM option indicate that the licensing model predicted a substantially higher cladding temperature and is conservative. The modeling techniques, such as nodalization and time step used in the benchmark analyses are consistent with those used in the PWR plant model. Thus, the benchmark analyses confirm that RELAP5 is adequate and conservative for application to the LOCA simulation in a PWR.

# APPENDIX H

## WILSON DRAG MODEL BENCHMARKS

Note: This appendix was originally added in its entirety in Revision 2 of BAW-10164, August, 1992.

In this appendix, Wilson drag benchmarks are compared with the NRC-approved code FOAM2 and with small break LOCA experiments performed at the Thermal-Hydraulic Test Facility (THTF), Oak Ridge National Laboratory (ORNL). The Wilson drag model is explained in section 2.1.3 of this topical report. The RELAP5/MOD2-B&W results for steady-state conditions are compared with FOAM2 calculations in Section H.1 and with Oak Ridge THTF data in section H.2; conclusions are given in section H.3.

Comparison of RELAP5/MOD2-B&W with FOAM2 Results

The NRC-approved computer code FOAM2[140] aids in analysis of small break loss-of-coolant accidents (SBLOCA). Its main objective is to determine, based on core void distribution, whether at any time during an SBLOCA transient the water content of the reactor core (as calculated by an appropriate LOCA code, such as RELAP5) is sufficient to cover the entire heated core with a combination of water and steam-water froth. If it determines that the core is uncovered, it calculates the swell level and steaming rate corresponding to the input core water content. If no core uncovery occurs, it will, at the user's option, calculate the mass flow and steaming rates.

RELAP5/MOD2-B&W estimates slug drag using the Wilson bubble rise correlation, whereas FOAM2 uses the Wilson bubble rise correlation[135] to directly calculate the core void distribution. FOAM2 does not include the B&W modification for the flow regime above $\alpha_g^* = 6.526$. Therefore, the core void distribution calculated by RELAP5/MOD2-B&W should be similar to FOAM2 results with potential for deviations at higher void fractions (that is, for j=3 in Equation 2.1.3-30.5).

A hypothetical reactor core was modeled as shown in Figure H.1. Low power steady-state RELAP5/MOD2-B&W cases were run for a variety of reactor powers (1.5 to 5.0% of full power) and

pressures (100 to 1600 psia); void profiles were compared with FOAM2 cases with the same water levels as were calculated by RELAP5. A listing of the RELAP5 cases is presented in Table H-1 and compared in Figures H.2 through H.13. RELAP5 data are plotted at the midpoint of each node because RELAP5 calculates an average void fraction for each node. It is assumed that void fraction changes linearly within all nodes, except the first node in which it is assumed that the inlet void fraction is zero.

Figures H.2 through H.13 demonstrate that, for equal core liquid inventories, RELAP5/MOD2-B&W acceptably predicts the void distributions and mixture levels calculated by FOAM2. Differences in mixture level for low pressure cases are caused partly by greater depletion of liquid inventory by RELAP5 at lower elevations, as compared to FOAM2, for which compensation is made at higher elevations.

Comparison with ORNL THTF Experiments[141]

The Thermal-Hydraulics Test Facility (THTF) is a large high pressure non-nuclear thermal-hydraulics loop. The facility was designed to simulate the thermal-hydraulics of a small-break loss-of-coolant accident (SBLOCA). The facility configuration is shown in Figure H.14.

The test section bundle contained 60 electrically-heated rods and four unheated rods which simulated control rod guide tubes. Rod diameter and pitch were typical of a 17 x 17 fuel assembly. Further details on the facility configuration and instrumentation is found in Reference 141.

The RELAP5 model for the THTF test loop is shown in Figure H.15. THTF runs 3.09.10i through 3.09.10n and 3.09.10aa through 3.09.10[141] were simulated using RELAP5/MOD2-B&W. The test conditions, which were also used as input to RELAP5, are given in

Table H.2. The axial power distribution of the test bundle was uniform.

Comparison of void distributions for all tests are shown in Figure H.16 through H.27. RELAP5/MOD2-B&W tends to predict slightly higher void fractions below the mixture level than the ORNL data. An adjustment has been made of the plots of ORNL data for which dryout occurred (which was true in all cases except 3.09.10i, cc, and ee). In Reference 141, the ORNL data was given at the centerline of intervals between pressure taps. This is appropriate for intervals in which there is a quasi-linear increase in void fraction within the interval, but not appropriate for dryout intervals. Near the dryout point, it is assumed that the void fraction within the dryout interval continued to increase at the same rate as the pre-dryout interval; the mixture level was calculated by determining the point along the extended slope at which the total area under the curve in the dryout interval would match the average void fraction. After making this adjustment, mixture level is quite well predicted.

Figures H.28 through H.33 compare RELAP5 calculated core vapor and cladding temperatures with ORNL THTF data. These figures show that RELAP5 is quite accurate, but slightly conservative in predicting the ORNL temperatures. The dip in the ORNL data at 11.0 ft is caused by grid effects on the heat transfer rate[141], which is not accounted for in the RELAP5 model. In case 3.09.10i, an anomolous surface temperature occcurs at an elevation of 2.7 meters; this is caused by the overly conservative temperature prediction of the Condie-Bengston IV film boiling correlation used at this point compared to the less conservative predictions of the McEligot single-phase vapor convection correlation applied at higher elevations. Given the overall complexity of the ORNL tests, RELAP5/MOD2-B&W achieved

excellent comparability of mixture level and clad temperature response.

## Conclusions

Comparison of RELAP5/MOD2-B&W benchmark cases with equivalent runs using the NRC-approved code FOAM2 and with ORNL THTF small break LOCA experiments shows good agreement between results. It is concluded that the Wilson drag option used to calculate interfacial drag in RELAP5-B&W, does a good job of matching void distributions and mixture levels calculated by the NRC-approved code FOAM2 and measured by ORNL small break LOCA experiments.

Table H.1. FOAM2 Comparison Benchmark Cases.

| Case | Power (percent) | Pressure (psia) | Equivalent Water Level (ft) |
|---|---|---|---|
| 1 | 5.0 | 100 | 2.77303 |
| 2 | 5.0 | 200 | 3.68117 |
| 3 | 5.0 | 400 | 3.74587 |
| 4 | 5.0 | 600 | 5.15504 |
| 5 | 5.0 | 800 | 4.32935 |
| 6 | 5.0 | 1200 | 3.95712 |
| 7 | 2.5 | 100 | 3.82168 |
| 8 | 2.5 | 400 | 4.51021 |
| 9 | 2.5 | 800 | 6.38204 |
| 10 | 2.5 | 1200 | 6.33372 |
| 11 | 1.5 | 1200 | 7.99433 |
| 12 | 1.5 | 1600 | 7.34294 |

Table H.2. ORNL Thermohydraulics Test Facility (THTF) Benchmark Cases.

| Case | Experiment | Pressure (psia) | Power Density (kw/ft) | Mass Flux ($lbm/hr/ft^2$) |
|---|---|---|---|---|
| 13 | 3.09.10i | 0.68 | 650 | 21943.9 |
| 14 | 3.09.10j | 0.33 | 610 | 9333.4 |
| 15 | 3.09.10k | 0.10 | 580 | 2306.5 |
| 16 | 3.09.10l | 0.66 | 1090 | 21461.4 |
| 17 | 3.09.10m | 0.31 | 1010 | 9313.0 |
| 18 | 3.09.10n | 0.14 | 1030 | 3395.2 |
| 19 | 3.09.10aa | 0.39 | 590 | 14938.7 |
| 20 | 3.09.10bb | 0.20 | 560 | 6961.9 |
| 21 | 3.09.10cc | 0.10 | 520 | 3706.1 |
| 22 | 3.09.10dd | 0.39 | 1170 | 14615.7 |
| 23 | 3.09.10ee | 0.19 | 1120 | 8111.9 |
| 24 | 3.09.10ff | 0.08 | 1090 | 3561.1 |

*Revised Table H.2 shown on page 5-260 per SER instruction on Table 2 (page 5-364).*

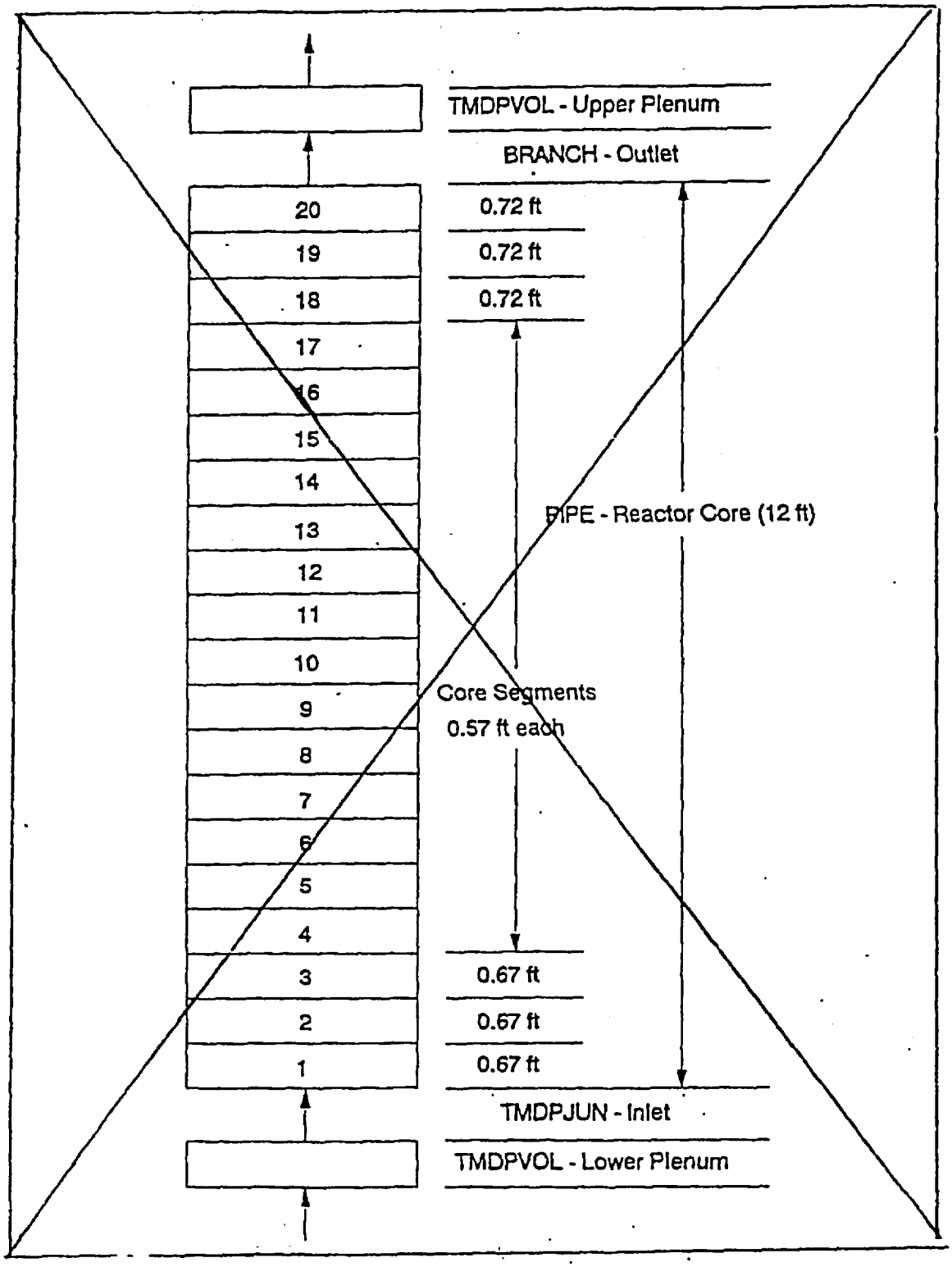


Figure H.1. RELAP5 Model of Hypothetical Reactor Core.

*Revised Figure H.1 shown on page 5-257 per SER instruction on Table 2 (page 5-364).*

Figure H.2. Comparison of RELAP5 and FOAM2 Predictions: 5% Decay Power, 100 Psia.

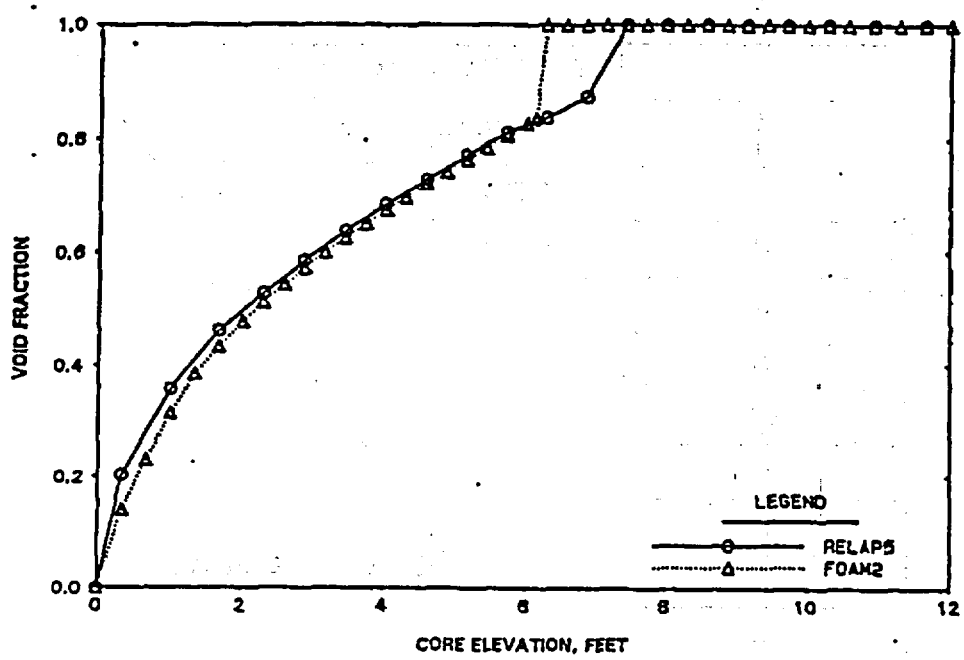


Figure H.3. Comparison of RELAP5 and FOAM2 Predictions: 5% Decay Power, 200 Psia.

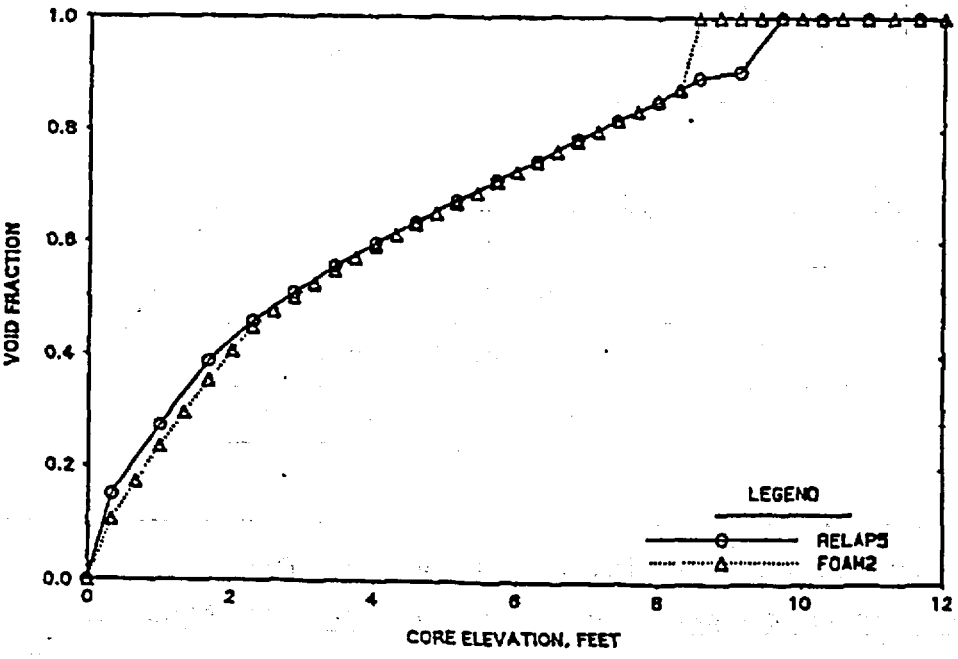

Figure H.4. Comparison of RELAP5 and FOAM2 Predictions:
5% Decay Power, 400 Psia.

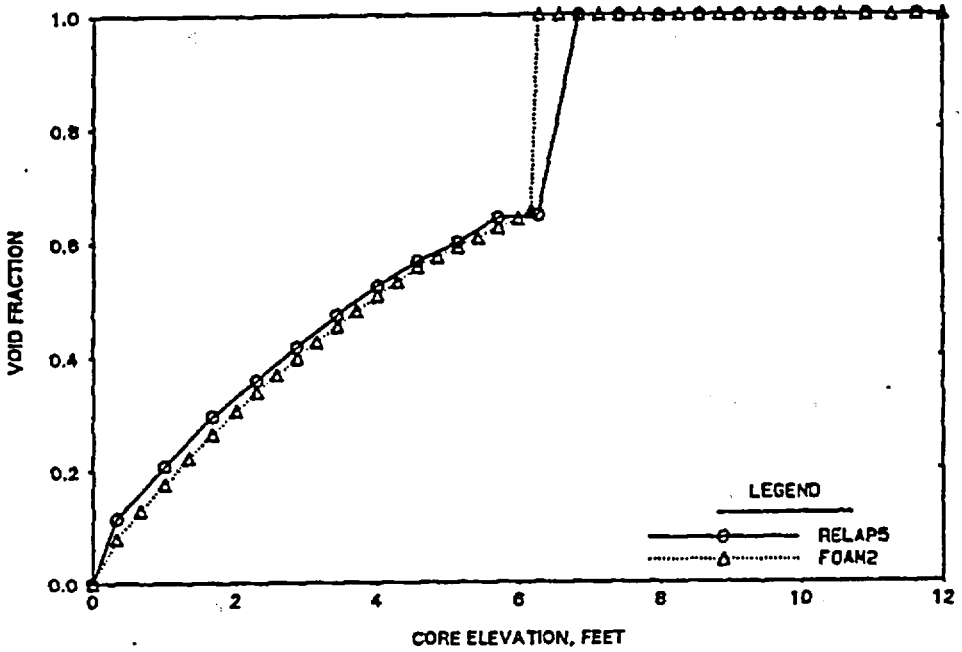


Figure H.5. Comparison of RELAP5 and FOAM2 Predictions:
5% Decay Power, 600 Psia.

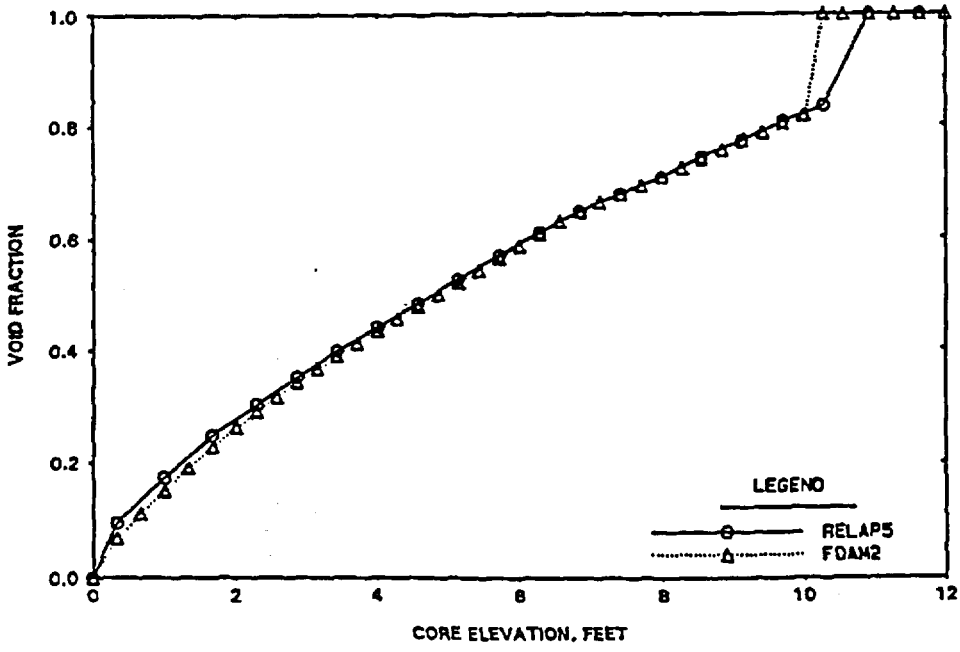

Figure H.6. Comparison of RELAP5 and FOAM2 Predictions:
5% Decay Power, 800 Psia.

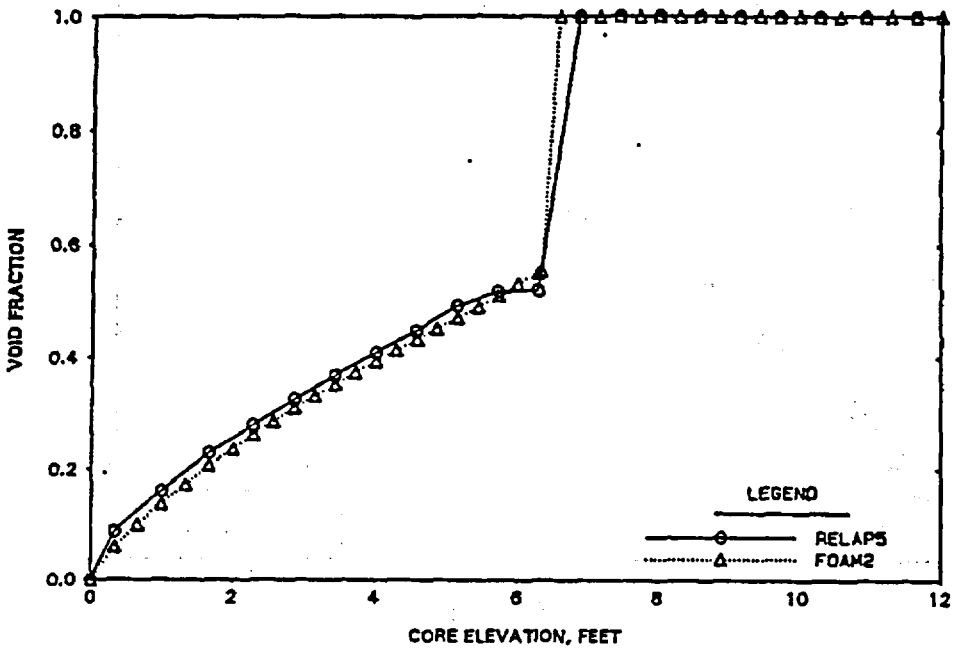


Figure H.7. Comparison of RELAP5 and FOAM2 Predictions:
5% Decay Power, 1200 Psia.

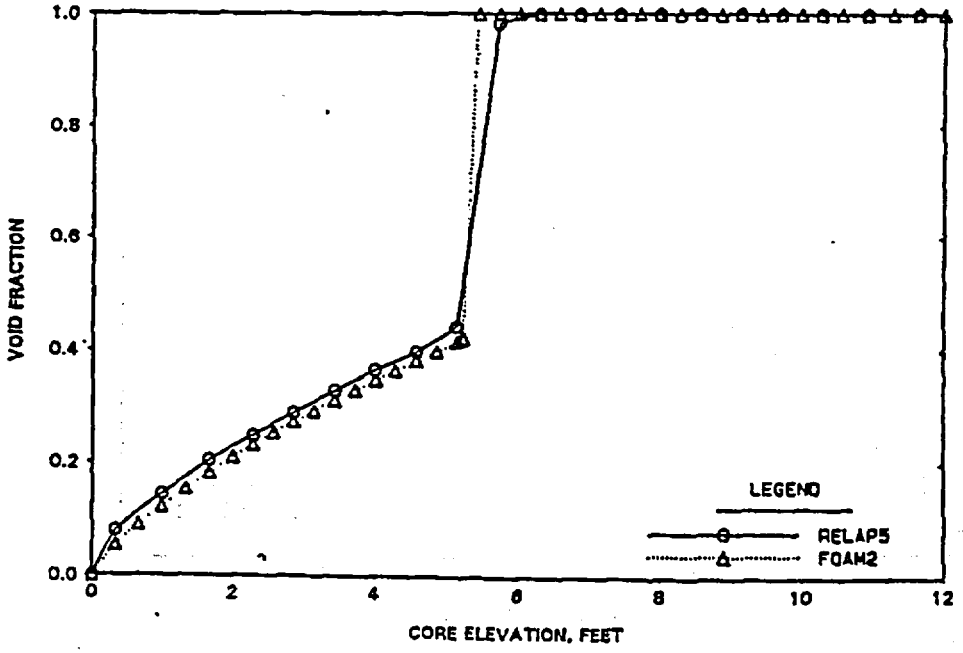

Figure H.8. Comparison of RELAP5 and FOAM2 Predictions:
2.5% Decay Power, 100 Psia.

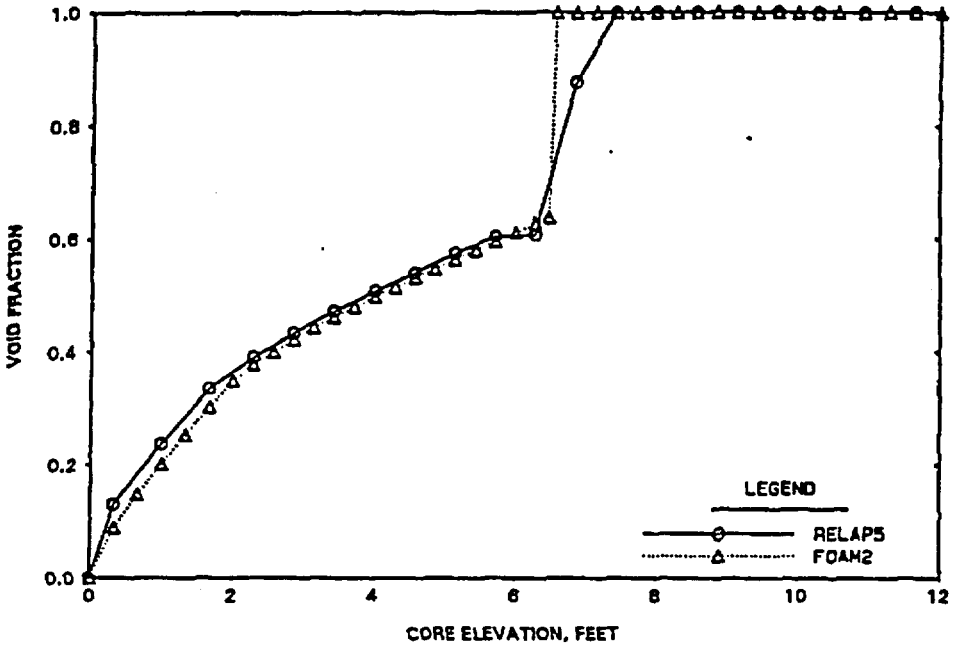


Figure H.9. Comparison of RELAP5 and FOAM2 Precdictions:
2.5% Decay Power, 400 Psia.

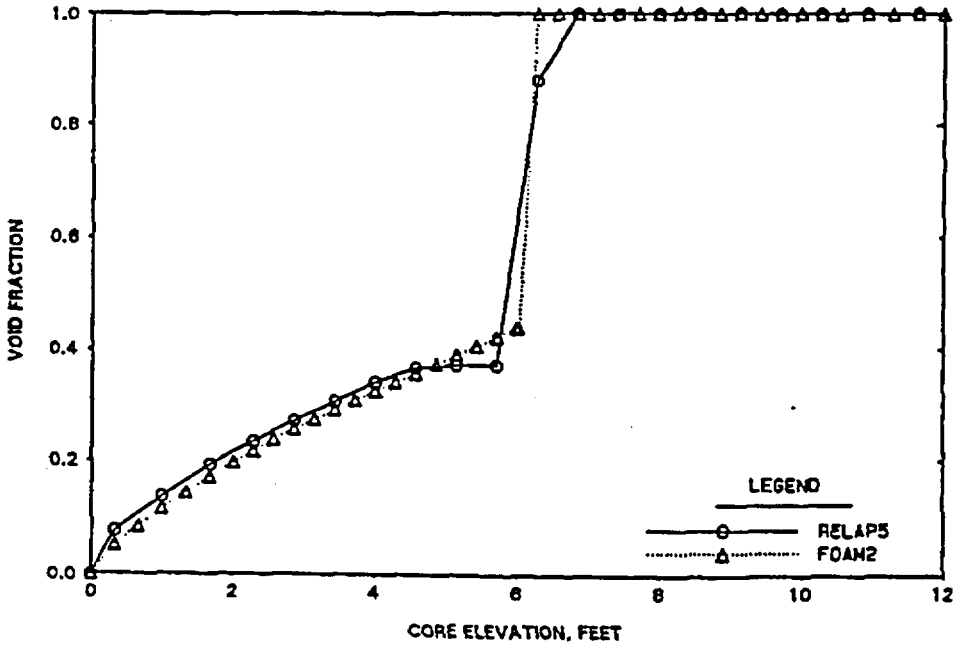

Figure H.10. Comparison of RELAP5 and FOAM2 Predictions: 2.5% Decay Power, 800 Psia.

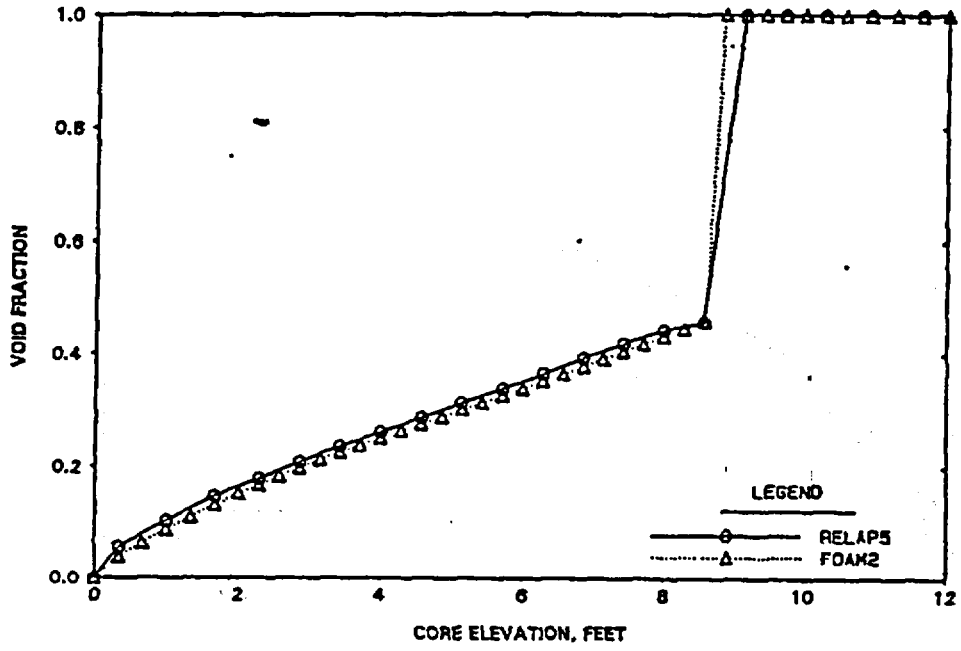


Figure H.11. Comparison of RELAP5 and FOAM2 Predictions: 2.5% Decay Power, 1200 Psia.

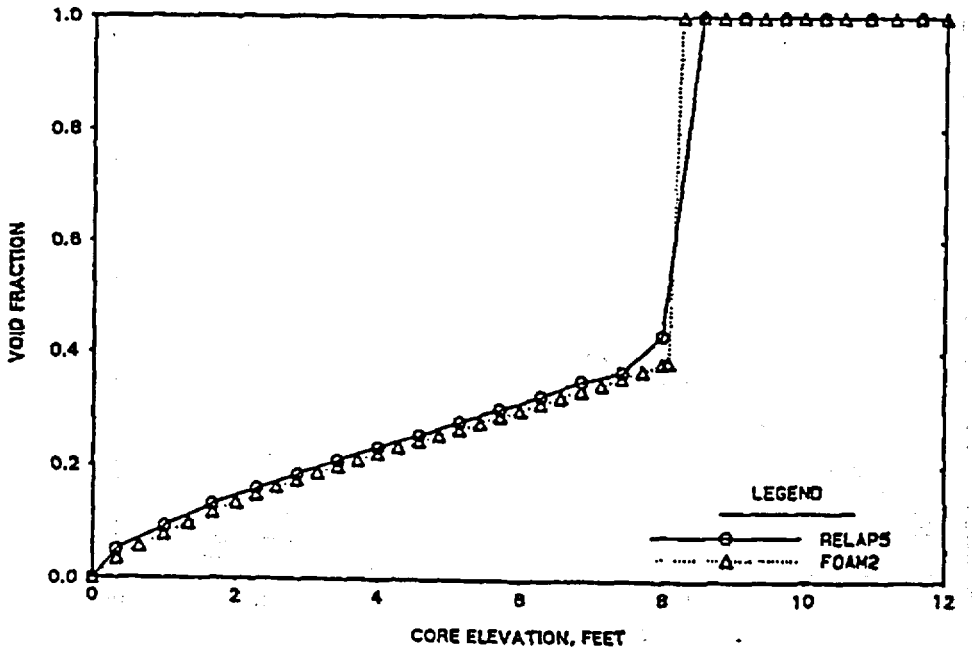

Figure H.12. Comparison of RELAP5 and FOAM2 Predictions:
1.5% Decay Power, 1200 Psia.

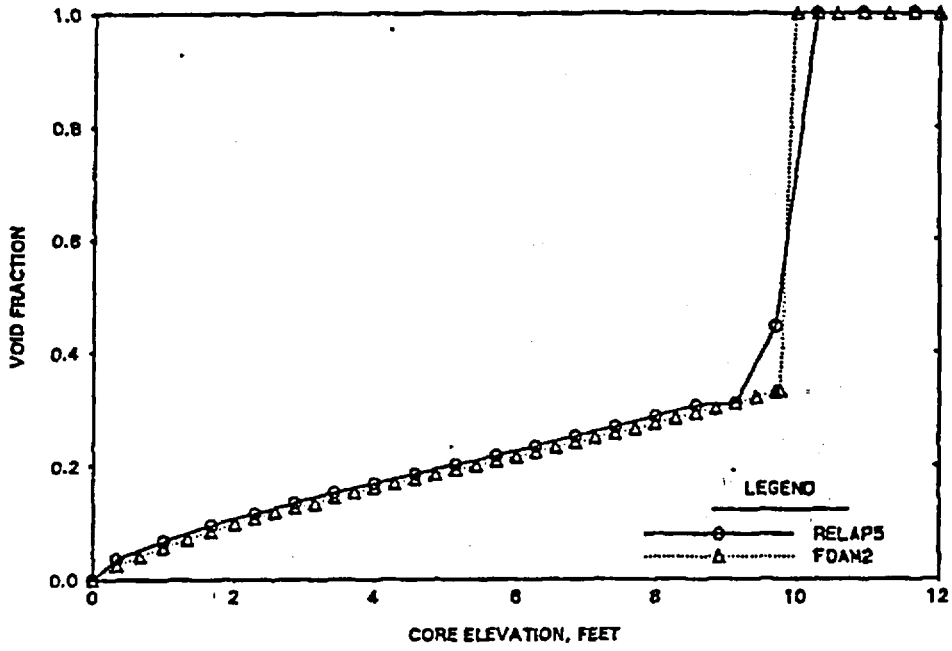


Figure H.13. Comparison of RELAP5 and FOAM2 Predictions:
1.5% Decay Power, 1600 Psia.

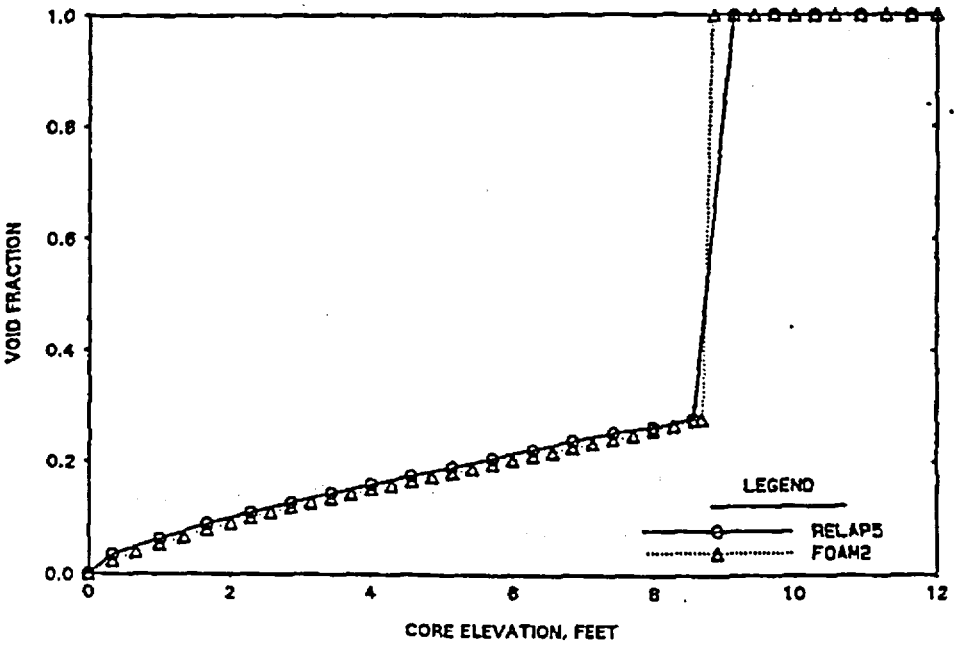

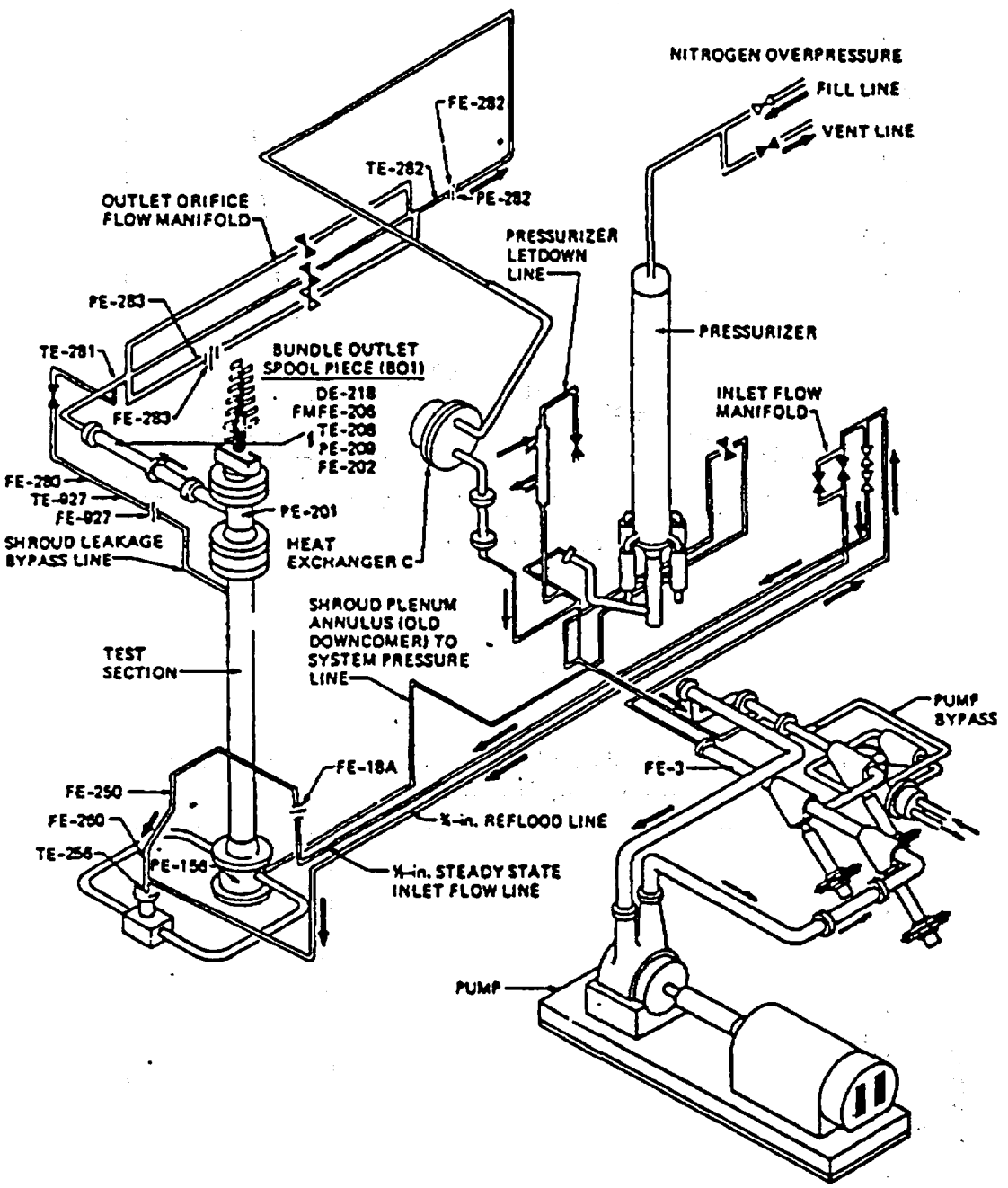


Figure H.14 - THTF in small break test configuration (Reference 141).

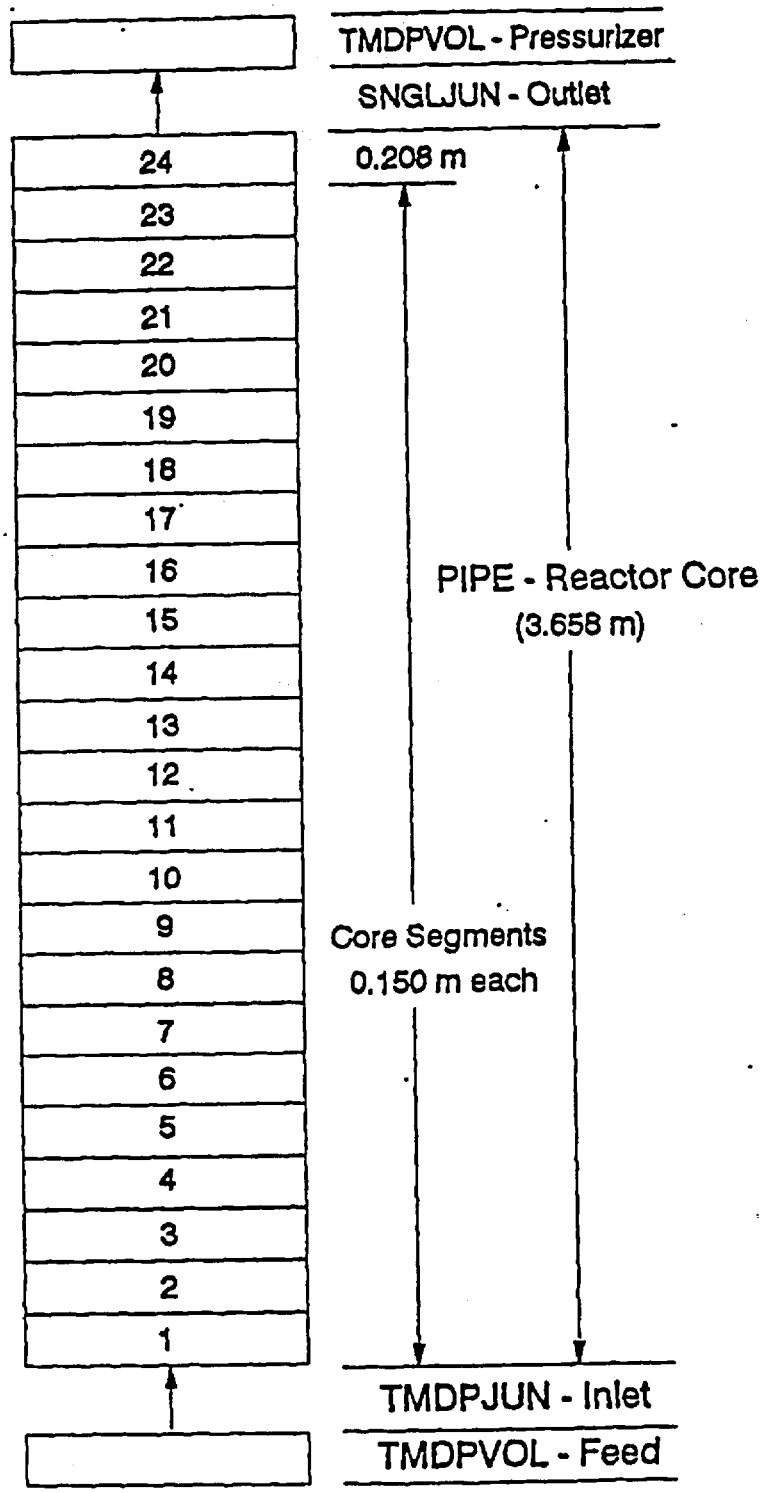


Figure H.15. RELAP Model of ORNL Thermal-Hydraulic Test Facility (THTF).

Figure H.16. Comparison Between RELAP5 Prediction and ORNL Test Data: 0.68 Kw/ft, 650 Psia.

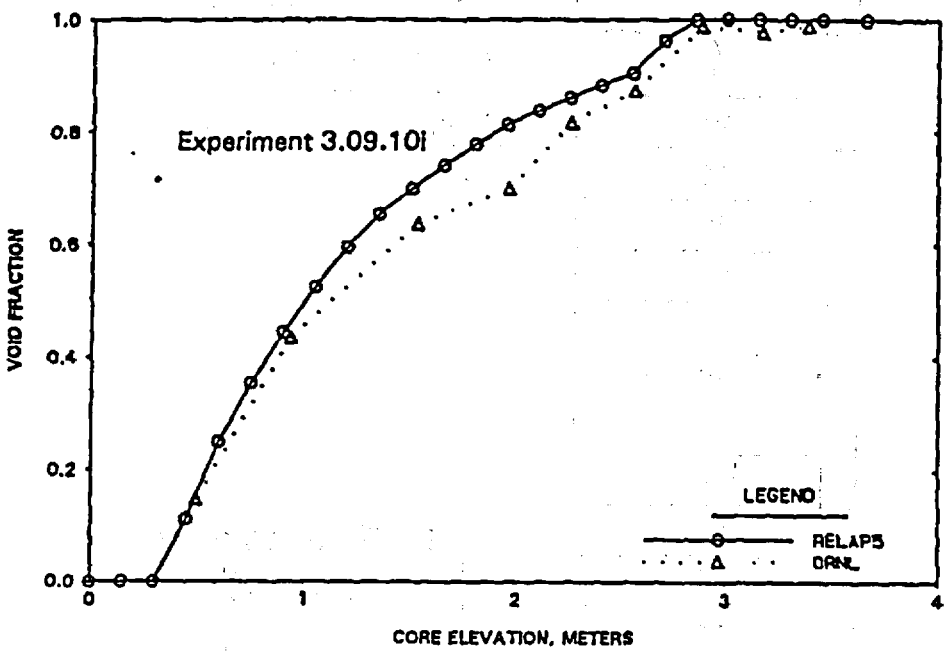


Figure H.17. Comparison Between RELAP5 Prediction and ORNL Test Data: 0.33 Kw/ft, 610 Psia.

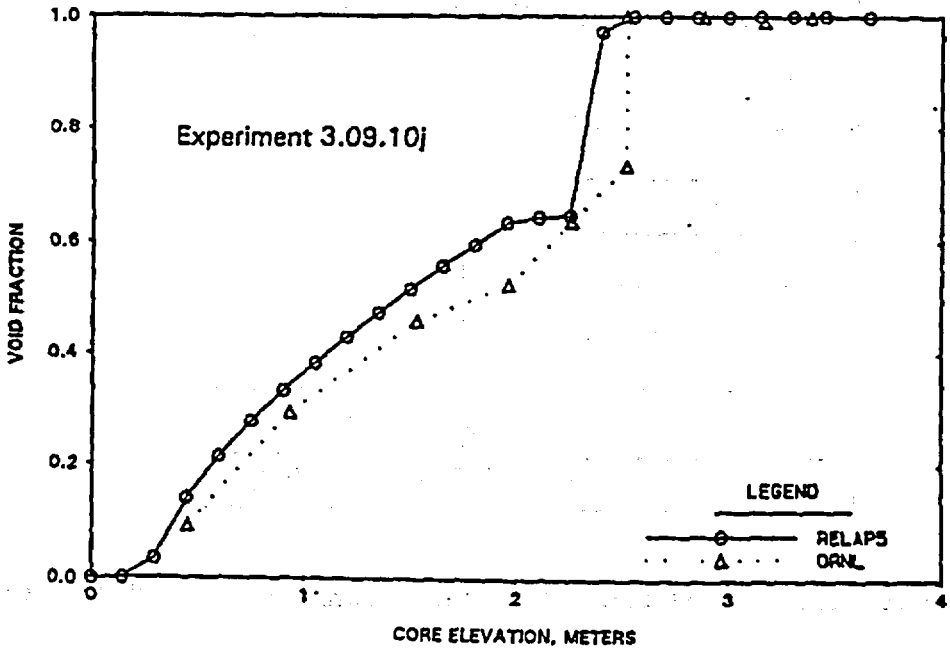

Figure H.18. Comparison Between RELAP5 Prediction and ORNL Test Data: 0.10 Kw/ft, 580 Psia.

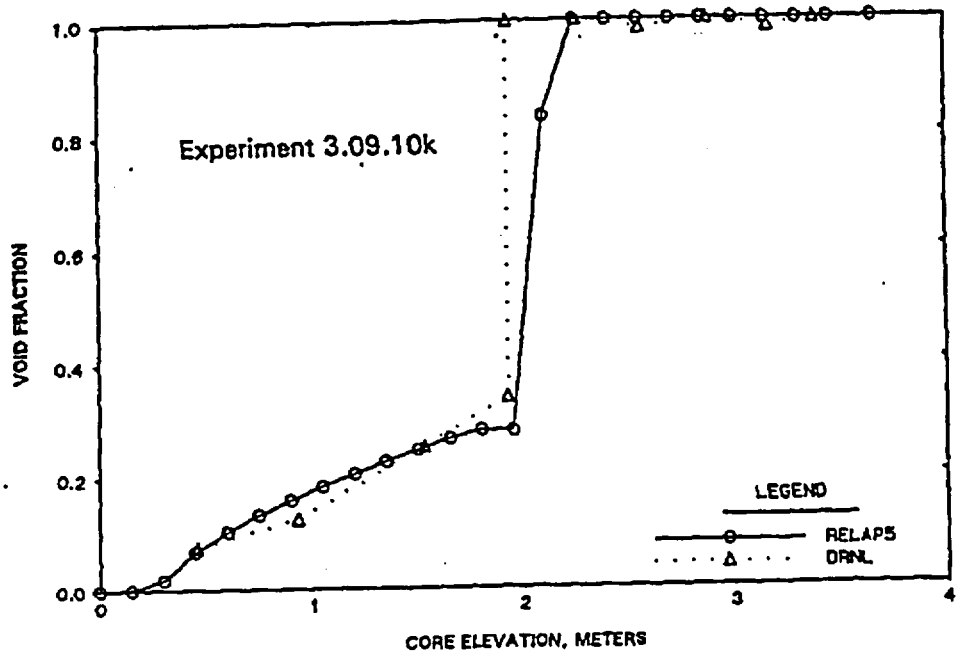


Figure H.19. Comparison Between RELAP5 Prediction and ORNL Test Data: 0.66 Kw/ft, 1090 Psia.

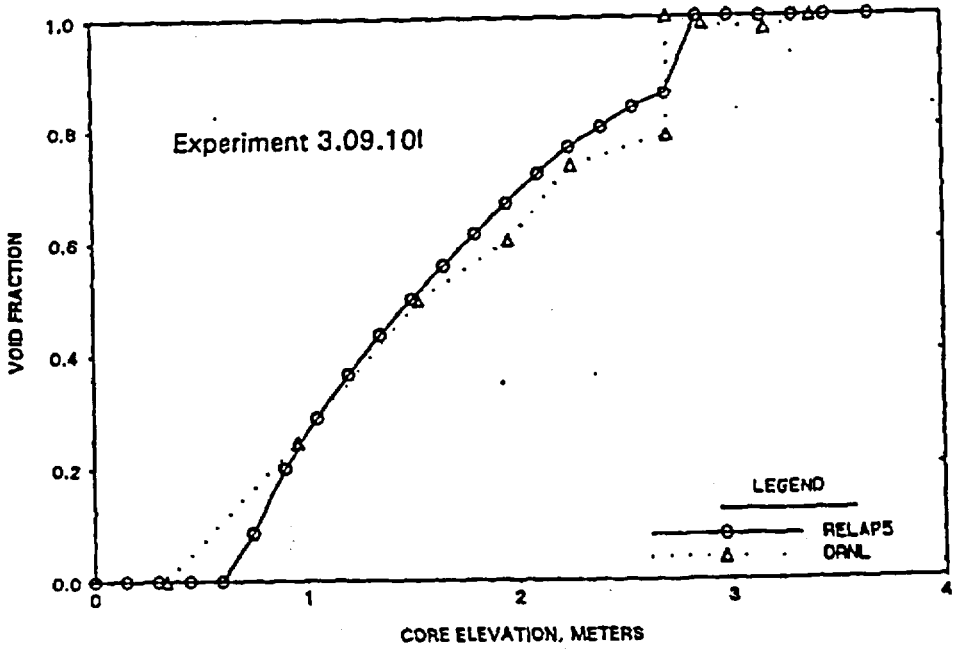

Figure H.20. Comparison Between RELAP5 Prediction and ORNL Test Data: 0.31 Kw/ft, 1010 Psia.

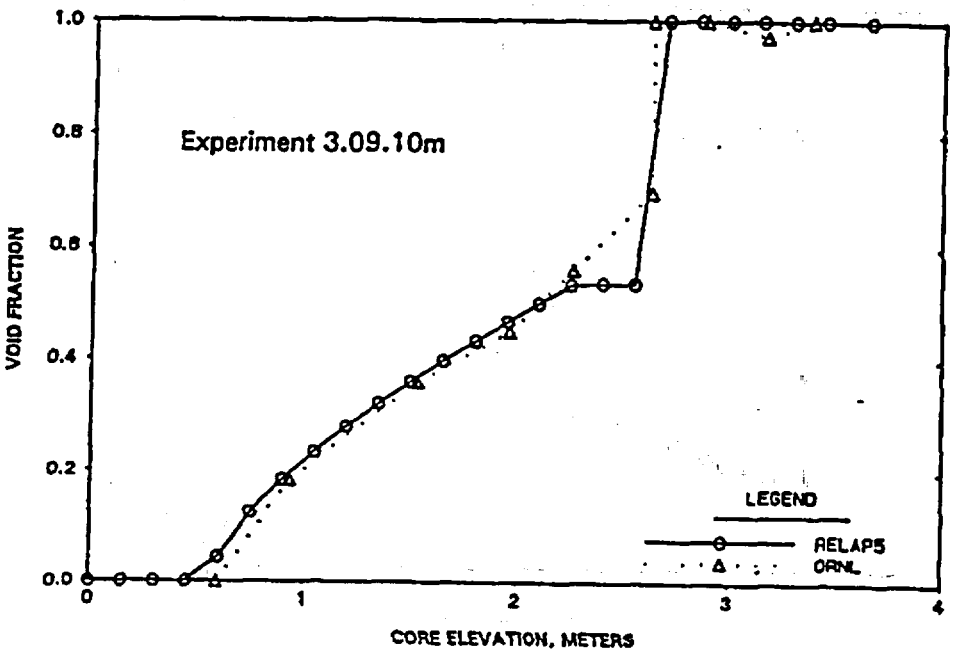


Figure H.21. Comparison Between RELAP5 Prediction and ORNL Test Data: 0.14 Kw/ft, 1030 Psia.

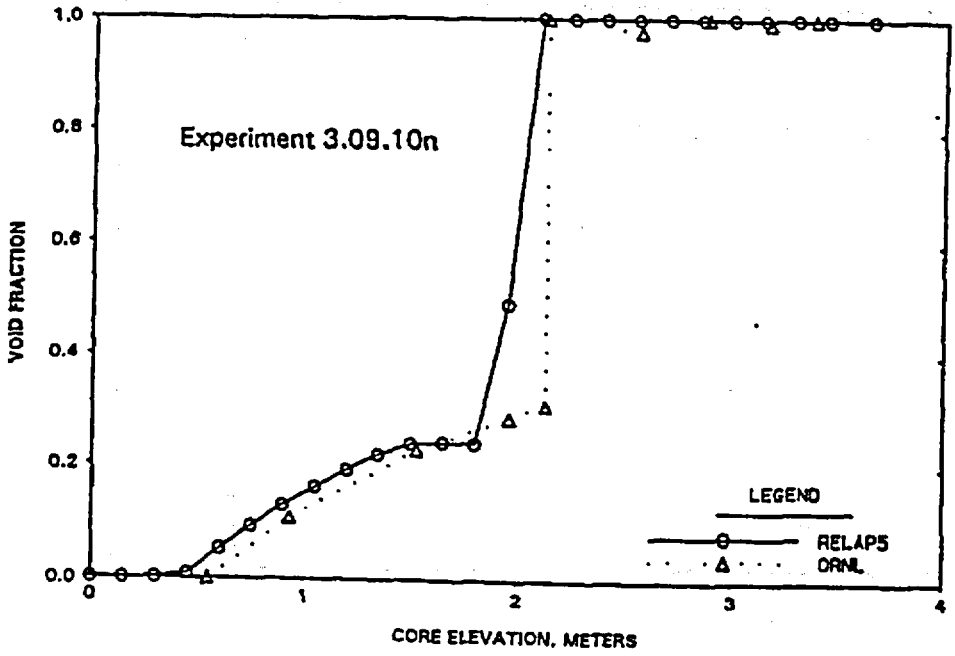

Figure H.22. Comparison Between RELAP5 Prediction and ORNL Test Data: 0.39 Kw/ft, 590 Psia.

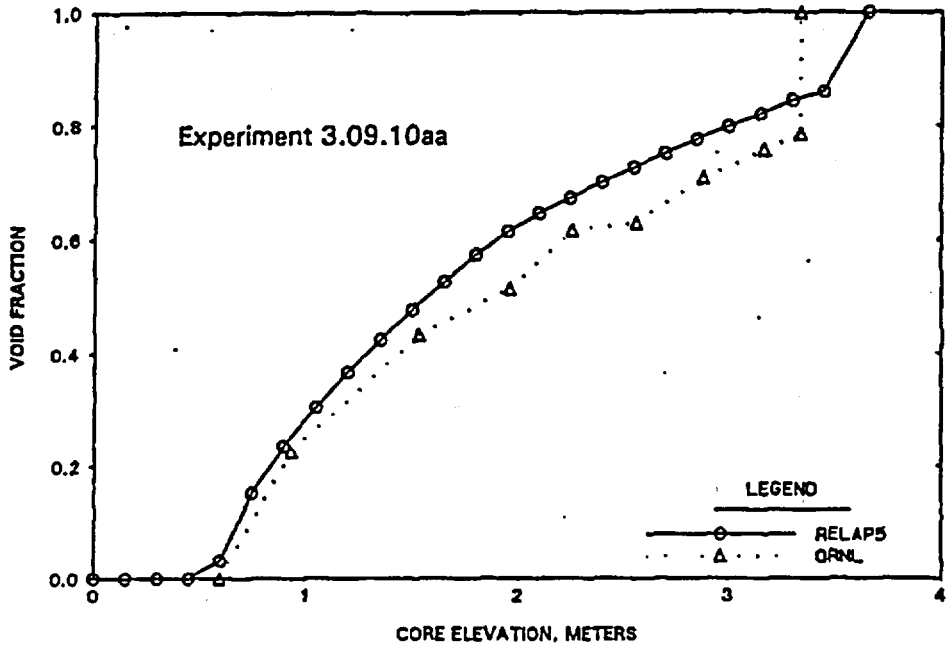


Figure H.23. Comparison Between RELAP5 Prediction and ORNL and ORNL Test Data: 0.20 Kw/ft, 560 Psia.

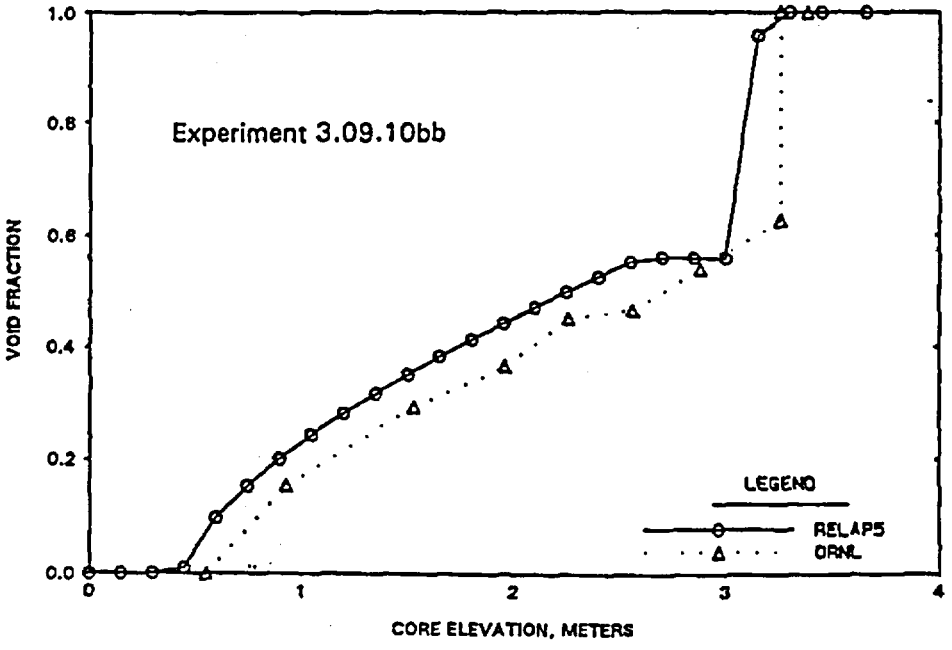

Figure H.24. Comparison Between RELAP5 Prediction and ORNL Test Data: 0.10 Kw/ft, 520 Psia.

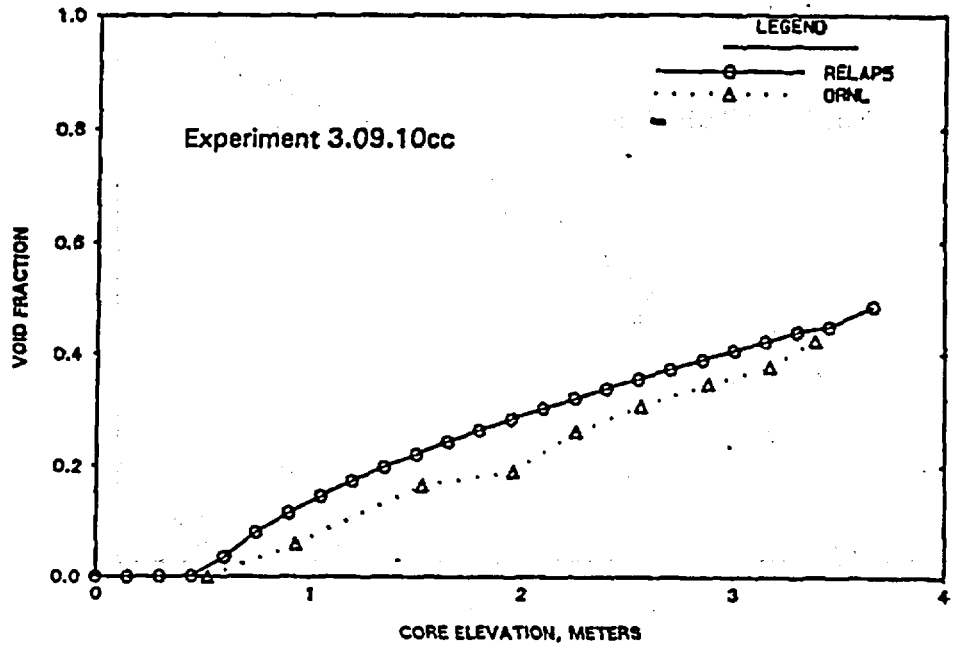


Figure H.25. Comparison Between RELAP5 Prediction and ORNL Test Data: 0.39 Kw/ft, 1170 Psia.

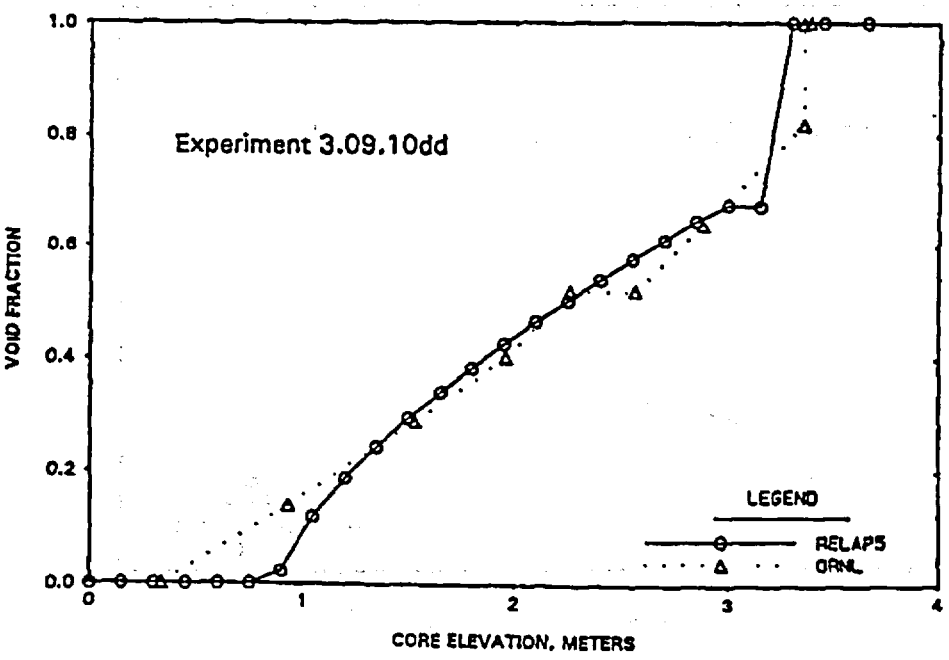

Figure H.26. Comparison Between RELAP5 Prediction and ORNL Test Data: 0.19 Kw/ft, 1120 Psia.

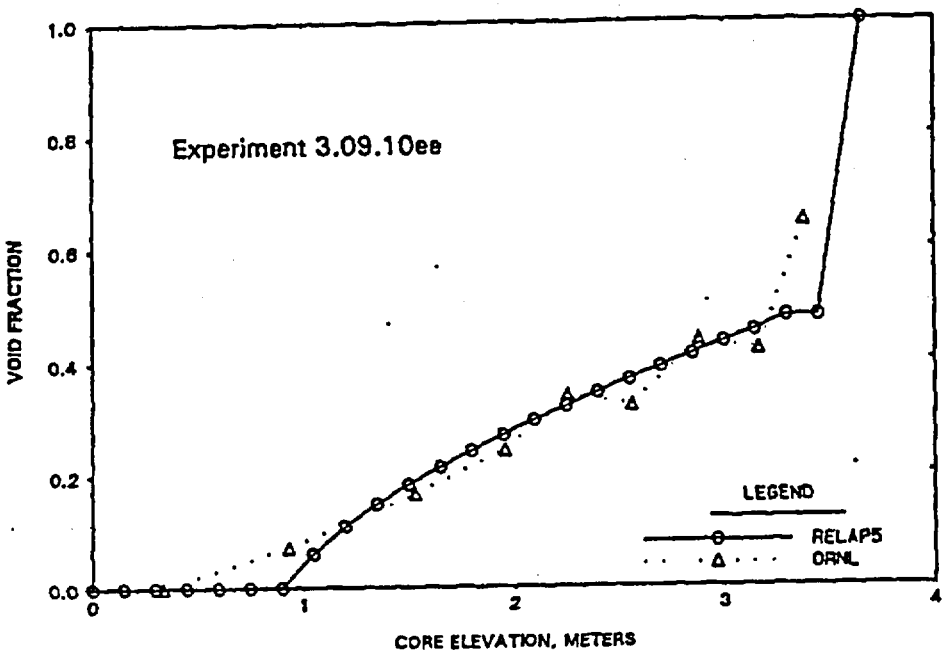


Figure H.27. Comparison Between RELAP5 Prediction and ORNL Test Data: 0.08 Kw/ft, 1090 Psia.

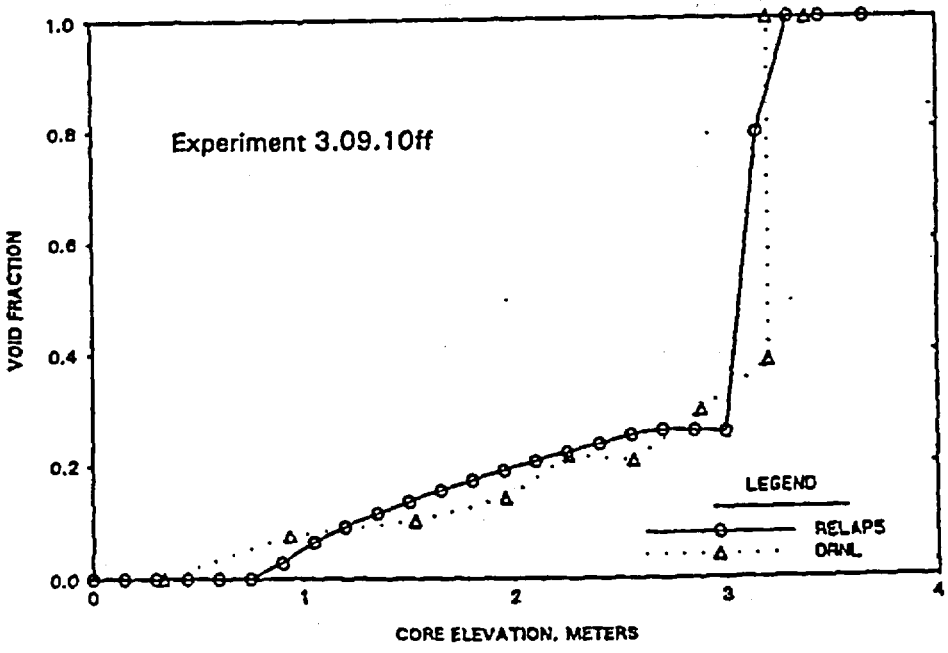

Figure H.28. Comparison Between RELAP5 Prediction and ORNL Test Data: 0.68 Kw/ft, 650 Psia.

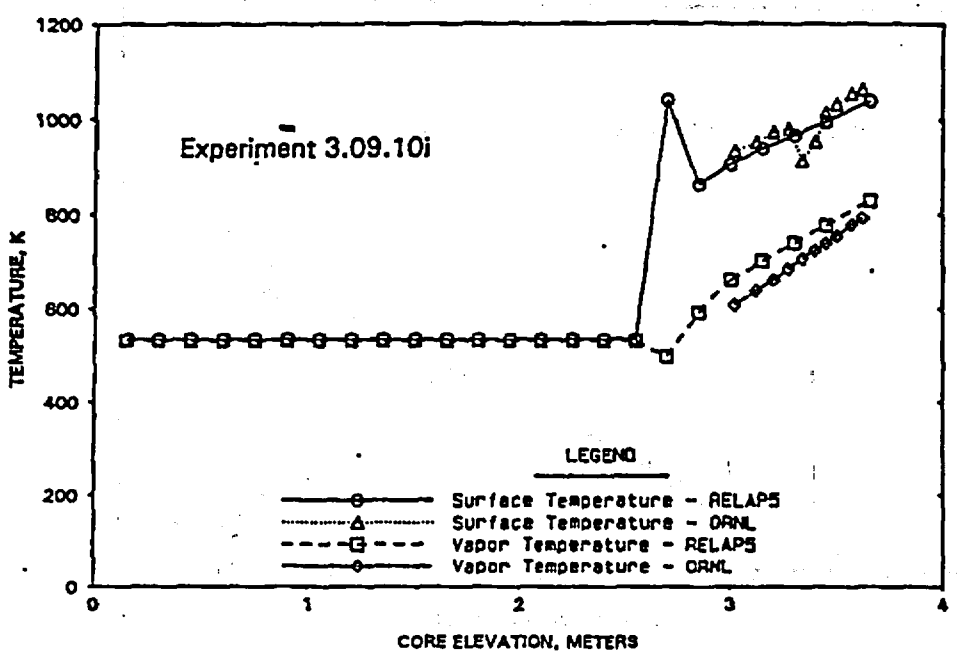


Figure H.29. Comparison Between RELAP5 Prediction and ORNL Test Data: 0.33 Kw/ft, 610 Psia.

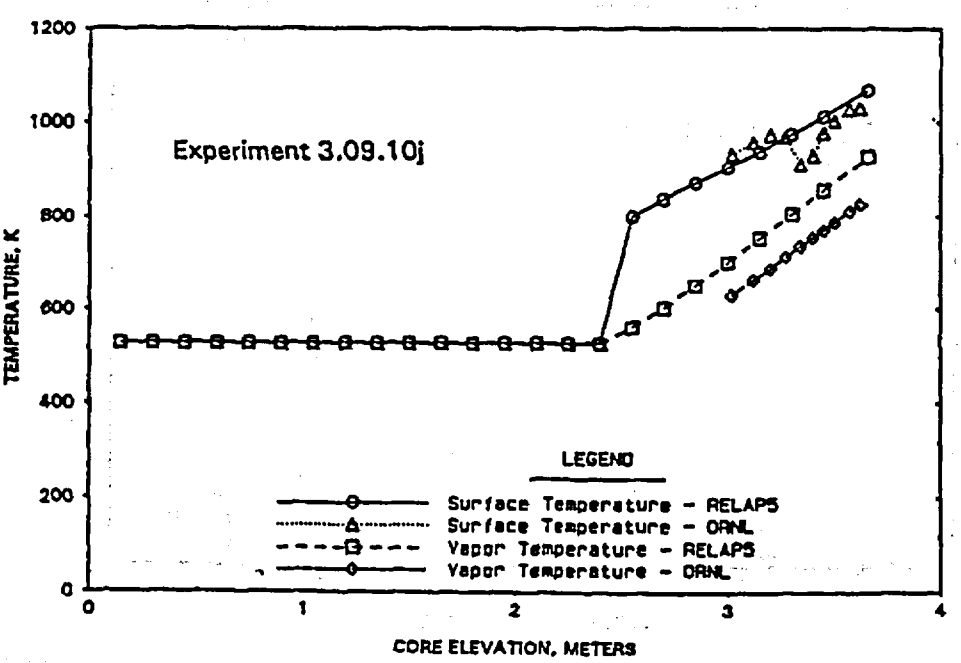

Figure H.30. Comparison Between RELAP5 Prediction and ORNL Test Data: 0.10 Kw/ft, 580 Psia.

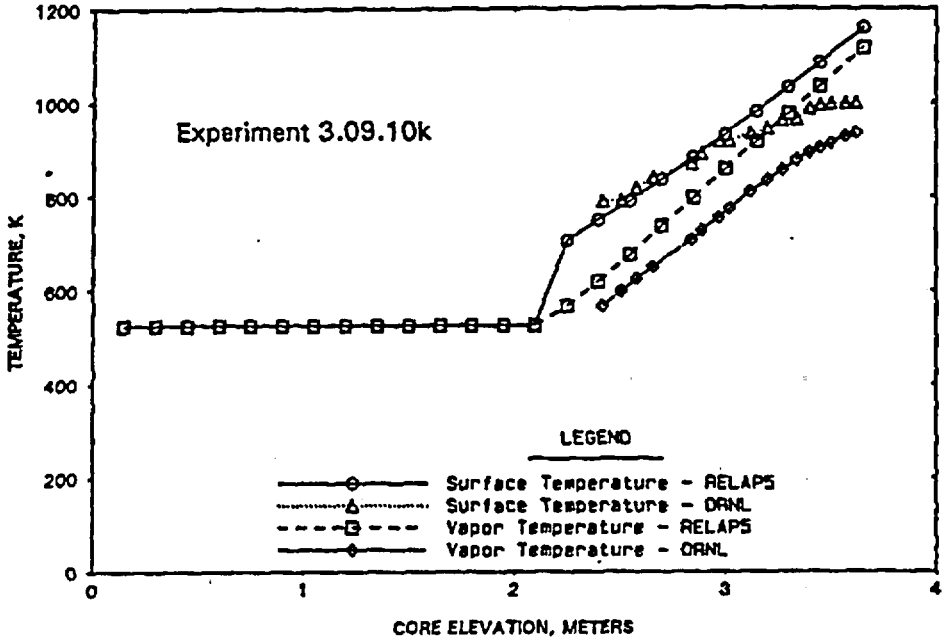


Figure H.31. Comparison Between RELAP5 Prediction and ORNL Test Data: 0.66 Kw/ft, 1090 Psia.

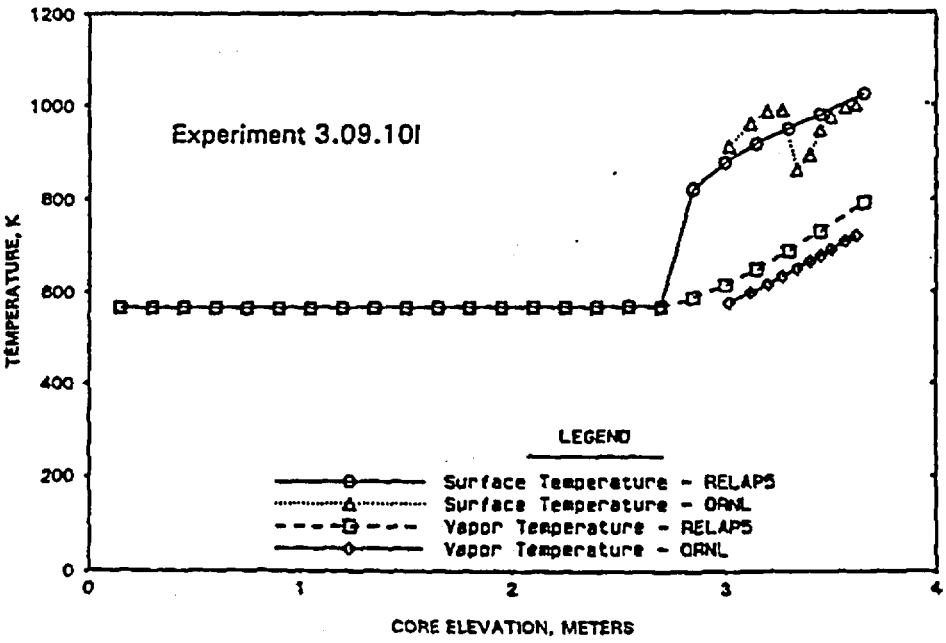

Figure H.32. Comparison Between RELAP5 Prediction and ORNL Test Data: 0.31 Kw/ft, 1010 Psia.

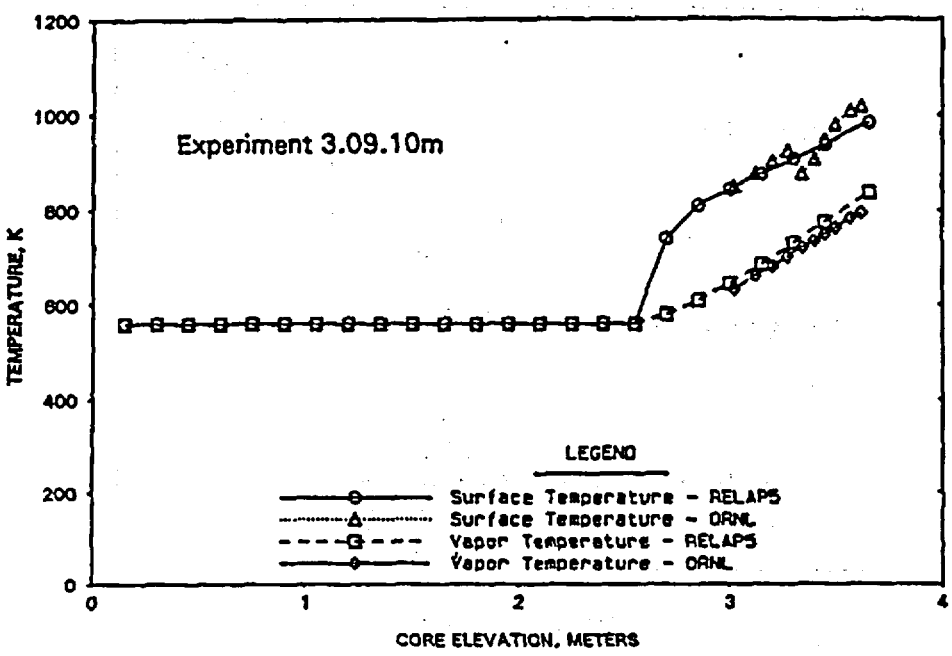


Figure H.33. Comparison Between RELAP5 Prediction and ORNL Test Data: 0.14 Kw/ft, 1030 Psia.

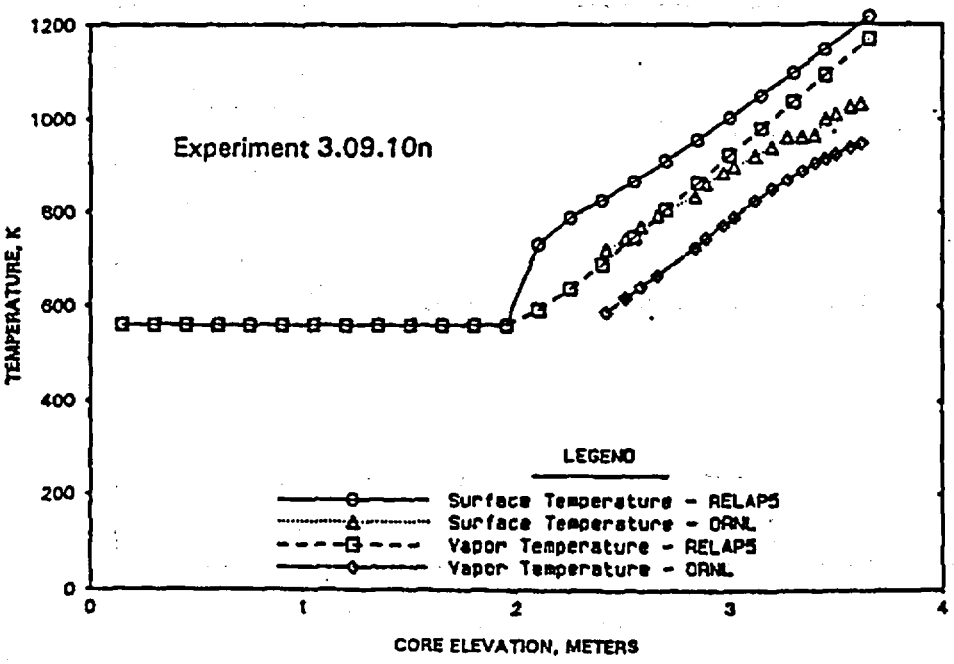

# APPENDIX I

## BWUMV CRITICAL HEAT FLUX CORRELATION

Note: This appendix was originally added in its entirety in Revision 2 of BAW-10164, August, 1992.

BWNT has developed the BWUMV (B&W Universal - Mixing Vane) CHF correlation for use in SBLOCA analysis. The correlation was generated using the NRC-approved methods in the BWCMV topical report, BAW-10159.[139] BWUMV is based on the BWCMV database extended to encompass additional data in the mid-flow regime. The correlation is for use with mixing grids.

A brief explanation of the CHF experiments conducted to measure BWUMV data are presented in section I.1, data reduction and derivation of the correlation in section I.2, and conclusions in section I.3.

## I.1. Critical Heat Flux Tests

BWUMV is based on published Westinghouse-sponsored CHF experimental data from the Columbia University Heat Transfer Research Facility (HTRF) with supplemental data from tests at the same facility sponsored by Nuclear Fuel Industries (NFI) of Japan. A description of this facility is provided in Reference 140. The Columbia University Heat Transfer Research Facility data (as given in Reference 140) has been used as the basis of other correlations in the past.

In the HTRF tests, the first indication of departure from nucleate boiling (DNB) was used as the one experimentally noted. This practice has been previously found acceptable and conservative by the NRC staff.

Most of the data used to develop BWUMV was previously used to develop BWCMV. The BWCMV database consisted of 70 tests performed for Westinghouse and 4 tests performed for NFI. From the Westinghouse sets only 22 tests (included mixing vane grid cores) qualified for this correlation. All the NFI tests qualified, yielding a total of 26 sets of tests with nearly 1,500 data points. They included six axial flux shapes, three heated

lengths, six grid spacings, six hydraulic diameters, three different grid designs, and both unit and guide tube geometries. For the local thermal-hydraulic conditions, pressure ranged from 1500 to 2400 psia, mass velocity from 1.0 to 3.5 million $lbm/hr/ft^2$, and CHF hydrodynamic qualities from -22 to +22 percent. This extensive database fully covers PWR operating ranges for both local and bundle (global) conditions. Further information on the development of BWCMV may be found in Reference 140.

BWUMV used all the BWCMV data plus mid-flow regime data from three additional Westinghouse tests:

## I.2. Derivation of Correlation

Because phenomenological models of CHF are not yet sufficiently accurate for most geometries, CHF is measured empirically using experimental facilities approximating reactor geometries. From these experimental measurements, a CHF correlation is derived; this correlation is an empirical regression of the experiments' independent variables. Four steps were used in the derivation of BWUMV:

1. A form of the correlation was chosen that accurately described the CHF data. The database used to derive BWUMV included a wide variety of bundle geometries, tested over a range of conditions (pressure, flow rates, and temperatures) which represent reactor conditions.

2. The level or magnitude of each independent variable for each run of the database was established. Independent variables were classified in two categories: local thermo-hydraulic conditions (such as velocity and quality) and bundle global conditions (such as heated

length and grid position). While global conditions were known, local conditions were calculated based on measured bundle values of flow, power, and system pressure. This was accomplished using the LYNX2 thermal-hydraulic computer code (Reference 141).

3. The correlation was developed; this included sorting of data by flow regime and optimization of the correlation coefficients. BWUMV coefficients were derived by sequential optimization, and verified using the final database.

4. Since BWUMV is an empirical correlation, there is a finite uncertainty associated with it. This uncertainty was quantified in a departure from nucleate boiling ratio (DNBR) design limit, consistent with the specified acceptable fuel design limit of Standard Review Plan 4.4 (NUREG 0800). DNBR is defined as:

$$\text{DNBR} = \frac{q''_{\text{CHF}}}{q''_{\text{actual}}} = \frac{\text{calculated CHF at a given location}}{\text{actual heat flux at that location}} .$$

A DNBR value of 1.0 implies transition to film boiling at that location. The higher the DNBR, the greater the margin to film boiling. Calculation of a DNBR value greater than this design limit provides assurance that there is at least a 95% probability at the 95% confidence level that a departure from nucleate boiling will not occur (95/95 design limit). As the final step in the derivation of the correlation, the 95/95 design limit was calculated and used to verify that the correlation describes CHF accurately and without bias. Verification included visual and numerical checks for bias with respect to all the independent variables.

## I.2.1. Correlation Form

The critical heat flux was assumed to depend on three parameters:

$$x_1 = \exp[P / (1000*Cl_P)],$$
$$x_2 = G/ (10^6*Cl_{MF}), \text{ and}$$
$$x_3 = X_{eth}.$$

where P is the system pressure in *Pa*, G is the mass flux in *kg/s/m²*, $X_{eth}$ is the quality at CHF, and $Cl_P$ and $Cl_{MF}$ are the English-to-metric conversion factors for pressure and mass flux, respectively. t

Based on the work of Farnsworth[142], a general polynomial form was assumed:

$$CHF = FLS (a_0 + a_1x_1 + a_2x_2 + a_3x_3^2 + a_4x_1^2 + a_5x_2 + a_6x_3|x_3|$$
$$a_7x_1x_2 + a_8x_1x_3 + a_9x_2x_3 + a_{10}x_1^3 + a_{11}x_2^3 + a_{12}x_3^3 +$$
$$a_{13}x_1x_2x_3) / F, \qquad \text{I-1}$$

*Revised Equation I-1 shown on Page 5-260 per SER instruction On Table 2 (page 5-364).* t

where FLS is the bundle specific multiplier used in BWCMV and is defined by

$$FLS = c_1 + c_2L + c_3S + c_4L^2 + c_5LS + c_6S^2, \qquad \text{I-2}$$

*Revised Equation I-2 shown on page 5-261 per SER instruction on Table 2 (page 5-364).* t

in which L = heated length,
S = spacer grid spacing, and
$c_i$ = empirically determined coefficients.

F is the non-uniform (Tong) factor which is set equal to one in the RELAP5/MOD2-B&W implementation of BWUMV.

From the BWCMV correlation[139], the empirical coefficients are:

[ b,c,d,e ]

I.2.2. Subchannel Analysis

Data reduction was required for the three Westinghouse tests which were not used in BWCMV. The experimental conditions for each of the tests (tests number 121, 160, and 164) are given in Table I.1.[140] Local conditions in each assembly subchannel were calculated using the thermo-hydraulic code LYNX2.[141] LYNX2 applies conservation relations at successive axial increments beginning at the channel inlet; downstream increments are considered singly and successively up to the channel exit. The conservation relations used include crossflow between adjacent subchannels. LYNX2 iterates over each axial increment until the differences between current and previous diversion crossflows meet a set convergence criteria. Within each iteration the code solves the conservation and crossflow relations of each subchannel and crossflow boundary.

For the three supplemental tests analyzed, one-eighth of the bundle was analyzed. Westinghouse Test 121 was performed on a 4x4 assembly and was divided into six subchannels as shown in Figure I.1. Westinghouse Tests 160 and 164 were performed with 5x5 assemblies and were divided into six subchannels as shown in

Figure I.2. The dimensions and parameters associated with each assembly are provided in Table I.2.

Based on the axial and radial heat profiles and input of bundle pressure, flow, power, and inlet temperature for each point, local conditions were determined for each assembly as given in Table I.3.

## I.2.3 Data Sorting and Coefficient Optimization

When the data points contained in Table I.3 are added to the data points in Reference 139, there are 1527 data points. These data points were used to obtain the coefficients $a_0$ through $a_{13}$ in Equation I-1 using the methods given in Reference 141. The data points cover the following ranges:

| | |
|---|---|
| Quality | -0.2160 to 0.6653 |
| Mass Flux (mlbm/hr-ft$^2$) | 0.405 to 3.871 |
| Pressure (psia) | 745 to 2455 |

The following coefficients were determined:

[ b,c,d,e ]

## I.2.4. Calculation of Design Limit and Verification

The statistical distribution of the mixing vane CHF data is shown in Figure I.3. Four data points were found to have measured-to-

predicted ratios which exceeded three standard deviations and were rejected from the database. The statistics of the remaining 1523 data points were:

| | |
|---|---|
| Number of data | 1523 |
| Mean | 1.0018 |
| Standard Deviation | 0.1016 |
| Coefficient of Variation | 0.1014 |

The 95/95 departure from nucleate boiling (DNB) design limit was calculated as 1.22.

Figures I.4, I.5, and I.6 show the measured-to-predicted ratios using BWUMV plotted against quality, pressure, and mass velocity, respectively. These figures show no bias of the correlation with respect to the independent variables.

## I.3. Conclusions

A new wide-range critical heat flux correlation has been developed based on 70 Westinghouse-sponsored and 4 NFI-sponsored mixing vane-type assembly experiments performed at the Columbia University Heat Transfer Test Facility. The new correlation, called BWUMV, has been demonstrated to have a favorable statistical distribution and to be unbiased relative to quality, pressure, and mass velocity. Based on the data used, BWUMV is applicable to CHF calculations of mixing vane rod assemblies for pressures and flow rates at or above 750 psia, and greater than $4.0 \times 10^5$ lbm/hr-ft$^2$, respectively.

Table I.1. Geometry of Westinghouse Bundles 121, 160, and 164.

| | Bundle Number | | |
|---|---|---|---|
| | 121 | 160 | 164 |
| Total Number of Rods | 16 | 25 | 25 |
| Number of Heated Rods | 16 | 25 | 25 |
| Rod Pitch (inches) | 0.555 | 0.496 | 0.496 |
| Rod Diameter (inches) | 0.422 | 0.374 | 0.374 |
| Heated Length (inches) | 96.0 | 96.0 | 168.0 |
| Rod-to-Wall Gap (inches) | 0.153 | 0.100 | 0.100 |
| Flow Area (square inches) | 3.489 | 3.796 | 3.796 |

Table I.2. Local Condition Analysis: Subchannel Parameters.

| | Subchannel No. | | | | | |
|---|---|---|---|---|---|---|
| | 1 | 2 | 3 | 4 | 5 | 6 |
| Test No. 121 | | | | | | |
| Subchannel Type | Corner | Wall | Unit | Wall | Unit | Unit |
| Flow Area (sq. in.) | 0.04877 | 0.13209 | 0.08408 | 0.06605 | 0.08408 | 0.02102 |
| Wetted Perimeter (in.) | 0.52970 | 1.21788 | 0.66288 | 0.60894 | 0.66288 | 0.16572 |
| Heated Perimeter (in.) | 0.16572 | 0.66288 | 0.66288 | 0.33144 | 0.66288 | 0.16572 |
| Test No. 160 | | | | | | |
| Subchannel Type | Corner | Wall | Unit | Wall | Unit | Unit |
| Flow Area (sq. in.) | 0.02745 | 0.08742 | 0.06808 | 0.08742 | 0.13616 | 0.06808 |
| Wetted Perimeter (in.) | 0.43387 | 1.08347 | 0.58748 | 1.08347 | 1.17495 | 0.58748 |
| Heated Perimeter (in.) | 0.14687 | 0.58748 | 0.58748 | 0.58748 | 1.17495 | 0.58748 |
| Test No. 164 | | | | | | |
| Subchannel Type | Corner | Wall | Unit | Wall | Unit | Unit |
| Flow Area (sq. in.) | 0.02745 | 0.08742 | 0.06808 | 0.08742 | 0.13616 | 0.06808 |
| Wetted Perimeter (in.) | 0.43387 | 1.08347 | 0.58748 | 1.08347 | 1.17495 | 0.58748 |
| Heated Perimeter (in.) | 0.14687 | 0.58748 | 0.58748 | 0.58748 | 1.17495 | 0.58748 |

Table I.3. Calculated Local Condition Values.

| | Point | Pressure psia | Mass Flux $lbm/hr/ft^2$ | Heat Flux $btu/hr/ft^2$ | Quality | |
|---|---|---|---|---|---|---|
| Test 121 | | | | | | |
| | 430 | 2015 | 405308 | 370043 | 0.2556 | |
| | 431 | 2015 | 721925 | 461763 | 0.0969 | |
| | 432 | 2015 | 704141 | 521065 | 0.0664 | |
| | 433 | 2015 | 916371 | 521065 | 0.0664 | |
| Test 160 | | | | | | |
| | 786 | 2115 | 527956 | 287300 | 0.3641 | |
| | 787 | 2385 | 531861 | 282880 | 0.3157 | |
| | 788 | 1805 | 541406 | 311610 | 0.3265 | |
| | 789 | 1515 | 519832 | 373490 | 0.5620 | |
| *Duplicate* | ~~789~~ | ~~1515~~ | ~~513721~~ | ~~373490~~ | ~~0.6653~~ | t |
| | 790 | 2115 | 532879 | 335920 | 0.3127 | |
| | 791 | 2405 | 519639 | 329290 | 0.2604 | |
| | 792 | 1800 | 531920 | 370175 | 0.4239 | |
| | 793 | 1815 | 516979 | 397800 | 0.4586 | |
| | 794 | 2075 | 508498 | 349180 | 0.3110 | |
| Test 164 | | | | | | |
| | 2055 | 1000 | 2554047 | 601121 | 0.2000 | |
| | 2056 | 1000 | 3018628 | 682772 | 0.1931 | |
| | 2057 | 1000 | 1588414 | 363385 | 0.3162 | |
| | 2058 | 1000 | 2035850 | 647578 | 0.2044 | |
| | 2059 | 1005 | 2518548 | 709520 | 0.1634 | |
| | 2060 | 1005 | 3030165 | 751754 | 0.1683 | |
| *Duplicate* | ~~2060~~ | ~~1005~~ | ~~3050214~~ | ~~611714~~ | ~~0.1980~~ | t |
| | 2061 | 1005 | 1103392 | 348591 | 0.4161 | |
| | 2062 | 1010 | 1575738 | 404069 | 0.3199 | |
| | 2063 | 760 | 1879028 | 372631 | 0.3371 | |
| | 2064 | 760 | 2634649 | 444754 | 0.2812 | |
| | 2065 | 765 | 3096974 | 713744 | 0.2090 | |

Table I.3 (continued). Calculated Local Condition Values.

| | Point | Pressure psia | Mass Flux lbm/hr/ft$^2$ | Heat Flux btu/hr/ft$^2$ | Quality |
|---|---|---|---|---|---|
| Test 164 (continued) | | | | | |
| *Duplicate* | ~~2065~~ | ~~765~~ | ~~3147021~~ | ~~468794~~ | ~~0.2528~~ |
| | 2066 | 755 | 1617322 | 374481 | 0.3567 |
| | 2067 | 750 | 2115662 | 392049 | 0.3122 |
| | 2068 | 750 | 1627688 | 338420 | 0.3935 |
| | 2069 | 745 | 1026514 | 327324 | 0.4569 |
| | 2070 | 750 | 1049376 | 347666 | 0.4291 |
| | 2071 | 1005 | 2120543 | 578597 | 0.2326 |
| | 2072 | 995 | 1044837 | 307906 | 0.4731 |
| | 2073 | 1005 | 558151 | 281092 | 0.6404 |
| | 2074 | 1000 | 547973 | 239483 | 0.5657 |
| | 2075 | 760 | 538561 | 378692 | 0.4393 |
| | 2076 | 755 | 545706 | 232086 | 0.6060 |

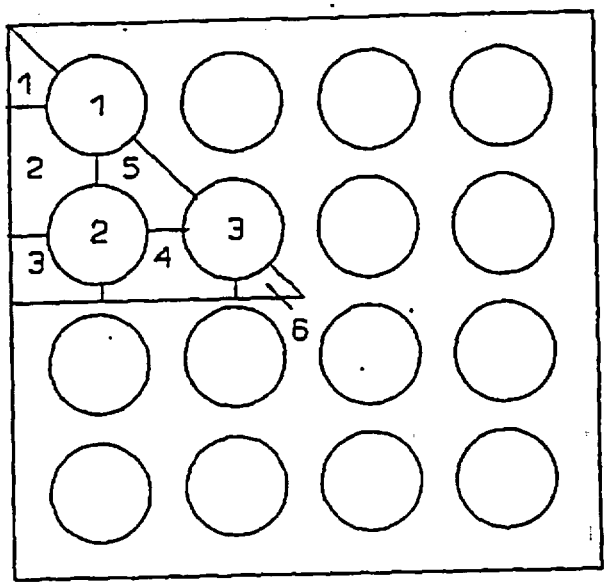


Figure I.1. Subchannel Model for Westinghouse Test 121.

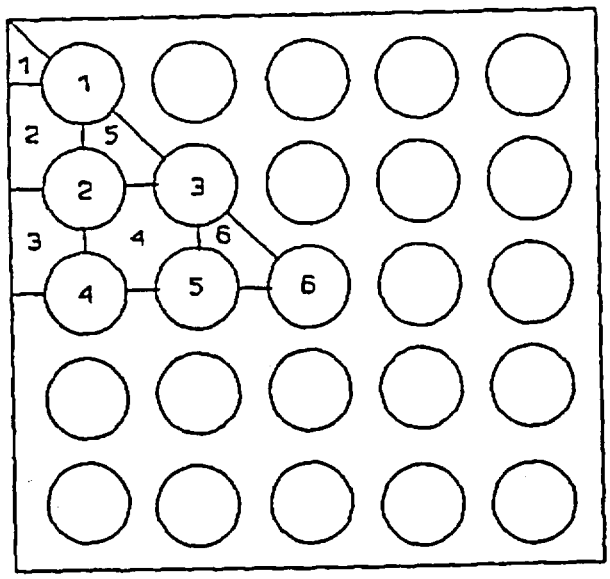


Figure I.2. Subchannel Model for Westinghouse Test 160 and 164.

FIGURE I.3. FREQUENCY DISTRIBUTION OF MIXING VANE CHF DATA.

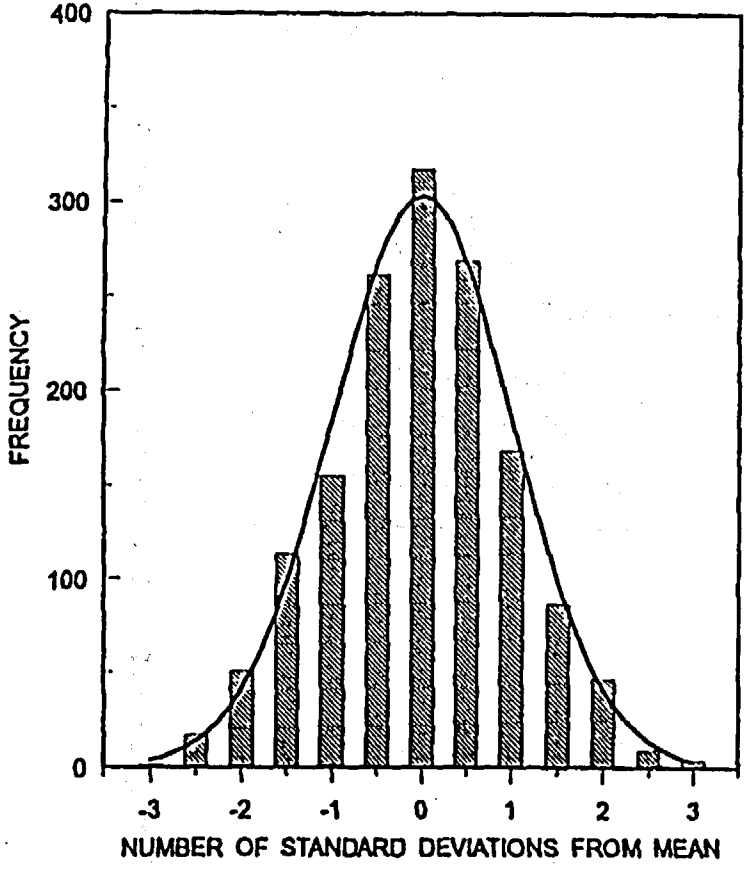


FIGURE I.4. MEASURED-TO-PREDICTED RATIOS OF BWUMV DATA: QUALITY.

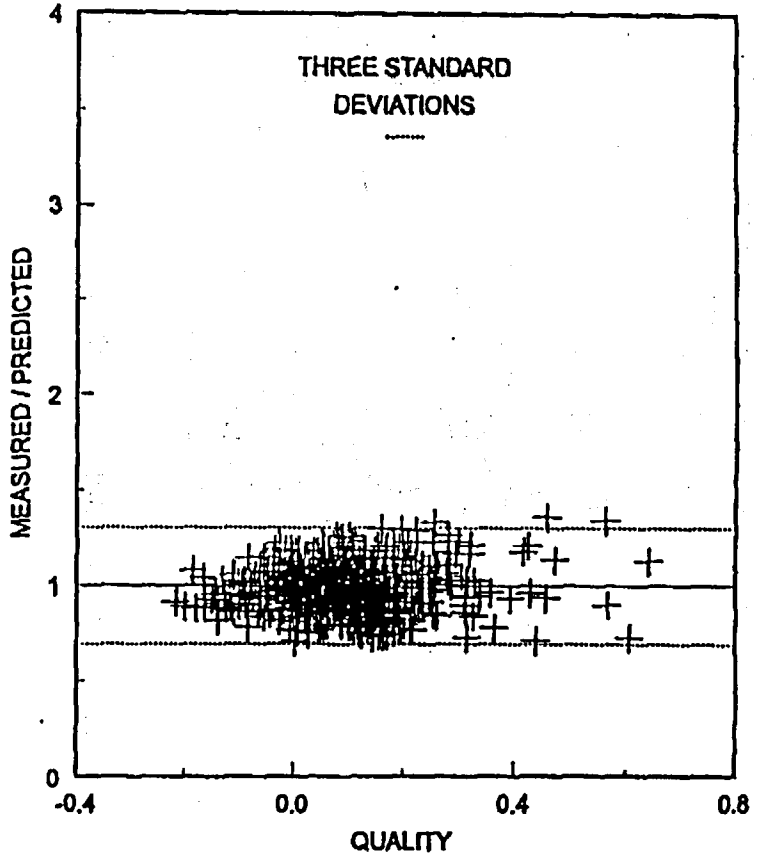

FIGURE I.5. MEASURED-TO-PREDICTED RATIOS OF BWUMV DATA: PRESSURE.

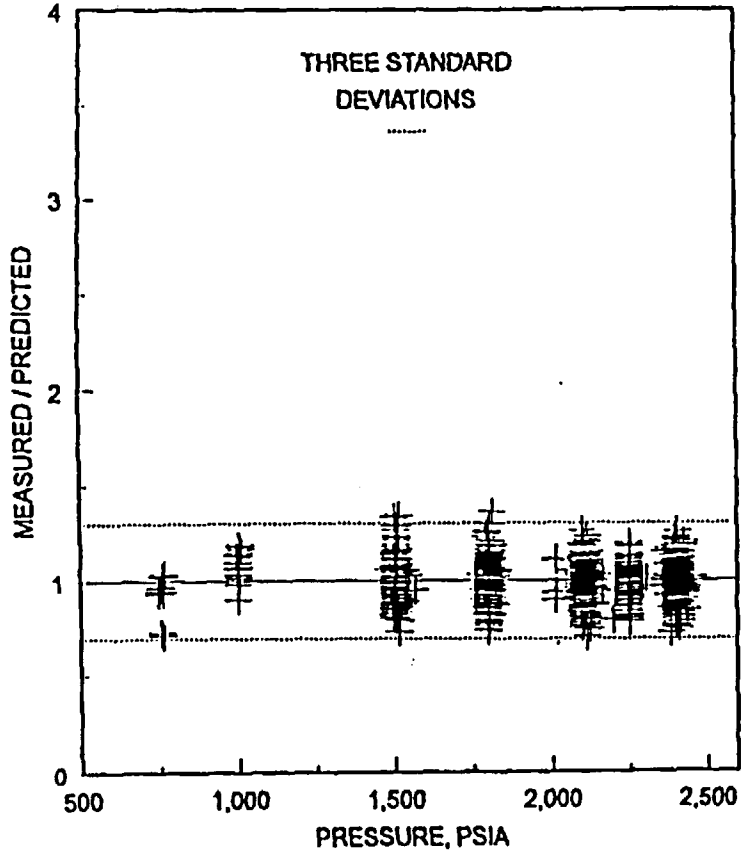


FIGURE I.6. MEASURED-TO-PREDICTED RATIOS OF BWUMV DATA: MASS FLUX.

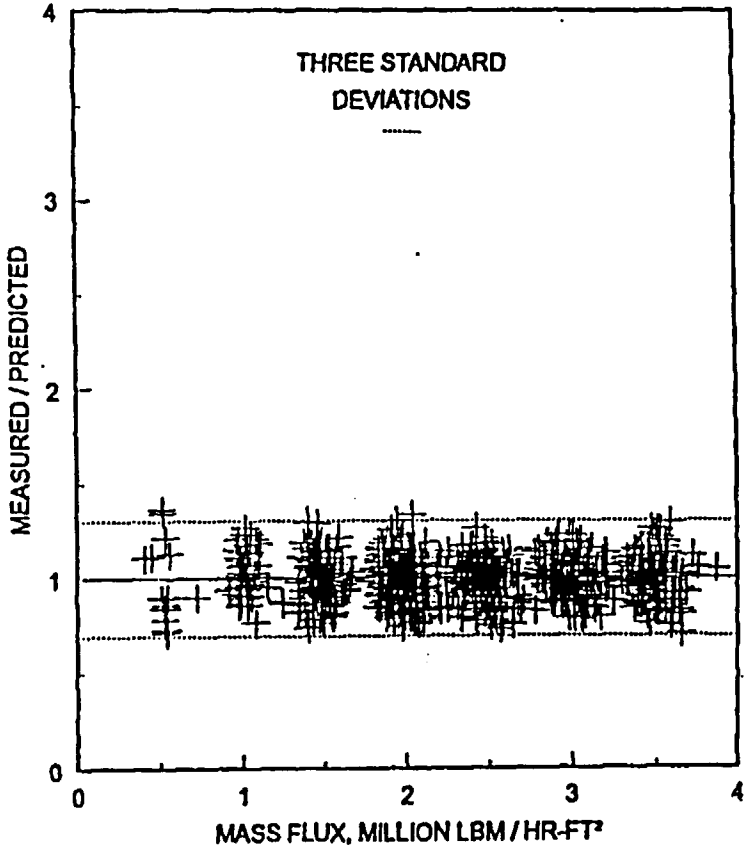

# APPENDIX J

## SBLOCA EM BENCHMARK

Note: This appendix was originally added in its entirety in Revision 2 of BAW-10164, August 1992.

## Introduction

Test SB-CL-18 was one of the SBLOCA experiments conducted in the ROSA-IV Large Scale Test Facility (LSTF) in 1988. This test was selected for International Standard Problem 26 (ISP-26) for benchmarking various system computer codes including RELAP5/MOD2 by participating organizations. BWNT also selected this test for benchmarking BWNT's version of RELAP5/MOD2 because it provides the various modes of a small break LOCA transient, from an initial system depressurization followed by pump coastdown and loss of two-phase circulation, reflux boiling, loop seal clearing and core level depression, core boiloff, and finally to accumulator injection and core recovering. This test simulates the break area equivalent to 5 percent of the cross sectional area of the pump discharge pipe with no pumped ECC injection.

The RELAP5 model for the ISP-26 program was obtained from EG&G. The model was verified against the system design data provided in Reference 142, and subsequently modified to implement the BWNT SBLOCA EM technology. The BWNT version of RELAP5/MOD2 was benchmarked with the revised model (BAW-10168, Revision 2) to demonstrate the analytical capability of the code in predicting the various modes of a SBLOCA transient. The following sections present a description of the ROSA-IV LSTF test facility, test conditions and calculational model, and a summary of results of the benchmark.

## Test Facility

ROSA-IV LSTF, as shown in Figure J.1, is a scaled model representation of a Westinghouse 4-loop PWR plant, with a fluid volume scaling ratio of 1 to 48. The 1 to 1 elevation scaling of the system is preserved because it has a first-order effect on SBLOCA transients. The core is simulated by 1064 electrically heated rods. A comparison of major design parameters of the LSTF

with the PWR is presented in Table J.1. The ROSA-IV system consists of a pressure vessel with two symmetrical loops, each representing two loops of the PWR plant. The pressurizer is connected to the intact loop. A brief description of the major components is provided below.

Pressure vessel:

The pressure vessel consists of an annular downcomer, lower plenum, simulated core with 16-7x7 bundles and 8 semi-crescent bundles on the periphery, and simulated upper plenum and upper head with 8 control rod guide tubes and 10 upper core support columns. Eight 3.4 mm holes are provided in the top flange of the core support barrel to simulate the downcomer-to-upper head bypass flow. An external pipe (1 inch, schedule 160) is used to connect the hot leg pipe to the upper downcomer for simulating hot leg nozzle leakage.

The core consists of 1064 electrically heated rods (9.5 mm OD) and 104 unheated rods (12.2 mm OD) with 9 spacer grids. The active heated length is 3660 mm (12 feet). The axial power distribution is a cosine profile with a 1.5 peak at the midplane.

Steam generator:

The primary side of the steam generator consists of inlet and outlet plenums, tube sheet, and 141 inverted U-tubes (1/48 of the PWR) with an inside diameter of 19.6 mm and a wall thickness of 2.9 mm. There are 9 groups of tubes with various lengths, and the average length is 19.7 m. In the secondary side, feedwater enters at the bottom of the boiler section, and two steam separators above the boiler section are used for moisture separation. The major components outside the steam generator vessel are main and auxiliary feedwater pumps and associated

piping, steam line and steam isolation valves, and steam condensation system.

Pressurizer:

The pressurizer is a 600 mm ID x 4200 mm height cylindrical vessel with a fluid volume of about 1/48 of the PWR. The pressurizer vessel is connected to the intact loop hot leg pipe by a surgeline (3 inch, schedule 160 pipe). The PORV and safety valves, heater, and spray system were installed to simulate those of the PWR, but they were not activated during the test.

Primary Coolant Pump:

The primary coolant pump is a canned-type centrifugal design. The impeller, casing, and suction and discharge configuration are similar to those of the PWR pump. The pump homologous head and torque curves are presented in Figures 5.2.43 and 5.2.44 of Reference 141.

Primary Coolant Pipe:

The primary loop is a 2x2 equal loop arrangement. Both the hot leg and cold leg pump discharge pipes have an inside diameter of 207 mm, and the inside diameter of the pump suction pipe is 168 mm.

Emergency Core Cooling System:

The ECCS consists of CCI, HPI, RHR and accumulator injection. The pumped ECCS was not activated in this test. The accumulator tank has a volume of 4.8 $m^3$, which is 50 percent larger than the scaled volume of 4 accumulator tanks in the PWR plant. The initial pressure of the cover gas was set at 4.51 MPa (654 psi) consistent with the value used in a PWR plant. There are two accumulator tanks, one each connected via a surgeline (4 inch, schedule 80 pipe) to the pump discharge piping.

## Model Description

The ROSA RELAP5 base model was originally developed by EG&G for the ISP-26 program. The model, shown in Figures J.2 and J.3, consists of 166 hydrodynamic volumes, 174 junctions, and 166 heat structures. Volume and junction parameters are calculated with non-equilibrium and non-homogeneous models. Steam generator secondaries, ECC injection, and system environmental heat losses are modelled in detail. The core axial power profile is modelled with six stacked heat structures over six 610 mm long axial fluid volumes. The upper head region is nodalized to allow for junctions to be connected at the elevations of the top of the control rod guide tube and at the elevation of the holes in the guide tube below the upper core support plate. This model was verified against the design data provided in Reference J-1.

For this benchmark the EG&G model was revised to implement the provision of the BWNT SBLOCA calculation model to be proposed in revision 2 of BAW-10168 (The BWNT SBLOCA evaluation model was under revision at the time of this benchmark. The planned release date for the evaluation model was about a month after the release of BAW-10164, Revision 2). Alterations were primarily in primary system nodalization in selected regions. The required changes are discussed below, and the resulting EM nodalization is presented in Figures J.4 and J.5.

The downcomer, component 108, is reduced from 9 to 6 volumes. Volume 1 of component 108 extends from the top of the original volume to the elevation corresponding to the top of the core. Volumes 2, 3, and 4 extend from the top of the core to the bottom of the core, similar to the core baffle region nodalization in a PWR plant model. Volumes 5 and 6 are made equal to the volume lengths of the lower plenum volumes, 120 and 116, respectively. The upper downcomer volumes, 100 and 104 remain unchanged.

The core, component 124, is increased from 6 to 20 volumes, and the original core heat structure is divided into two heat structure groups, one representing 360 high power rods and the other 704 low power rods. Each heat structure is divided into 20 stacked heat structures with axial length equal to the corresponding fluid volume lengths. The core is divided into 20 unequal axial lengths such that each grid is located at the node boundary, and the axial power distribution is modified accordingly. No separate fluid channel is modelled for the high power heat structure because the core fluid temperature measurements indicate good mixing between the high power and low power bundles.

The upper plenum region, components 128, 132 and 136 in the original model, is increased from 3 to 6 volumes, and the heat structure is redistributed in accordance with the volume length.

The steam generator inlet nozzles (components 208-2 and 408-2) are 50 degrees inclined from horizontal (typical of the PWR design). In order to utilize the horizontal flow stratification model, these components are changed from the 50 degree vertical orientation to a 14 degree horizontal orientation to provide adequate draining of water from the steam generator inlet plenum through the hot leg to the pressure vessel.

The two volume nodalization in the steam generator plenum region in the original model is maintained instead of one volume in the plant model, because the LSTF plenum volume is oversized (1/24 of a PWR). The steam generator tubesheet is combined with the upper volume of the plenum region on both inlet and outlet sides. In order to simulate the differential draining of fluid in the steam generator tubes observed in the experiment, the steam generator tube volume is divided into two parallel channels, one representing 78 short tubes (types 1 through 4 in Figure 5.3.4b

of Reference 142), and the other 63 long tubes (types 5 through 9 in Figure 5.3.4b of Reference 142). Each channel contains 16 volumes, eight volumes each on the upflow and downflow sides. The tube heat structures are revised in accordance with the corresponding fluid volume lengths.

The pump suction piping is increased from 9 to 10 volumes (6 for the downflow and 4 for the upflow). The noding changes are primarily in the downflow side (components 232 and 432 for broken and intact loops respectively) including horizontal section of the U-bend to improve spatial representation that affects fluid conditions and timing of the pump suction seal clearing. Volume 1 represents the steam generator outlet nozzle (40 degree bend), and volumes 2 through 5 represent the vertical section of the downflow side with the bottom volume substantially smaller than the others. Volume 6 models the horizontal section of the U-bend. The upflow side (components 236 and 436 for broken and intact loops respectively) is represented by 4 volumes similar to the original model. Heat structures are redistributed accordingly.

The intact loop pump discharge piping is increased from 3 to 4 volumes, and the heat structure is revised accordingly.

The pressurizer surgeline volume is reduced from 3 volumes to 1 volume. The elevation change from the pressurizer outlet to the hot leg is conserved.

The revised model consists of 223 volumes, 233 junctions, and 280 heat structures. Volume and junction parameters are calculated with non-equilibrium and non-homogeneous models similar to the base model except for the core region where equilibrium modeling is used. In addition, the Wilson drag model is applied to vertical volumes in the pressure vessel and primary loops.

Counter current flow limiting (CCFL) is applied to the junctions at the steam generator plenum and tube inlets. The Wallis correlation from Reference 145 is used in the steam generator tube inlet junction, and the CCFL correlation based on the UPTF data from Reference 146 is used in the steam generator plenum inlet junction. The results of the CCFL calculation will be discussed later. The SBLOCA EM heat transfer model is used for the core heat transfer calculation. This model uses the BWUMV CHF correlation to calculate DNB, and permits return to nucleate boiling when rewetting is calculated during the post-DNB period.

A discharge coefficient of 1.1 is used for subcooled flow and two-phase flow up to 70 percent void fraction, and the two-phase coefficient is reduced to 0.77 for void fraction greater than 70 percent. These relative values were used to match a measured flow, and are consistent with the relationship of discharge coefficients with respect to void fraction discussed in Volume 2 Section 4.3.2.3 of BAW-10168, Revision 2.

Results of the Benchmark

The steady-state initial conditions for the benchmark are presented along with the test conditions in Table J.2. To demonstrate model stability relative to time advancement, the EM model was run with a time step advancement of 0.05 seconds (base case) and with a reduced time step of 0.005 seconds. Figures 6 through 10 show the results of the time step study, and confirm that the reduced time step advancement does not change the results. A comparison of the results of the base case (RELAP5/MOD2 EM) with the experimental data identified with instrumentation tag names listed in Reference 142 is presented in Table J.3 and Figures J.11 through J.36 below.

The calculated sequence of major events are presented along with the test data in Table J.3. Due to a facility power limitation,

the initial core power is only 14 percent of the scaled PWR power. To compensate for the power deficiency during the early phase of the transient, the initial core power was maintained for approximately 38 seconds after the reactor scram (8.3 seconds) until it matched the decay power rate based on the initial core power equivalent to the scaled PWR power. Thereafter, the power was reduced in accordance with the decay power curve. The calculation was forced to model this simulation.

The transient was initiated at time zero by opening the leak, and thereby causing a flow of subcooled fluid out the break, resulting in a rapid system depressurization followed by pump coastdown and loss of two-phase circulation. Then, the system enters the refluxe cooling mode until clearing of the pump suction seals. The loop seal clearing was accompanied by changes in discharge flow characteristics and system depressurization. Reflux cooling was lost as the primary system depressurized rapidly below the secondary side pressure. Figures J.11, J.12 and J.13 show the leak flow rate, the primary system pressure response, and pressurizer liquid level, respectively. The figures show that the predictions are in good agreement with the experimental results. The secondary system pressure responses are presented in Figures J.14 and J.15. These figures also demonstrate good agreement between the calculations and the experimental results. The pressure perturbation during the early phase of the transient is caused by actuation of relief valves.

The differential pressures for the pump suction downflow and upflow sides in Figures J.16 through J.19 show good agreement in loop seal responses between the calculations and the experimental results. The calculations show that the broken loop seal cleared slightly ahead of the intact loop seal because of its proximity to the leak. But the experimental data seemed to indicate that the both loop seals cleared almost simultaneously. The predicted

time of loop seal clearing is about 16 seconds later than the experiment due to under-prediction of the leak flow. Note that the measured initial differential pressure in the downflow side is approximately 5 KPa higher than that of the calculations. This could be caused by the lower tap instrumentation pipe, for the differential pressure measurement (DPE070/DPE210 in Figure 6.11c of Reference 142), extending below the bottom of the horizontal pipe in the pump suction U-bend. This would be sufficient to produce the additional required static head; but no detailed instrumentation design information is available to confirm the hypothesis.

Figures J.20 and J.21 show differential pressures in the core and downcomer, respectively. The system hydrostatic head balance caused the first core depression during clearing of the pump suction seals. Because of liquid holdup in the steam generator upflow sides, the core level decreased below the level corresponding to the bottom of the pump suction pipe (1.86 m above the bottom of the core). Prior to clearing of the pump suction seals, the remaining fluid in the primary system for core cooling was centered in the pressure vessel and steam generator upflow sides. Following loop seal clearing, the core was reflooded from the bottom by downcomer fluid and from the top by draining of the steam generator upflow side fluid. The second core depression was predicted at 320 seconds, approximately 80 seconds earlier than the experiment.

Since both the experiment and calculation have the same core level depression and downcomer level at their respective time of loop seal clearing (140 seconds for the experiment and 156 seconds for the calculation), and the bottom flooding was not sufficient to match core boil-off, the second core depression was greatly influenced by the top flooding. Figures J.22 through J.25 show differential pressures in the steam generator plenums

and tubes for the upflow side. These plots show the differential pressure in the inlet plenum for the experiment is greater than that for the calculation, and vice-a-versa for the tubes as a result of the system hydrostatic balance. The cross-sectional area of the inlet plenum is approximately four times larger than that of the tubes. Thus, water in the inlet plenums became a major source of coolant for the top flooding. Furthermore, Figures J.22 and J.23, and the differential pressure in the vessel upper plenum in Figure J.26 also show a prolong draining period in the experiment that resulted in delaying the second core depression for approximately 80 seconds. Because the calculated second core depression occurred earlier, and continuous core depression reduced steam generation, this resulted in a faster system depressurization between 350 and 420 seconds as shown in Figure J.12.

Figures J.27 and J.28 show the differential pressures in the steam generator long and short tube groups for the downflow sides. The downflow side drained faster than the upflow side following pump coastdown. Figures J.29 and J.30 show the accumulator flow rates. As a result of the larger depressurization rate calculated during the second core depression (discussed above), the accumulator pressure set point was reached earlier in the calculation than in the experiment. The calculated flow rate is conservatively less than that of the experiment. The increase in accumulator flow after 500 seconds for both the calculation and experiment is caused by a faster system depressurization following quenching of the upper core that reduced steam production.

The temperature responses for various thermocouple locations are presented in Figures J.31 through J.36. Two major core liquid level depressions cause core heater rod temperature excursions. The first of these depressions occurs as a result of loop seal

clearing. Depletion of the core inventory occurs rapidly with water remaining in the steam generator inlet plenum and tubes. That leads to a highly voided core region but not to complete voiding. The retained water prevents superheating within the RELAP control volumes resulting in an underprediction of both vapor and cladding temperatures. Although observable as potentially nonconservative, the underprediction of cladding temperatures at loop seal clearing is not of significant consequence. This phase of SBLOCA has been studied in numerous experiments and consistently found to be of short duration and limited temperature excursion. The more important aspect of core liquid depletion during loop seal clearing is that the inventory during and after the excursion provides the initial liquid inventory for the core boildown phase. Because cladding temperature excursions can only occur at relatively high void fractions, approximately 0.95 or greater, the fact that excursions were calculated demonstrates that the core inventory during and after loop seal clearing was reasonably well predicted. This is further evidenced by the timing of the second temperature excursion.

The second temperature excursion occurred during the core boildown phase. Because this excursion is not limited in duration or extent and is highly dependent on ECCS design and capacity, it is appropriate and significant that the cladding temperature and other controlling parameters be conservatively predicted. Although the temperatures during the experiment were not significant relative to LOCA acceptance criteria, it is evident that the modelling successfully and conservatively established conditions under which the cladding temperature was overpredicted. The heatup period was longer and the temperature excursion higher than the experiment; thereby, confirming the conservatism of the modelling.

The CCFL model was applied to junctions at the steam generator plenum and tube inlets. Figures J.37 through J.39 show the calculated values of $j_f^*$, $j_g^*$, and the Wallis constant, C, respectively, at the broken loop steam generator tube inlet. Figures J.40 through J.42 show the CCFL parameters at the broken loop steam generator plenum inlet. In Figures J.39 and J.42, the value for C is set to zero when the flow is co-current. When the flow is counter current, the maximum value for the liquid downflow is limited by the CCFL correlation.

b,c,d,e

From these figures it can be observed that, during the counter current flow period, the RELAP5 calculated flow satisfies the CCFL correlation. In Figure J.39, the calculated constant C exceeds the input value only when the liquid velocity is near zero. Figure J.37 also shows that, from 100 to 140 seconds, the flow in the short tube is co-current and the flow in the long tube is counter current.

Conclusions

RELAP5/MOD2-B&W calculated the major events of the ROSA-IV SB-CL-18 experiment; blowdown, two-phase natural circulation, reflux boiling and liquid holdup, pump suction seal clearing, core liquid level depression, and accumulator injection and core recovery in the proper sequence. The benchmark calculated the overall system responses in good agreement with the experimental data. The code also conservatively predicted heater rod surface temperature during the boil-off phase of the transient.

The SBLOCA EM features and nodalization described in Volume 2 of BAW-10168, Revision 2 are sufficient to meet the calculational needs for the benchmark analysis. The results of the analysis demonstrate that the BWNT version of RELAP5/MOD2 can adequately predict system thermal-hydraulic responses during SBLOCA.

Table J.1. Major Design Parameters of LSTF and PWR.

| Items | LSTF | PWR | PWR/LSTF |
|---|---|---|---|
| Pressure, MPa | 16 | 16 | 1 |
| Hot Leg Temp, K | 598 | 598 | 1 |
| Cold Leg Temp, K | 562 | 562 | 1 |
| No. of Fuel Rods | 1064 | 50952 | 48 |
| Core Height, m | 3.66 | 3.66 | 1 |
| Core Power, MW | 10* | 3423 | NA* |
| Fluid Volume, $m^3$ | 7.23 | 347 | 48 |
| Power/Volume, $MW/m^3$ | 1.4* | 9.9 | NA* |
| Core Inlet Flow, Kg/s | 48.8* | 16700 | NA* |
| Downcomer Width, m | 0.053 | 0.26 | 4.91 |
| Hot Leg Pipe ID, m | 0.207 | 0.737 | 3.56 |
| No. of Loops | 2 | 4 | 2 |
| No. of Tubes/SG | 141 | 3382 | 24 |
| Ave Length of Tubes, m | 19.7 | 20.2 | 1 |
| CL PS Pipe ID, m | 0.168 | 0.787 | 4.69 |
| CL PD Pipe ID, m | 0.207 | 0.699 | 3.37 |
| Acc Pressure, MPa | 4.51 | 4.24 | 1 |

* Initial core power is limited to 14 percent of the scaled PWR power. To compensate for the power deficiency during the early phase of the transient, the initial core power was maintained for 47 seconds before power reduction in accordance with the decay power curve.

Table J.2. Initial Test Conditions.

| Items | Test[143] | RELAP5 |
|---|---|---|
| Pressurizer Pressure, MPa | 15.5 | 15.5 |
| Hot Leg Fluid Temp. K | 599 | 600 |
| Cold Leg Fluid Temp. K | 563 | 564 |
| Core Power, MW | 10 | 10 |
| Core Inlet Flow, Kg/s | 48.7 | 48.2 |
| Pressurizer Water Level, m | 2.7 | 2.7 |
| Primary Coolant Pump Speed (IL/BL) RPM | 769/796 | 828/828 |
| SG Secondary side Pressure, MPa | 7.3 | 7.3 |
| Steam Flow, Kg/s | 2.7 | 2.8 |
| SG Secondary Side Level, m | 10.8 | 9.0 |

Table J.3. Sequence of Events.

| Events | Time, Seconds | |
|---|---|---|
| | Test[143] | RELAP5 |
| Break Initiation | 0.0 | 0.0 |
| Reactor Scram | 9.0 | 8.3 |
| ESFAS Signal | 12.0 | 12.6 |
| Main Steam Line Isolation | 14.0 | 14.0 |
| Main Feedwater Isolation | 16.0 | 16.0 |
| Pressurizer Empty | 25.0 | 60.0 |
| Loss of Two-Phase Circulation | 75.0 | 107.0 |
| Loop Seal Clearing | 140.0 | 156.0 |
| Accumulator Injection | 455.0 | 430.0 |
| Core Recovered | 540.0 | 560.0 |

Figure 1. ROSA Large Scale Test Facility Configuration.

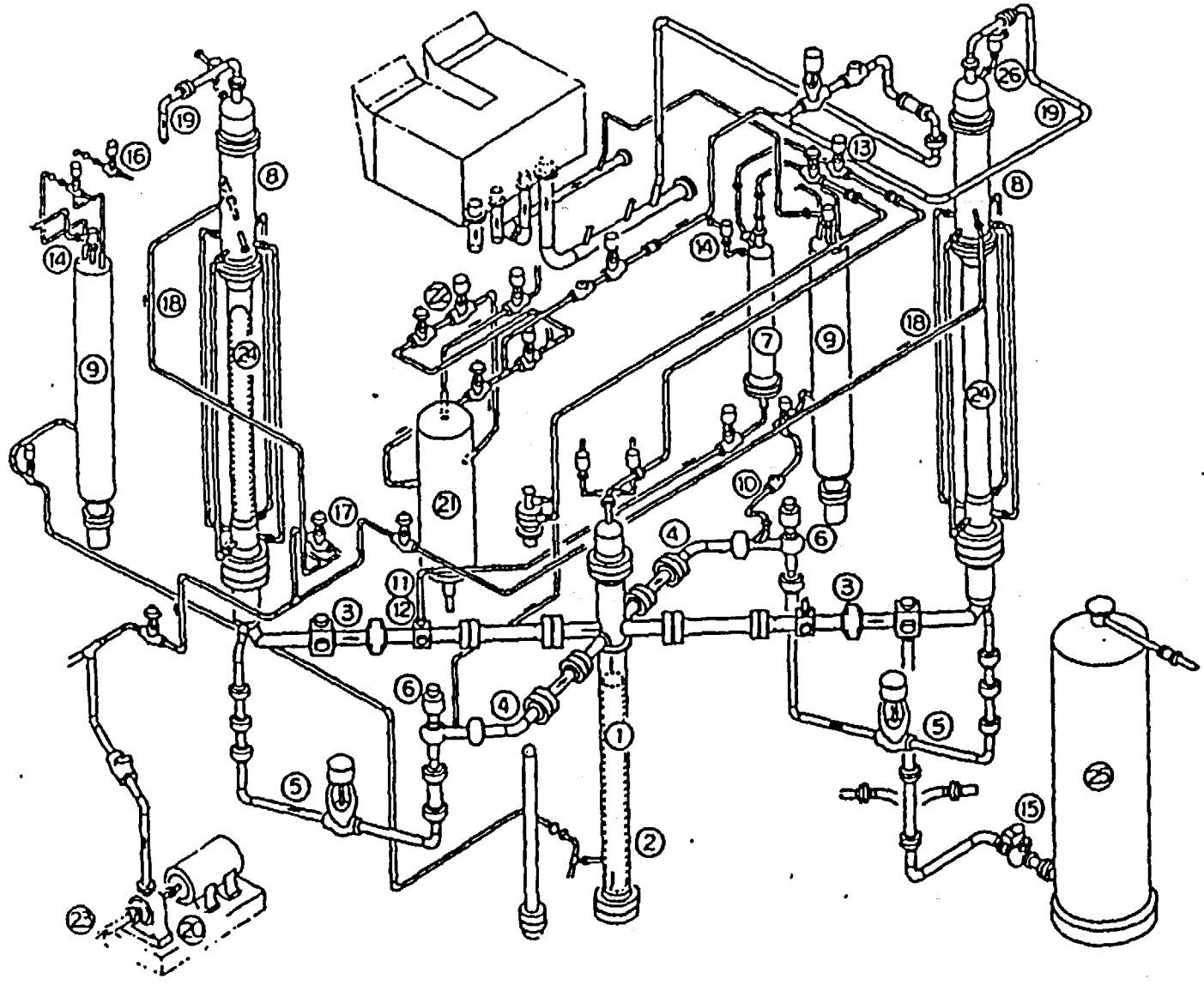

1. Simulated core
2. Reactor pressure vessel
3. Hot leg
4. Cold leg
5. Crossover leg
6. RCS pump
7. Pressurizer
8. Steam generator
9. Accumulator
10. ACC piping
11. HPIS piping
12. RHR piping
13. Pressure control vent valve
14. Relief valve
15. Break initiation valve
16. N2 supply valve
17. Feed water control valve
18. Feed water line
19. Main steam line
20. Feed water pump
21. Jet condenser
22. Main steam valve
23. Cooling tower line
24. Steam generator tubes
25. Break flow storage tank
26. Safety valve

FIGURE J.2. ROSA NODING DIAGRAM FOR PRESSURE VESSEL.

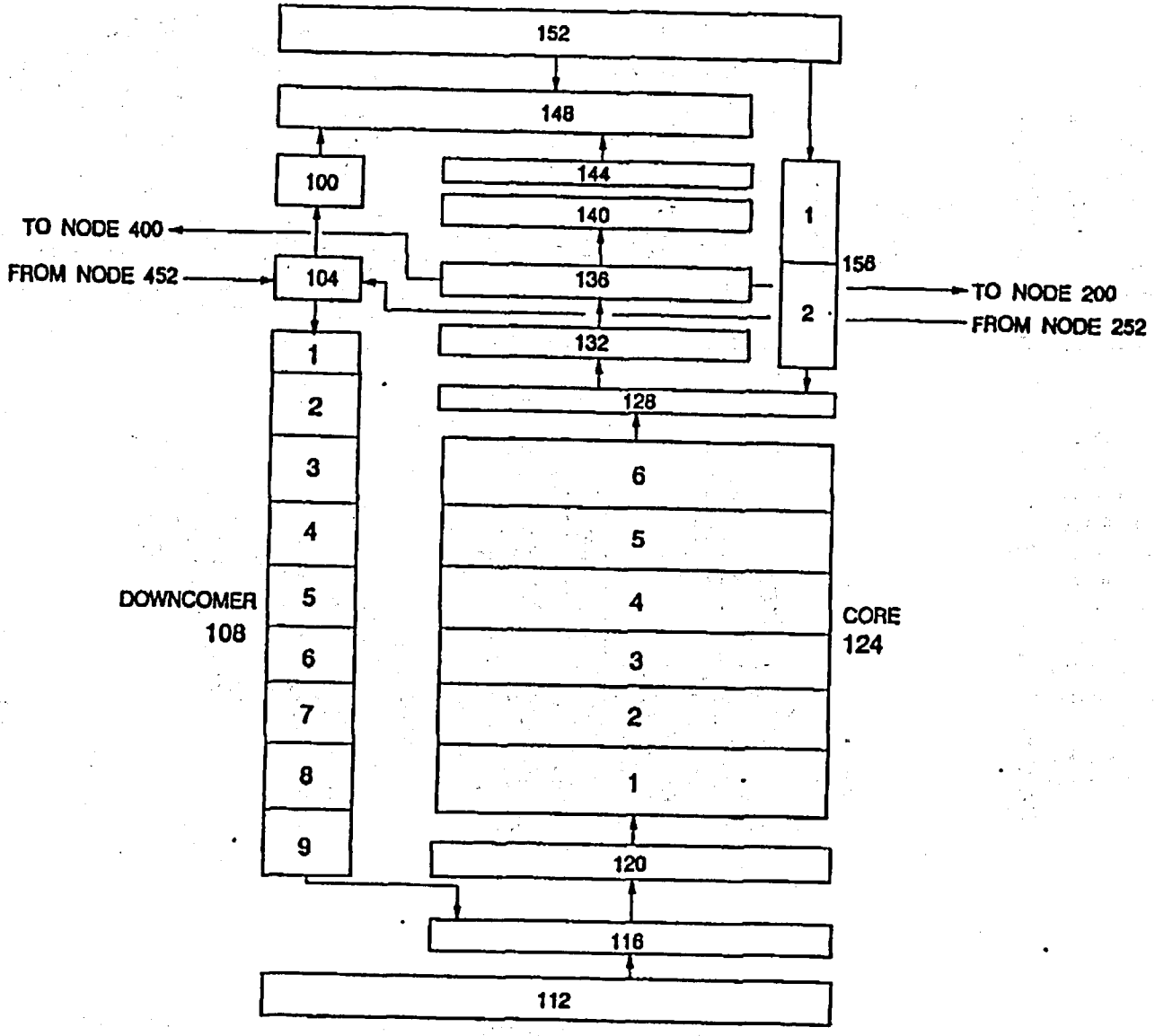

FIGURE J.3. ROSA NODING DIAGRAM FOR PRIMARY LOOPS.

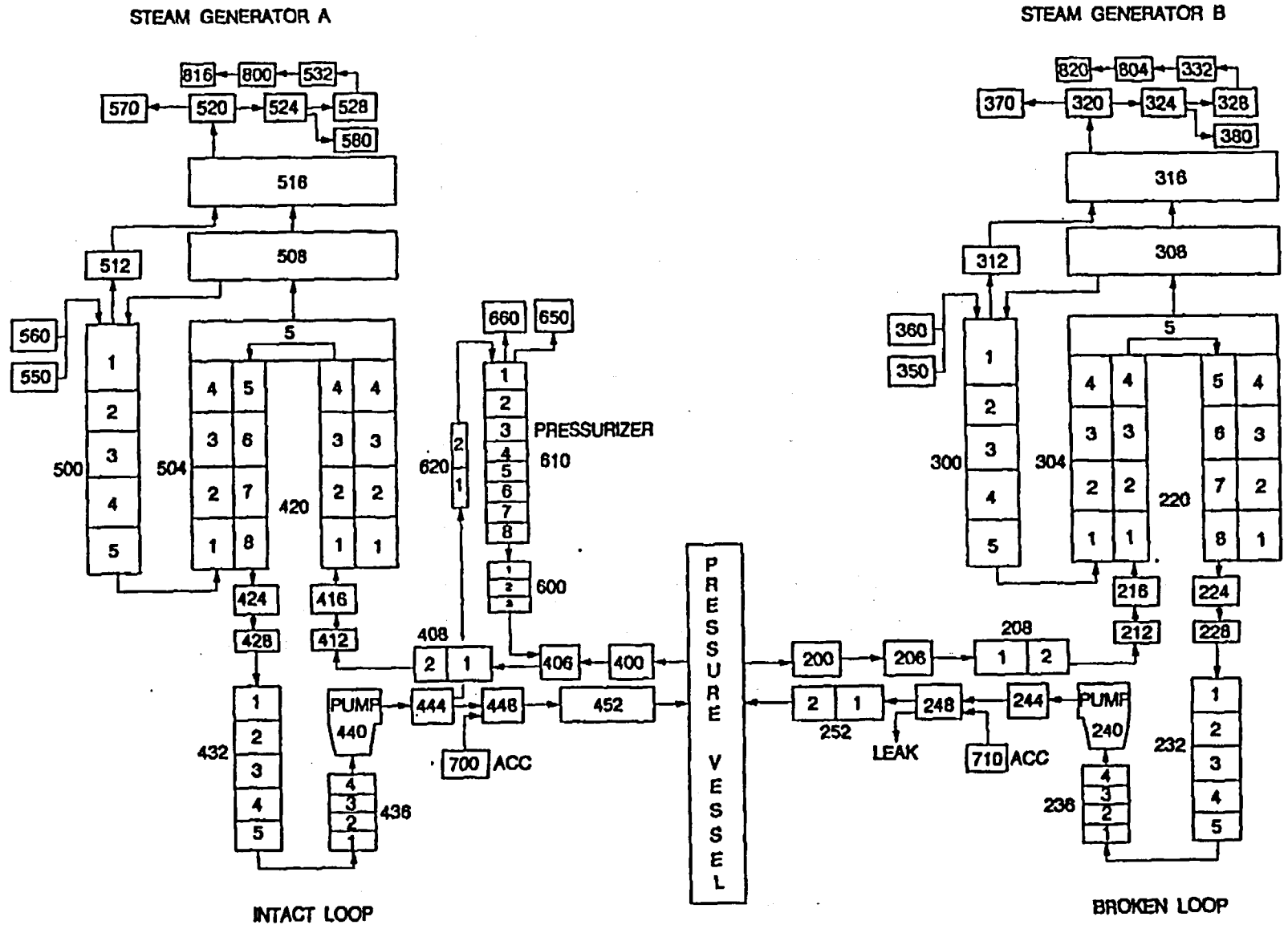

FIGURE J.4. ROSA SBLOCA EM NODING DIAGRAM FOR PRESSURE VESSEL.

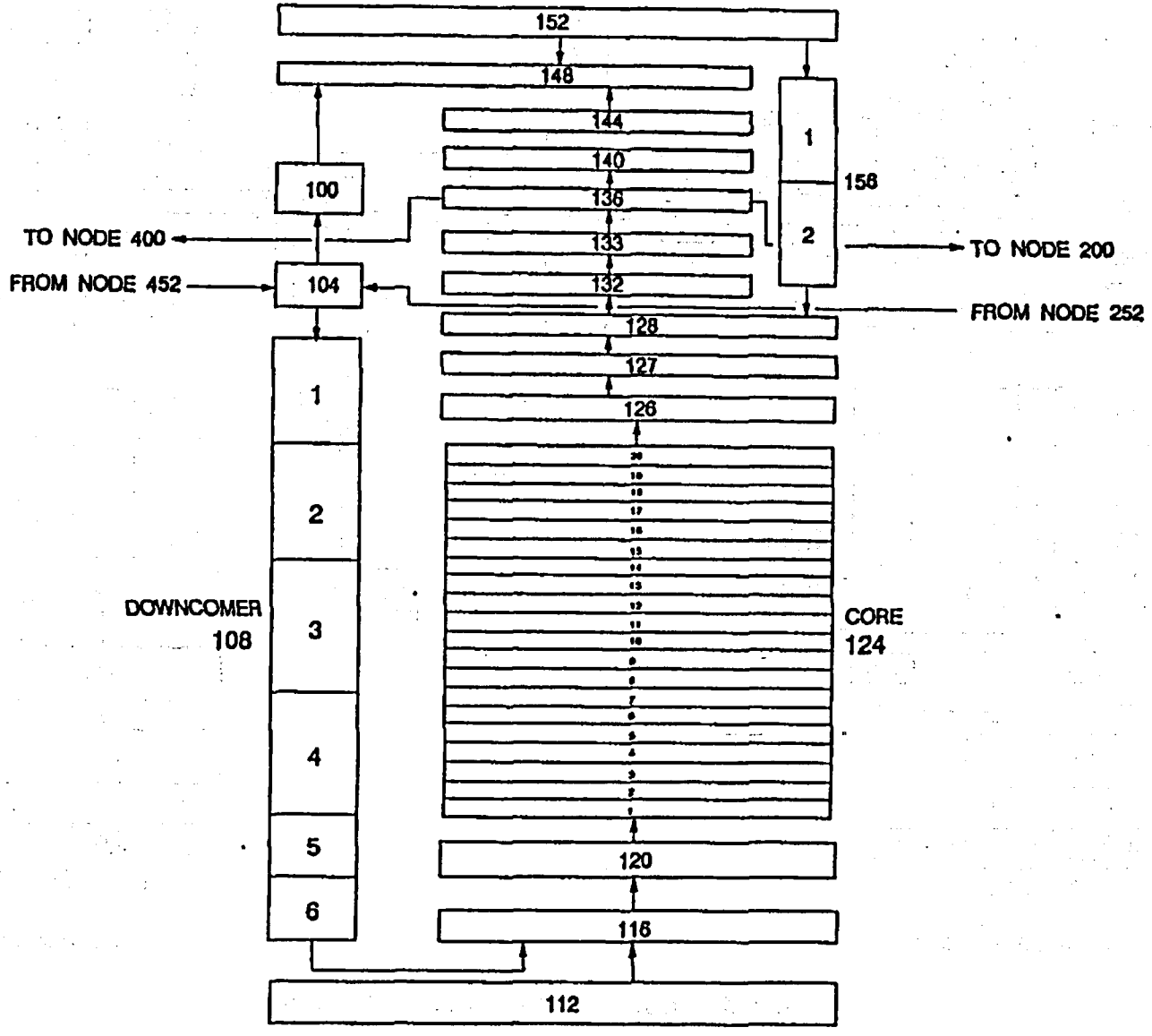

FIGURE J.5. ROSA SBLOCA EM NODING DIAGRAM FOR PRIMARY LOOPS.

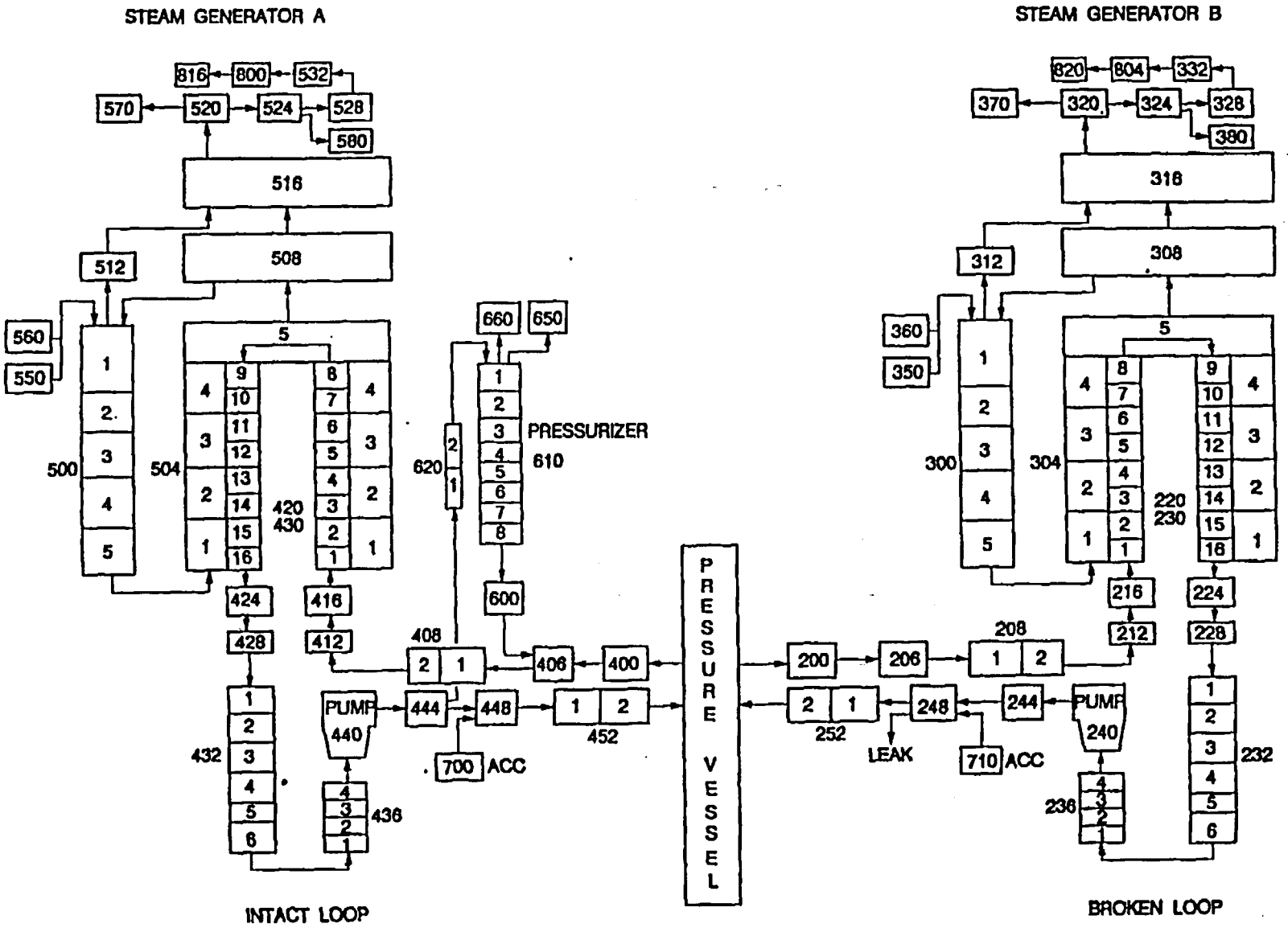

FIGURE J.6. LEAK FLOW RATE.

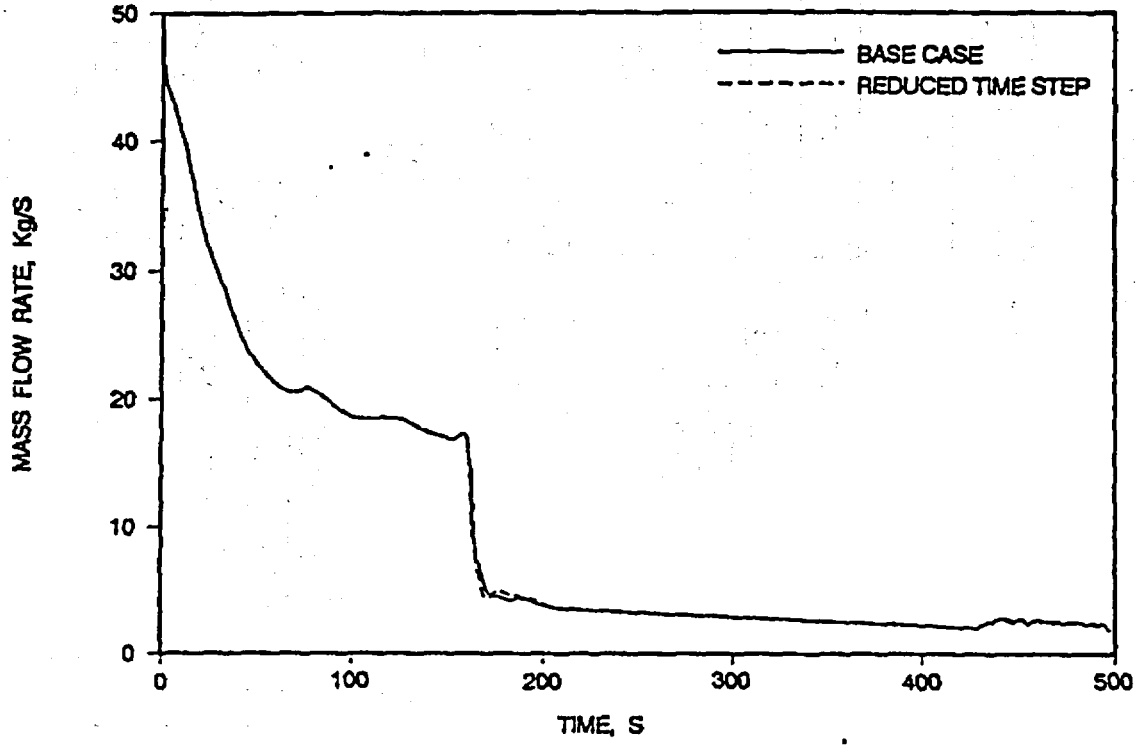


FIGURE J.7. PRIMARY SYSTEM PRESSURE.

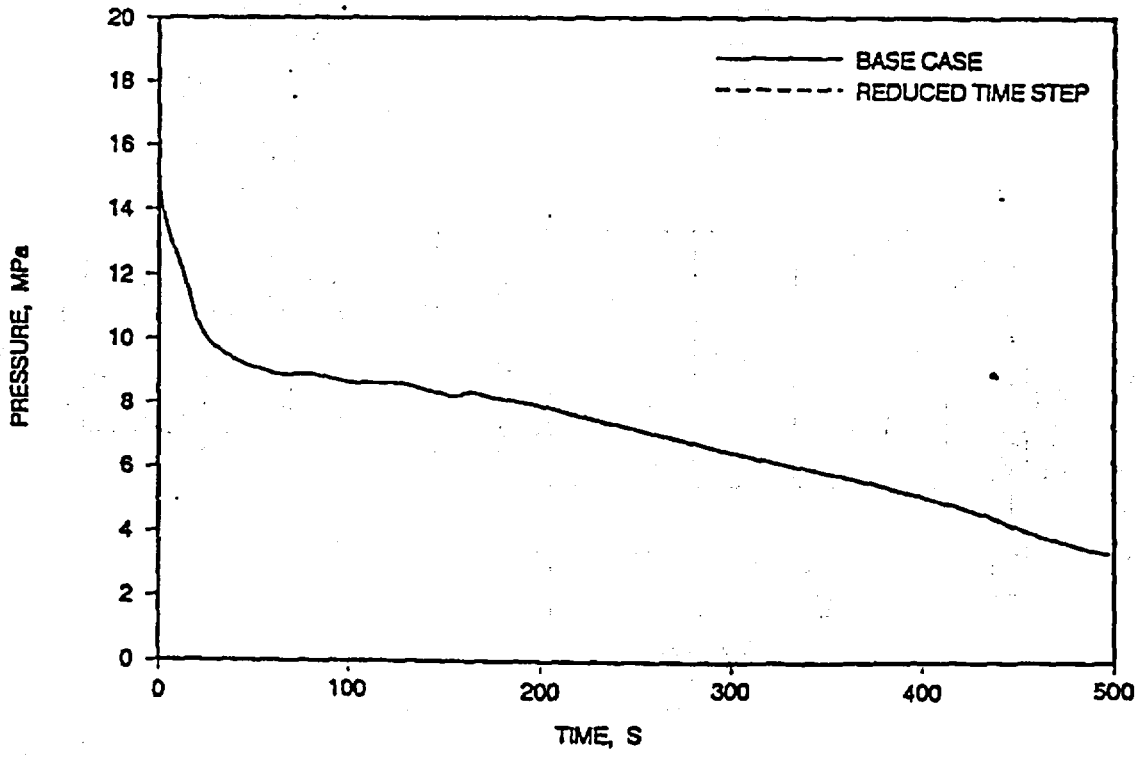

FIGURE J.8. CORE DIFFERENTIAL PRESSURE.

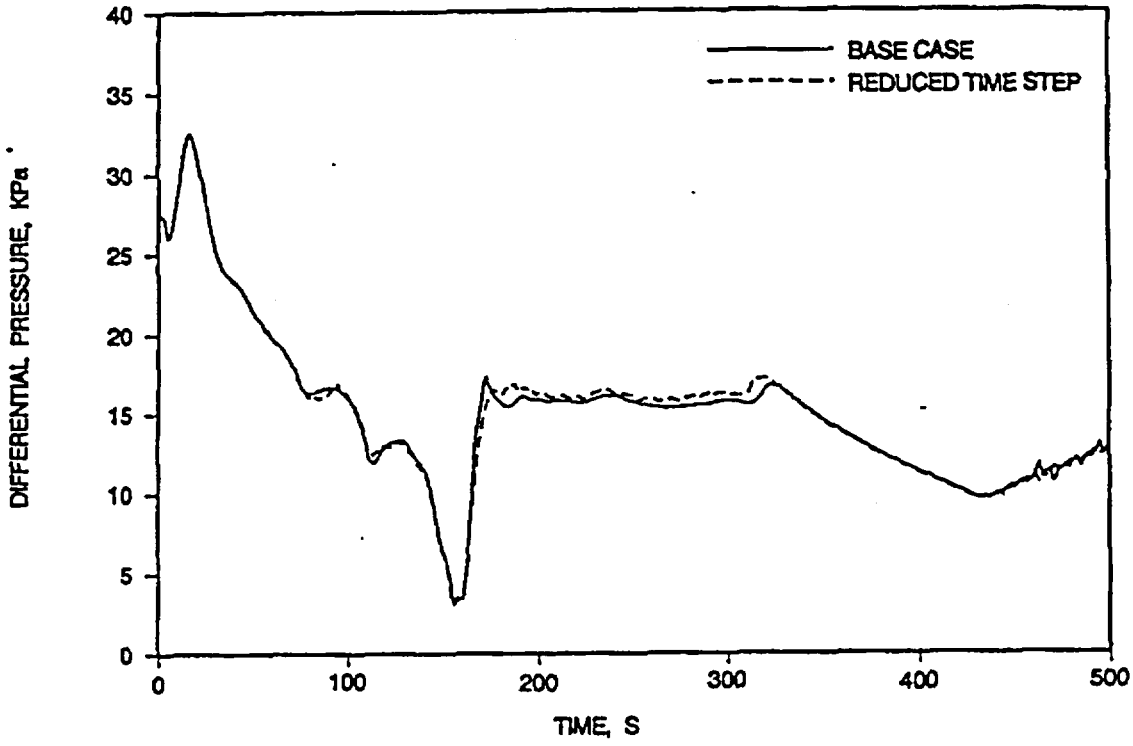


FIGURE J.9. INTACT LOOP PUMP SUCTION SEAL DOWNFLOW DIFFERENTIAL PRESSURE.

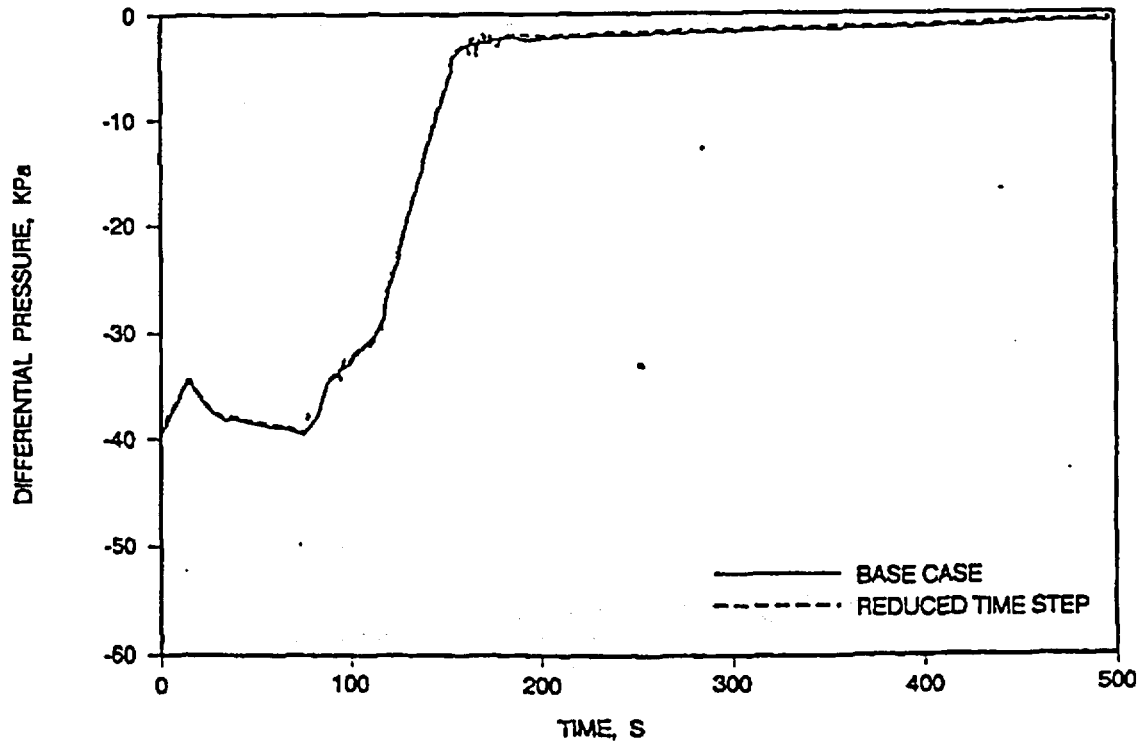

FIGURE J.10. BROKEN LOOP PUMP SUCTION SEAL DOWNFLOW DIFFERENTIAL PRESSURE.

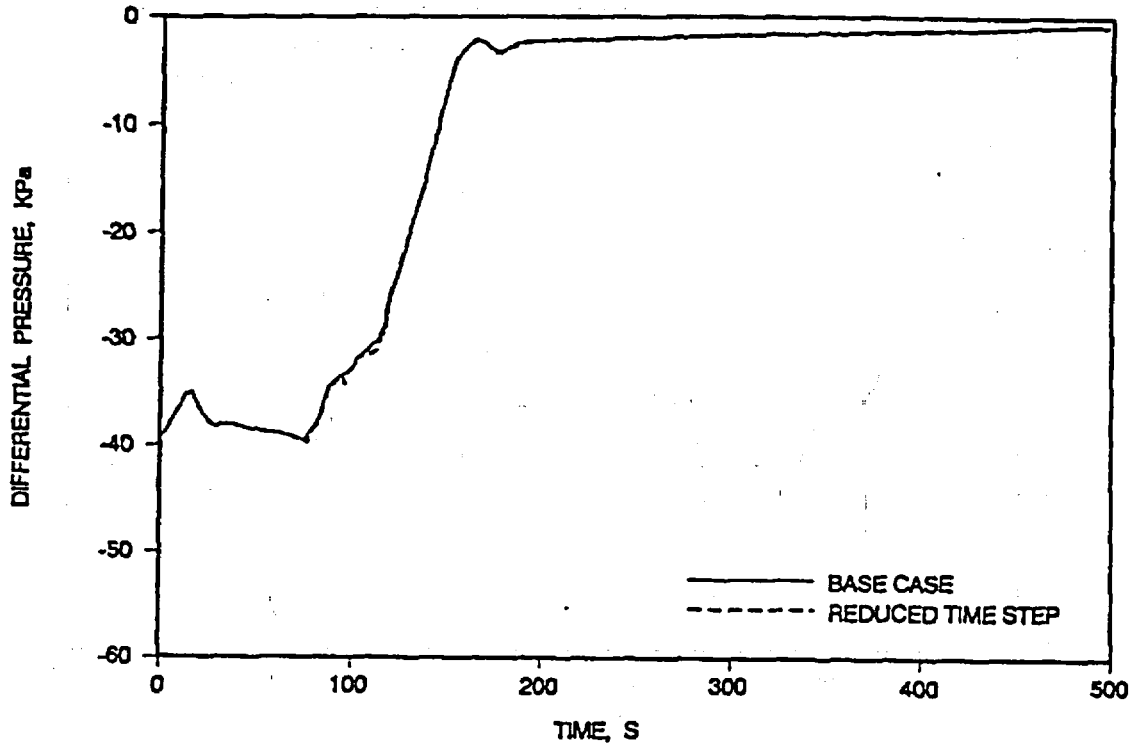


FIGURE J.11. LEAK FLOW RATE.

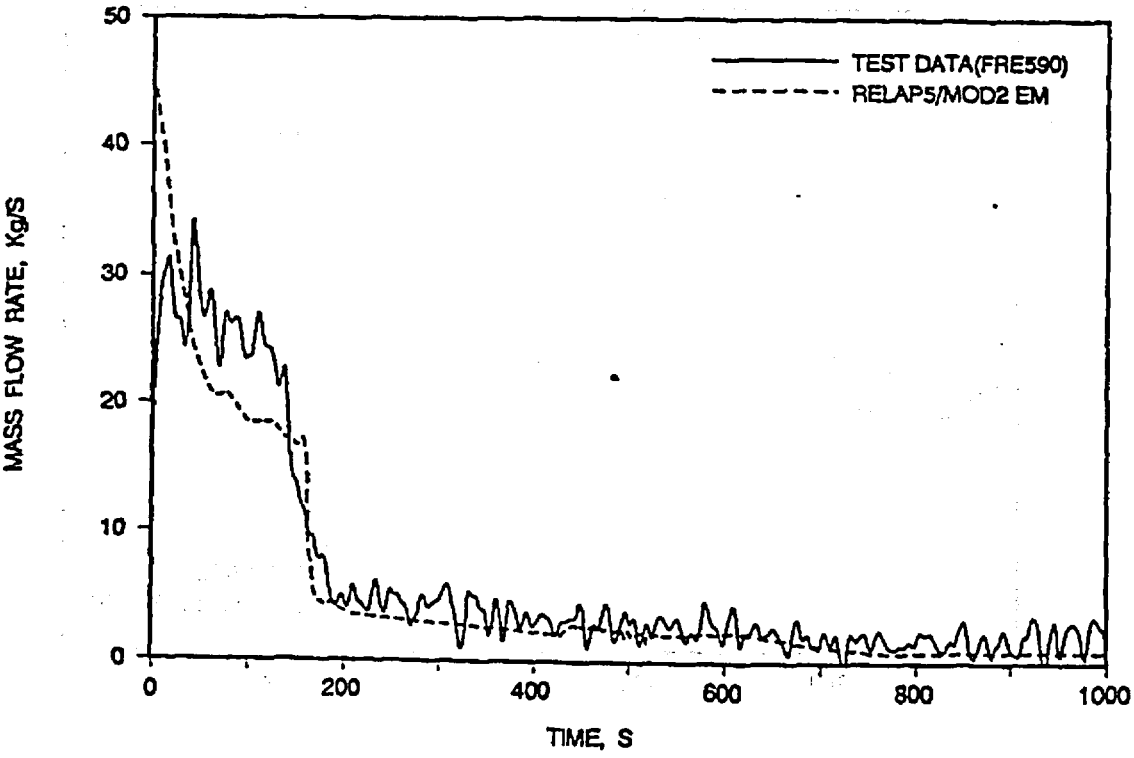

FIGURE J.12. PRIMARY SYSTEM PRESSURE.

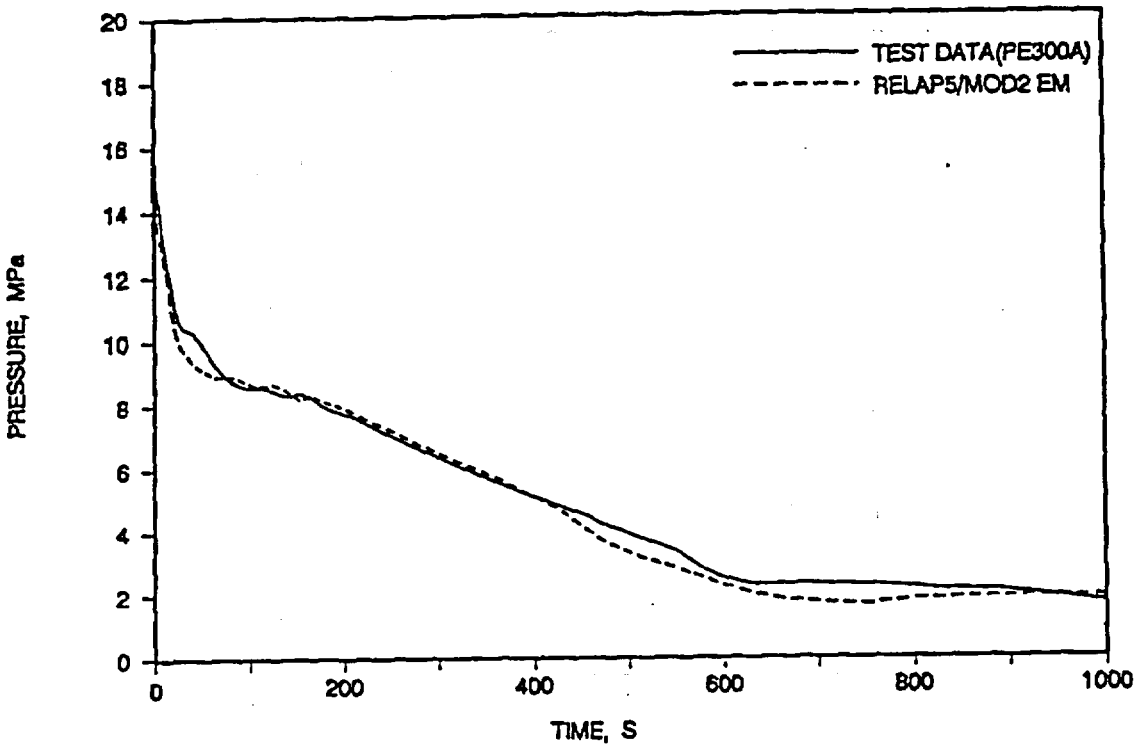


FIGURE J.13. PRESSURIZER LEVEL.

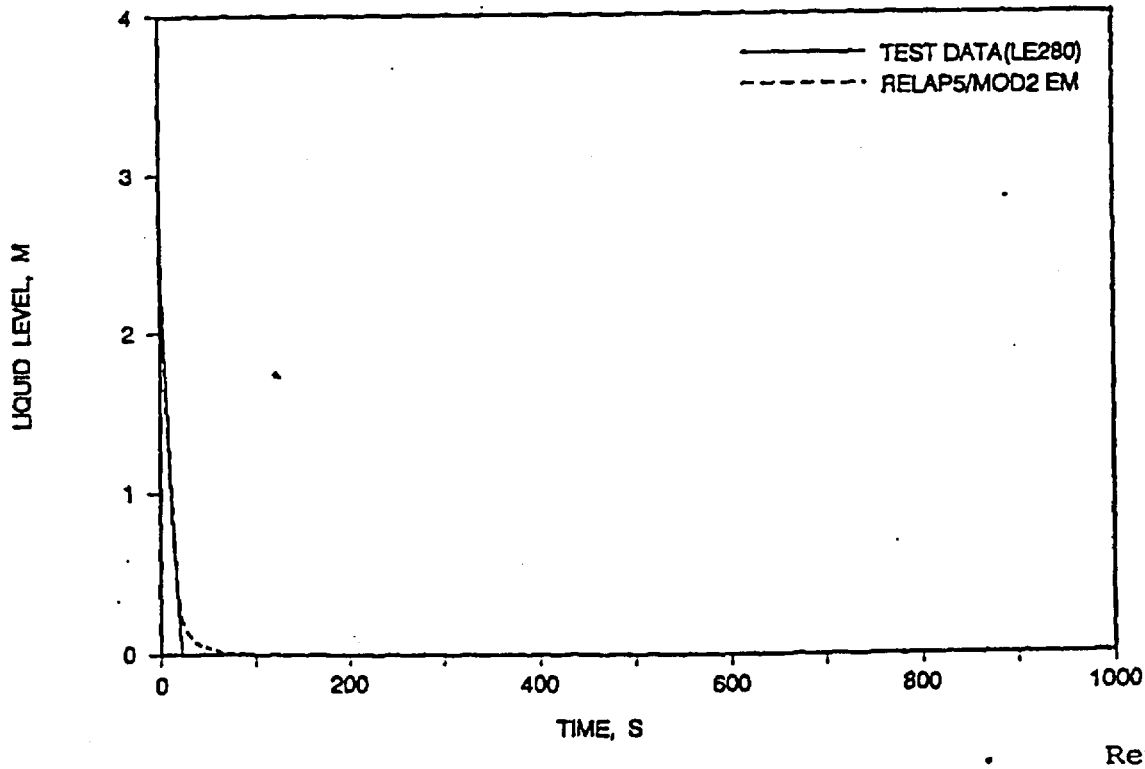

FIGURE J.14. INTACT LOOP STEAM GENERATOR PRESSURE.

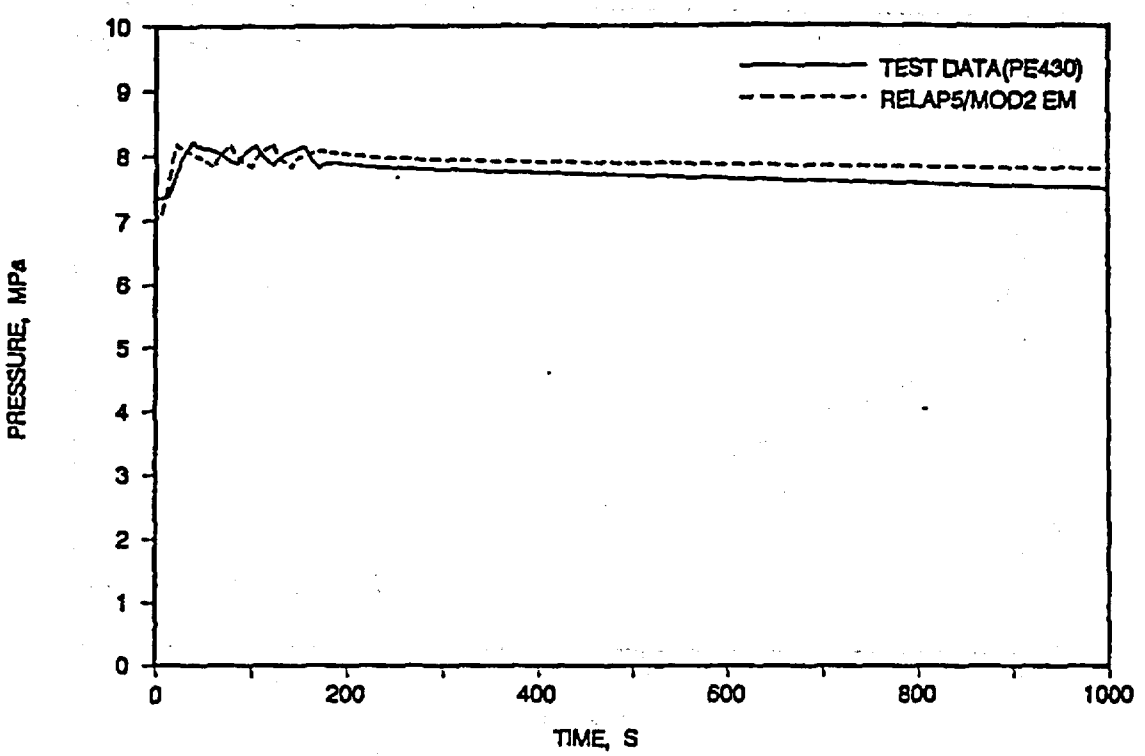


FIGURE J.15. BROKEN LOOP STEAM GENERATOR PRESSURE.

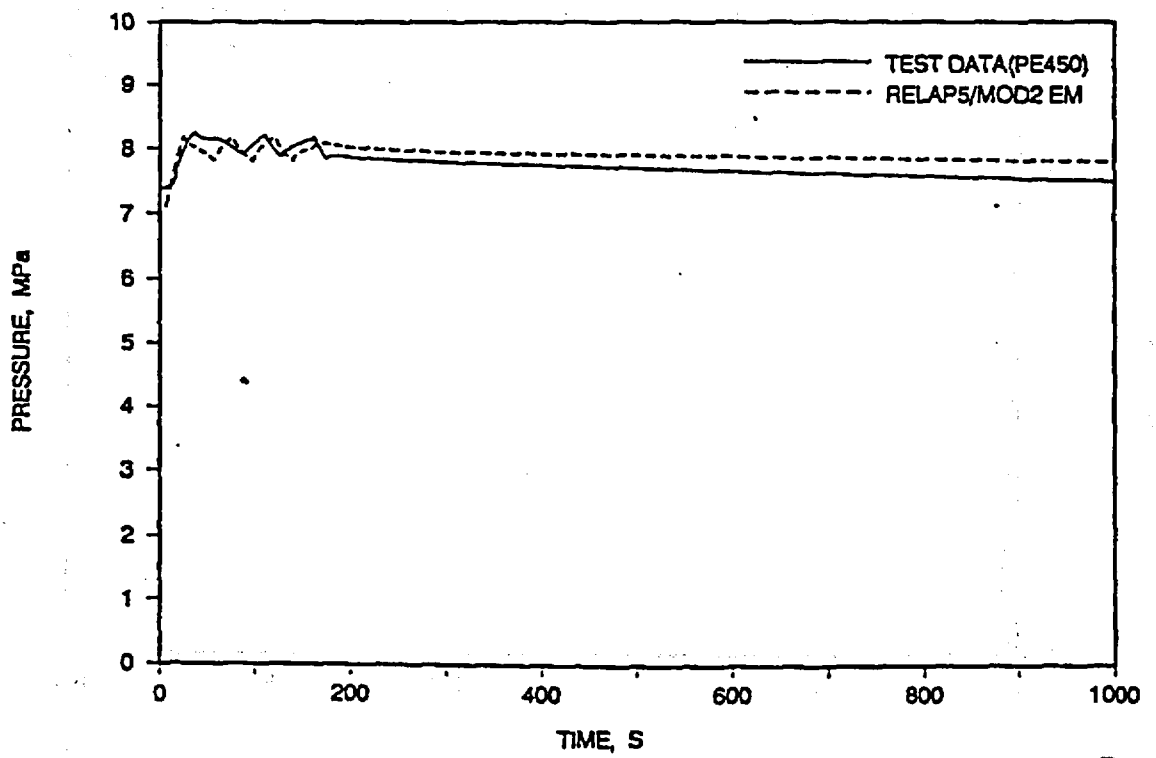

FIGURE J.16. INTACT LOOP PUMP SUCTION SEAL DOWNFLOW DIFFERENTIAL PRESSURE.

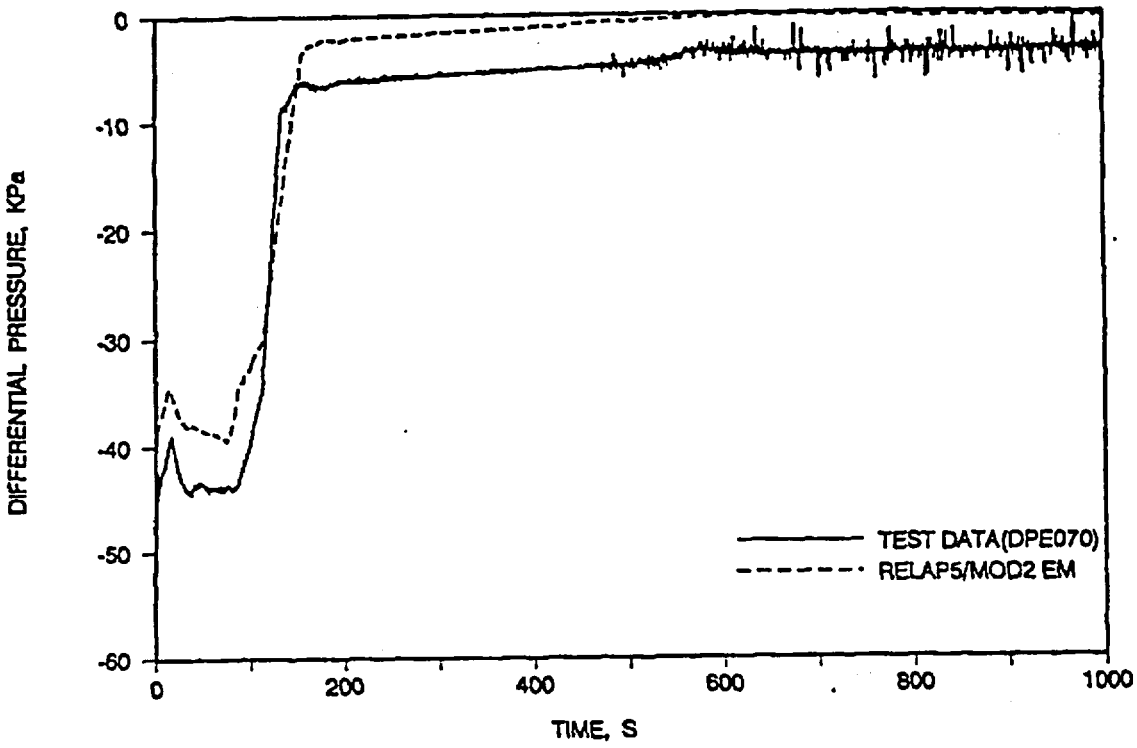


FIGURE J.17. INTACT LOOP PUMP SUCTION SEAL UPFLOW DIFFERENTIAL PRESSURE.

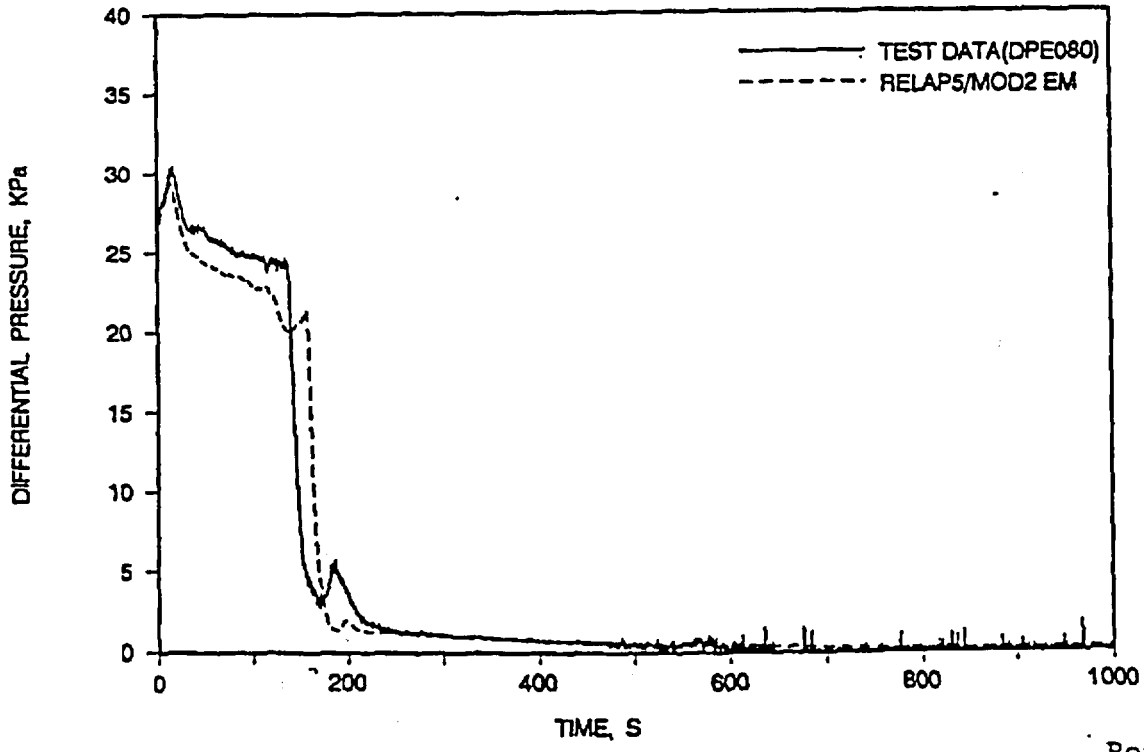

FIGURE J.18. BROKEN LOOP PUMP SUCTION SEAL DOWNFLOW DIFFERENTIAL PRESSURE.

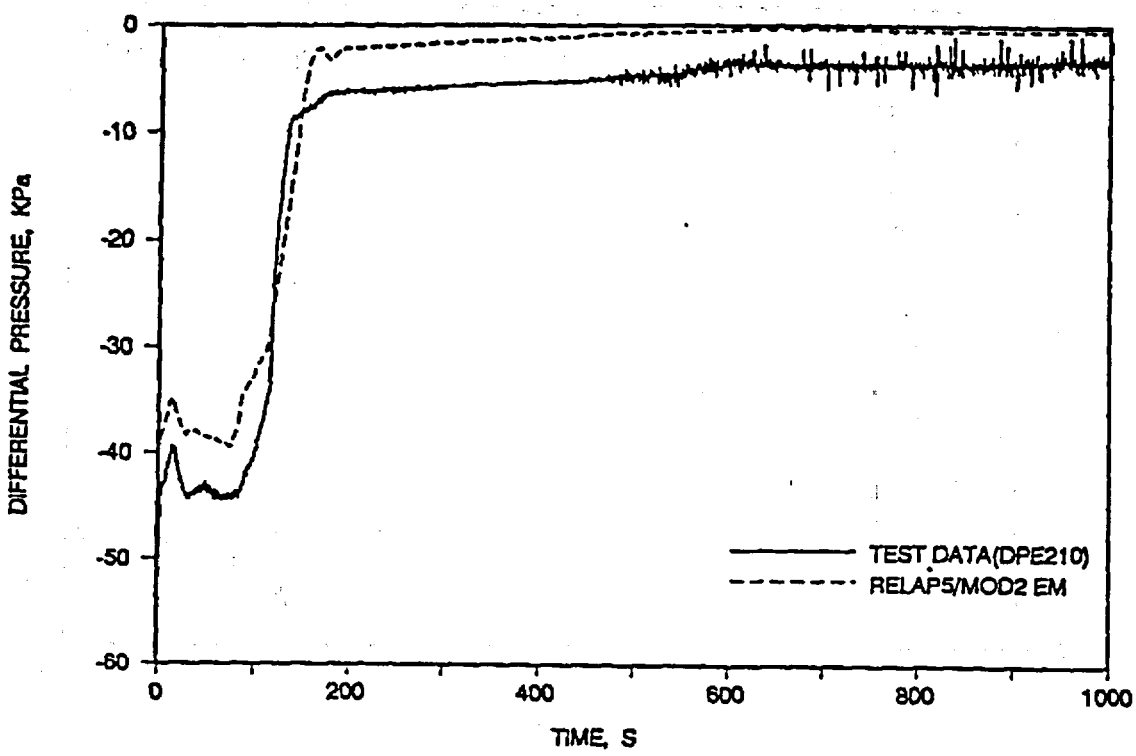


FIGURE J.19. BROKEN LOOP PUMP SUCTION SEAL UPFLOW DIFFERENTIAL PRESSURE.

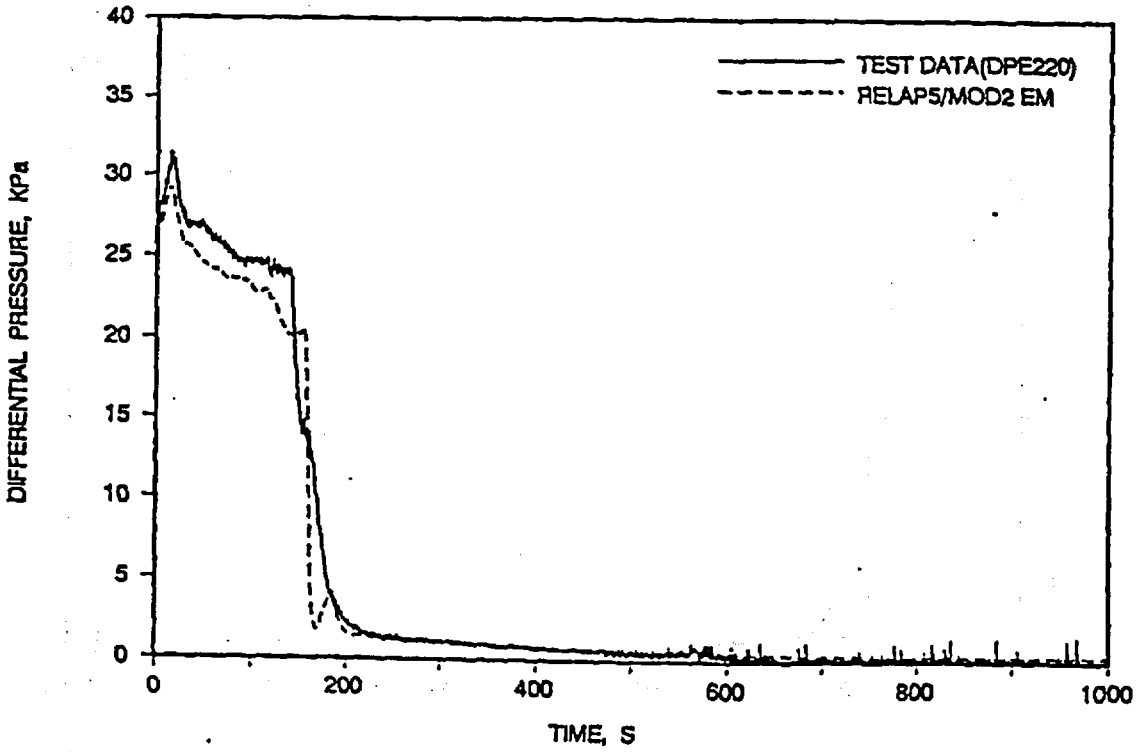

FIGURE J.20. CORE DIFFERENTIAL PRESSURE.

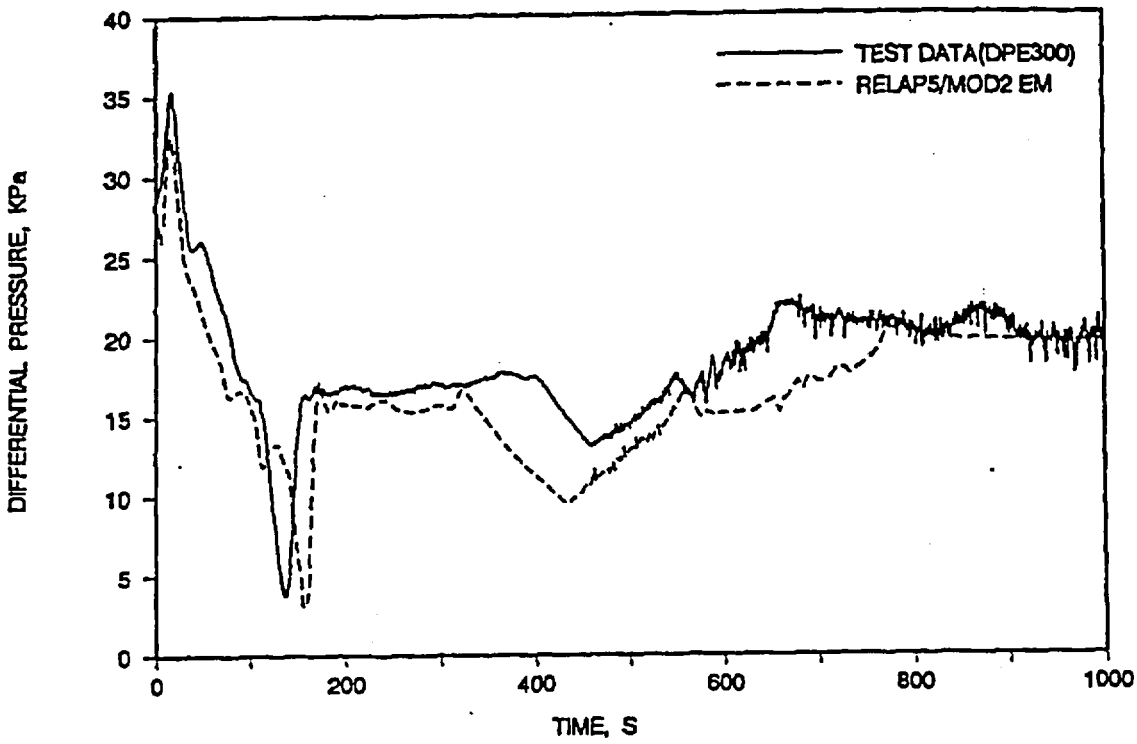


FIGURE J.21. DOWNCOMER DIFFERENTIAL PRESSURE.

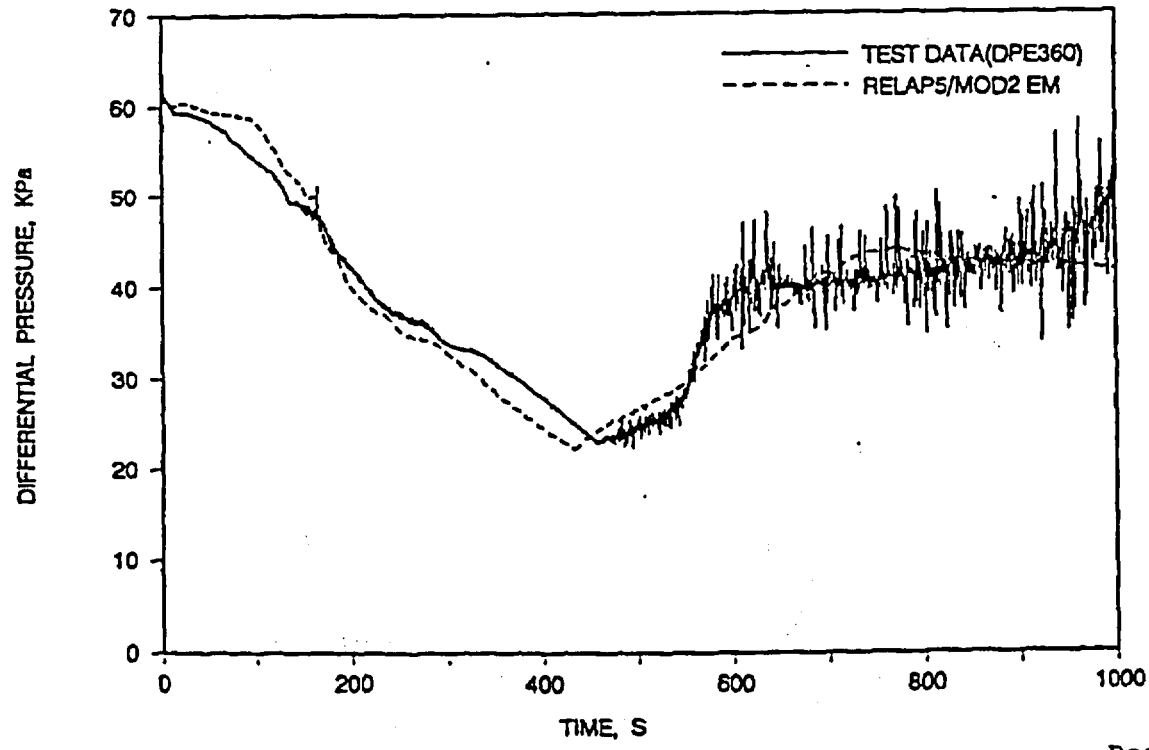

FIGURE J.22. INTACT LOOP STEAM GEN. INLET PLENUM DIFFERENTIAL PRESSURE.

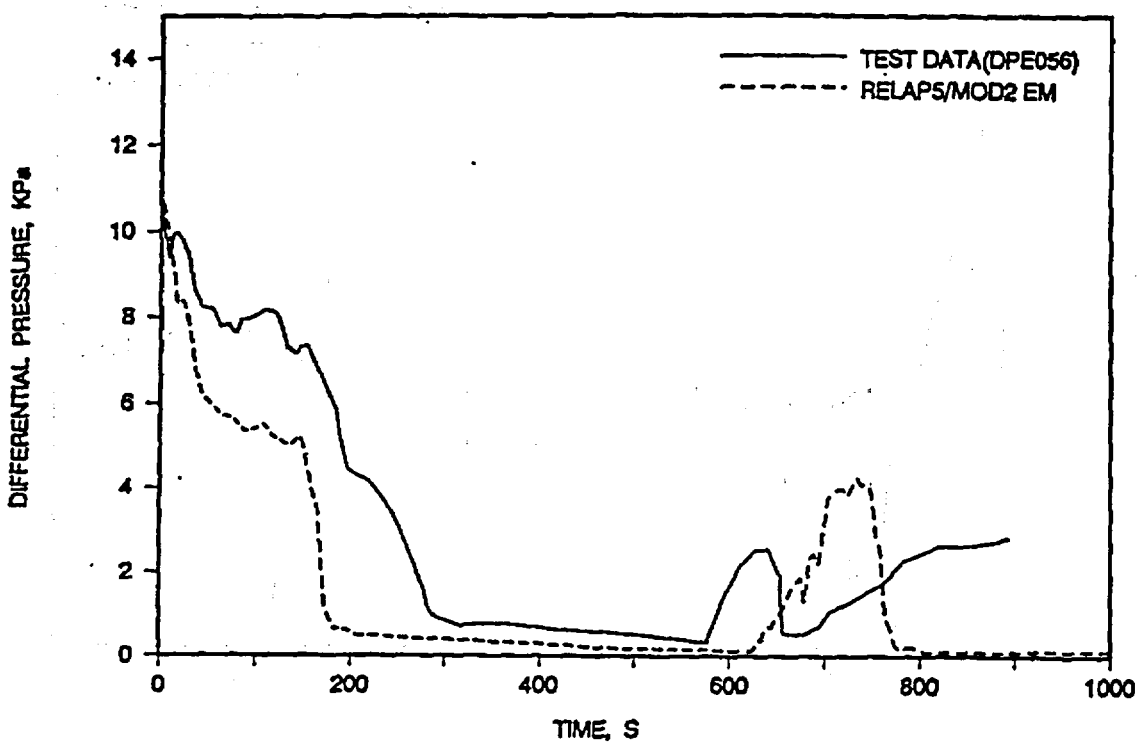


FIGURE J.23. BROKEN LOOP STEAM GEN. INLET PLENUM DIFFERENTIAL PRESSURE.

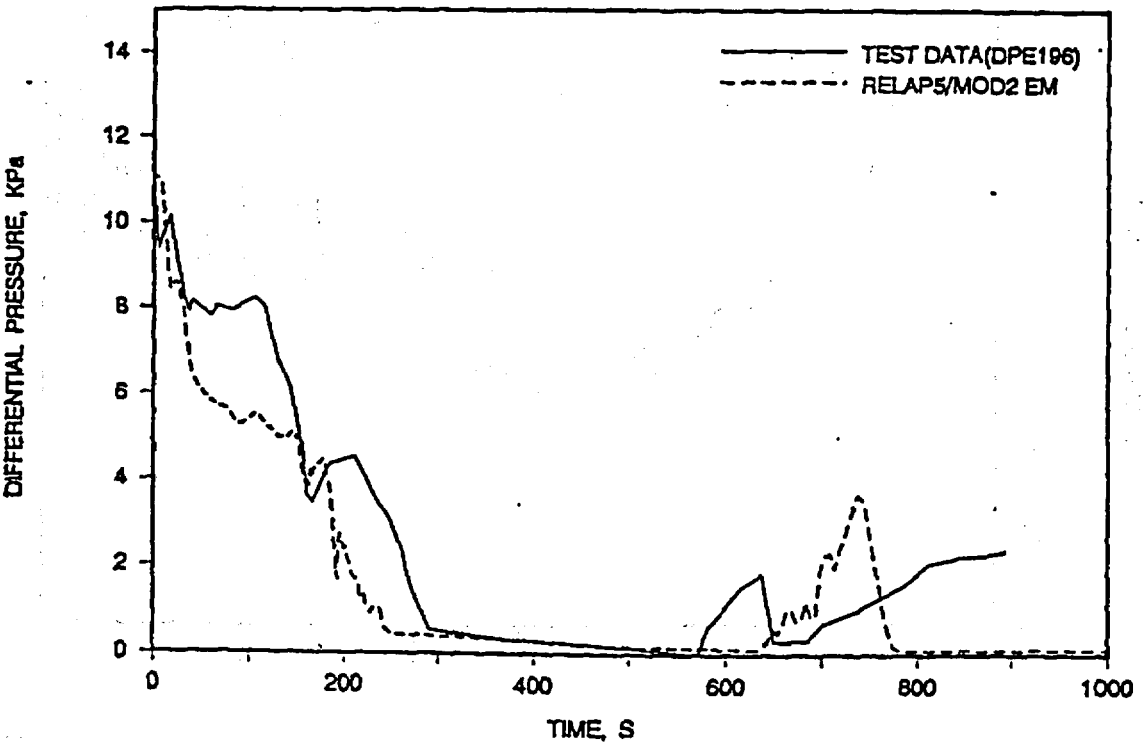

FIGURE J.24. INTACT LOOP STEAM GEN. TUBE UPFLOW DIFFERENTIAL PRESSURE.

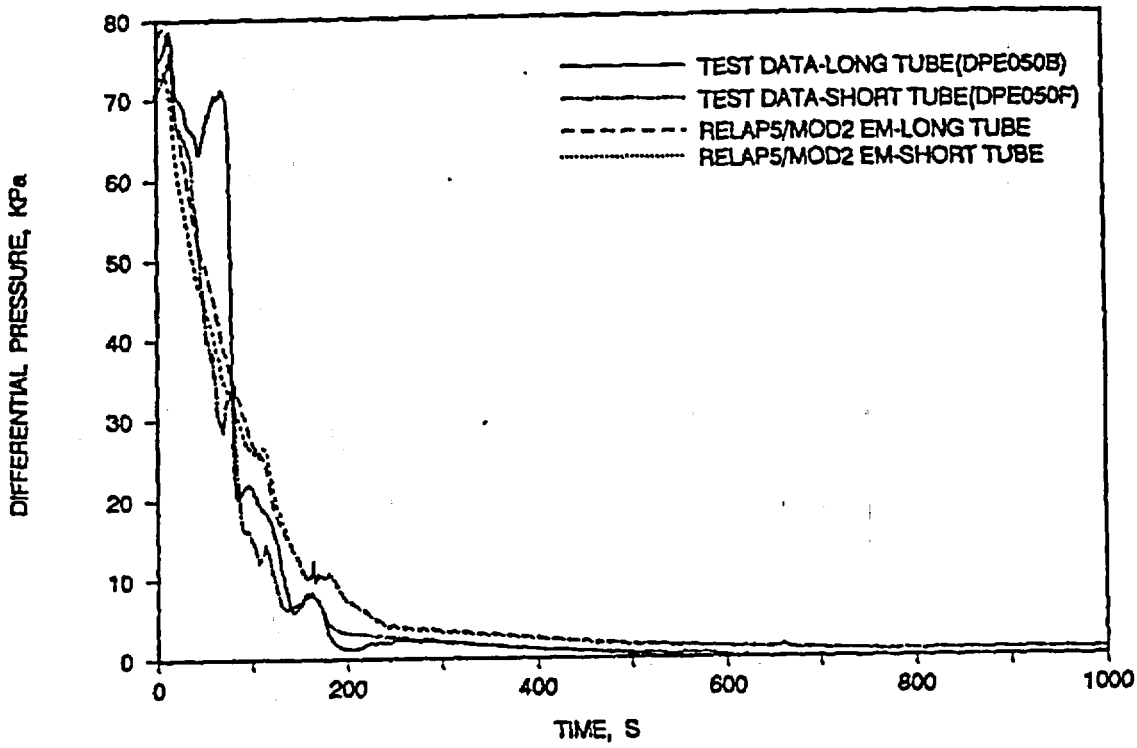


FIGURE J.25. BROKEN LOOP STEAM GEN. TUBE UPFLOW DIFFERENTIAL PRESSURE.

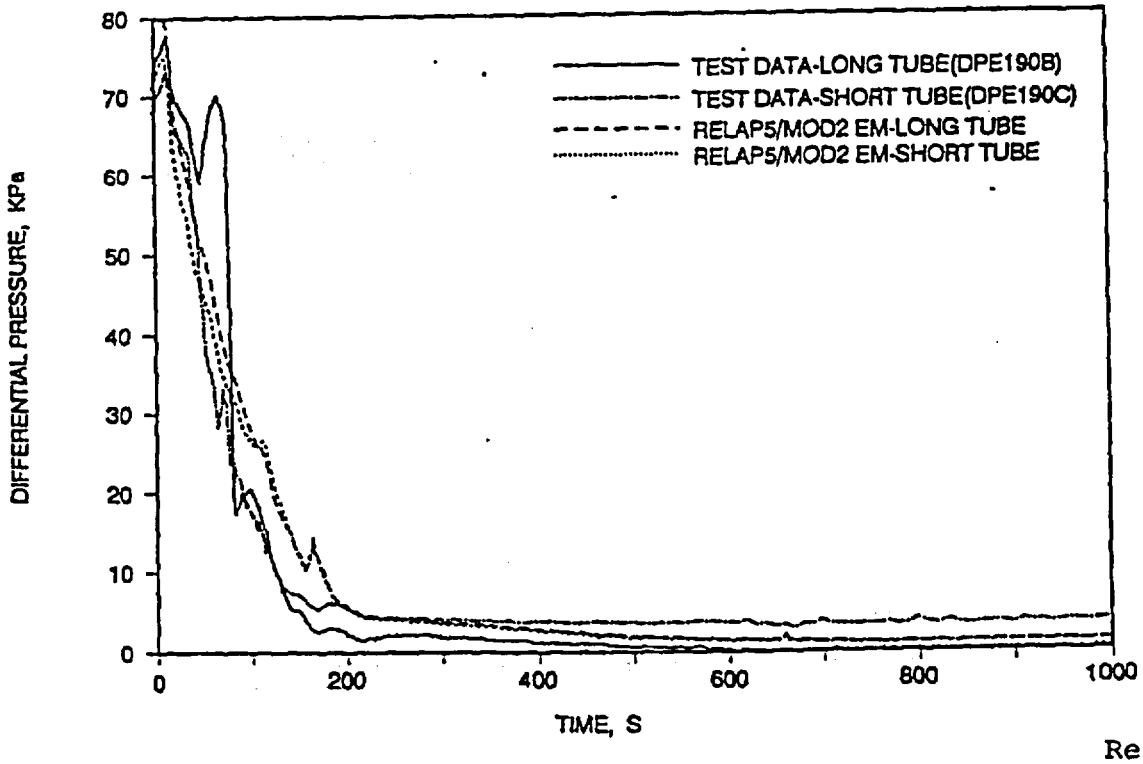

FIGURE J.26. UPPER PLENUM DIFFERENTIAL PRESSURE.

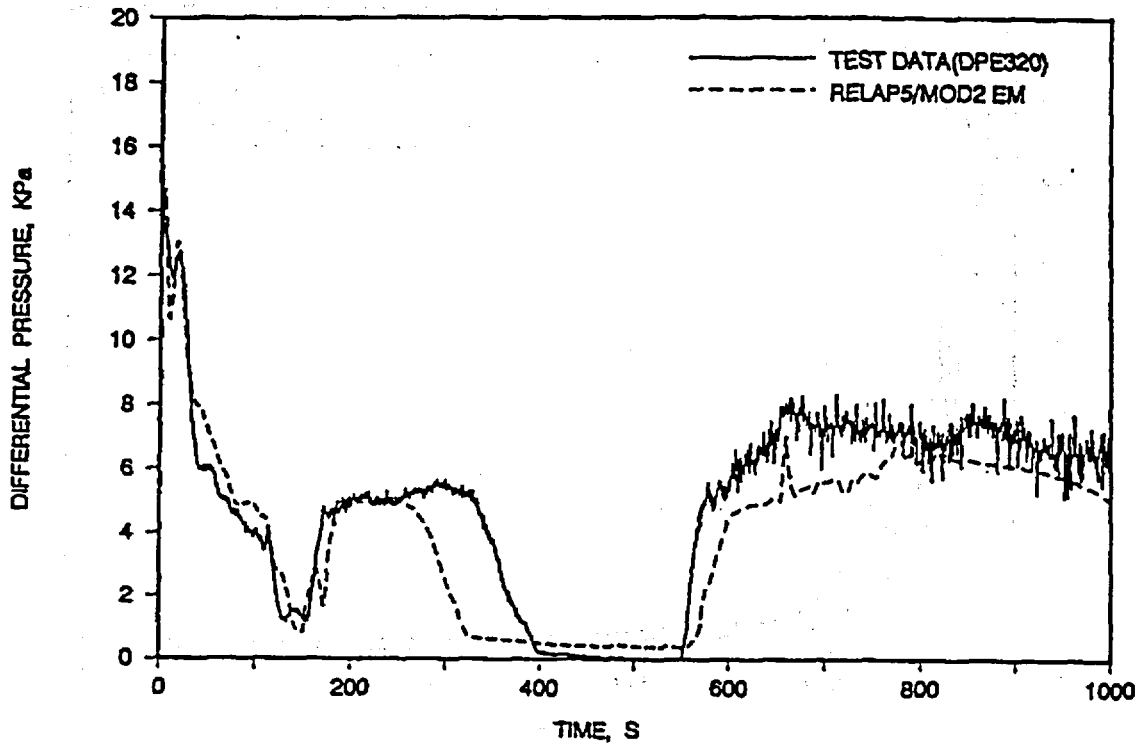


FIGURE J.27. INTACT LOOP STEAM GEN. TUBE DOWNFLOW DIFFERENTIAL PRESSURE.

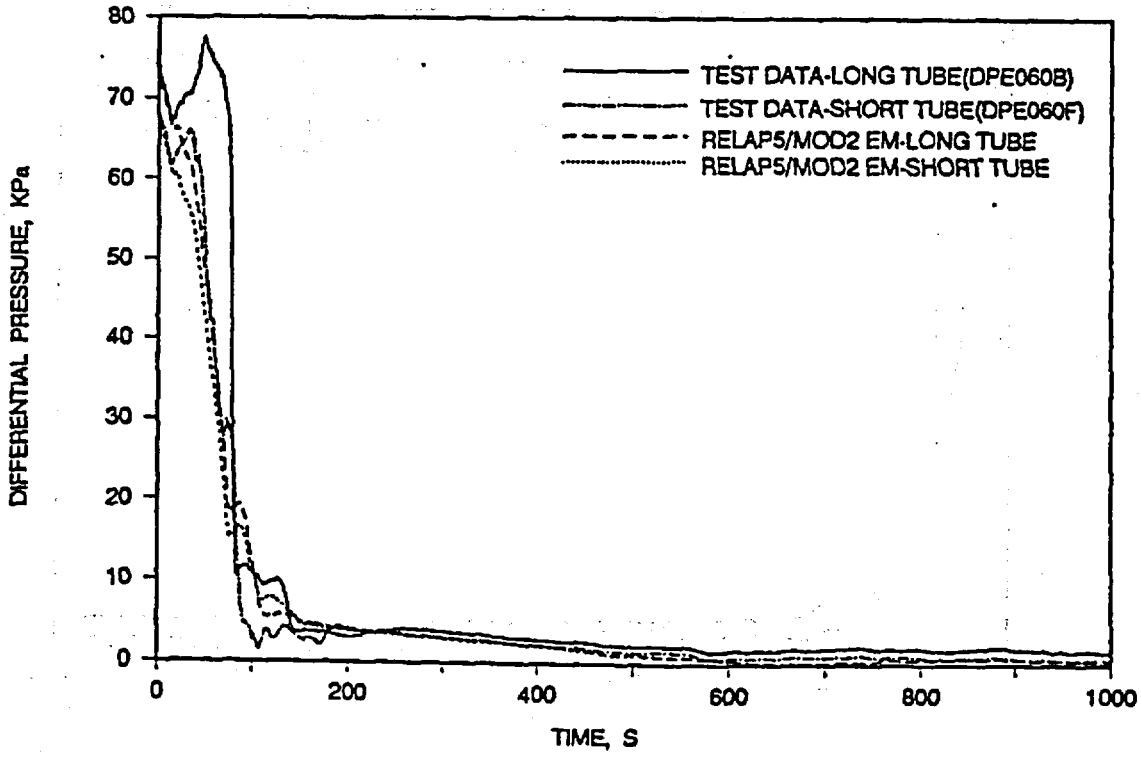

FIGURE J.28. BROKEN LOOP STEAM GEN. TUBE DOWNFLOW DIFFERENTIAL PRESSURE.

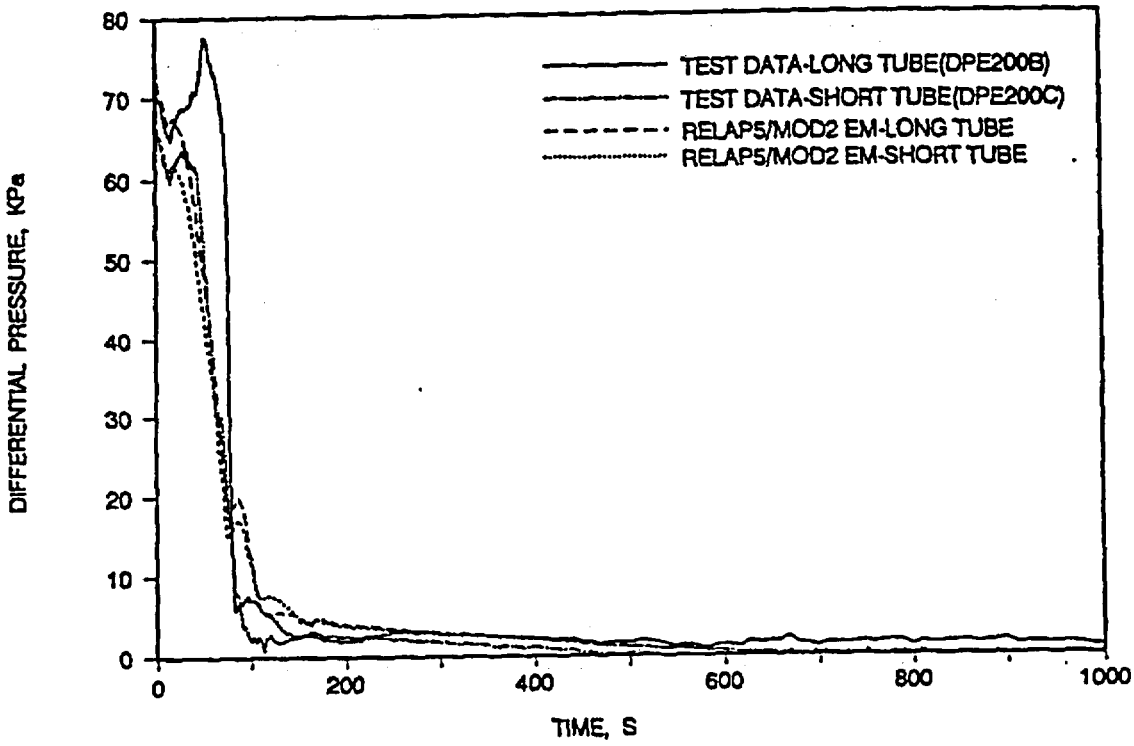


FIGURE J.29. INTACT LOOP ACCUMULATOR FLOW RATE.

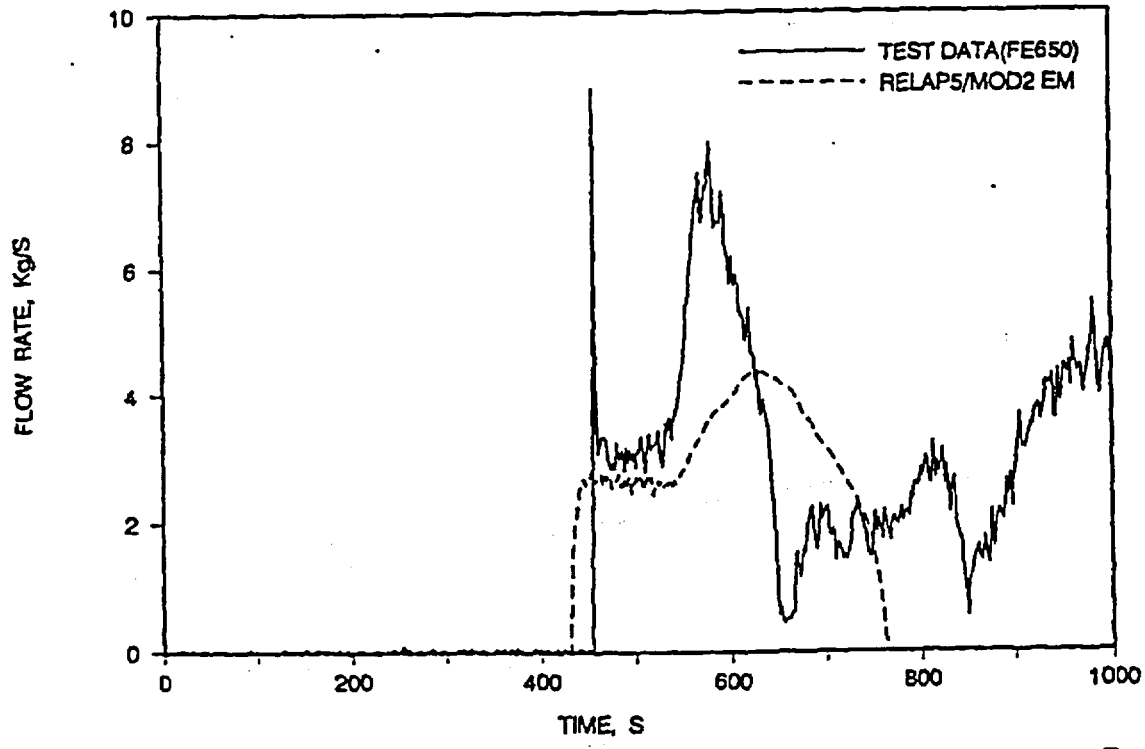

FIGURE J.30. BROKEN LOOP ACCUMULATOR FLOW RATE.

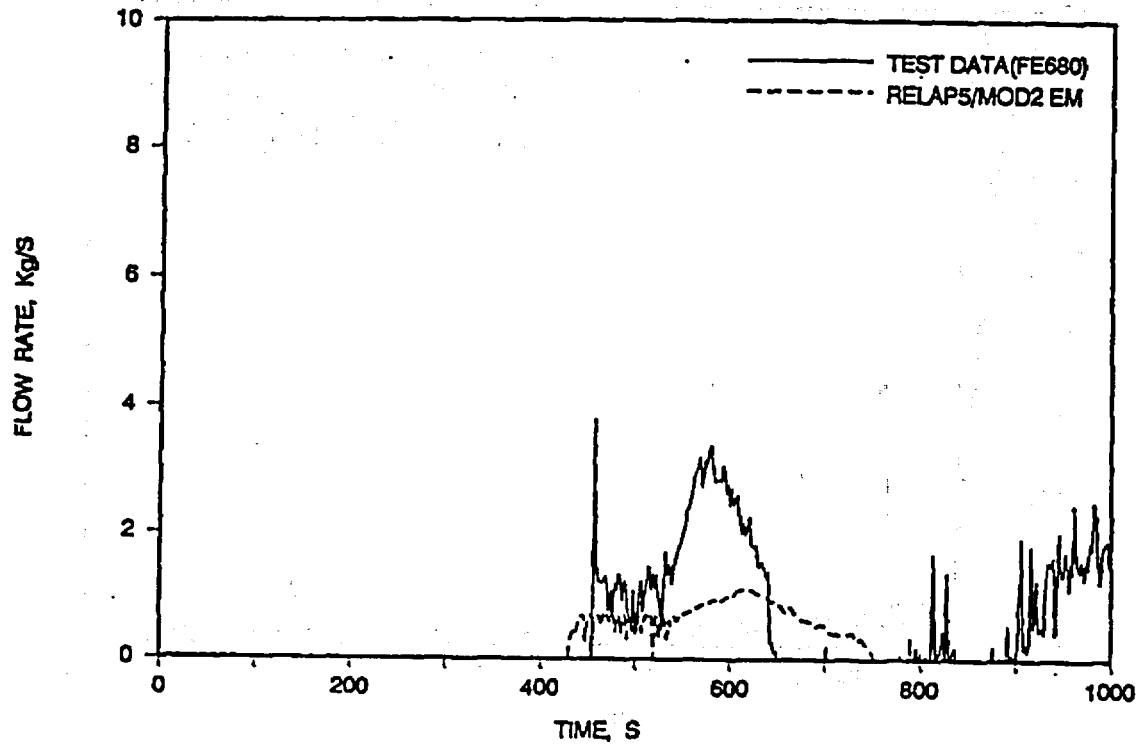


FIGURE J.31. HOT ROD SURFACE TEMPERATURE - ELEV 0.05 M.

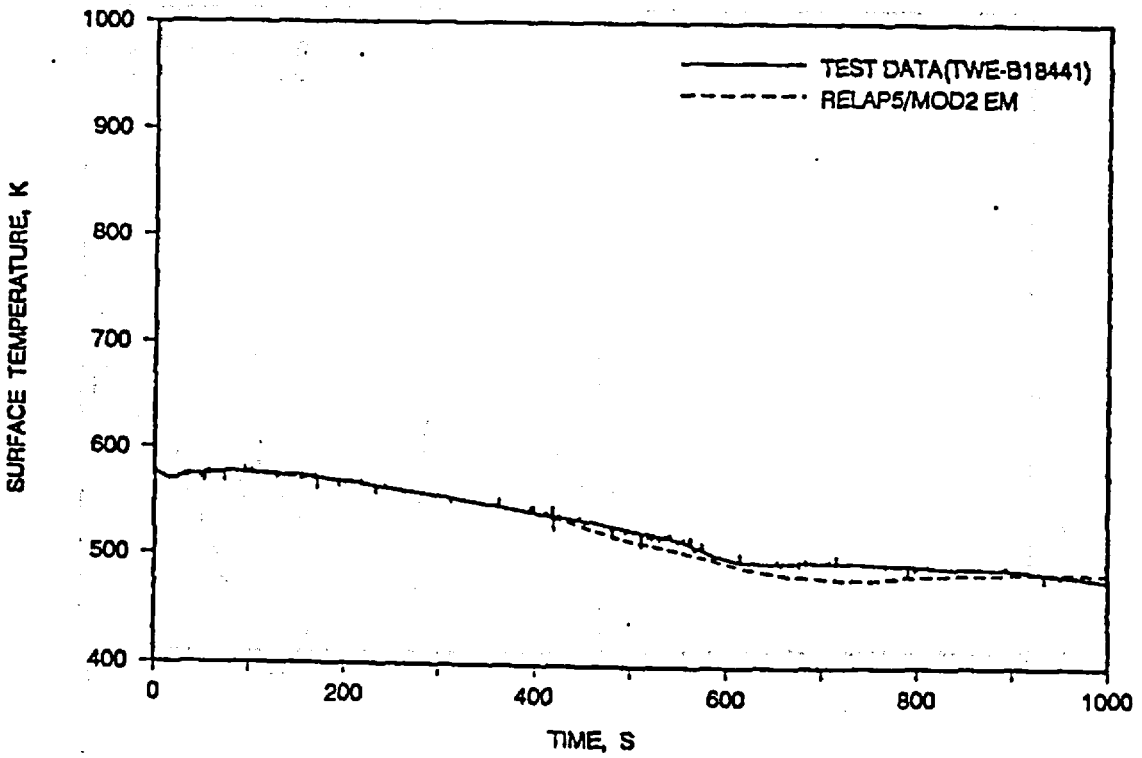

FIGURE J.32. HOT ROD SURFACE TEMPERATURE - ELEV 1.018 M.

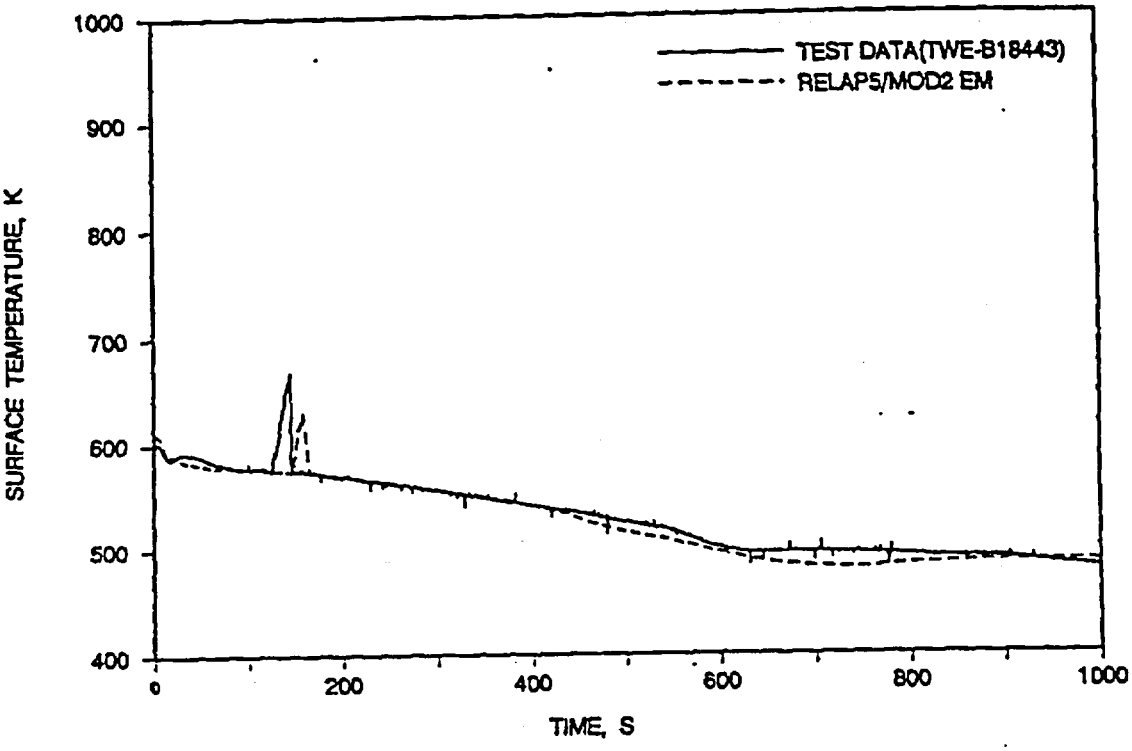


FIGURE J.33. HOT ROD SURFACE TEMPERATURE - ELEV 1.83 M.

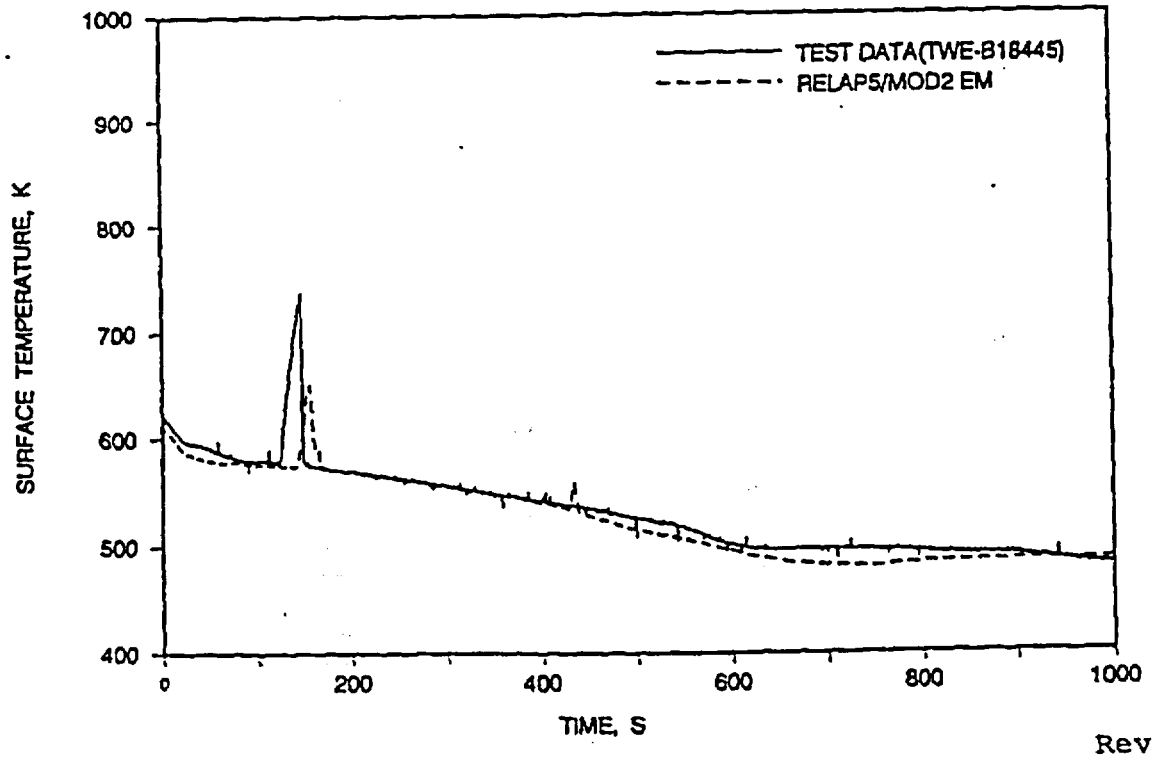

FIGURE J.34. HOT ROD SURFACE TEMPERATURE - ELEV 2.236 M.

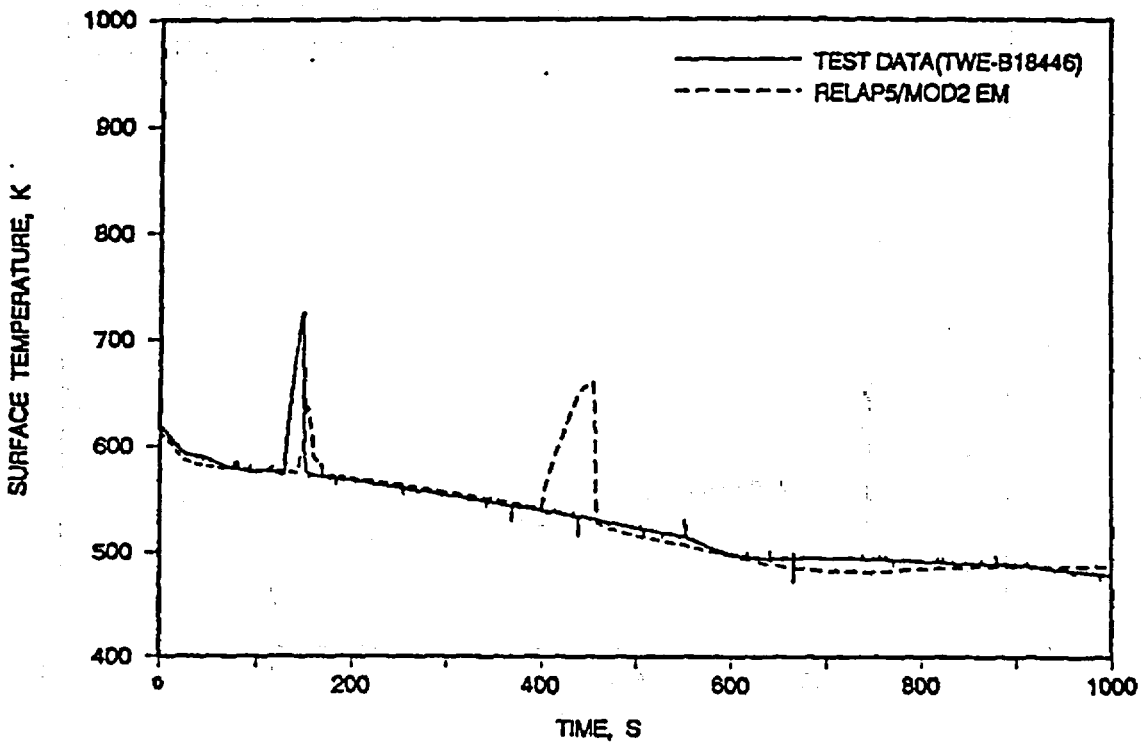


FIGURE J.35. HOT ROD SURFACE TEMPERATURE - ELEV 3.048 M.

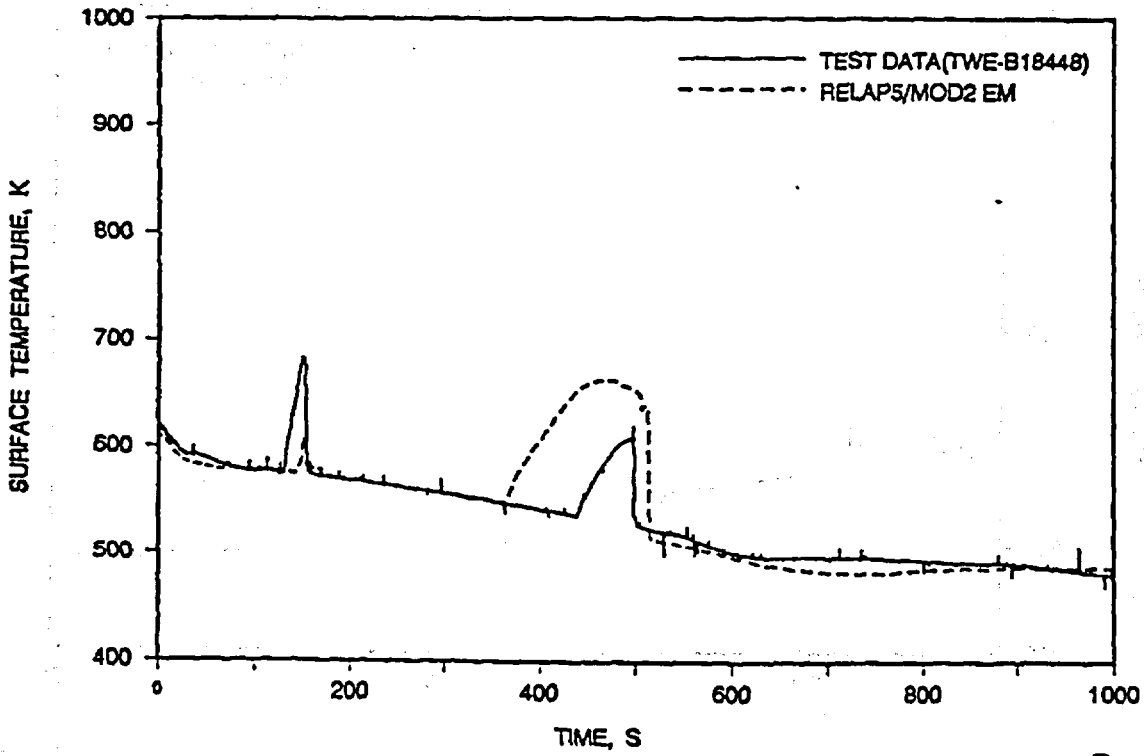

FIGURE J.36. HOT ROD SURFACE TEMPERATURE - ELEV 3.61 M.

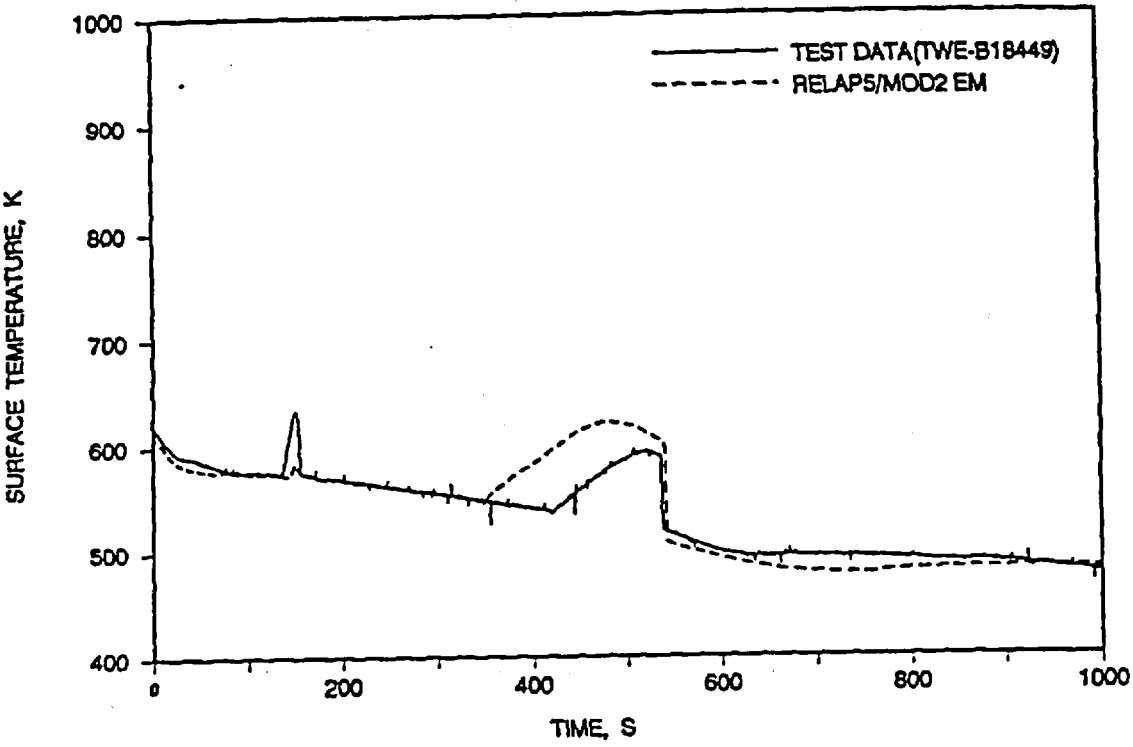


FIGURE J.37. DIMENSIONLESS LIQUID VELOCITY AT STEAM GENERATOR TUBE INLET.

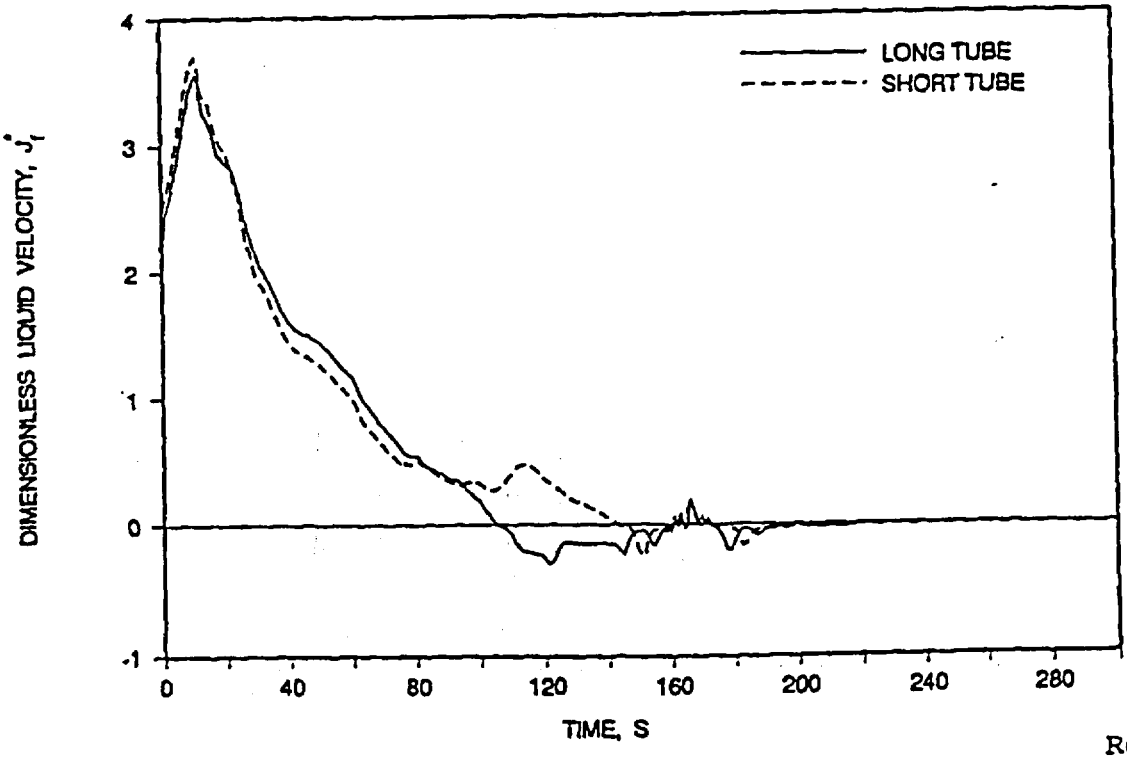

FIGURE J.38. DIMENSIONLESS VAPOR VELOCITY AT STEAM GENERATOR TUBE INLET.

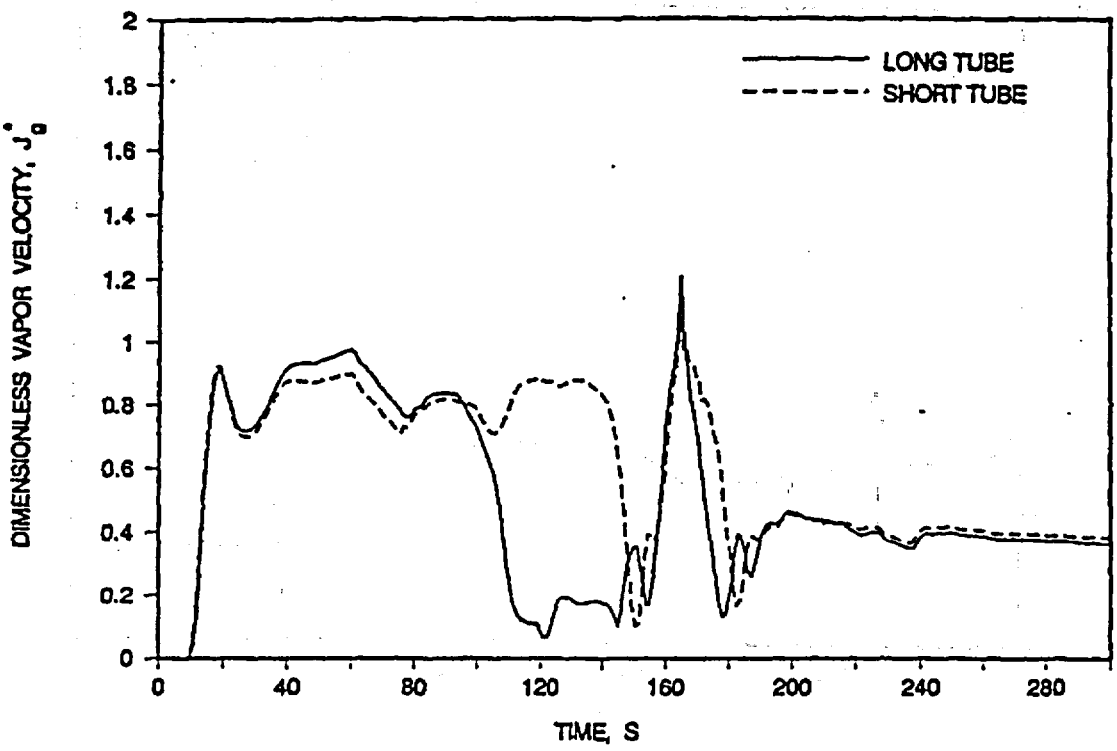


FIGURE J.39. WALLIS CONSTANT AT STEAM GENERATOR TUBE INLET.

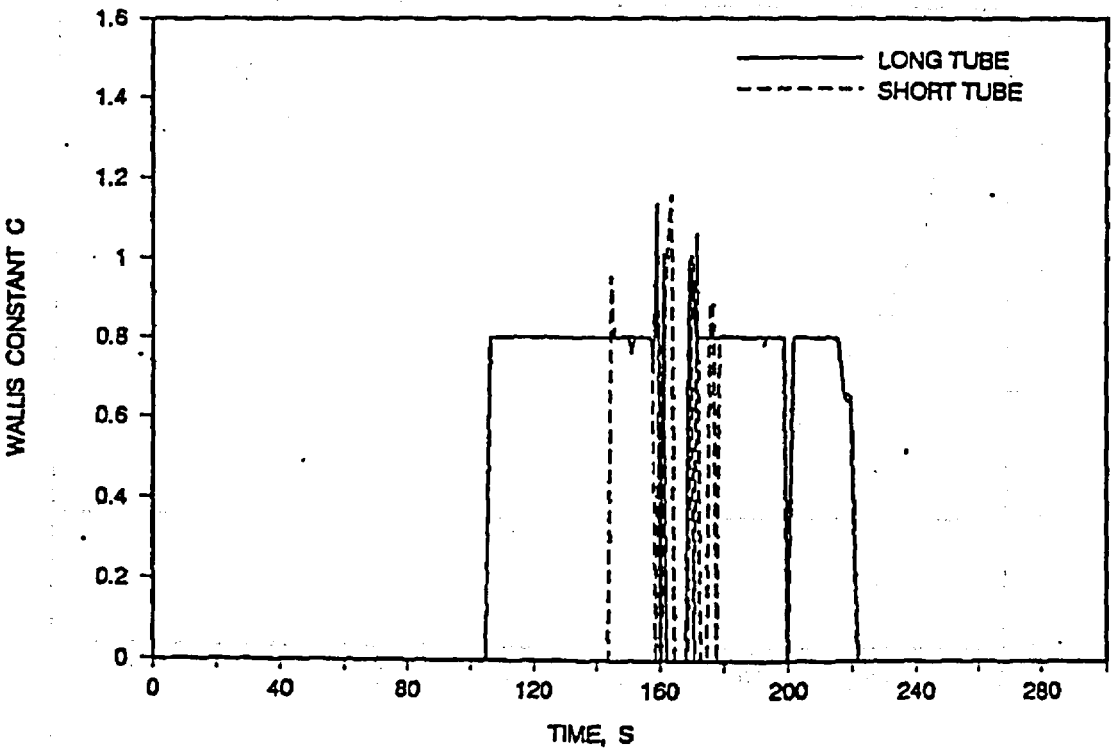

FIGURE J.40. DIMENSIONLESS LIQUID VELOCITY AT STEAM GEN. PLENUM INLET.

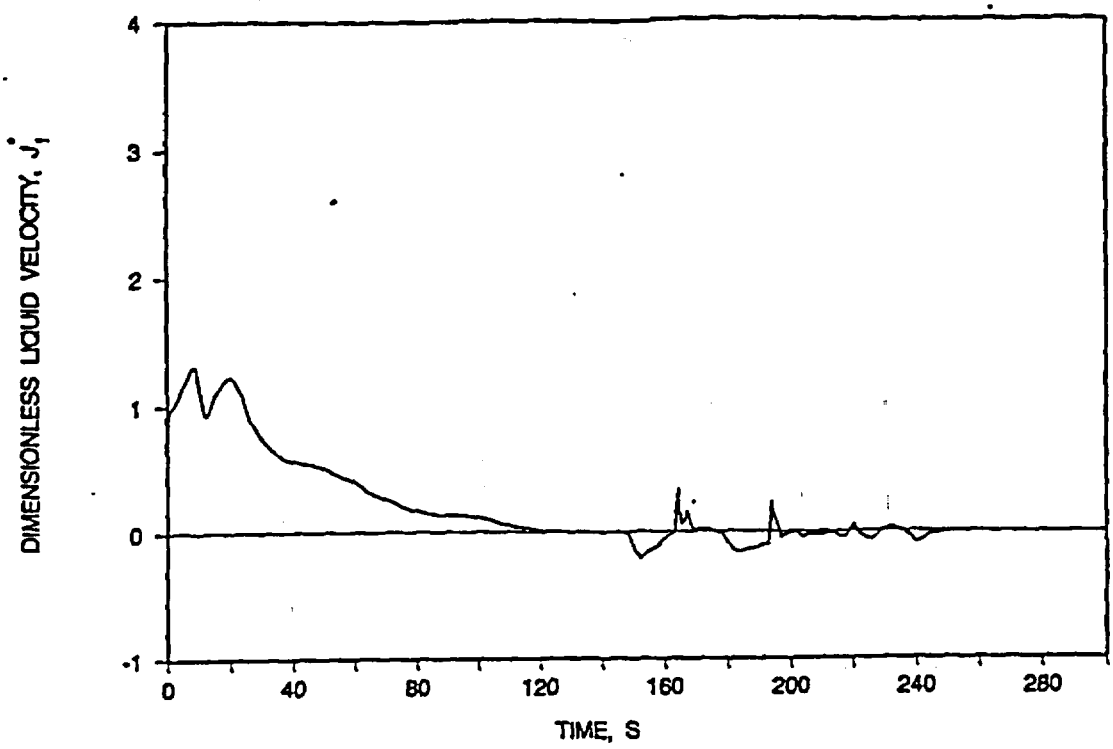


FIGURE J.41. DIMENSIONLESS VAPOR VELOCITY AT STEAM GEN. PLENUM INLET.

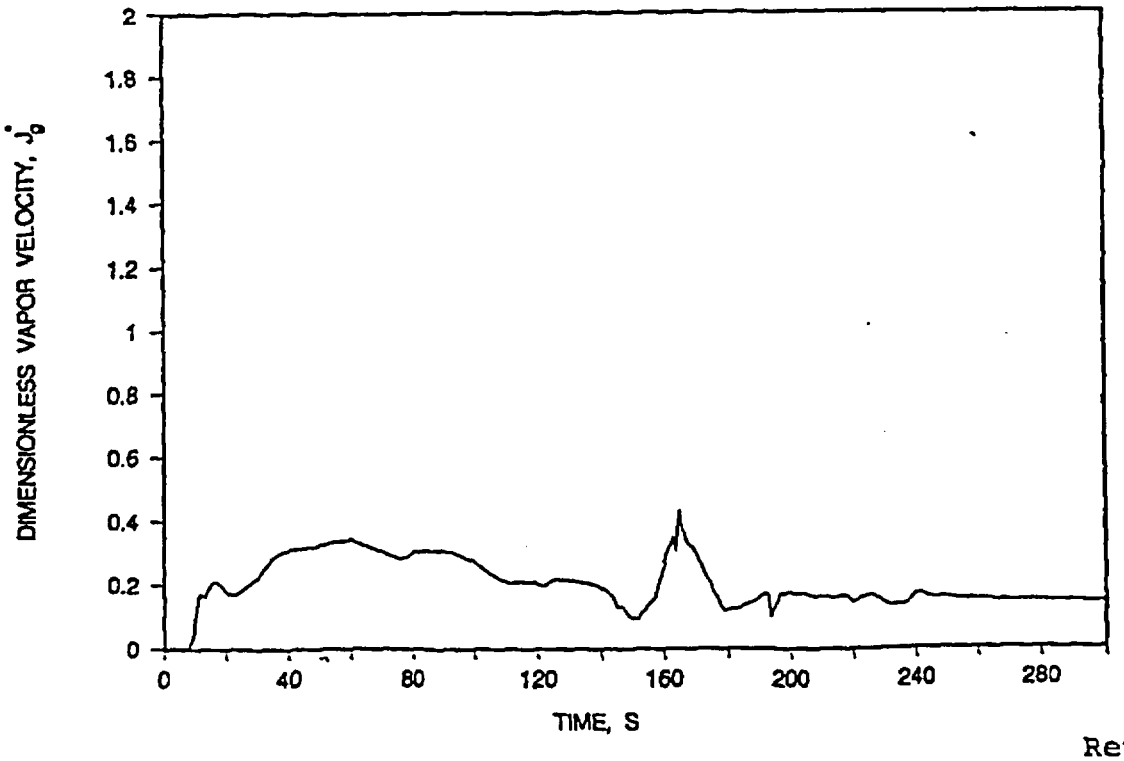

FIGURE J.42. WALLIS CONSTANT AT STEAM GENERATOR PLENUM INLET.

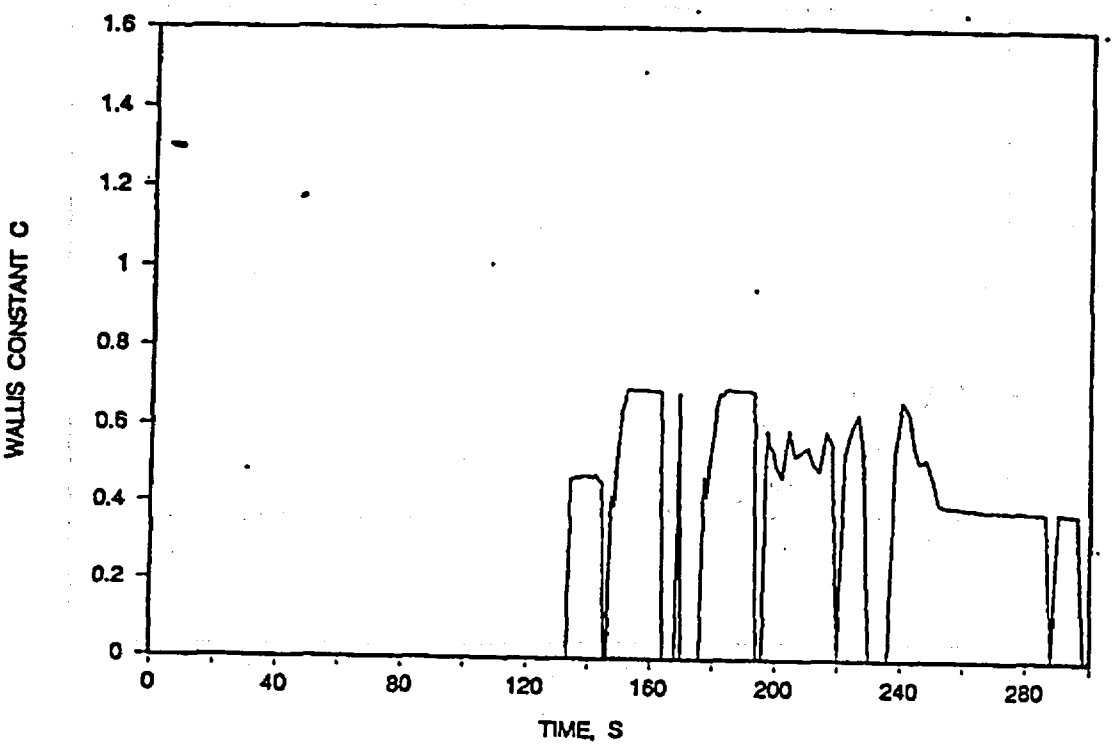

# APPENDIX K

## 19-TUBE OTSG BENCHMARKS

Note: This Appendix was originally added in its entirety in Revision 3 of BAW-10164, October, 1992.

Various benchmarks of the RELAP5/MOD2-B&W code or models have been presented in Appendices G, H, I, and J to verify the code formulation and implementation. They were included to support a variety of licensing applications in nuclear steam supply systems (NSSSs) with U-tube steam generators. These benchmarks demonstrate a general thermal-hydraulic adequacy, for both stand-alone tests and integral system tests, that is applicable to other NSSS designs as well. This appendix is added to include an additional benchmark to augment the existing calculational results, specifically to support licensing analyses of B&W-designed NSSSs.

One of the unique features of the B&W-designed NSSS is the once-through steam generator (OTSG). Accurate prediction of the OTSG performance is required to demonstrate the adequacy of the methods used. This benchmark, against B&W-proprietary data for a 19-tube OTSG, is included to show that the RELAP5/MOD2-B&W formulation and input modeling techniques used to model OTSGs are acceptable for the licensing applications.

## K.1. Introduction

Babcock & Wilcox performed numerous tests on model 19-tube and 37-tube once-through steam generators at the Alliance Research Center (ARC) Nuclear Steam Generator Test Facility (NSGTF). The objectives of these tests were to demonstrate the characteristics of B&W-designed steam generators and to provide data for computer code development. BWNT simulated two sets of model 19-tube tests with RELAP5/MOD2-B&W. The first set of benchmarks are to steady-state tests to show the ability of the code to predict the shell side nucleate boiling length at various power levels. The second benchmark is a comparison to a loss-of-feedwater (LOFW) flow test to demonstrate the ability of the code to predict boil-down and refill of a once-through steam generator.

## K.2. Facility Description

The ARC NSGTF (Figure K-1) provided the capability of testing steam generators at full system pressure and temperature conditions using water as the test fluid. The primary system of the NSGTF was a closed circuit test loop consisting of a natural gas-fired furnace (simulating reactor heat input to the primary fluid), a pressurizer, flow control valves, flow measuring elements, and a water conditioning system.

The secondary system of the NSGTF was a closed circuit test loop consisting of steam flow control valves, steam flow measuring elements, feedwater heaters, back pressure control valves, a flash tank, circulating pumps, feedwater control valves, feedwater flow measuring elements, feedwater bypass valves, and a water conditioning system.

The model steam generator was a single pass, counterflow, tube and shell heat exchanger (Figure K-2). It consisted of 19 full-length tubes 5/8-inch in diameter spaced on a triangular pitch on 7/8-inch centers. The tube bundle was enclosed in a hexagonal shell 3.935 inches across flats and was held in place by 16 tube support plates spaced at approximately 3-foot intervals. The tube support plates were drilled in a manner to simulate the broached pattern of a full-size tube support plate.

Primary flow entered at the top of the steam generator, flowed downward through the tubes, and exited at the bottom. The secondary fluid was introduced via an external downcomer, entered the tube bundle at the bottom, boiled on the outside of the tubes, and exited at the top. When run in the standard once-through steam generator mode, the feedwater was raised to saturation by mixing it with steam from the tube region via a steam bleed pipe. This bleed pipe simulated the aspirator port in the full size prototype.

## K.3. RELAP5/MOD2-B&W Model Description

The 19-tube OTSG was represented with eleven axial control volumes in the primary tube region and the secondary shell region (Figure K-3). Similarly, eleven heat structures simulated the 19 inconel 600 tubes to provide primary-to-secondary heat transfer. The external downcomer was modeled with five axial control volumes that represented the piping from the steam/feedwater mixer region to the tube bundle inlet. Feedwater aspiration was provided by a single junction component that connected the tube bundle region to the external downcomer. Feedwater flow, feedwater temperature, secondary pressure, primary inlet flow, primary inlet temperature, and primary pressure were input as boundary conditions using time-dependent volume and time-dependent junction components.

Special features, available in RELAP5/MOD2-B&W, were employed in the 19-tube OTSG model. First, the Becker critical heat flux correlation was used on the shell side of the tube heat structure to provide a better prediction of the dryout point in the OTSG. Second, the interphase drag in the slug and annular-mist flow regimes was reduced by use of the default multipliers developed for regions of small hydraulic diameters. This model produces results similar to the Wilson bubble rise model for pressures above 200 psia and provides a better prediction of liquid mass in the tube region. Finally, a linear ramp was applied to the Chen boiling suppression factor, $S_f$, such that it was reduced from the calculated value to zero over a void fraction of 0.99 to 1.0. This prevented the Chen heat transfer coefficient from becoming unrealistically large as the void fraction approached 1.0 on the shell side of the OTSG.

## K.4. Comparison to Steady-State Boiling Length Tests

In 1969 the Alliance Research Center performed a series of steady-state tests on the model 19-tube OTSG to determine the nucleate boiling length as a function of scaled power level.[152]

Each test was performed with primary pressure, primary inlet conditions, feedwater conditions, and secondary pressure held constant. The nucleate boiling length (dryout location) was determined from primary tube and secondary side thermocouples.

The boundary conditions for five, 2700 MWt plant-scaled tests are shown in Table K.1. Using these boundary conditions, a steady-state calculation of each test was performed using RELAP5/MOD2-B&W. Also, for comparison purposes, each test was simulated with RELAP5/MOD2 Cycle 36.05. The calculated boiling lengths are compared to the measured values in Table K.2. and Figure K-4.

The results show that the boiling lengths predicted by RELAP5/MOD2-B&W are in good agreement with the data over the range of simulated power levels. Furthermore, the RELAP5/MOD2-B&W predictions represent a significant improvement over the base RELAP5/MOD2 results at power levels less than 80 percent of scaled full power. This is primarily due to use of the Becker critical heat flux correlation in the RELAP5/MOD2-B&W simulation. That correlation, developed from heated rod bundle dryout data, provides a higher CHF value at reduced feedwater flow rates; whereas, the Biasi-Zuber CHF correlation combination used in RELAP5/MOD2 predicts early dryout in an OTSG as the feedwater flow (power level) decreases.

## K.5. Comparison to OTSG LOFW Test

ARC performed several loss-of-feedwater tests on the 19-tube model OTSG.[153] One LOFW test, Run 29, performed on December 16, 1977, was benchmarked with RELAP5/MOD2-B&W. This test was a loss-of-feedwater from scaled full power conditions consistent with a 2772 MWt plant.

The model OTSG was initialized to full scaled power consistent with a 2772 MWt plant. The test was initiated by the simultaneous trip of the feedwater pump and closure of the

feedwater isolation valve. The OTSG was allowed to boil dry. After the OTSG boiled dry, feedwater was turned on by starting the feedwater pump and by opening the feedwater isolation valve.

An attempt was made to hold the primary inlet temperature, primary flow and secondary pressure constant during the test. Primary outlet temperature, secondary steam flow, and secondary steam temperature were measured and recorded during the test.

The RELAP5/MOD2-B&W model was initialized to the test initial conditions shown in Table K.3. The predicted primary and secondary fluid temperatures are compared in Figures K-5 and K-6, respectively, to the measured values just prior to test initiation. The feedwater flow, primary inlet temperature, primary flow, and secondary pressure values that were measured during the test were input as boundary conditions. The calculated steam flow and primary outlet temperature are compared to the measured data in Figures K-7 and K-8, respectively. The code predictions are in good agreement with data, indicating that the calculated heat transfer is similar to that observed during the test.

The differences between observed and calculated results are primarily due to the sudden changes in heat transfer as the control volumes in the tube region systematically dryout and, later, refill. The addition of control volumes in the boiling region would decrease the magnitude of the step changes, but the number of steps would increase. The resulting prediction of primary outlet temperature would be approximately the same as the current prediction.

## K.6. Summary and Conclusions

Steady-state performance tests performed on a model 19-tube OTSG were benchmarked with RELAP5/MOD2-B&W and RELAP5/MOD2 Cycle 36.05. Those benchmarks demonstrate that the BWNT slug-drag

model and the Becker critical heat flux correlation properly predict the nucleate boiling length in the OTSG over a wide range of power levels and transient conditions. Furthermore, RELAP5/MOD2-B&W provides a significantly improved prediction of the nucleate boiling length than does RELAP5/MOD2 Cycle 36.05 at power levels less than eighty percent full power.

In addition, a loss-of-feedwater test performed on a model 19-tube OTSG from scaled full power conditions was benchmarked with RELAP5/MOD2-B&W. The code calculation was in good agreement with the measured values of primary outlet temperature and steam flow during the dryout and refill phases of the test.

Therefore, the 19-tube OTSG benchmarks serve two main purposes. First, they validate the OTSG application of the Becker correlation and the BWNT slug and annular-mist drag models. Secondly, they demonstrate that the methods used with RELAP5/MOD2-B&W properly predict the steady-state and transient heat transfer behavior in an OTSG. Together with the other benchmarks they confirm that RELAP5/MOD2-B&W is acceptable for multi-purpose licensing applications in NSSSs with either U-tube or once-through steam generators.

Table K.1. Model 19-Tube OTSG Conditions for Steady-State Boiling Length Tests.

| Power Level (Percent) | Feedwater Temperature (F) | Feedwater Flow (lbm/hr) | Prim. Inlet Temperature (F) | Prim. Exit Temperature (F) |
|---|---|---|---|---|
| b,c,d,e | | | | |

Table K.2 Comparison of Predicted and Measured Boiling Lengths for a 19-Tube Model OTSG.

| Power Level (Percent) | Boiling Length, ft. | | |
|---|---|---|---|
| | RELAP5/MOD2 Cycle 36.05 | RELAP5/MOD2-B&W | Test Data |
| b,c,d,e | | | |

Table K.3. Initial Conditions for 19-Tube Model OTSG LOFW Test.

| Parameter | Model OTSG | RELAP5/MOD2-B&W |
|---|---|---|
| Primary System Pressure, psia | [ b,c,d,e ] | |
| Primary Inlet Temperature, F | | |
| Primary Exit Temperature, F | | |
| Primary System Flow, lbm/hr | | |
| Secondary System Pressure, psia | | |
| Feedwater Temperature, F | | |
| Steam Discharge Temperature, F | | |
| Feedwater Flow, lbm/hr | | |
| Heat Transfer Rate, Btu/s | | |

*Input values.

Figure K-1. Schematic Diagram of the Nuclear Steam Generator Test Facility.

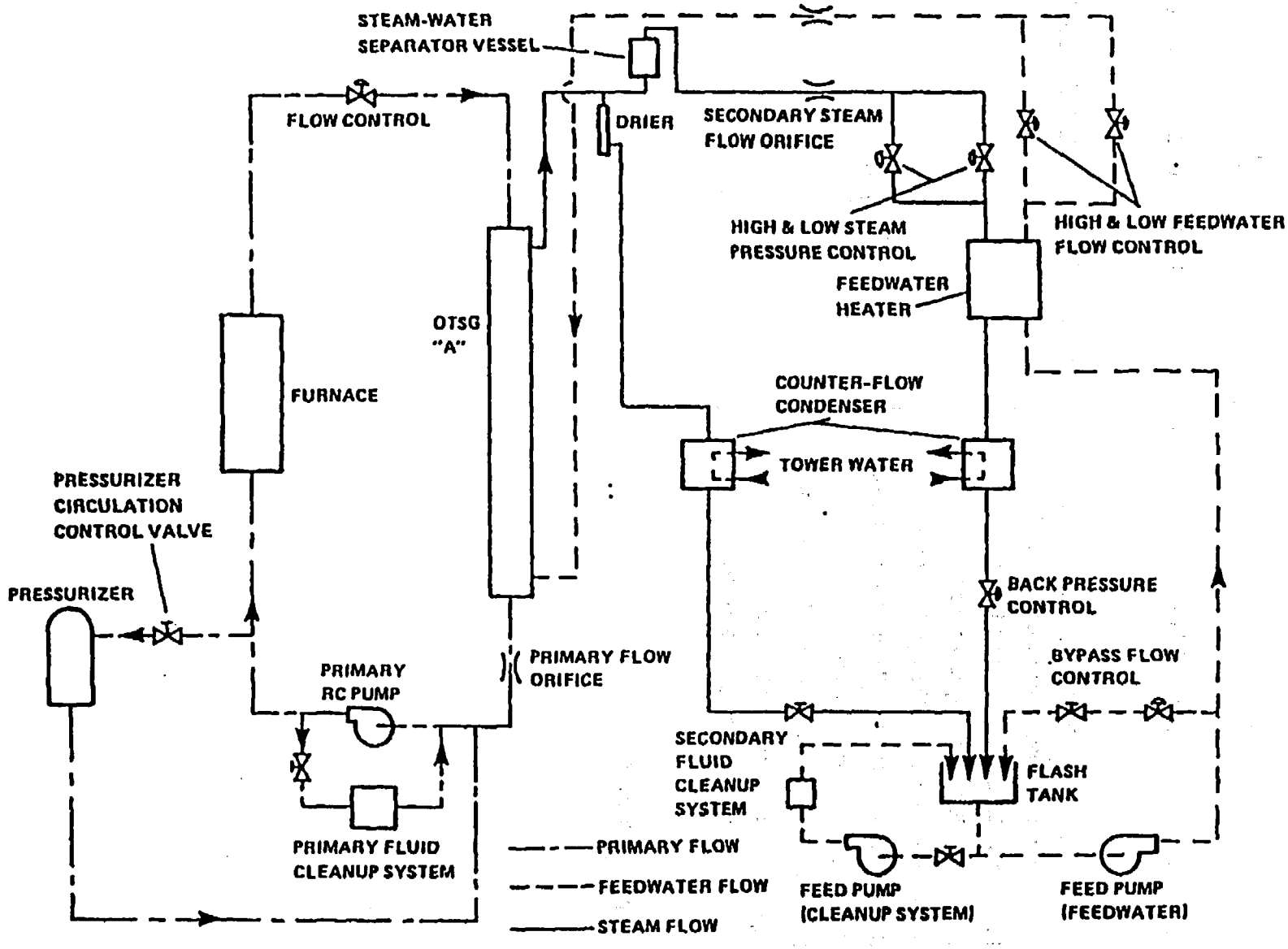

Figure K-2. 19-Tube Once-Through Steam Generator and Downcomer.

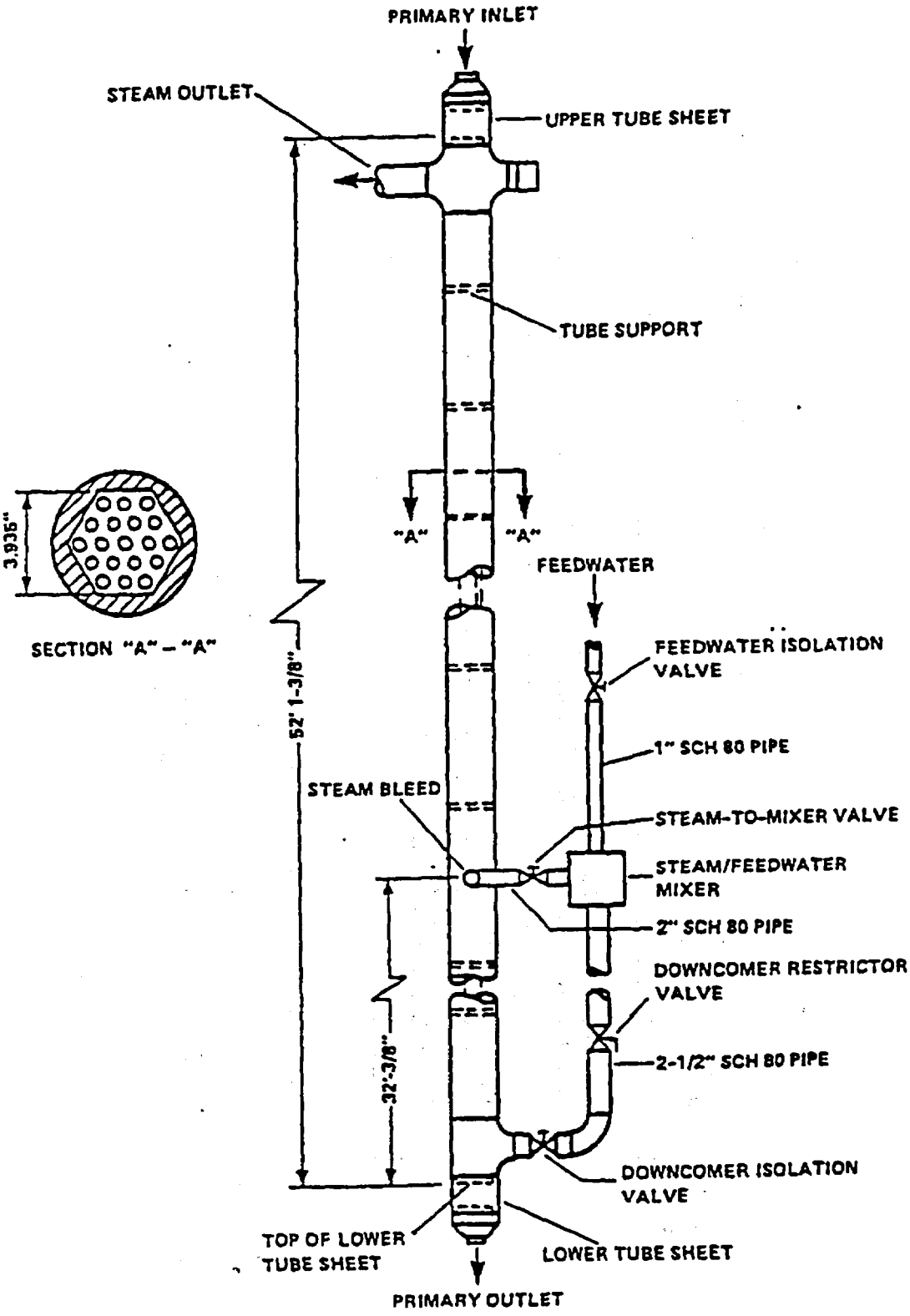

FIGURE K-3. RELAP5/MOD2-B&W MODEL OF 19-TUBE OTSG.

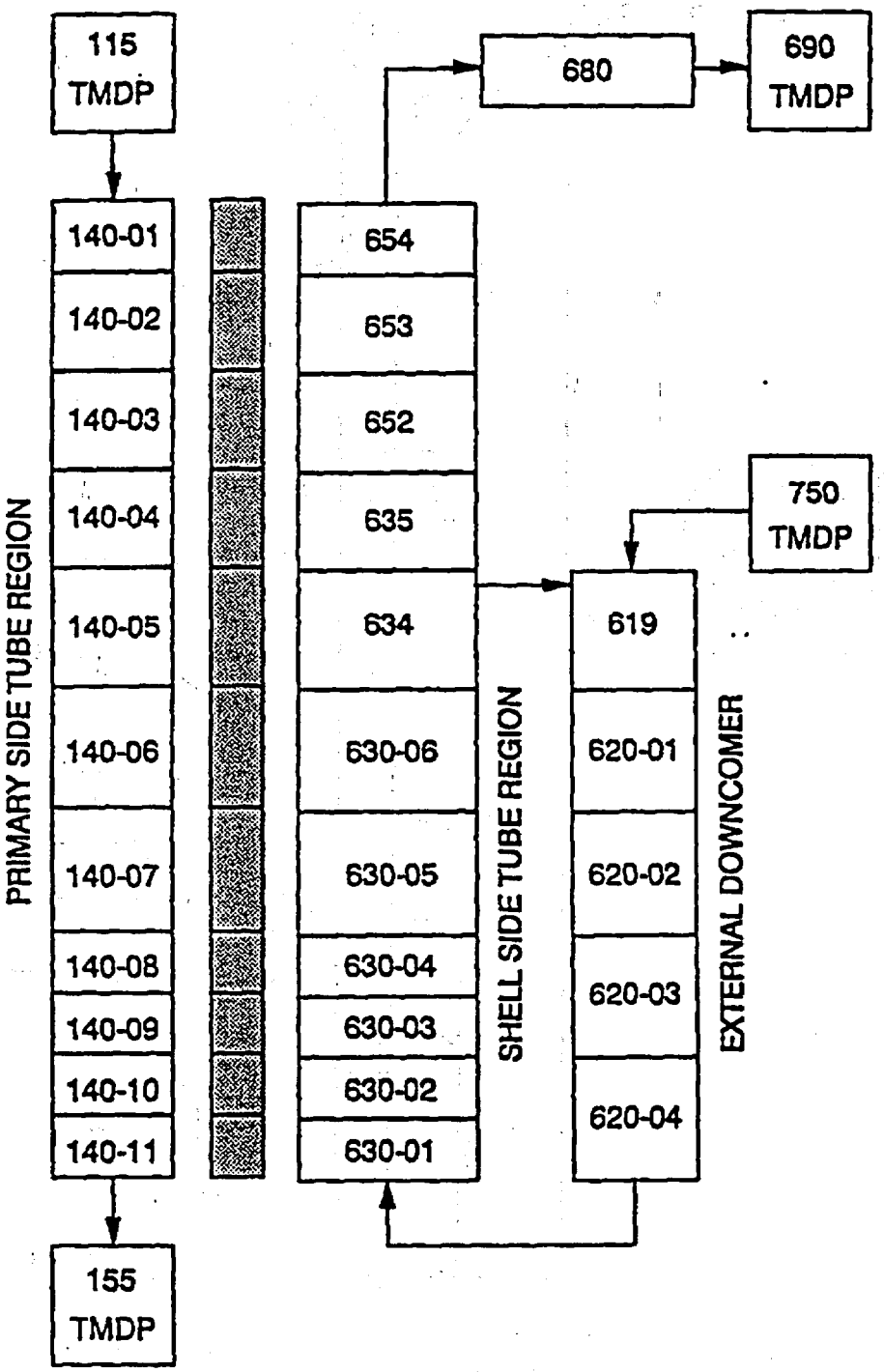

FIGURE K-4. COMPARISON OF MEASURED AND PREDICTED BOILING LENGTHS IN A MODEL 19-TUBE OTSG.

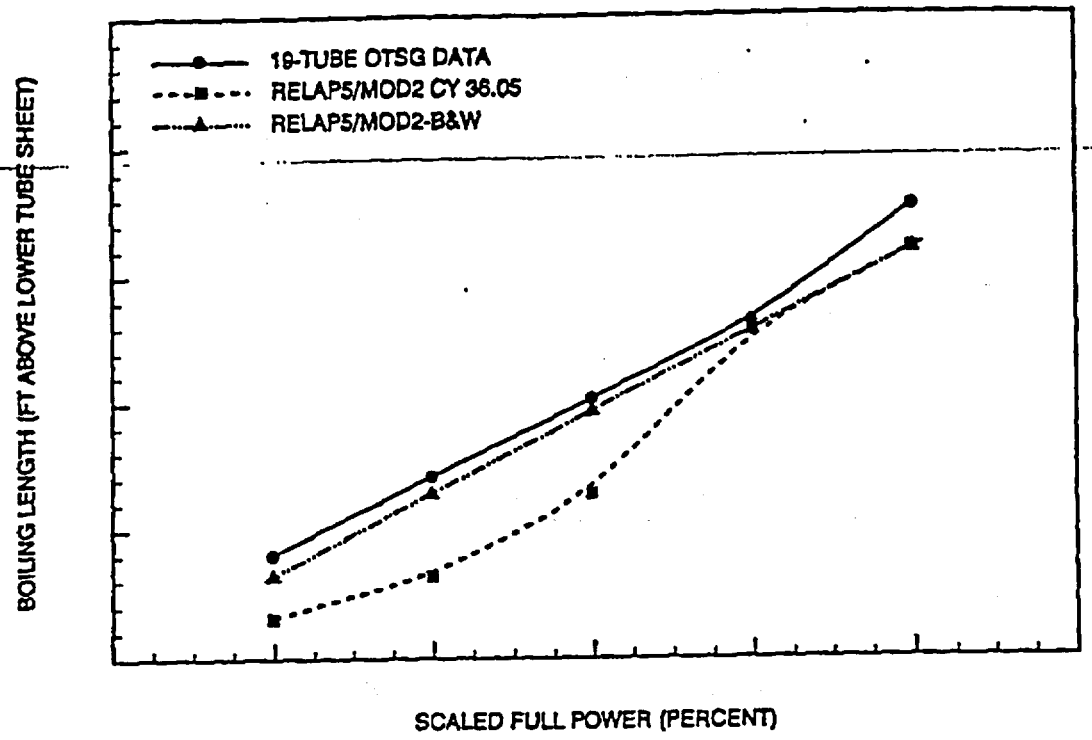


FIGURE K-5. COMPARISON OF MEASURED AND PREDICTED INITIAL PRIMARY SYSTEM FLUID TEMPERATURES FOR 19-TUBE OTSG LOFW TEST.

b,c,d,e

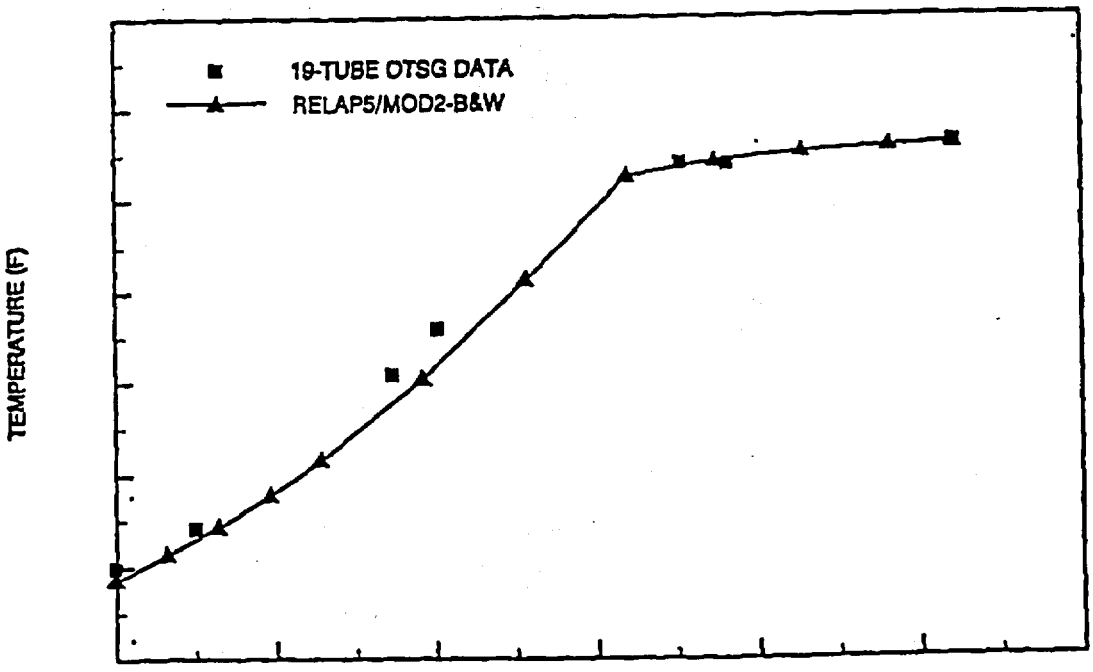

FIGURE K-6. COMPARISON OF MEASURED AND PREDICTED INITIAL SECONDARY SYSTEM FLUID TEMPERATURES FOR 19-TUBE OTSG LOFW TEST.

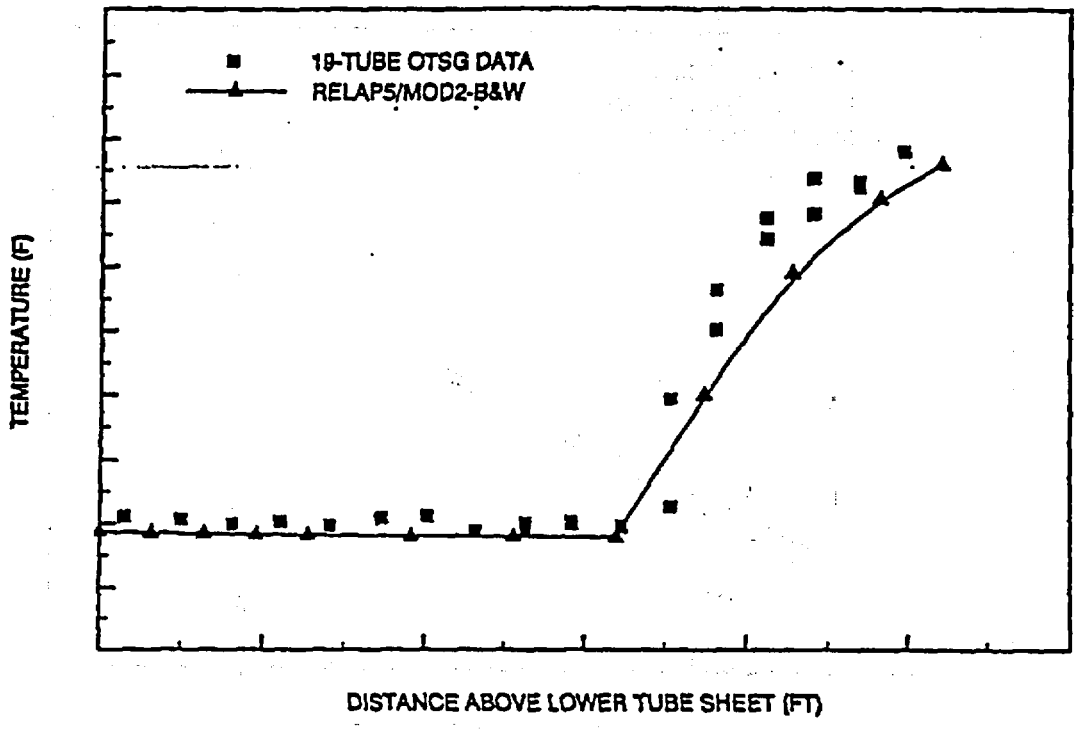


FIGURE K-7. COMPARISON OF MEASURED AND PREDICTED STEAM FLOW DURING 19-TUBE OTSG LOFW TEST.

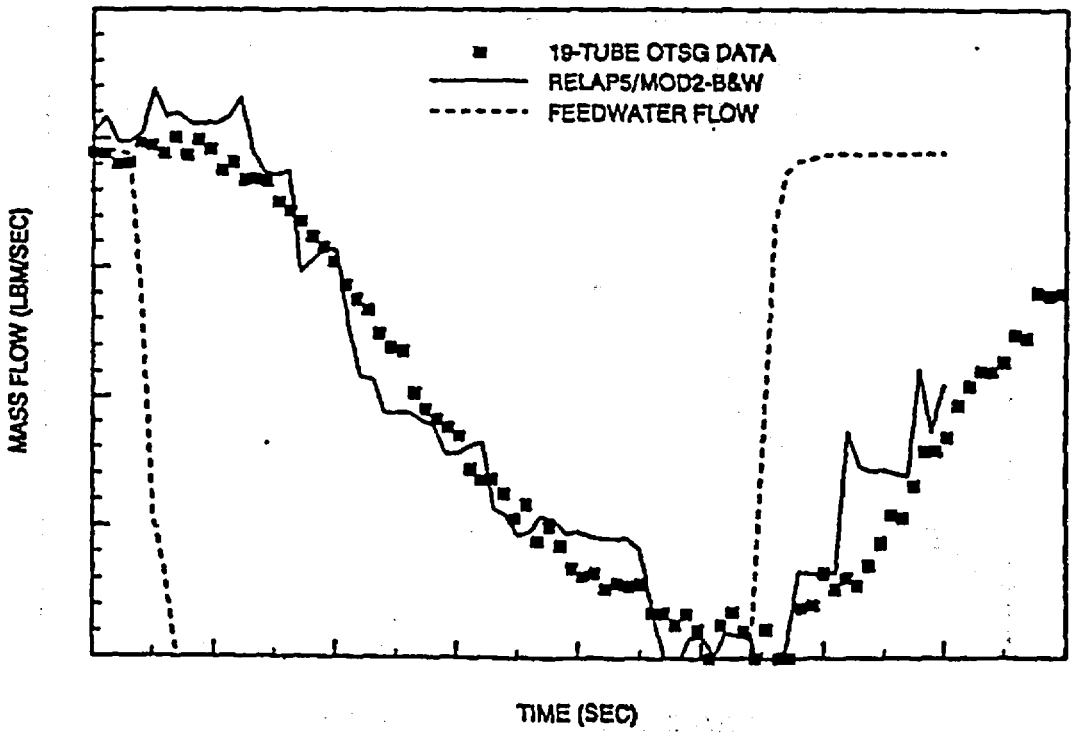


b,c,d

FIGURE K-8. COMPARISON OF MEASURED AND PREDICTED PRIMARY OUTLET TEMPERATURES DURING 19-TUBE OTSG LOFW TEST.

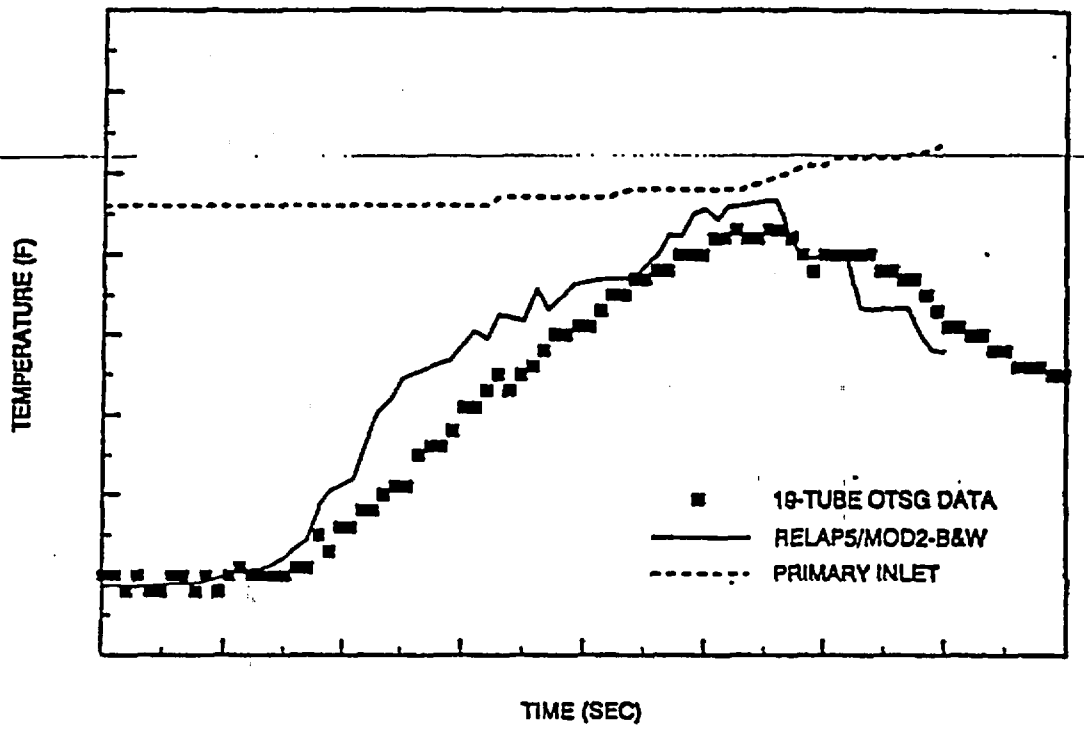


b,c,d,e

# APPENDIX L

## MIST BENCHMARK WITH RELAP5/MOD2-B&W

Note: This Appendix was originally added in its entirety in Revision 3 of BAW-10164, October 1992.

This appendix was added to provide an integral system benchmark of a simulated small break loss-of-coolant accident in a nuclear steam supply system (NSSS) with once-through steam generators (OTSGs). This benchmark of RELAP5/MOD2-B&W code, with the support Appendices G, H, I, J and K, is used to verify the code formulation and implementation. These benchmarks collectively demonstrate a general thermal-hydraulic adequacy, for both stand-alone tests and integral system tests, that is applicable to NSSS designs containing U-tube steam generators or OTSGs.

This benchmark was performed against Multi-Loop Integral System Test facility data. The facility was chosen because it contains all of the unique features of a B&W-designed NSSS. The specific test benchmarked with RELAP5/MOD2-B&W was chosen because the scaled break size corresponds to the worst small break size for B&W-designed plants. The benchmark is included to show that the code formulation and input modeling techniques used to model a scale-model B&W-plant are acceptable for licensing application use.

## L.1. Introduction

The Multi-Loop Integral System Test (MIST) facility is a scale model of a Babcock & Wilcox lowered-loop 177 fuel assembly pressurized water reactor. Design, fabrication and testing of the facility was sponsored by Babcock & Wilcox, the Babcock & Wilcox Owners Group (BWOG), the Nuclear Regulatory Commission, and the Electric Power Research Institute. The facility was fabricated to provide data on the transient response of B&W PWRs during small-break loss-of-coolant accidents (SBLOCA), steam generator tube ruptures (SGTRs) and feed-and-bleed cooling. The data generated by MIST testing is used to determine the adequacy of thermal-hydraulic computer codes to predict the phenomena exhibited during these events.

To demonstrate that RELAP5/MOD2 adequately predicts the dominant phenomena, the MIST program management group sponsored three pre-test and five post-test predictions.[154] Similarly, the BWOG sponsored several additional RELAP5/MOD2 post-test predictions of MIST tests.[155-160] These benchmarks clearly show that RELAP5/MOD2 properly predicts the phenomena exhibited during SBLOCA and SGTR events. However, in many of the benchmarks the code underpredicted collapsed liquid level in the core region because the code underpredicted the phase slip in the slug flow regime.

Consequently, BWNT modified the RELAP5/MOD2 interphase drag models to reduce the interphase drag forces in the slug and annular-mist flow regimes. The revised models were verified by comparisons to separate effects tests and to core level predictions by the FOAM2 computer code.[161] As further justification of this code modification, MIST test 320201 was re-analyzed. The prediction of this scaled 50 $cm^2$ pump discharge break test with the revised version of RELAP5/MOD2-B&W is discussed in this Appendix. Section L.2 provides a simple description of the MIST facility. A detailed description is provided in Reference 162. The RELAP5/MOD2-B&W input model is discussed in Section L.3. The results of the revised benchmark are compared to MIST data and to the original RELAP5/MOD2 prediction in Section L.4. A summary and conclusions are provided in Section L.5. References are listed in Section 4 of the main text.

## L.2. MIST Facility Description

The MIST facility was a scaled, two-by-four (two hot legs and four cold legs) model of a B&W, lowered-loop, nuclear steam supply system. MIST was designed to operate at plant-typical pressures and temperatures. Experimental data obtained from this facility during post-SBLOCA testing are used for computer code benchmarking.

MIST consisted of two 19-tube once-through steam generators; a reactor vessel with heated core and external downcomer; pressurizer; two hot legs; and four cold legs, each with a scaled reactor coolant pump. Other loop components in MIST included a closed secondary system, four simulated reactor vessel vent valves (RVVVs), a pressurizer power-operated relief valve, hot leg vents and reactor vessel upper-head vents, high pressure injection (HPI), core flood system, and critical flow orifices for scaled leak simulation. The system was also capable of noncondensible gas addition at selected loop sites. The MIST facility is illustrated in Figure L-1.

The reactor coolant system of MIST was scaled according to the following criteria, listed in order of decreasing priority: elevation, post-SBLOCA flow phenomena, component volume, and irrecoverable pressure drop. Consequently, MIST retained full plant elevations throughout the primary system and the steam generator secondaries. Key interfaces were maintained including the hot leg spillover, upper and lower tube sheets of the steam generators, cold leg low point, pump discharge spillover, cold and hot leg nozzle centerlines, core, and points of emergency core cooling system injection. Only the elevations of several non-flow regions were compromised, primarily to optimize power-to-volume scaling. Also, the MIST hot legs and cold legs were oversized with respect to ideal power-to-volume scaling (plant/MIST power ratio is 817). This atypicality was necessary to preserve prototypical two-phase flow characteristics, match irrecoverable pressure losses in the piping, and preserve prototypical cold leg Froude number.

As with any scaled facility, the metal surface area-to-fluid volume ratio of MIST was considerably greater than the plant value. As a result, guard heaters were used, in conjunction with passive insulation, on the steam generator secondaries and on all primary coolant components to minimize model heat losses.

However, the guard heaters did not compensate for all the loop heat losses. Therefore, core power was increased to offset these uncompensated heat losses.

MIST instrumentation was selected and distributed based on input from experimenters and code analysts. This instrument selection process considered the needs of code benchmarking, indications of thermal-hydraulic phenomena, and system closure. MIST instrumentation consisted of measurements of temperature, pressure, and differential pressure. Fluid level and phase indications were provided by optical viewports, gamma densitometers, conductivity probes, and differential pressures. Mass flow rates in the circulation loop were measured using venturis and a cooled thermocouple, and at the system boundaries using Coriolis flowmeters and weigh scales. Approximately 850 MIST instruments were interfaced to a computer-controlled, high-speed data acquisition system.

## L.3. RELAP5/MOD2-B&W Model Description

The base RELAP5/MOD2-B&W input model is identical to that used in the original post-test prediction[155] and is discussed in detail in Reference 163. The model simulates all of the MIST primary reactor coolant system piping, active components and ancillary systems. Specifically, the complete model represents the reactor vessel, an external annular downcomer, two hot legs, a pressurizer, two once-through steam generators, four cold legs, four reactor coolant pumps, reactor vessel vent valves, a core flood tank, high point vents, high- and low-pressure emergency core cooling system injection, high elevation auxiliary feedwater, primary and secondary metal mass, and guard heaters.

Special features of the model include the reactor vessel noding arrangement, the cold leg-to-downcomer connections, and the two-radial region steam generators. The reactor vessel noding arrangement models the full height core region and the vessel

exit region noding scheme preserves the two-phase flow splits during boiling pot mode.

The cold legs utilize a double flow path connection to the external reactor vessel downcomer so that counter-current two-phase flow can be predicted. In other words, this connection scheme allows steam from the upper downcomer to enter the cold leg while liquid drains from the cold leg into the lower downcomer.

The final model feature represents the primary steam generator (SG) tube region with two radial regions. One region (three tubes) represents the tubes directly wetted by auxiliary feedwater (AFW) injection on the shell side of the SG. The other region (16 tubes) represents the tubes in contact with secondary steam (dry tubes).

The base RELAP5/MOD2-B&W model was modified for this re-analysis. Most notably, the revised slug drag model was implemented in the core and the shell side of the steam generator. The revised slug drag model is designed for use in these regions where the hydraulic diameters are small and boiling takes place.

In addition to the revised slug drag model, the reactor vessel and downcomer models were modified slightly. The core region was modified so that twenty control volumes represent the full height core instead of the three control volumes used in the original prediction. This increase in core detail is required to maintain consistency with the models used to develop the revised slug drag model. Furthermore, the outer annulus region in the vessel outlet was revised to include three control volumes rather than one so that the mixture level would properly reside below the RVVV during the loop draining period. Also, the RVVV junction was modified to enter the bottom of the upper downcomer control volume to better predict the steam condensation there. This last

modification is consistent with latest MIST benchmark models. A schematic of the RELAP5/MOD2-B&W model of MIST is shown in Figure L-2.

## L.4. Prediction of MIST Test 320201 with Revised RELAP5/MOD2-B&W

The original post-test prediction of MIST test 320201 with Version 5.0 of RELAP5/MOD2-B&W is discussed in detail in Reference 155. The models used in this simulation with that code version are identical to those described in Revision 0 of this code topical report. A simple summary of the re-analysis with Version 14.0 is provided here and a comparison is made between the original and revised predictions. The Version 14.0 models used in this simulation are identical to those contained in Revision 3 of this code topical.

### L.4.1. MIST Initialization

The MIST facility was capable of only ten percent full-scaled power. Therefore, the facility was initialized to the conditions existing approximately 145 seconds after trip. Consequently, MIST was initialized in natural circulation with the core power equal to 3.5 percent scaled power plus an additional 0.4 percent scaled power for uncompensated heat losses. Other initial conditions were:

1. Primary system pressure corresponding to 22 F core exit subcooling.
2. Pressurizer level five feet above the bottom of the pressurizer.
3. Steam generator pressure of 1010 psia.
4. Steam generator secondary level controlled to five feet above the lower tube sheet by throttling high elevation AFW injection.

The MIST initial conditions for Test 320201 are shown in Table L.1 with the calculated values from the RELAP5/MOD2-B&W model.

## L.4.2. Summary of Results

The test was initiated by turning off the pressurizer heaters and opening the leak. When the pressurizer level reached one foot, full HPI flow was started, steam generator secondary refill using full capacity AFW was initiated, the core decay heat ramp was activated, and the RVVV control was placed in automatic.

When the leak was opened the system began a subcooled blowdown. The hot leg and core exit fluid saturated and the primary depressurization rate decreased as the hot fluid flashed. The primary system depressurization continued until the steam produced from flashing of the hot leg fluid interrupted natural circulation at approximately one minute.

The interruption of natural circulation stopped the primary system depressurization because the onset of gross boiling in the core exceeded the volumetric discharge of the break. Steam that was formed in the core collected in the reactor vessel upper head and displaced the mixture level below the RVVV elevation. Steam passed through the RVVVs into the reactor vessel downcomer. As the steam collected in the downcomer, it depressed the liquid level to the cold leg nozzle elevation. With the cold leg nozzles partially uncovered, the rate of condensation of the core steam on the cold HPI liquid in the cold legs increased. Consequently, the primary system depressurization resumed. Shortly thereafter, the depressurization rate increased as the trapped hot leg steam bubble depressed the liquid levels in the SG tubes below the tube sheets, establishing high-elevation boiler-condenser mode (BCM) heat transfer. The depressurization was further augmented as the leak site saturated.

Upon re-establishment of SG heat transfer at three minutes, the primary system depressurization resumed and continued as long as the AFW was flowing. When the secondary levels reached the

control setpoint at eight minutes, AFW flow stopped. Without significant primary-to-secondary heat transfer, the primary system depressurization slowed as the only mode of energy removal was leak-HPI cooling.

The primary system depressurized slowly because of leak-HPI cooling while the SG secondary pressures remained relatively constant. The residual primary-to-secondary heat transfer was offset by steam line heat losses to ambient. Therefore, the SG pressures remained constant. Approximately, twenty-eight minutes after test initiation, the primary system depressurized below the secondary system pressure. At that time, SG secondary side blowdown was initiated. AFW injection reactivated as flashing and boil-off reduced the secondary level blow the control setpoint. Consequently, the reactivation of AFW injection re-initiated high elevation BCM heat transfer and the primary system depressurization rate increased. The increase in depressurization rate caused flashing within the primary system. Also, the dramatic increase in primary system steam condensation in the SG tubes caused liquid to relocate from the vessel into the hot legs. Consequently, these two effects caused a decrease in core collapsed liquid level.

As the secondary system blowdown continued, the secondary depressurization rate decreased to a rate limited by the facility condenser. The blowdown rate was sufficient to maintain a primary-to-secondary temperature differential. The resulting primary-to-secondary heat transfer, in combination with leak-HPI cooling, sustained a primary system depressurization for the duration of the event. Reactor vessel collapsed liquid levels increased as flashing decreased and as core flood tank flow suppressed core boiling and aided system refill.

The RELAP5/MOD2-B&W Version 14.0 prediction of primary system pressure is in good agreement with the data (Figure L-3). The

predictions of interruption of natural circulation, high elevation BCM cooling, and leak-HPI cooling are consistent with the observation. The final depressurization caused by SG blowdown is calculated to occur earlier than observed because the MIST operator opened the blowdown valve 2.5 minutes after the primary pressure equalized with the secondary pressure (Table L.2). The SG blowdown was automatically initiated in the simulation when the primary and secondary system pressures equalized.

The response predicted by Version 14.0 was similar to the Version 5.0 prediction. As expected, the change in the interphase drag had little impact on the primary system pressure response. However, the Version 14.0 prediction showed a later actuation of the SG blowdown and a better primary system pressure prediction during the blowdown. The delayed blowdown occurred because the Version 14.0 prediction of the "A" SG pressure was lower than the Version 5.0 prediction when AFW was terminated (Figure L-4). The pressure was lower because the revised MIST model used in the Version 14.0 prediction had subcooled liquid in the pressurizer surge line and lower head. Since the fluid entering the hot leg was colder, less flashing occurred, reducing two-phase natural circulation. The net result was less heat transfer to the secondary system. The Version 5.0 prediction exhibited a lower primary pressure during the blowdown because the secondary level swell was overpredicted, providing more primary-to-secondary heat transfer than was observed in the test.

The reactor vessel collapsed liquid level predicted by Version 14.0 was also in good agreement with MIST data (Figure L-5). During the test, the reactor vessel mixture level quickly fell below the RVVVs and stabilized above the hot leg nozzles. This mixture level translated to a collapsed liquid level of approximately 19 feet above the upper face of the lower SG tube sheet. Both post-test predictions showed the same behavior.

However, the Version 5.0 simulation underpredicted the collapsed liquid level because it overpredicted the void fractions in the mixture region. The Version 14.0 prediction, with the revised slug drag model and finer core noding, provided an excellent calculation of collapsed liquid level for the same approximate mixture level. Furthermore, the revised prediction properly calculated reactor vessel collapsed liquid level during the SG blowdown phase of the transient. The collapsed liquid level decreased during this phase as flashing in the reactor vessel increased the void fraction in the mixture region.

In addition to an improved reactor vessel liquid level prediction, the Version 14.0 post-test prediction also displayed an improved SG secondary collapsed liquid level prediction (Figure L-6). RELAP5/MOD2-B&W Version 5.0 overpredicted the secondary level swell during the SG blowdown, resulting in significant carryout of liquid. The Version 14.0 prediction incorporated the revised slug drag model in the SG tube region. The revised slug drag model significantly reduced the level swell and produced a collapsed liquid level calculation that was in good agreement with the data. Furthermore, the accurate calculation of mixture level by Version 14.0 during the SG blowdown provided an accurate calculation of primary-to-secondary heat transfer and gave an improved primary pressure prediction as compared to the Version 5.0 results.

## L.5. Summary and Conclusions

A post-test prediction of MIST test 320201, a scaled 50 $cm^2$ cold leg pump discharge break, was performed with Version 14.0 of the RELAP5/MOD2-B&W computer code. The models employed in that prediction are identical to those contained in Version 19.0, and described in this revision to the code topical. The calculation included the BWNT modified interphase drag modeling in the reactor vessel and steam generator secondary components to reduce the calculated interphase drag force in the slug flow regime.

The results were compared to the MIST test data and the original post-test prediction that was performed with Version 5.0 of RELAP5/MOD2-B&W.

That comparison showed the calculated primary and secondary pressure responses were in good agreement with the data and were similar to the original predictions. However, the reduced interphase drag forces predicted by Version 14.0 provided a significant improvement in calculated collapsed liquid levels in the reactor vessel and the steam generator secondary as compared to the Version 5.0 calculations. Furthermore, the collapsed liquid levels predicted by Version 14.0 are in excellent agreement with the MIST data. Therefore, it is concluded that the revised slug drag model is appropriate for use in regions of small hydraulic diameter.

This benchmark demonstrates the accuracy and adequacy of the RELAP5/MOD2-B&W code for prediction of the phenomena expected to occur during a postulated SBLOCA in a plant with OTSGs. In combination with the other benchmark cases, it confirms that the RELAP5/MOD2-B&W code is appropriate for licensing applications of B&W-designed NSSSs.

Table L.1. Comparison of MIST Initial Conditions to RELAP5/MOD2-B&W Values.

| Parameter, Units | MIST Value | RELAP5/MOD2-B&W Value |
|---|---|---|
| Primary Pressure, psia | 1730.0 | 1726.5 |
| Secondary Pressure, psia | 1010.0 | 1010.0 |
| Core Exit Temperature, F | 592.0 | 593.4 |
| SG Exit Temperature, F | 551.0 | 550.3 |
| Core Exit Subcooling, F | 22.0 | 22.0 |
| Core Power, Btu/s | 117.0 | 119.5 |
| Pressurizer Level, ft | 5.0 | 5.0 |
| SG Secondary Level, ft | 4.8 | 5.0 |
| Core Flow Rate, lbm/s | 1.86 | 1.86 |

t

*Revised Table L.1 shown on page 5-285 per SER instruction on Table 2 (page 5-364).*

Table L.2. Sequence of Events.

| Event | MIST Observation Seconds | Ver 5.0 Prediction Seconds | Ver 14.0 Prediction Seconds |
|---|---|---|---|
| Leak opened | 0 | 0 | 0 |
| Primary saturates | 12 | 31 | 34 |
| Pzr level reaches one foot (HPI, AFW, and DH ramp started) | 30-42 | 60 | 57 |
| Hot leg U-bend voiding interrupts natural circ. (Loop A/Loop B) | 54/42 | 85/130 | 130/90 |
| High elev BCM begins (Loop A/Loop B) | 170/175 | 180/185 | 180/180 |
| Break saturates | 190 | 130 | 140 |
| Secondary refilled and AFW shutoff (SG A/SG B) | 480/480 | 490/440 | 480/480 |
| Primary and secondary pressures equalize | 1560 | 1500 | 1650 |
| Secondary blowdown | 1710 | 1500 | 1650 |
| CFT injection begins | 1920 | 1680 | 1800 |

t

*Revised Table L.2 shown on page 5-288 per SER instruction on Table 2 (page 5-364).*

Figure L-1. MIST Facility

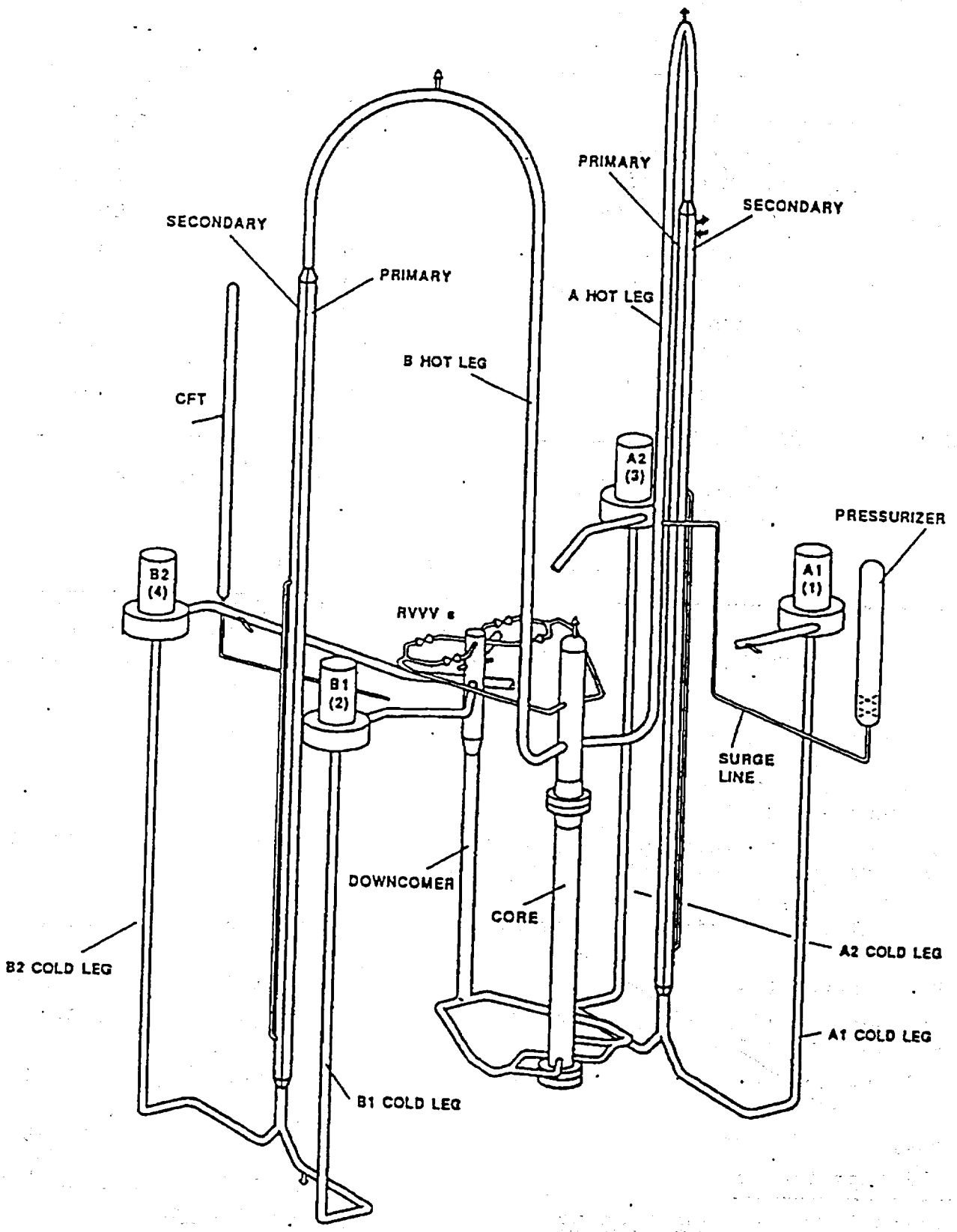

FIGURE L-2. RELAP5/MOD2-B&W MODEL OF THE MIST FACILITY.

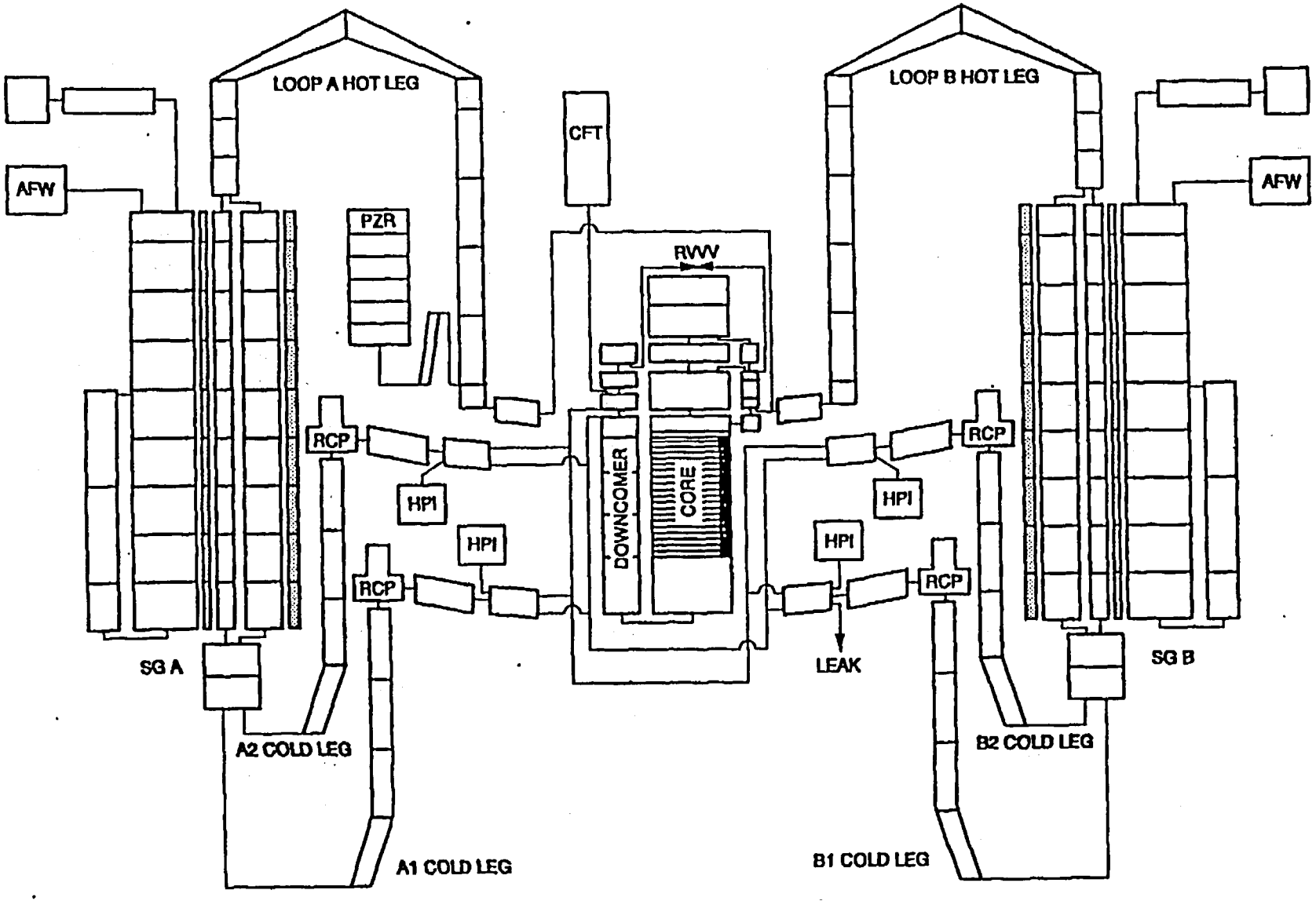

FIGURE L-3. COMPARISON OF PREDICTED AND OBSERVED PRIMARY PRESSURES FOR MIST TEST 320201.

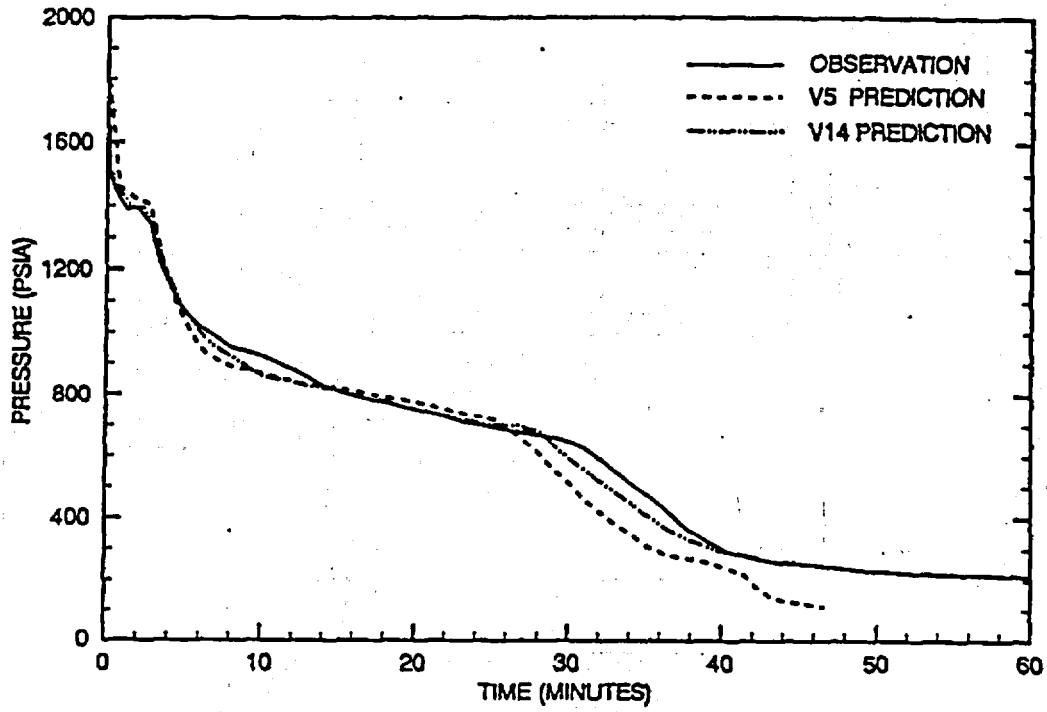


FIGURE L-4. COMPARISON OF PREDICTED AND OBSERVED SECONDARY SYSTEM PRESSURES FOR MIST TEST 320201.

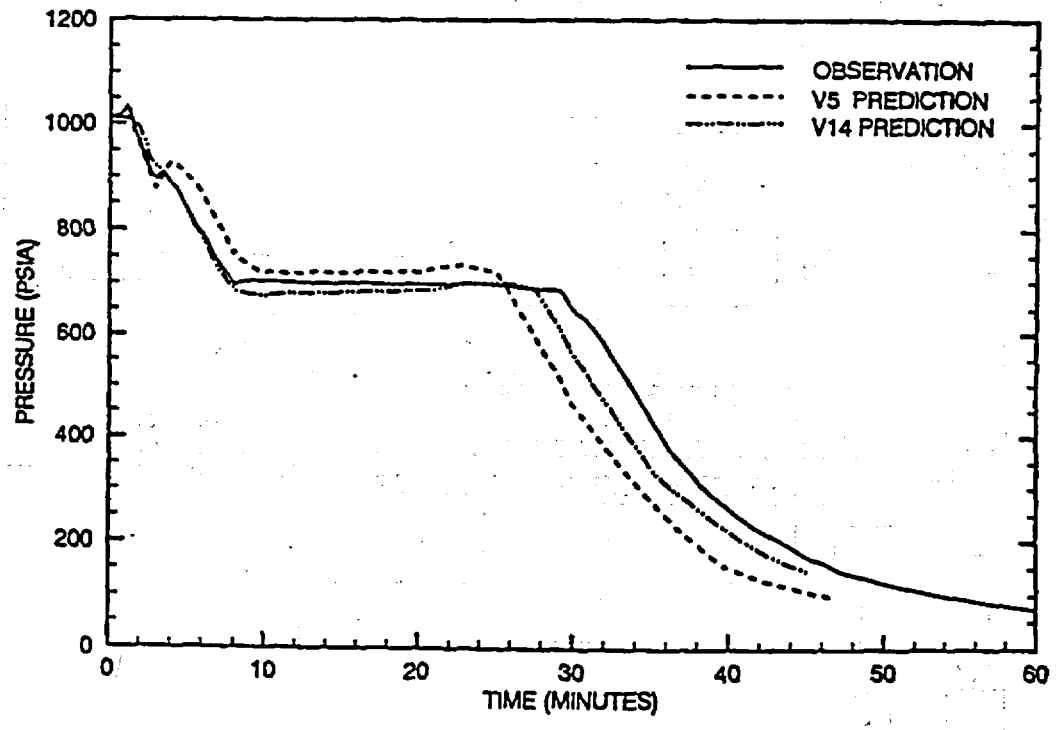

FIGURE L-5. COMPARISON OF PREDICTED AND OBSERVED REACTOR VESSEL LIQUID LEVELS FOR MIST TEST 320201.

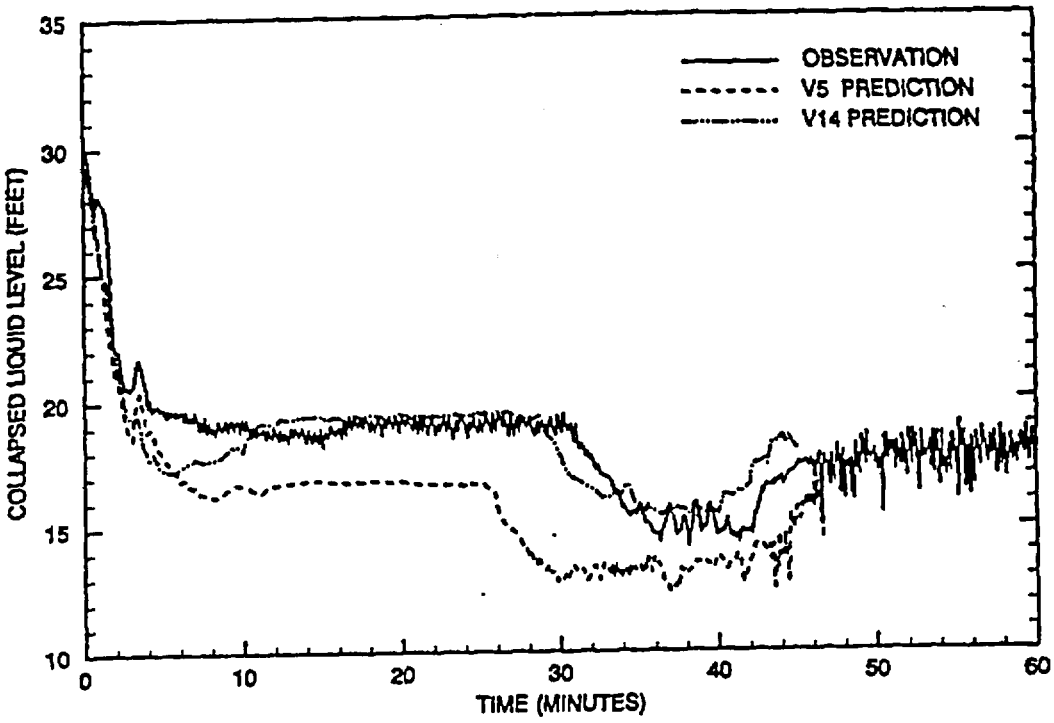


FIGURE L-6. COMPARISON OF PREDICTED AND OBSERVED SG SECONDARY LIQUID LEVELS FOR MIST TEST 320201.